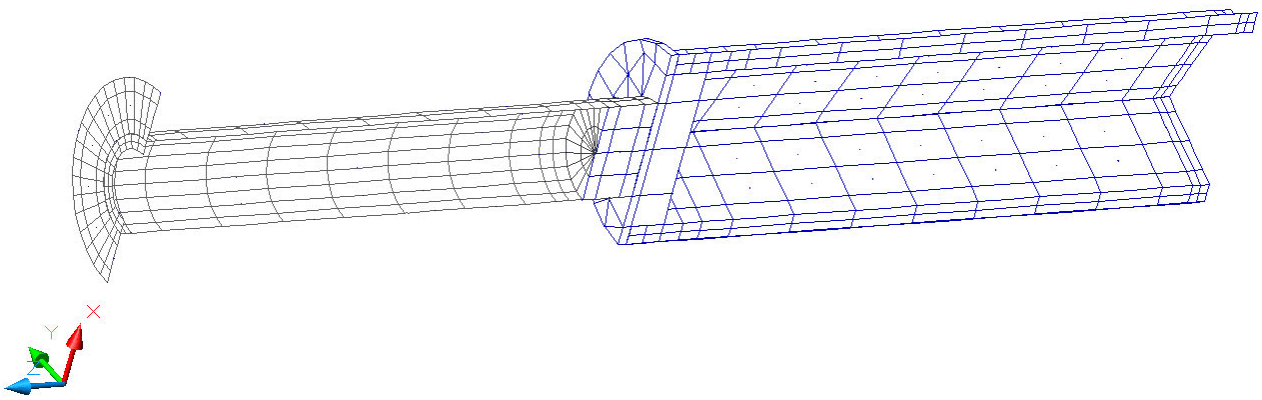

(Note: the positive x-axis is oriented towards the top of the package and the positive z-axis towards the package closure end)

Figure 3.6-11 – 'Hidden Line' View of MURR FHE and Spacer Quarter Symmetry Thermal Model

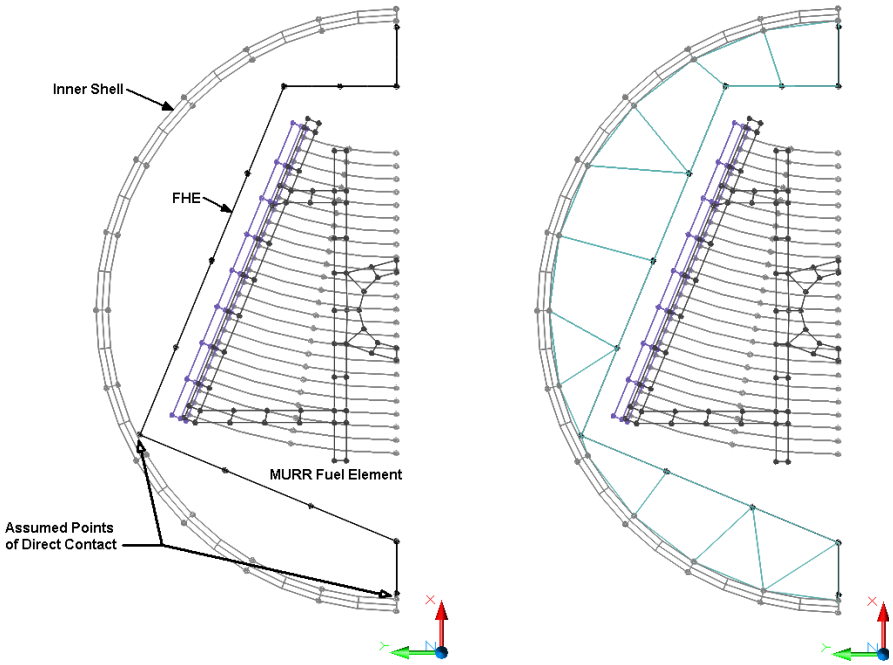

Modeling Showing Direct Contact **Modeling with 'Solid' Elements for Air**

Figure 3.6-12 – Thermal Model of MURR Fuel Element and FHE within Inner Shell

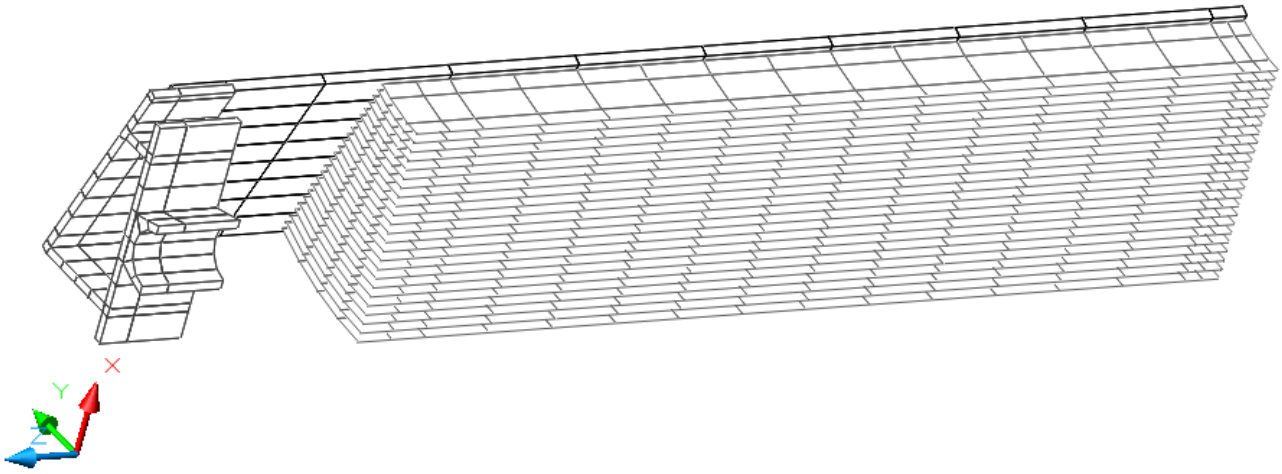

MURR Fuel Element Model, Side View of Quarter Symmetry Model

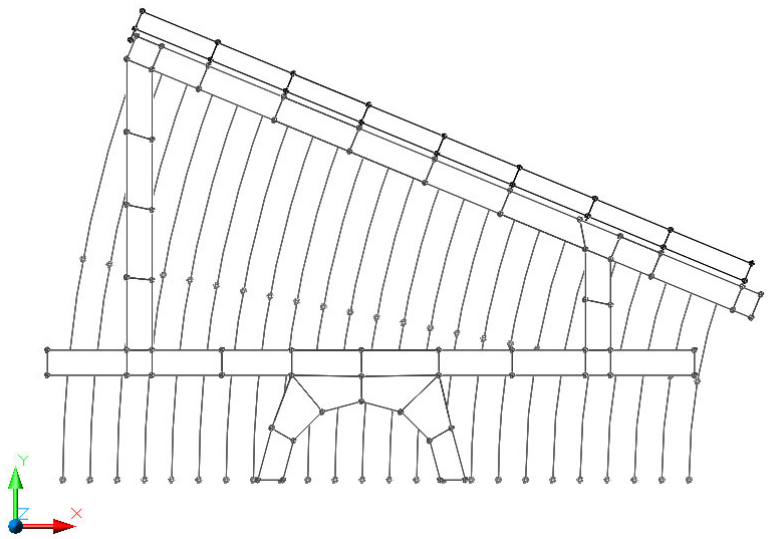

MURR Fuel Element Model, End View of Quarter Symmetry Model

Figure 3.6-13 – Side and End Views of MURR Fuel Element Thermal Model

This page left intentionally blank.

4.0 CONTAINMENT

4.1 Description of the Containment System

The containment function of the ATR FFSC is to confine the fuel elements or loose plates within the packaging during Normal Conditions of Transport (NCT) and Hypothetical Accident Conditions (HAC).

The package body is a stainless steel weldment that consists of two nested shells. The outer shell is an 8-in square stainless steel tube with a 3/16-in thick wall, and the inner shell is a 6-in diameter stainless steel tube with a 0.120-in thick wall. Components are joined using full-thickness fillet welds (i.e., fillet welds whose leg size is nominally equal to the lesser thickness of the parts joined) and full and partial penetration groove welds. The end of the body is welded closed with 0.88-in plate.

The lid end of the package is closed with a simple closure device. The closure engages with the body using a bayonet style design. There are four lugs, uniformly spaced on the closure, that engage with four slots in the mating body fixture. The closure is secured by two retracting spring loaded pins, rotating the closure through 45°, and releasing the spring loaded pins such that the pins engage with the mating holes on the body. When the pins are properly engaged with the mating holes the closure is locked and cannot be removed unintentionally.

The containment boundary is defined as the boundary of the cavity formed by the closure and inner stainless steel tube. For criticality control purposes, the fuel element must remain within this boundary during NCT and HAC. No seals or gaskets are utilized within the package.

To prevent unauthorized operation, a small post on the closure is drilled to receive a tamper indicating device (TID) wire. An identical post is located on the body and is also drilled for the TID wire. For ease in operation, there are two TID posts on the body. There are only two possible angular orientations for the closure installation and the duplicate TID post on the body enables TID installation in both positions.

4.1.1 Type A Fissile Packages

The ATR FFSC is classified as a Type A Fissile package. The Type A Fissile package is constructed and prepared for shipment so that there is no loss or dispersal of the radioactive contents, and no significant increase in external surface radiation levels, and no substantial reduction in the effectiveness of the packaging during normal conditions of transport. The fissile material is contained within the containment boundary. Chapter 6.0, *Criticality Evaluation*, demonstrates that the package remains subcritical under normal and hypothetical accident conditions.

The ATR FFSC contains four radioactive isotopes: U-234, U-235, U-236, and U-238. The A_2 value for U-235 and U-238 is unlimited, while the minimum A_2 value for U-234 and U-236 is 0.16 Ci for slow lung absorption. To compute the mixture A_2 for the HEU payloads, the maximum value of 1200 g U-235 is assumed, with a low weight fraction of 90% to maximize the mass of uranium. Therefore, the total mass of uranium is 1200/0.9 = 1333 g U. The maximum weight percents of U-234 (1.2%) and U-236 (0.7%) are assumed to maximize the mass of these isotopes. The balance is treated as U-238. For this conservative isotopic mix, the mixture A_2 is

0.164 Ci. The package activity for this mixture is 0.103 Ci (mostly due to U-234); therefore, the package contains approximately $0.6A_2$.

For LEU payloads, the maximum value of 1,681 g U-235 is taken for ATR LEU fuel (from Section 1.2.2.7, *ATR LEU Fuel Element*), with a low weight fraction of 19.55% (19.75% - 0.20%). The total mass of uranium is 1,681/0.1955 = 8,598 g U. The maximum weight percentages are $2(10^{-7})$% for U-232, 0.26% for U-234, and 0.46% for U-236. The mixture A_2 for the LEU mixture is 0.165 Ci. The package activity for this mixture is 0.148 (again, mostly due to U-234); therefore the package contains approximately $0.9A_2$.

4.1.2 Type B Packages

The content of the ATR FFSC package is high-enriched uranium with approximately $0.9A_2$ for release purposes. As a fissile package the ATR FFSC must meet the release rates for Type B packages when required by the total amount of radioactive material. However, because the A_2 value of the contents is less than 1 A_2, the package is classified as Type A and there are no release limits except as necessary for criticality control.

4.2 Containment under Normal Conditions of Transport

The ATR FFSC payloads listed in Section 1.2.2, *Contents*, are confined within the packaging under NCT. This is verified by full-scale testing, as discussed in Section 2.6, *Normal Conditions of Transport*. The test units survived the NCT drop tests with minimal damage to the packaging and no damage to the fuel elements. The maximum internal pressure in the package does not exceed atmospheric pressure because the closure is not sealed with a gasket or other sealing material. Because the ATR FFSC is a Type A Fissile package, leakage rate testing is not required.

4.3 Containment under Hypothetical Accident Conditions

The radioactive material contents of the ATR FFSC package must meet the containment requirements of 10 CFR §71.55(e) such that the package would be subcritical under the HAC.

The test program demonstrates that the package contains the fuel elements or loose fuel plates under the HAC events sufficient to maintain criticality control. The full-scale HAC drop tests summarized in Section 2.7, *Hypothetical Accident Conditions*, confirm the HAC performance of the package. The closure remained intact throughout all the drop sequences, and the fuel element remained confined within the inner stainless steel tube. The non-fissile end boxes on the fuel element shattered as expected but the fueled portion of the element remained intact and retained its geometry. There was no dispersal of fissile material. The criticality evaluation presented in Section 6.0, *Criticality Evaluation*, evaluates the contents in the most reactive credible configuration and with water moderation as required.

Because the ATR FFSC package is a Type A Fissile package and the contents are less than 1 A_2, the performance requirements of 10 CFR §71.51 do not apply.

4.4 Leakage Rate Tests for Type B Packages

The ATR FFSC is a Type A Fissile package; therefore, this section does not apply.

5.0 SHIELDING EVALUATION

Compliance of the ATR FFSC with respect to the dose rate limits established by 10 CFR §71.47[1] for normal conditions of transport (NCT) or 10 CFR §71.51(a)(2) for hypothetical accident conditions (HAC) are satisfied when limiting the package to the contents specified in Section 1.2.2, *Contents*, and verified by measurement.

Prior to transport, the ATR FFSC shall be monitored for both gamma and neutron radiation to demonstrate compliance with 10 CFR §71.47. Although the ATR FFSC will likely be shipped exclusive use, dose rates will be sufficiently low to allow non-exclusive use transport, if desired.

Shielding materials are not specifically provided by the ATR FFSC. Because the contents are essentially unshielded, the HAC dose rates at one meter will not be significantly different from the NCT dose rates at one meter. This result ensures that the post-HAC, allowable dose rate of 1 rem/hr a distance of one meter from the package surface per 10 CFR §71.51(a)(2) will be met.

[1] Title 10, Code of Federal Regu1ations, Part 71 (10 CFR 71), *Packaging and Transportation of Radioactive Material*.

This page left intentionally blank.

6.0 CRITICALITY EVALUATION

The following analyses demonstrate that the ATR FFSC complies with the requirements of 10 CFR §71.55[1] and §71.59.

The analysis in the main body of Chapter 6 (Sections 6.2 through 6.6, 6.8, and 6.9) pertains only to the ATR high enriched uranium (HEU) fuel element and ATR loose plate basket. Any discussion of the ATR fuel element or ATR FHE in these sections is limited solely to the ATR HEU fuel element and ATR HEU FHE. Additional payloads are added as appendices.

The analysis for MIT and MURR HEU fuel is contained in Appendix B (Section 6.10, *Criticality Analysis for MIT and MURR Fuel*). Any discussion of the MIT and MURR fuel elements and MURR FHE in these sections is limited solely to the MIT and MURR HEU fuel elements and the MURR HEU FHE.

The analysis for the small quantity payloads is contained in Appendix C (Section 6.11, *Criticality Analysis for Small Quantity Payloads*).

The analysis for the ATR U-Mo demonstration element was previously contained in Appendix D (Section 6.12, *Criticality Analysis for the U-Mo Demonstration Element*). This analysis and any associated results have been removed as the ATR U-Mo demonstration element is no longer a possible payload.

The analysis for the Cobra fuel element is contained in Appendix E (Section 6.13, *Criticality Analysis for the Cobra Fuel Element*).

The analysis for the ATR low enriched uranium (LEU) fuel element, MURR LEU fuel element and design demonstration element (DDE), MIT LEU fuel element and DDE, and NBSR DDE is contained in Appendix F (Section 6.14, *Criticality Analysis for ATR, MURR, MIT, and NBSR LEU Fuel Elements and/or DDEs*).

The air transport analysis in Section 6.7 applies to all payloads except those documented in Section 6.14 (for which the applicable air transport analysis is also documented in Section 6.14).

6.1 Description of Criticality Design

The results presented in this section are for all payload types.

6.1.1 Design Features Important for Criticality

A comprehensive description of the ATR FFSC is provided in Section 1.2, *Packaging Description*, and in the drawings in Appendix 1.3.2, *Packaging General Arrangement Drawings*. This section summarizes those design features important for criticality.

No poisons are utilized in the package.

For the ATR HEU and LEU fuel element payloads, the separation provided by the packaging (outer tube minimum flat-to-flat dimension of 7.9-in, inner tube maximum inner diameter of

[1] Title 10, Code of Federal Regulations, Part 71 (10 CFR 71), *Packaging and Transportation of Radioactive Material*.

5.814-in), along with the limit on the number of packages per shipment, is sufficient to maintain criticality safety.

For the ATR loose plate payload, in addition to the packaging design features noted above, moderation of the loose plates is controlled by the loose plate basket, which confines the fuel plates to a rectangular area.

For the MURR/MIT HEU and LEU fuel element payloads, in addition to the packaging design features noted above, the MURR and MIT fuel handling enclosures (FHEs) restrict postulated fuel element pitch expansion under hypothetical accident conditions.

For the small quantity payload analysis, the fuel is modeled as a homogenized mixture of uranium and water. Therefore, the packaging itself is sufficient to maintain criticality safety, as the fuel handling enclosures and fuel structural materials are not credited in the analysis.

For the Cobra fuel element analysis, in addition to the packaging design features noted above, the Cobra FHE is credited for normal conditions of transport.

For the NBSR DDE payload, the applicable fuel handling enclosure or protective material is conservatively not credited.

6.1.2 Summary Table of Criticality Evaluation

The upper subcritical limit (USL) for ensuring that the ATR FFSC (single package or package array) is acceptably subcritical, as determined in Section 6.8 (for HEU plate-fuel), Section 6.11.8 (for the small quantity payload), and Section 6.13.8 (for the Cobra fuel element) is:

$$USL = 0.9209$$

The USL for ATR, MURR, MIT, and NBSR LEU fuel elements and/or DDEs is calculated on a case-by-case basis in Section 6.14.6.

The package is considered to be acceptably subcritical if the computed k_{safe} (k_s), which is defined as $k_{effective}$ (k_{eff}) plus twice the statistical uncertainty (σ), is less than or equal to the USL, or:

$$k_s = k_{eff} + 2\sigma \leq USL$$

The USL is determined on the basis of a benchmark analysis and incorporates the combined effects of code computational bias, the uncertainty in the bias based on both benchmark-model and computational uncertainties, and an administrative margin. The results of the benchmark analysis indicate that the USL is adequate to ensure subcriticality of the package.

<u>ATR HEU Fuel Element and ATR Loose Plate Basket</u>

The packaging design is shown to meet the requirements of 10 CFR 71.55(b) when the package is limited to either one 1200 g U-235 ATR HEU fuel element, or 600 g U-235 in the form of ATR loose fuel plates. Moderation by water in the most reactive credible extent is utilized in both the NCT and HAC analyses. In the single package NCT models, full-density water fills the accessible cavity, while in the single package HAC models, full-density water fills all cavities. In the fuel element models, the most reactive credible configuration is utilized by maximizing the gap between the fuel plates. Maximizing this gap maximizes the moderation and hence the reactivity because the system is under moderated. In the loose plate model, no credit is taken for the dunnage plates and the optimal pitch and fuel arrangement is utilized. In all single package models, 12-in of water reflection is utilized.

In the NCT and HAC array cases, partial moderation is considered to maximize array interaction effects. A 9x9x1 array is utilized for the NCT array, while a 5x5x1 array is utilized in the HAC array. In all array models, 12-in of water reflection is utilized.

The maximum results of the ATR HEU fuel element criticality calculations are summarized in Table 6.1-1. The maximum calculated k_s is 0.8362, which occurs for the optimally moderated NCT array case. The NCT array is more reactive than the HAC array because the NCT array is larger, and moderation is allowed in both conditions. In this case, the fuel element is moderated with full-density water, the inner tube is moderated with 0.3 g/cm^3 water, and void is modeled between the insulation and outer tube.

The maximum results of the loose plate basket criticality calculations are summarized in Table 6.1-2. The maximum calculated k_s is 0.7747, which occurs for the optimally moderated NCT array case. The NCT array is more reactive than the HAC array because the NCT array is larger, and moderation is allowed in both conditions. In this case, the loose fuel plate basket is moderated with full-density water, the inner tube is moderated with 0.5 g/cm^3 water, and void is modeled between the insulation and outer tube.

It may be noted when comparing Table 6.1-1 and Table 6.1-2 the fuel element payload is more reactive than the loose plate basket payload.

MURR and MIT HEU Fuel Element

A summary of the MURR and MIT HEU fuel element analysis is provided in Section 6.10.1.2. The summary table is also provided as Table 6.1-3 for convenience.

Small Quantity Payload

A summary of the small quantity payload analysis is provided in Section 6.11.1.2. The summary table is also provided as Table 6.1-4 for convenience.

Cobra Element

A summary of the Cobra element analysis is provided in Section 6.13.1.2. The summary table is also provided as Table 6.1-5 for convenience.

Air Transport Analysis

The air transport analysis applies to all licensed payloads except the ATR LEU, MURR LEU, MIT LEU, and NBSR LEU payloads. The air transport analysis for these LEU payloads is documented in Section 6.14. In the air transport analysis, 2000 g U-235 is modeled as a sphere moderated with the hydrogenous packaging materials and reflected with 20 cm of water. The hydrogenous packaging materials include 100 g polyethylene and 4000 g neoprene. Maximum reactivity is achieved when the fissile material is divided into a 1500 g U-235 inner sphere moderated with polyethylene and neoprene and an outer sphere consisting of 500 g U-235 uranium metal. The maximum calculated k_s is 0.6074 for the most reactive air transport case, which is far below the USL.

ATR, MURR, MIT, and NBSR LEU Fuel Elements and/or DDEs

A summary of the ATR, MURR, MIT, and NBSR LEU fuel elements and/or DDEs is provided in Section 6.14.1.2. The summary table is also provided as Table 6.1-6 for convenience.

Table 6.1-1 – Summary of Criticality Evaluation (ATR Fuel Element Payload)

Normal Conditions of Transport (NCT)	
Case	k_s
Single Unit Maximum	0.4224
9x9 Array Maximum	0.8362
Hypothetical Accident Conditions (HAC)	
Case	k_s
Single Unit Maximum	0.4524
5x5 Array Maximum	0.7453
USL = 0.9209	

Table 6.1-2 – Summary of Criticality Evaluation (ATR Loose Plate Payload)

Normal Conditions of Transport (NCT)	
Case	k_s
Single Unit Maximum	0.4020
9x9 Array Maximum	0.7747
Hypothetical Accident Conditions (HAC)	
Case	k_s
Single Unit Maximum	0.4363
5x5 Array Maximum	0.6979
USL = 0.9209	

Table 6.1-3 – Summary of Criticality Evaluation (MURR/MIT Payload)

	MURR	**MIT**
Normal Conditions of Transport (NCT)		
Case	k_s	k_s
Single Unit Maximum	0.44807	0.36978
9x9 Array Maximum	0.85643	0.65658
Hypothetical Accident Conditions (HAC)		
Case	k_s	k_s
Single Unit Maximum	0.54584	0.43666
5x5 Array Maximum	0.85881	0.67309
USL = 0.9209		

Table 6.1-4 – Summary of Criticality Evaluation (Small Quantity Payload)

Normal Conditions of Transport (NCT)	
Case	k_s
Single Unit Maximum	0.6478
10 Package Array Maximum	0.8943
Hypothetical Accident Conditions (HAC)	
Case	k_s
Single Unit Maximum	0.7244
4 Package Array Maximum	0.8222
USL = 0.9209	

Table 6.1-5 – Summary of Criticality Evaluation (Cobra Element)

Normal Conditions of Transport (NCT)	
Case	k_s
71.55(b)(d): Single Unit Maximum	0.4032
71.55(d), 71.59: 9x9x1 Array Maximum	0.7389
Hypothetical Accident Conditions (HAC)	
Case	k_s
71.55(e): Single Unit Maximum	0.4996
71.55(e), 71.59: 5x5x1 Array Maximum	0.7643
USL = 0.9209	

Table 6.1-6 – Summary of Criticality Evaluation (LEU Fuel Elements and DDEs)

	ATR LEU	MURR LEU	MIT LEU	NBSR LEU
Normal Conditions of Transport (NCT)				
Case	k_s	k_s	k_s	k_s
Single Unit Maximum	0.42385	0.5063	0.42693	0.39137
Array Maximum	0.79375 (8×8)	0.86146 (8×8)	0.68613 (9×9)	0.65257 (9×9)
Hypothetical Accident Conditions (HAC)				
Case	k_s	k_s	k_s	k_s
Single Unit Maximum	0.45393	0.58572	0.52045	0.50968
Array Maximum	0.72607 (5×5)	0.86625 (5×5)	0.72735 (5×5)	0.74897 (5×5)
Upper Subcritical Limit (USL)				
	0.91942	0.92071	0.92288	0.92348
Air Transport Analysis				
	k_s = 0.71171		USL = 0.90868	

6.1.3 Criticality Safety Index

The HAC array calculations are performed for 2N packages and the NCT array calculations are performed for at least 5N packages. The number of packages modeled for each payload type is summarized in Table 6.1-7, along with the value of N. Note that for many of the NCT array cases, the number of packages modeled conservatively exceeds the 5N value. The 10 CFR §71.59 criticality safety index (CSI) is computed as 50/N and is provided in Table 6.1-7 for each payload type.

Table 6.1-7 – Summary of Criticality Safety Indices

Payload	NCT Array (# Packages)	HAC Array (# Packages)	N	CSI
ATR HEU fuel element	81	25	12.5	4.0
ATR loose plates				
MIT HEU fuel element				
MURR HEU fuel element				
Cobra fuel element				
Small Quantity Payload	10	4	2.0	25.0
ATR LEU fuel element	≥ 64	25	12.5	4.0
MURR LEU fuel element and DDE				
MIT LEU fuel element and DDE				
NBSR DDE				

6.2 Fissile Material Contents

The package can accommodate either (i) one ATR Mark VII fuel element, or (ii) a loose plate basket filled with ATR Mark VII fuel plates.

6.2.1 Fuel Element

Four different ATR Mark VII fuel element types are available: standard (7F), non-borated (7NB), non-borated hybrid (7NBH), and non-fueled plate 19 (YA). These fuel element types are described in Section 1.2.2, *Contents*. The 7NB fuel element is the only fuel element that does not contain boron, and is conservatively utilized in the criticality analysis.

Each fuel element contains up to 1200 g U-235, enriched up to 94 wt.%. The U-235 mass per plate is provided in Table 6.2-1. These values are generated by scaling up the U-235 loading for a 1075 g U-235 fuel element, as the 1200 g limit has been selected to envelope future increases in the loading. The weight percents of the remaining uranium isotopes are 1.2 wt.% U-234 (max), 0.7 wt.% U-236 (max), and 5.0-7.0 wt.% U-238. Each fuel element contains 19 curved fuel plates. Fuel plate 1 has the smallest radius, while fuel plate 19 has the largest radius, as shown in Figure 6.2-1. The as-modeled fuel element is shown in Figure 6.2-2. The fuel "meat" is uranium aluminide (UAl_x) mixed with additional aluminum. In the following paragraphs, the details of the fuel element are provided.

The key fuel element dimensions and tolerances utilized in the criticality models are summarized on Figure 6.2-1. Fuel plate 1 is nominally 0.080-in thick, fuel plates 2 through 18 are nominally 0.050-in thick, and fuel plate 19 is nominally 0.100-in thick. The plate thickness tolerance is +0.000/-0.002-in for all plates. The fuel meat is nominally 0.02-in thick for all 19 plates. The plate cladding material is aluminum ASTM B 209, 6061-0. Fuel element side plates are fabricated of ASTM B 209, aluminum alloy 6061-T6 or 6061-T651. All aluminum alloys are modeled as pure aluminum. The fuel element side plates have a minimum thickness of 0.182-in. Channels 2 through 10 have a width of 0.078 ± 0.007-in, while channels 11 through 19 have a width of 0.077 +0.008/-0.006-in. These tolerances represent average and not localized channel width. Therefore, the maximum average channel width is 0.085-in. For an actual fuel element, the channel width may exceed these tolerances in localized areas. The local maximum is 0.087-in.

The arc length of the fuel meat changes from plate to plate. This arc length varies based on the distance from the edge of the fuel meat to the fuel element side plate, as defined for each plate on Figure 6.2-1. This dimension is 0.245-in (max)/0.145-in (min) for fuel plates 1 and 19, 0.145-in (max)/0.045-in (min) for fuel plates 2 through 17, and 0.165-in (max)/0.065-in (min) for fuel plate 18. The smaller this dimension, the larger the arc length of the fuel meat.

The active fuel length varies between a minimum of 47.245-in (= 49.485 – 2*1.12) and a maximum of 48.775-in (= 49.515 – 2*0.37) for all fuel plates.

It is demonstrated in Section 6.4.1.2.1, *Fuel Element Payload Parametric Evaluation*, that reactivity increases with increasing meat arc length. Therefore, the arc length is modeled at the maximum value. To determine the number densities of the fuel meat, it is first necessary to compute the volume of the fuel meat. The volume of the fuel meat for each plate is the maximum arc length of the meat multiplied by the fuel length (48-in) and meat thickness (0.02-

in). The fuel length and meat thickness are treated as fixed quantities in all fuel element models, and the use of these dimensions is justified in Section 6.4.1.2.1.

The fuel meat volume for each of the 19 fuel plates is provided in Table 6.2-1. The mass of U-235 per plate utilized in the analysis is also provided in Table 6.2-1. The U-235 gram density for each fuel plate is also computed. Note that the U-235 gram density is higher in the inner plates compared to the outer plates.

The fuel itself is a mixture of UAl_x and aluminum. The density of this mixture is proportional to the U-235 gram density, as shown in Table 6.2-2. These data are perfectly linear, and a linear fit of the data is $\rho_2 = 0.8733\rho_1 + 2.5357$, where ρ_2 is the total gram density of the mixture, and ρ_1 is the gram density of the U-235 in the mixture. This equation is used to compute the total mixture gram density provided as the last column in Table 6.2-1.

From the fuel volumes, U-235 gram densities, and total mixture densities provided in Table 6.2-1, the number densities for the fuel region of each fuel plate may be computed. These number densities are provided in Table 6.2-3. The U-235 weight percent is assumed to be the maximum value of 94%. Representative weight percents of 0.6% and 0.35% are assumed for U-234 and U-236, respectively, and the balance (5.05%) is modeled as U-238.

6.2.2 Loose Fuel Plates

The loose plate basket may transport up to 600 g of U-235 in the form of ATR Mark VII fuel plates. These plates are described in Section 6.2.1, *Fuel Element*, although the loose plates may be flat as well as curved. The widths of the fuel meat for flat plates are the same as the fuel meat arc lengths provided in Table 6.2-1.

Because an integer number of plates will be transported, for computational purposes it is useful to modify the mass of U-235 per plate so that the total U-235 mass per package adds to 600 g. The column labeled “Number of Plates to 600 g” in Table 6.2-4 is simply the total desired mass (600 g) divided by the mass of U-235 per plate (from Table 6.2-1) and gives an estimate of the number of plates of each type required to reach 600 g U-235. Detailed models are developed for only four plates: 3, 5, 8, and 15. It is demonstrated in the analysis that it is sufficient to bound all of the plates by modeling these four. The number of plates modeled and the modeled mass of U-235 per plate are provided as the last two columns in Table 6.2-4.

In fuel element calculations, it has been determined that the fuel element is the most reactive when the arc length of the fuel “meat” is maximized. Therefore, all loose plate models utilize fuel plates with maximized fuel meat arc length. Also, because it has been determined that nominal fuel meat thickness (0.02-in) and nominal active fuel length (48.0-in) may be utilized with negligible effect on the reactivity, all loose plate models utilize these nominal dimensions. The overall plate thickness tolerance is +0.000/-0.002-in, and the loose plates are modeled at the minimum thickness of 0.048-in by reducing the cladding thickness by 0.001-in.

The number densities utilized in the models are provided in Table 6.2-5. These number densities are computed using the same method utilized in the fuel element models, although the U-235 mass per plate has been slightly adjusted as necessary so that the models always have 600 g U-235.

The active fuel length is modeled as 48-in for all fuel plates, consistent with the treatment of the fuel elements. The axial regions outside the active fuel region are conservatively ignored. The

width of cladding from the fuel meat to the edge of the plate is modeled as 0.045-in for all of the fuel plates, which is the minimum dimension from the fuel meat to the fuel element support structure. The actual plates are wider than modeled because the plates extend into the fuel element support structure and this additional width is neglected.

Table 6.2-1 – Fuel Element Volume and Gram Densities

Plate	Fuel Meat Arc Length (cm)	Fuel Meat Volume (cm^3)	U-235 Mass Per Plate (g)	U-235 density, ρ_1 (g/cm^3)	Total UAl_x + Al Density, ρ_2 (g/cm^3)
1	4.2247	26.2	27.1	1.04	3.44
2	5.0209	31.1	32.5	1.04	3.45
3	5.2764	32.7	43.2	1.32	3.69
4	5.5319	34.3	45.1	1.32	3.69
5	5.7873	35.8	58.2	1.62	3.95
6	6.0427	37.4	60.9	1.63	3.96
7	6.2982	39.0	63.6	1.63	3.96
8	6.5536	40.6	66.3	1.63	3.96
9	6.8090	42.2	69.0	1.64	3.96
10	7.0644	43.8	71.7	1.64	3.97
11	7.3198	45.3	74.3	1.64	3.97
12	7.5752	46.9	77.0	1.64	3.97
13	7.8306	48.5	79.7	1.64	3.97
14	8.0860	50.1	82.4	1.64	3.97
15	8.3414	51.7	85.2	1.65	3.98
16	8.5968	53.2	71.4	1.34	3.71
17	8.8521	54.8	73.6	1.34	3.71
18	9.0058	55.8	60.1	1.08	3.48
19	8.9039	55.1	58.7	1.06	3.47
Total	--	824.5	1200.0	--	--

Table 6.2-2 – Fuel Density Equation

U-235 Density (g/cm^3) ρ_1	Total Fuel Density (g/cm^3) ρ_2
1.00	3.409
1.30	3.671
1.60	3.933
Linear Fit: $\rho_2 = 0.8733\rho_1 + 2.5357$	

Table 6.2-3 – Fuel Element Number Densities

Plate	U-234 (atom/b-cm)	U-235 (atom/b-cm)	U-236 (atom/b-cm)	U-238 (atom/b-cm)	Aluminum (atom/b-cm)	Total (atom/b-cm)
1	1.7026E-05	2.6560E-03	9.8475E-06	1.4089E-04	5.2187E-02	5.5010E-02
2	1.7156E-05	2.6763E-03	9.9226E-06	1.4196E-04	5.2153E-02	5.4998E-02
3	2.1711E-05	3.3869E-03	1.2557E-05	1.7966E-04	5.0974E-02	5.4574E-02
4	2.1618E-05	3.3724E-03	1.2503E-05	1.7889E-04	5.0998E-02	5.4583E-02
5	2.6648E-05	4.1571E-03	1.5413E-05	2.2051E-04	4.9696E-02	5.4115E-02
6	2.6746E-05	4.1724E-03	1.5470E-05	2.2132E-04	4.9670E-02	5.4106E-02
7	2.6790E-05	4.1791E-03	1.5495E-05	2.2168E-04	4.9659E-02	5.4102E-02
8	2.6830E-05	4.1854E-03	1.5518E-05	2.2201E-04	4.9649E-02	5.4098E-02
9	2.6867E-05	4.1911E-03	1.5539E-05	2.2232E-04	4.9639E-02	5.4095E-02
10	2.6901E-05	4.1965E-03	1.5559E-05	2.2260E-04	4.9630E-02	5.4092E-02
11	2.6933E-05	4.2015E-03	1.5577E-05	2.2287E-04	4.9622E-02	5.4089E-02
12	2.6963E-05	4.2061E-03	1.5595E-05	2.2311E-04	4.9614E-02	5.4086E-02
13	2.6990E-05	4.2105E-03	1.5611E-05	2.2334E-04	4.9607E-02	5.4083E-02
14	2.7017E-05	4.2145E-03	1.5626E-05	2.2356E-04	4.9600E-02	5.4081E-02
15	2.7077E-05	4.2239E-03	1.5661E-05	2.2406E-04	4.9585E-02	5.4075E-02
16	2.2037E-05	3.4377E-03	1.2746E-05	1.8235E-04	5.0889E-02	5.4544E-02
17	2.2037E-05	3.4377E-03	1.2745E-05	1.8235E-04	5.0889E-02	5.4544E-02
18	1.7683E-05	2.7586E-03	1.0228E-05	1.4633E-04	5.2016E-02	5.4949E-02
19	1.7487E-05	2.7279E-03	1.0114E-05	1.4470E-04	5.2067E-02	5.4967E-02

Table 6.2-4 – Loose Plate Data

Plate	Number of Plates to 600 g U-235	Modeled Number of Plates	Modeled U-235 Mass Per Plate (g)
1	22.12	-	-
2	18.47	-	-
3	13.89	14	42.9
4	13.30	-	-
5	10.32	10	60.0
6	9.84	-	-
7	9.43	-	-
8	9.05	9	66.7
9	8.70	-	-
10	8.37	-	-
11	8.07	-	-
12	7.79	-	-
13	7.53	-	-
14	7.28	-	-
15	7.04	7	85.7
16	8.40	-	-
17	8.16	-	-
18	9.99	-	-
19	10.22	-	-

Table 6.2-5 – Loose Plate Number Densities (as-modeled)

Plate	U-234 (atom/b-cm)	U-235 (atom/b-cm)	U-236 (atom/b-cm)	U-238 (atom/b-cm)	Aluminum (atom/b-cm)	Total (atom/b-cm)
3	2.1539E-05	3.3600E-03	1.2458E-05	1.7823E-04	5.1018E-02	5.4591E-02
5	2.7492E-05	4.2887E-03	1.5901E-05	2.2749E-04	4.9477E-02	5.4037E-02
8	2.6975E-05	4.2081E-03	1.5602E-05	2.2322E-04	4.9611E-02	5.4085E-02
15	2.7249E-05	4.2508E-03	1.5760E-05	2.2548E-04	4.9540E-02	5.4059E-02

This page left intentionally blank.

PLATE NO.	DIM A $^{+.000}_{-.002}$	DIM B MIN	DIM B MAX
1	.080	.145	.245
2	.050	.045	.145
3	.050	.045	.145
4	.050	.045	.145
5	.050	.045	.145
6	.050	.045	.145
7	.050	.045	.145
8	.050	.045	.145
9	.050	.045	.145
10	.050	.045	.145
11	.050	.045	.145
12	.050	.045	.145
13	.050	.045	.145
14	.050	.045	.145
15	.050	.045	.145
16	.050	.045	.145
17	.050	.045	.145
18	.050	.065	.165
19	.100	.145	.245

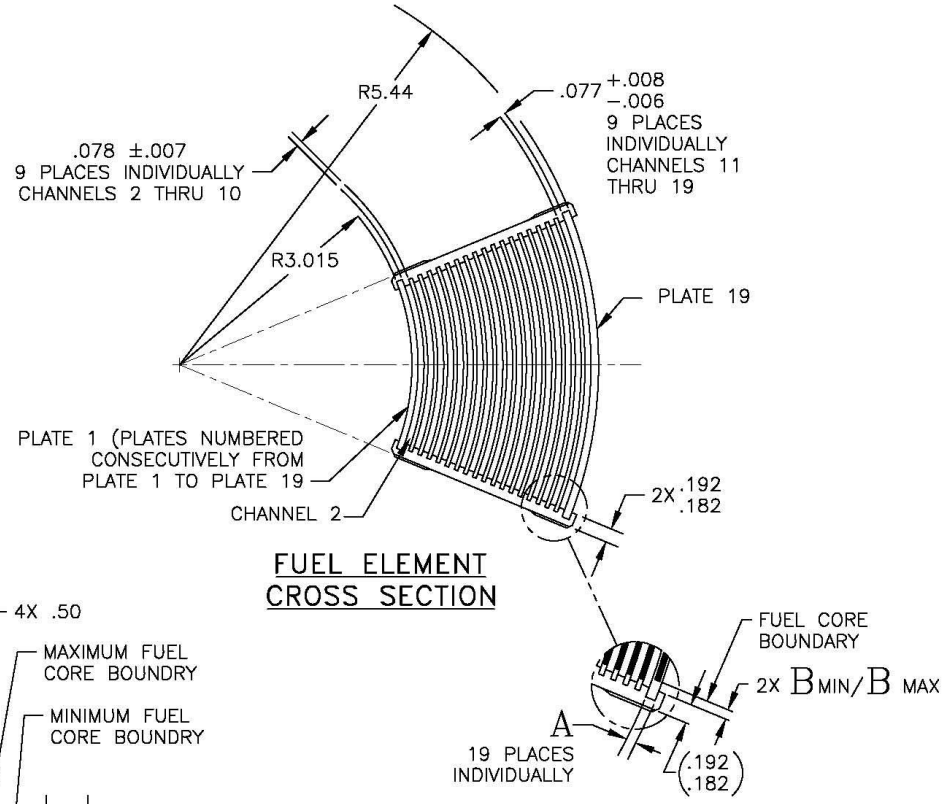

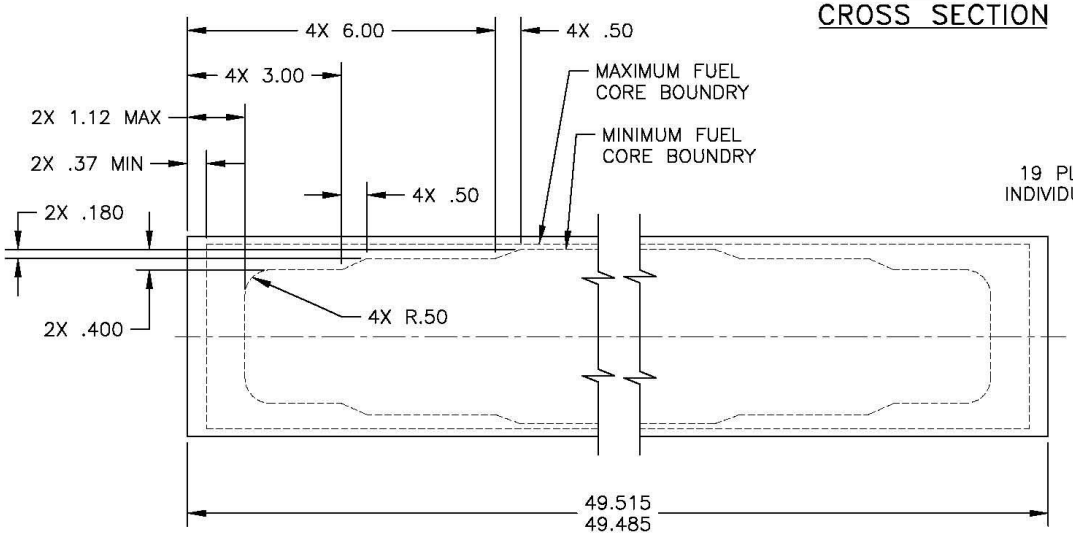

Figure 6.2-1 – ATR Fuel Element Dimensions

This page left intentionally blank.

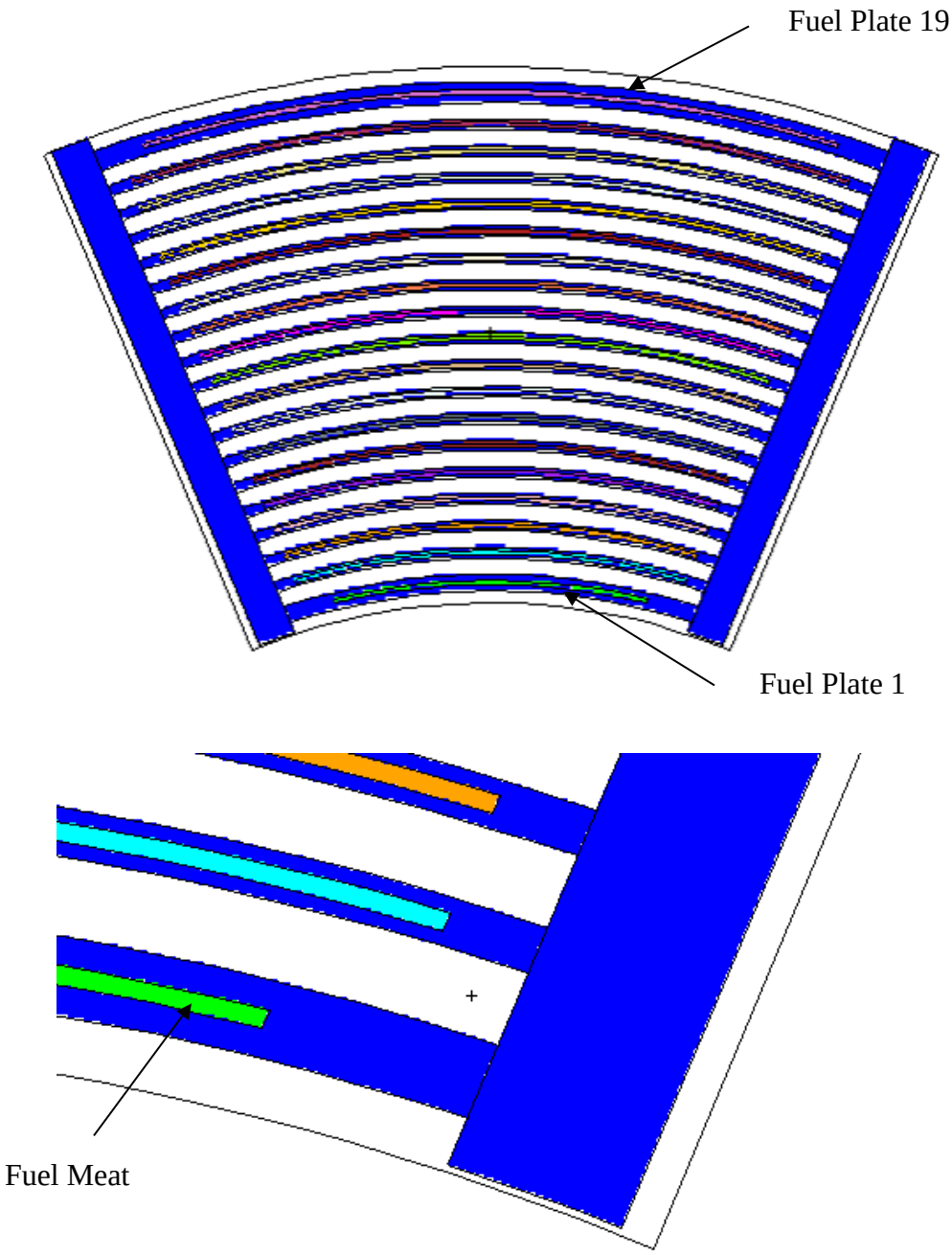

Figure 6.2-2 – Fuel Element Model

6.3 General Considerations

Criticality calculations for the ATR FFSC are performed using the three-dimensional Monte Carlo computer code MCNP5[2]. Descriptions of the fuel assembly geometric models are given in Section 6.3.1, *Model Configuration*. The material properties for all materials used in the models are provided in Section 6.3.2, *Material Properties*. The computer code and cross section libraries used are provided in Section 6.3.3, *Computer Codes and Cross-Section Libraries*. Finally, the most reactive configuration is provided in Section 6.3.4, *Demonstration of Maximum Reactivity*.

6.3.1 Model Configuration

Models are developed for both the fuel element and loose plate basket payloads.

6.3.1.1 Fuel Element Payload

The model configuration is relatively simple. Most packaging details are conservatively ignored, particularly at the ends. Because the package is long and narrow, array configurations will stack only in the lateral directions (e.g., 5x5x1). Therefore, the end details, for both the package and the fuel element, are conservatively ignored external to the active fuel region, and these end regions are simply modeled as full-density water.

The package consists of two primary structural components, a circular inner tube and a square outer tube, as shown in Appendix 1.3.2, *Packaging General Arrangement Drawings*. The inner tube has a nominal outer diameter of 6-in and a nominal thickness of 0.12-in. The outer tube has a nominal outer dimension of 8-in and a nominal thickness of 0.188-in. A layer of insulating material 1-in thick is wrapped around the inner tube.

For the inner tube, tolerances are based upon ASTM A269[3]. The tolerance on the outer diameter (OD) is ± 0.030-in, and the tolerance on the wall thickness is ±10%. Tolerances are selected to minimize the spacing between the fuel elements in the array configuration. This spacing is minimized using the maximum OD and minimum wall thickness. Using the minimum wall thickness also reduces parasitic neutron absorption in the steel. Therefore, the modeled tube OD is 6.03-in, the modeled wall thickness is 0.108-in, and the modeled tube ID is 5.814-in.

For the outer tube, the wall thickness tolerance is ±10% based upon ASTM A554[4] (the tolerance for the optional use of ASTM A240[5] also falls within this value). Using the minimum wall thickness of 0.169-in reduces parasitic neutron absorption in the steel. Reactivity in the array cases is maximized by minimizing the outer dimensions of the square. A bounding tolerance of 0.1-in is assumed for this dimension based on drawing tolerance in Appendix 1.3.2, *Packaging General Arrangement Drawings*, for a modeled OD of 7.9-in. The as-fabricated packages will meet this tolerance.

---

[2] MCNP5, "*MCNP – A General Monte Carlo N-Particle Transport Code, Version 5; Volume II: User's Guide*," LA-CP-03-0245, Los Alamos National Laboratory, April, 2003.

[3] ASTM A269-02a, *Standard Specification for Seamless and Welded Austenitic Stainless Steel Tubing for General Service*.

[4] ASTM A554-03, *Standard Specification for Welded Stainless Steel Mechanical Tubing*.

[5] ASTM A240-03, *Standard Specification for Chromium and Chromium-Nickel Stainless Steel Plate, Sheet, and Strip for Pressure Vessels and for General Applications*.

In the NCT single package models, the inner tube, insulation, and outer tube are modeled explicitly, as shown in Figure 6.3-1 and Figure 6.3-2. Although negligible water ingress is expected during NCT, the inner cavity of the package is assumed to be flooded with water because the package lid does not contain a seal. However, the region between the insulation and the outer tube will remain dry because water cannot enter this region. The Fuel Handling Enclosure (FHE) is conservatively ignored. Modeling the FHE would decrease water reflection in the single package model. However, the neoprene along the sides of the FHE is modeled explicitly using a thickness of 1/8-in. Because neoprene will reduce the reactivity due to parasitic absorption in chlorine, chlorine is removed from the neoprene, and the density is reduced accordingly. In the model, the fuel element is conservatively positioned at the radial center of the inner tube to maximize neutron reflection. The package is reflected with 12-in of full-density water.

The HAC single package model is essentially the same as the NCT single package model. Damage in the drop tests was shown to be negligible and concentrated at the ends of the package (See Section 2.12.1). As the ends of the package are not modeled, this end damage does not affect the modeling. The various side drops resulted in only minor localized damage to the outer tube, and no observable bulk deformation of the package. Therefore, the minor damage observed will not impact the reactivity. The insulation is replaced with full-density water, and the region between the insulation and outer tube is also filled with full-density water (see Figure 6.3-3). The treatment of the FHE is the same as the NCT single package model. Cases are developed both with and without the FHE neoprene, and with and without chlorine in the neoprene.

As a result of the drop tests, limited damage to the fuel element was observed. The bottom end box sheared off from the main body, although this condition has no effect on the criticality models because the fuel element is not modeled beyond the active fuel region. Limited damage to the fuel element plates was observed at the ends, although this damage is over a short length in a region of low reactivity worth. Slight localized buckling of the fuel plates was also observed in the region of the fuel element side plate vent openings, as the fuel plates are not as well supported in these regions. Because the observed fuel element damage is minor and will have only a negligible effect on reactivity, no damaged fuel element models are developed.

In the NCT array models, a 9x9x1 array is utilized. Although the FHE would survive NCT events with no damage, the FHE is conservatively ignored and the fuel elements are pushed toward the center of the array. Because the fuel elements are transported in a thin (~0.01-in) plastic bag, this plastic bag is assumed to act as a boundary for partial moderation effects. The plastic bag is not modeled explicitly, because it is too thin to have an appreciable effect on the reactivity. Therefore, it is postulated that the fuel element channels may fill with full-density water, while the region between the fuel element and inner tube fills with variable density water. The partial moderation effects that could be achieved by modeling the FHE explicitly are essentially addressed by the partial moderation analysis using the plastic bag. Also, modeling the FHE explicitly would result in the fuel elements being significantly pushed apart, which is a less reactive condition. Axial movement of the fuel elements is not considered because axial movement would increase the effective active height of the system and reduce the reactivity due to increased leakage. The presence of chlorine-free neoprene is also considered.

In the HAC array models, a 5x5x1 array is utilized. The HAC array models are essentially the same as the NCT array models, except additional cases are developed to determine the reactivity

effect of allowing variable density water in the region between the inner and outer tubes. Cases are also developed with and without the insulation, and with and without chlorine-free neoprene. The FHE is conservatively ignored for the reasons stated in the previous paragraph. Because the NCT and HAC models are very similar and the NCT models utilize a larger array, the NCT array models are more reactive than the HAC array models.

The detailed moderation assumptions for the array cases are discussed more fully in Section 6.5, *Evaluation of Package Arrays under Normal Conditions of Transport*, and Section 6.6, *Package Arrays under Hypothetical Accident Conditions*.

6.3.1.2 Loose Plate Basket Payload

The NCT and HAC single package models are shown in Figure 6.3-4 and Figure 6.3-5, respectively. The NCT and HAC packaging models, including tolerances, are consistent with the values used in the fuel element analysis. The difference is that the aluminum loose plate basket and payload of fuel plates is inserted into the cavity. The loose plate basket does not contain neoprene.

The dimensions of the loose plate basket are provided on the packaging general arrangement drawings. The wall thickness of the basket in the central rectangular region is 0.19 ± 0.06-in. The cavity width is 4.5 ± 0.06-in, and the cavity height is 1.62 ± 0.06-in. The basket wall thickness is modeled at the minimum thickness of 0.13-in to minimize absorption in the aluminum. The inner dimensions of the basket are modeled at the maximum values of 4.56-in x 1.68-in to maximize the volume available for moderation. The radial supports are neglected in the MCNP models.

In the actual loaded configuration, the loose plates are bundled so that the plates are in close contact, and aluminum dunnage plates are used to fill the void space to prevent lateral movement. In the criticality models, the dunnage plates are conservatively ignored. Modeling the dunnage plates would severely restrict the volume available for water moderation. Because no dunnage plates are modeled, the fuel plates are allowed to arrange in the most reactive geometry, including non-regular pitches. Flat plates are modeled rather than curved plates because flat plates are much simpler to model. It is demonstrated that flat plates and curved plates are neutronically equivalent.

Axial movement of the fuel plates is not considered, because this motion would be negligible and is precluded by the basket design, which has a cavity length of 50.5-in. The fuel plates are approximately 49.5-in long, although only the 48-in active length is modeled.

In the NCT and HAC single package models, the fuel basket is centered in the cavity to maximize water reflection, and all water is at full density to maximize moderation and reflection.

In the NCT array analysis, four different plate types are examined: 3, 5, 8, and 15. Plate type 5 is shown to be the most reactive. A number of both regular and non-regular pitches are utilized in order to find the most reactive condition. Plate type 5 is used in all single package and array analyses.

In the NCT array models, a 9x9x1 array is utilized. Water is assumed to be present inside the cavity at a density that maximizes reactivity. To bound any potential damage to the loose plate basket, the rectangular region of each basket is pushed toward the radial center of the array until

contact is made with the circular tube. This geometry is not considered credible because the ribs will maintain concentricity between the basket and cavity.

In the HAC array models, a 5x5x1 array is utilized. Water is assumed to be present inside the cavity and between the inner and outer tubes at a density that maximizes reactivity. The detailed moderation assumptions for the array cases are discussed more fully in Section 6.5, *Evaluation of Package Arrays under Normal Conditions of Transport*, and Section 6.6, *Package Arrays under Hypothetical Accident Conditions.*

The fuel plates are modeled as undamaged in both the NCT and HAC models. As a result of the drop tests, limited buckling of the fuel plates was observed at the end, although this damage is over a short length in a region of low reactivity worth. Because the observed fuel plate damage is minor and will have only a negligible effect on reactivity, no damaged fuel plate models are developed. Also, any anticipated damage is bounded because the most reactive pitch is modeled for both uniform and non-uniform conditions, and the damaged condition is essentially a subset of the conditions already modeled.

6.3.2 Material Properties

The fuel meat compositions are provided in Table 6.2-3 and Table 6.2-5 for the fuel element and loose plates, respectively. The fuel plate cladding is aluminum alloy 6061-0, while the side plates may be either aluminum alloy 6061-T6 or 6061-T651. From a criticality perspective, these alloys are essentially aluminum, and in the MCNP models all aluminum alloy structural materials are modeled as pure aluminum with a density of 2.7 g/cm^3. The material properties of the remaining packaging and moderating materials are described in the following paragraphs.

The inner and outer tubes of the package are constructed from stainless steel 304. Although MCNP is used in the calculations, the standard compositions for stainless steel 304 are obtained from the SCALE material library[6], which is a standard set accepted for use in criticality analyses. The stainless steel composition and density utilized in the MCNP models are provided in Table 6.3-1.

The insulation material utilized in the NCT models has a density of 6 pounds per cubic foot (0.096 g/cm^3). The insulation is composed of Al_2O_3 and SiO_2 in approximately equal quantities, with small (<1 wt%) quantities of other minor constituents. It is assumed in this analysis that the material is simply 50% Al_2O_3 and 50% SiO_2 by weight and the impurities are neglected. Insulation material properties are provided in Table 6.3-2.

Neoprene (C_4H_5Cl) has a density of 1.23 g/cm^3, and the chemical composition is provided in Table 6.3-3. Because chlorine is a neutron absorber, for models in which the chlorine has been deleted, a density of 0.737 g/cm^3 is utilized.

Water is modeled with a density ranging up to 1.0 g/cm^3 and the chemical formula H_2O. The S(α,β) card LWTR.60T is used to simulate hydrogen bound to oxygen in water.

[6] *Standard Composition Library*, NUREG/CR-0200, Rev. 6, Volume 3, Section M8, ORNL/NUREG/CSD-2/V3/R6, September 1998.

6.3.3 Computer Codes and Cross-Section Libraries

MCNP5 v1.30 is used for the criticality analysis[7]. All cross sections utilized are at room temperature (293.6 K). The uranium isotopes utilize preliminary ENDF/B-VII cross section data that are considered by Los Alamos National Laboratory to be more accurate than ENDF/B-VI cross sections. ENDF/B-V cross sections are utilized for chromium, nickel, and iron because natural composition ENDF/B-VI cross sections are not available for these elements. The remaining isotopes utilize ENDF/B-VI cross sections. Titles of the cross sections utilized in the models have been extracted from the MCNP output and provided in Table 6.3-4. As discussed in Section 6.3.2, the S(α,β) card LWTR.60T is also used to simulate hydrogen bound to water.

Cases are run with a minimum 2500 neutrons per generation for 250 generations, skipping the first 50. The 1-sigma uncertainty is approximately 0.001 for most cases.

6.3.4 Demonstration of Maximum Reactivity

Fuel Element Payload

The reactivities of the NCT and HAC single package cases are small, with $k_s < 0.5$.

The NCT and HAC array cases are similar. For the NCT array, a 9x9x1 array is utilized, while in the HAC array, a smaller 5x5x1 array is utilized. Because negligible damage was observed in the drop tests, the package dimensions are the same between the NCT and HAC models. Dimensions of both the fuel element and packaging are selected to maximize reactivity, and close-water reflection is utilized. In the fuel element, the fuel meat width and channel width are maximized, as this condition is the most reactive. In both NCT and HAC array cases, flooding with partial moderation is allowed in the central cavity, and the fuel elements are pushed toward the center of the array. In the fuel element models, the FHE is not modeled explicitly because the FHE would increase the fuel element spacing and decrease the reactivity. Any partial moderation effects of the FHE are essentially addressed by the partial moderation analysis for the fuel element itself.

In the NCT array models, insulation is modeled between the inner and outer tubes, while in the HAC array models, this region may have water, void, or insulation. In both sets of models, chlorine-free neoprene is modeled adjacent to the fuel element side plates, although the effect on the reactivity is small. No models in which the neoprene is allowed to decompose and homogeneously mix with the water are developed, as this scenario is already bounded by the variable water density search.

The NCT array is more reactive than the HAC array, primarily because the NCT array is significantly larger. The most reactive case (Case E23) results in a $k_s = 0.8362$, which is below the USL of 0.9209.

Loose Plate Basket Payload

The reactivities of the NCT and HAC single package cases are small, with $k_s < 0.5$.

To facilitate model preparation, only four different plate types are examined: 3, 5, 8, and 15. The fuel meat width is maximized in all loose plate models, as this condition has been shown to

[7] MCNP5, "*MCNP – A General Monte Carlo N-Particle Transport Code, Version 5; Volume II: User's Guide*," LA-CP-03-0245, Los Alamos National Laboratory, April 2003.

maximize reactivity. For simplicity, plate types are not mixed in the same model. An optimum pitch search is performed to determine the most reactive condition. Both regular and non-regular pitches are examined. Plate 5 is the most reactive because its small width allows this plate to "double stack" along the width of the basket, resulting in a higher level of moderation compared to the larger plates. Plates 1 through 4 are smaller than Plate 5, but the low uranium loading of these plates results in a higher number of plates to achieve 600 g U-235, and the larger number of plates results in less moderation. In actual practice, plates of any type may be combined in a single loose plate basket, although random combinations of plates would be less reactive than modeling all plates as type 5.

The actual loose plate basket may accept either flat or curved plates. However, plates are modeled as flat rather than curved to facilitate model preparation. It is demonstrated that flat plates are neutronically equivalent to curved plates.

The array geometry and modeling assumption for the loose plate basket payload are similar to those described above for the fuel element payload. The NCT array is more reactive than the HAC array, primarily because the NCT array is significantly larger. The most reactive NCT configuration is with full-water density between the fuel plates, a water density of 0.5 g/cm^3 between the basket and the inner pipe, and void between the insulation and the outer tube. The axial regions beyond the active fuel are modeled as water to maximize reflection. The most reactive case (Case LG5) results in a k_s = 0.7747, which is below the USL of 0.9209. Note that the most reactive loose plate basket case is less reactive than the most reactive fuel element payload case.

Table 6.3-1 – SS304 Composition

Component	Wt.%
C	0.08
Si	1.0
P	0.045
Cr	19.0
Mn	2.0
Fe	68.375
Ni	9.5
Density = 7.94 g/cm^3	

Table 6.3-2 – Insulation Composition

Component	Wt.%
Al	26.5
Si	23.4
O	50.2
Density = 0.096 g/cm^3	

Table 6.3-3 – Neoprene Composition

Component	Wt.%
H	5.7
C	54.3
Cl	40.0
Density = 1.23 g/cm^3	

Table 6.3-4 – Cross Section Libraries Utilized

Isotope/Element	Cross Section Label (from MCNP output)
1001.62c	1-h-1 at 293.6K from endf-vi.8 njoy99.50
6000.66c	6-c-0 at 293.6K from endf-vi.6 njoy99.50
8016.62c	8-o-16 at 293.6K from endf-vi.8 njoy99.50
13027.62c	13-al-27 at 293.6K from endf-vi.8 njoy99.50
14000.60c	14-si-nat from endf/b-vi
15031.66c	15-p-31 at 293.6K from endf-vi.6 njoy99.50
17000.66c	17-cl-0 at 293.6K from endf-vi.0 njoy99.50
24000.50c	njoy
25055.62c	25-mn-55 at 293.6K from endf/b-vi.8 njoy99.50
26000.55c	njoy
28000.50c	njoy
92234.69c	92-u-234 at 293.6K from t16 u234la4 njoy99.50
92235.69c	92-u-235 at 293.6K from t16 u235la9d njoy99.50
92236.69c	92-u-236 at 293.6K from t16 u236la2d njoy99.50
92238.69c	92-u-238 at 293.6K from t16 u238la8h njoy99.50

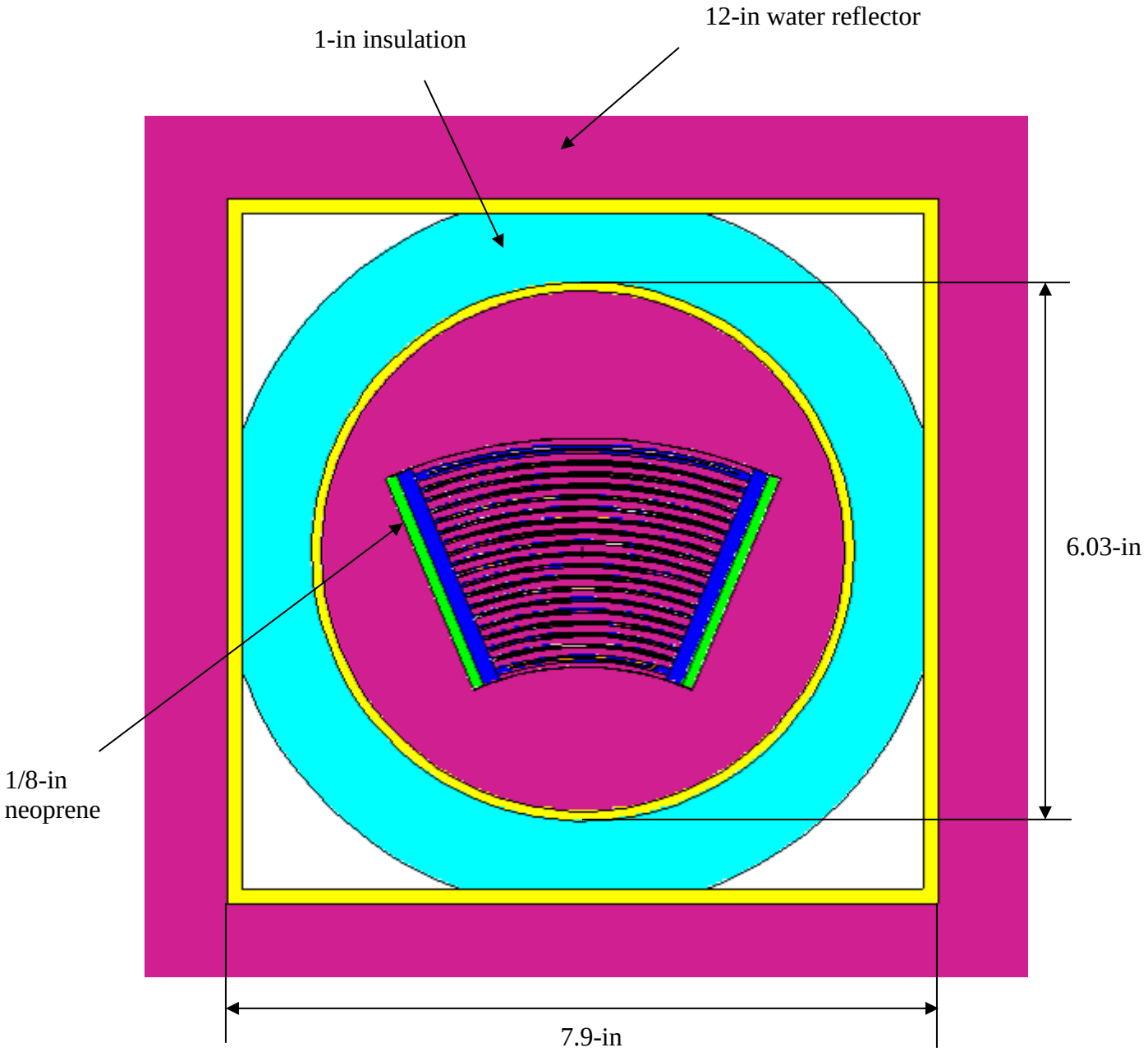

Figure 6.3-1 – NCT Single Package Model, Fuel Element (planar view)

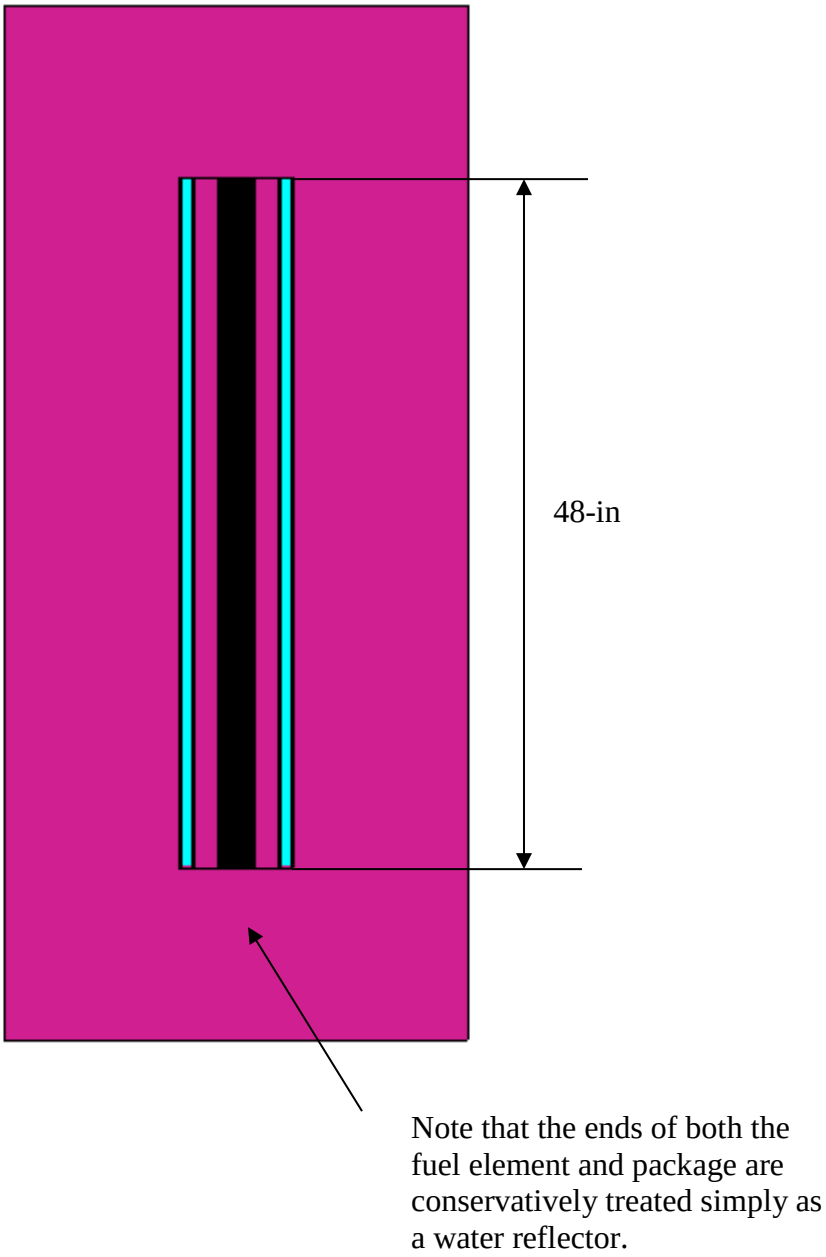

Figure 6.3-2 – NCT Single Package Model, Fuel Element (axial view)

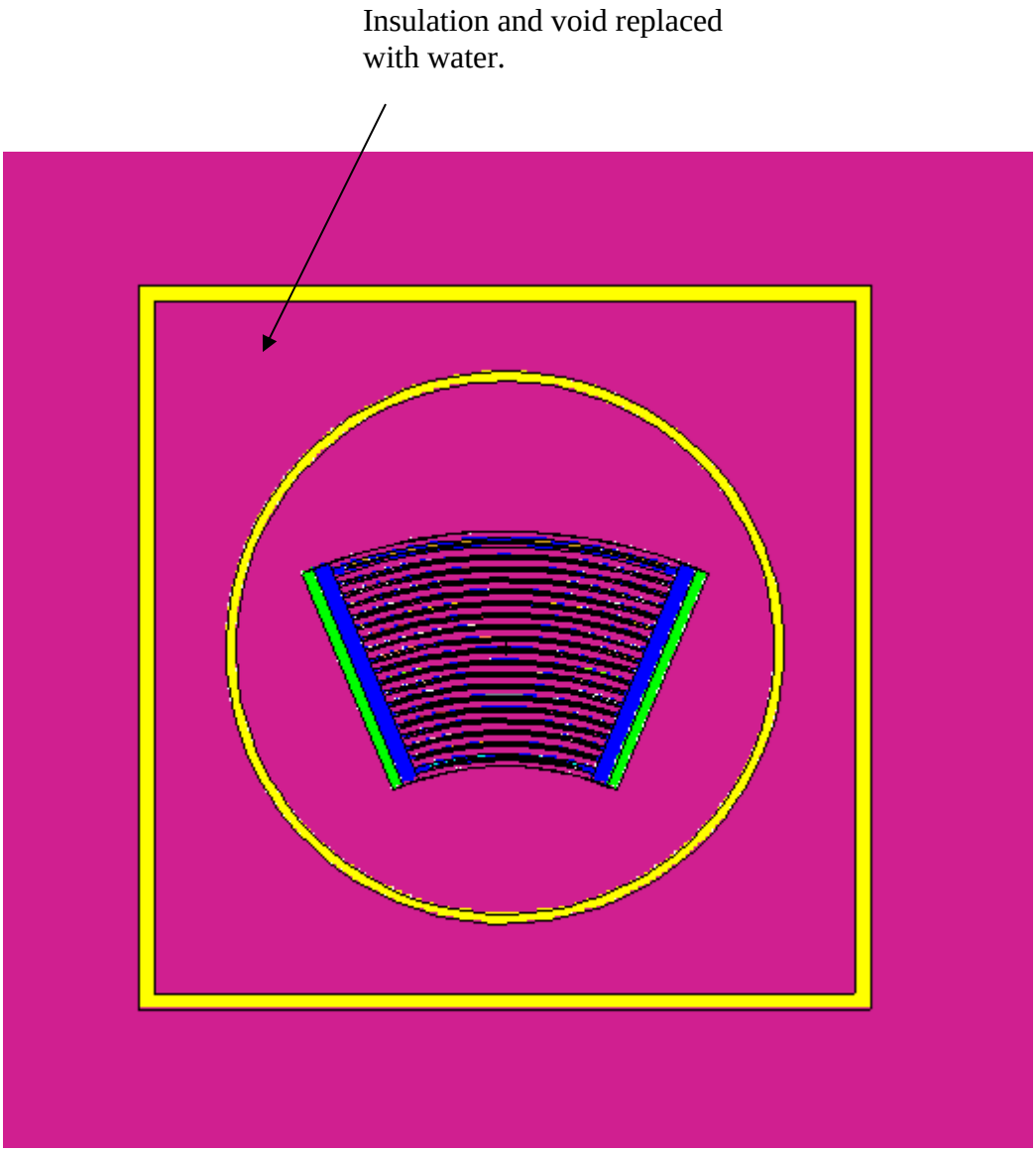

Figure 6.3-3 – HAC Single Package Model, Fuel Element (planar view)

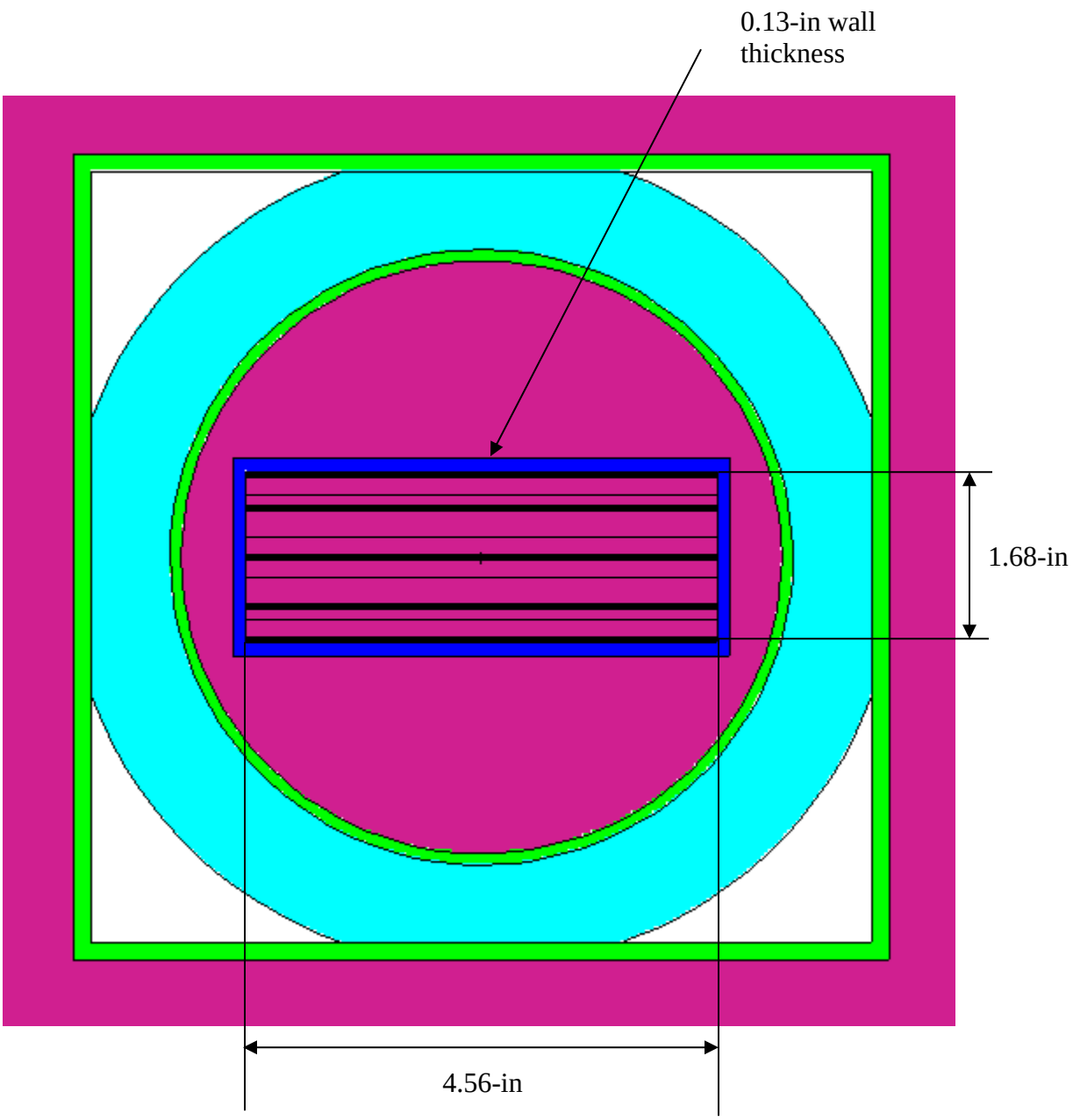

Figure 6.3-4 – NCT Single Package Model, Basket (planar view)

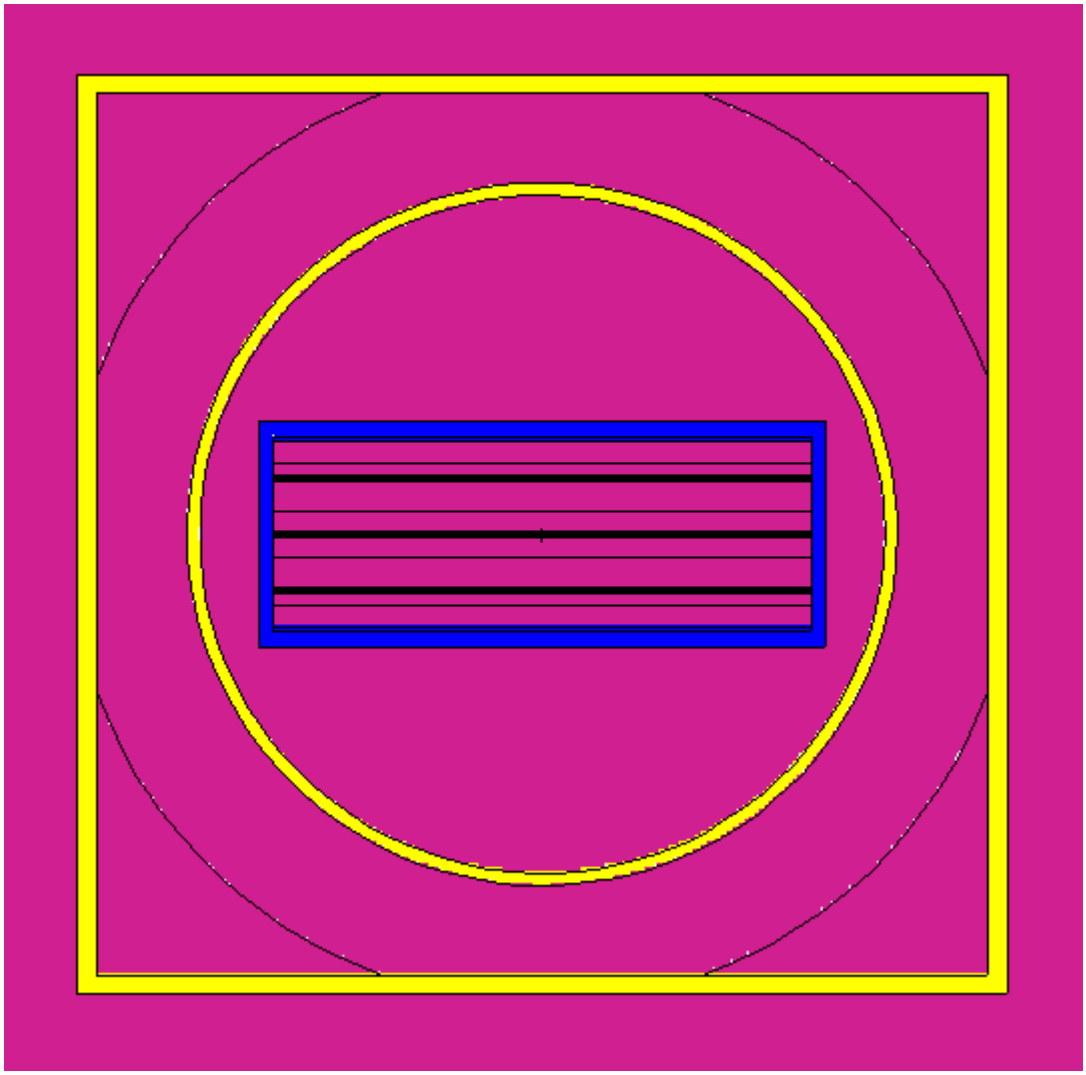

Case LB3

Figure 6.3-5 – HAC Single Package Model, Basket (planar view)

6.4 Single Package Evaluation

Compliance with the requirements of 10 CFR §71.55 is demonstrated by analyzing an optimally moderated damaged and undamaged, single-unit ATR FFSC. The figures and descriptions provided in Section 6.3.1, *Model Configuration*, describe the basic geometry of the single-unit models.

6.4.1 Single Package Configuration

6.4.1.1 NCT Configuration

6.4.1.1.1 Fuel Element Payload

The geometry of the NCT single package configuration is discussed in Section 6.3.1, *Model Configuration*. The inner tube is flooded with full-density water. The fuel element geometry is consistent with the most reactive fuel element model, including tolerances, as determined in Section 6.4.1.2.1, *Fuel Element Payload Parametric Evaluation*. Consistent with the most reactive HAC single package model, neoprene from the FHE is modeled at the sides of the fuel element. Chlorine is conservatively removed from the neoprene because chlorine acts as a poison. The package is reflected with 12-in of water.

Two cases are developed. In Case A1, the modeled channel width is 0.085-in, and in Case A2, the modeled channel width is 0.089-in. A channel width of 0.089-in is the maximum local channel width (0.087-in) with an additional margin of 0.002-in. The larger channel width is achieved by reducing the cladding thickness. Case A2 is more reactive, although the reactivity is low, with k_s = 0.42239. This result is below the USL of 0.9209. Results are provided in Table 6.4-1.

6.4.1.1.2 Loose Plate Basket Payload

The selection of the bounding fuel plate and development of the various plate arrangements are presented in conjunction with the NCT array analysis in Section 6.5.1.2, *Loose Plate Basket Payload*. It is determined that Plate 5 may be used as a bounding plate type for criticality purposes. Because the aluminum dunnage has not been credited, the plates are allowed to become arranged in the most reactive configuration within the loose plate container. The most reactive fuel plate arrangements determined in the NCT array analysis are used in the NCT single package analysis. The NCT single package models are reflected with 12-in of water.

The 10 Type 5 plates are modeled as 5 plates of double fuel meat width to allow two plates to be present side by side. The top and bottom plates are in contact with the fuel basket inner surfaces, and the center plate is always in the center of the basket. The two off-center plates are shifted in 0.1-cm increments away from the center plate so that the pitch is non-regular. When the pitch is non-regular, the maximum pitch is given as a “max” value in the results table.

A figure showing the general NCT model geometry is provided in Figure 6.3-4. Results are provided in Table 6.4-2. Six cases are run, with small variations in the plate arrangement. The maximum reactivity occurs for Case LA4, with k_s = 0.40199. This result is below the USL of 0.9209. The pitch of this case is non-regular. The top, center, and bottom plates are centered in the lattice locations with a base pitch of 1.036-cm, while the off-center plates are shifted 0.3-cm from the center plate. Note that the most reactive NCT array case peaks with the off-center

plates shifted 0.2-cm rather than 0.3-cm, although this difference is most likely due to statistical fluctuation.

6.4.1.2 HAC Configuration

6.4.1.2.1 Fuel Element Payload Parametric Evaluation

Prior to development of a single package model, a parametric analysis is performed to determine the impacts of various fuel element tolerances on the reactivity. This parametric analysis considers the effects of a number of parameters, such as fuel meat arc length, fuel meat thickness, channel width, and active fuel length.

Because the ATR fuel element is complex, with 19 unique fuel plates and 19 unique fuel material descriptions, performing this parametric study on an actual fuel element would be cumbersome. Rather, the approach utilized is to perform the parametric study on a system of 19 identical flat plates. This geometry mimics the ATR fuel element to determine trends in the data. Note that the reactivity of the 19 flat plate model is not identical to the reactivity of an actual ATR fuel element due to geometrical and material differences, although the trends are the same. The most reactive model variations are then incorporated into the ATR fuel element model.

In the parametric models, 1200 g U-235 is equally distributed between 19 identical flat plates. The base configuration consists of plates with a fuel meat width of 2.65-in (6.7355 cm; the average nominal meat arc length), active fuel height of 48-in, fuel meat thickness of 0.02-in, fuel cladding thickness of 0.015-in (total plate thickness of 0.050-in), and fuel channel thickness of 0.078-in. The geometry of Case B1 is shown in Figure 6.4-1. A total of 12 parametric models are developed, as summarized below.

Case ID	Case Description
B1	Base case
B2	Increase width of fuel meat by 0.1-in
B3	Decrease width of fuel meat by 0.1-in
B4	Increase thickness of fuel meat by 0.002-in
B5	Decrease thickness of fuel meat by 0.002-in
B6	Increase thickness of fuel meat by 0.002-in but decrease the cladding thickness to maintain a nominal plate thickness
B7	Decrease thickness of fuel meat by 0.002-in but increase the cladding thickness to maintain a nominal plate thickness
B8	Increase water channel thickness to 0.085-in
B9	Increase water channel thickness to 0.085-in by reducing the cladding thickness
B10	Decrease active fuel length to 47.0-in
B11	Reduce cladding thickness to the minimum value of 0.008-in
B12	Combine cases B2 and B9

In Cases B2 through B12, each case is identical to the base case B1 with the exception of the changes identified in the table above. The pitch, which is the sum of the plate thickness and

channel thickness, is treated as a dependant variable and is allowed to vary as the independent parameters are changed. For example, in Case B5, decreasing the thickness of the fuel meat decreases the pitch, although the channel thickness remains constant. The detailed model description of the parametric cases is summarized in Table 6.4-3.

The results of the parametric analysis are summarized in Table 6.4-4. Because the uncertainty in the calculation is ~0.001, a difference of at least 0.002 (2 milli-k, abbreviated mk) between the various cases is required in order to distinguish a real effect from statistical fluctuation. The results indicate a reactivity increase of 4.3 mk for Case B2, when the width of the fuel meat is increased, and a decrease of 5.4 mk for Case B3, when the width of the fuel meat is decreased. Therefore, reactivity increases when the width of the fuel meat is maximized.

The nominal thickness of the fuel meat is 0.02-in. No tolerance on the fuel meat is defined because the fuel plates are fabricated using a rolling process. A thickness tolerance of 0.002-in (±10%) is assumed for computational purposes. In Cases B4 and B5, the fuel meat thickness is adjusted for constant channel thickness and variable pitch, while for Cases B6 and B7 the fuel meat thickness is adjusted for constant plate thickness and nominal pitch. The reactivity fluctuations are within 2 mk in all four cases, and it is concluded that a nominal fuel meat thickness of 0.02-in is acceptable for modeling purposes.

In Case B8, the water channel thickness is increased to 0.085-in (increase in pitch), while in Case B9 the water channel thickness is increased to the maximum by artificially reducing the cladding thickness (nominal pitch). Both cases B8 and B9 show large reactivity gains of 9.6 and 12.9 mk, respectively, indicating that reactivity increases when the water channel thickness increases.

In Case B10, the active fuel length is reduced to a lower bound value of 47.0-in. The reactivity increase is within statistical fluctuation. It may be inferred that increasing the active fuel length would also result in a reactivity effect within statistical fluctuation.

In Case B11, the cladding is reduced to the minimum value of 0.008-in, and the reactivity increases by 5.5 mk. This reactivity gain is likely due to the more compact geometry, as the pitch reduces considerably. This scenario is not directly applicable to an ATR fuel element because the pitch is fixed by the side plates and such a minimum pitch is not possible.

The only cases that show a statistically significant increase are B2, B8, B9, and B11. In Case B12, the increased fuel meat width of Case B2 and increased channel width of Case B9 are combined. This model geometry bounds Case B8, and Case B11 is incorporated in an approximate manner because the cladding thickness has been reduced to accommodate the larger channel. The reactivity of Case B12 represents an increase of 19.5 mk over base Case B1.

6.4.1.2.2 Fuel Element Payload

The geometry of the HAC single package configuration is discussed in Section 6.3.1, *Model Configuration*. Based on the parametric evaluation, three HAC single package ATR fuel element models are developed in order to verify the trends indicated in the parametric analysis: (1) Case C1, a nominal (base) model, (2) Case C2, a conservative model with the increased channel width consistent with Case B9, and (3) Case C3, an optimized model with both increased channel width and increased meat arc length. In all three models, the FHE neoprene is ignored and a nominal pitch is utilized (i.e., the centerline radial locations of the 19 plates are the same in each model). Note that in Cases C1 and C2, the fuel number densities are computed using nominal fuel meat arc lengths and thus do not correspond to the values in Table 6.2-3. In

the increased channel width models, the channel width is increased by removing cladding. This approach is highly conservative, because it is unlikely (if not impossible) to maximize the channel width between each plate. In an actual fuel element, maximizing the channel width between two plates would likely minimize the channel width between the next two plates, as the overall plate thickness is held to a rather tight tolerance.

The HAC single package results are provided in Table 6.4-5. As expected from the parametric analysis, Case C2 is more reactive than Case C1 (by 13.7 mk), and Case C3 is more reactive than Case C1 (by 17.2 mk). Therefore, it may be concluded that reactivity is maximized in the ATR fuel element by maximizing the fuel meat arc length and maximizing the channel width between the fuel plates. This optimized fuel element is used in all models using the fuel element payload (including NCT single package, NCT array, and HAC array models).

In Cases C1, C2, and C3, the neoprene of the FHE is ignored and treated as full-density water. In Cases C4 and C5, the effect of neoprene is evaluated. Neoprene is a hydrocarbon with the chemical formula C_4H_5Cl. Neoprene is present on the FHE and is used to cushion the fuel element. In Case C4, 1/8-in of neoprene is modeled along the sides of the fuel element (see Figure 6.3-3). The small strips of neoprene above and below the fuel element are neglected because these strips are of insufficient mass to affect the reactivity in any appreciable manner. Inclusion of the neoprene has a pronounced negative effect on the reactivity, presumably due to absorption in the chlorine. In Case C5, the chlorine is deleted from the neoprene, and the density is reduced accordingly. Eliminating the chlorine from the neoprene may be postulated to be a result of decomposition during a fire, although such a scenario is not credible. Case C5 is slightly more reactive than Case C3, although the effect may simply be statistical fluctuation. It may be concluded that chlorine-free neoprene has a negligible effect on the reactivity.

Because the fuel may be transported inside of a plastic bag, it is conservatively assumed that the water density inside of the inner tube can vary independently of the water density inside of the fuel element. To maximize neutron reflection, full-density water is always modeled inside of the tube external to the fuel element, and the fuel element is centered laterally within the tube. In Cases C6 through C10, Case C5 is run with a range of water densities between the fuel plates, and maximum water density in all other regions of the model. Reactivity drops as the water density is reduced between the fuel plates, indicating that the system is under moderated.

Case C5 is the most reactive case when comparing Cases C1 through C10. In Case C11, Case C5 is rerun with the channel width increased from 0.085-in to 0.089-in. A channel width of 0.089-in is the maximum local channel width (0.087-in) with an additional margin of 0.002-in. The larger channel width is achieved by reducing the cladding thickness. Case C11 is the most reactive, with k_s = 0.45237. This result is below the USL of 0.9209.

6.4.1.2.3 Loose Plate Basket Payload

The selection of the bounding fuel plate and development of the various plate arrangements are presented in conjunction with the NCT array analysis in Section 6.5.1.2, *Loose Plate Basket Payload*. The most reactive fuel plate arrangements determined in the NCT array analysis are used in the HAC single package analysis. This arrangement will also be the most reactive in the HAC single package models because both the NCT and HAC models are flooded and behave in a similar manner.

A figure showing the general HAC model geometry is provided in Figure 6.3-5. Results are provided in Table 6.4-6. Six cases are run, with small variations in the plate arrangement. The maximum reactivity occurs for Case LB3, with k_s = 0.43629. This result is below the USL of 0.9209. The pitch of this case is non-regular. The top, center, and bottom plates are centered in the lattice locations with a base pitch of 1.036-cm, while the off-center plates are shifted 0.2-cm from the center plate.

6.4.2 Single Package Results

Following are the tabulated results for the single package cases. The most reactive configurations are listed in boldface.

Table 6.4-1 – NCT Single Package Results, Fuel Element

NCT Case					
Case ID	**Filename**	**Moderator Density (g/cm^3)**	**k_{eff}**	**σ**	**k_s ($k+2\sigma$)**
A1	NS_M100	1.0	0.41068	0.00097	0.41262
A2	**NS_M100_C89**	**1.0**	**0.42021**	**0.00109**	**0.42239**

Table 6.4-2 – NCT Single Package Results, Loose Plate Basket

Case ID	**Filename**	**Pitch (cm)**	**k_{eff}**	**σ**	**k_s ($k+2\sigma$)**
LA1	NS_N5P52	1.036	0.39898	0.00091	0.40080
LA2	NS_N5P52A	1.136 (max)	0.39847	0.00096	0.40039
LA3	NS_N5P52B	1.236 (max)	0.39856	0.00097	0.40050
LA4	**NS_N5P52C**	**1.336 (max)**	**0.40007**	**0.00096**	**0.40199**
LA5	NS_N5P52D	1.436 (max)	0.39881	0.00095	0.40071
LA6	NS_N5P52E	1.491 (max)	0.39751	0.00095	0.39941

Table 6.4-3 – Parametric Analysis Input Data, Fuel Element

Parameter	B1	B2	B3	B4	B5	B6
Fuel Arc (cm)	6.7355	6.9895	6.4815	6.7355	6.7355	6.7355
Meat thickness (in)	0.02	0.02	0.02	0.022	0.018	0.022
Active fuel height (in)	48	48	48	48	48	48
Channel (in)	0.078	0.078	0.078	0.078	0.078	0.078
Cladding (in)	0.015	0.015	0.015	0.015	0.015	0.014
Total plate (in)	0.050	0.050	0.050	0.052	0.048	0.050
Pitch (in)	0.128	0.128	0.128	0.130	0.126	0.128
Volume (cm^3)	41.7164	43.2895	40.1432	45.8880	37.5447	45.8880
U-235 (g)	63.2	63.2	63.2	63.2	63.2	63.2
U-235 density (g/cm^3)	1.51	1.46	1.57	1.38	1.68	1.38
UAlx+Al density (g/cm^3)	3.86	3.81	3.91	3.74	4.00	3.74
N U-234	2.4865E-05	2.3962E-05	2.5840E-05	2.2605E-05	2.7628E-05	2.2605E-05
N U-235	3.8789E-03	3.7380E-03	4.0309E-03	3.5263E-03	4.3099E-03	3.5263E-03
N U-236	1.4382E-05	1.3859E-05	1.4945E-05	1.3074E-05	1.5980E-05	1.3074E-05
N U-238	2.0576E-04	1.9828E-04	2.1382E-04	1.8705E-04	2.2862E-04	1.8705E-04
N U-Al	5.0157E-02	5.0391E-02	4.9905E-02	5.0742E-02	4.9442E-02	5.0742E-02
Total	5.4281E-02	5.4365E-02	5.4190E-02	5.4491E-02	5.4024E-02	5.4491E-02

Parameter	B7	B8	B9	B10	B11	B12
Fuel Arc (cm)	6.7355	6.7355	6.7355	6.7355	6.7355	6.9895
Meat thickness (in)	0.018	0.02	0.02	0.02	0.02	0.02
Active fuel height (in)	48	48	48	47	48	48
Channel (in)	0.078	0.085	0.085	0.078	0.078	0.085
Cladding (in)	0.016	0.015	0.0115	0.015	0.008	0.0115
Total plate (in)	0.050	0.050	0.0430	0.050	0.036	0.0430
Pitch (in)	0.128	0.135	0.128	0.128	0.114	0.128
Volume (cm^3)	37.5447	41.7164	41.7164	40.8473	41.7164	43.2895
U-235 (g)	63.2	63.2	63.2	63.2	63.2	63.2
U-235 density (g/cm^3)	1.68	1.51	1.51	1.55	1.51	1.46
UAlx+Al density (g/cm^3)	4.00	3.86	3.86	3.89	3.86	3.81
N U-234	2.7628E-05	2.4865E-05	2.4865E-05	2.5394E-05	2.4865E-05	2.3962E-05
N U-235	4.3099E-03	3.8789E-03	3.8789E-03	3.9615E-03	3.8789E-03	3.7380E-03
N U-236	1.5980E-05	1.4382E-05	1.4382E-05	1.4688E-05	1.4382E-05	1.3859E-05
N U-238	2.2862E-04	2.0576E-04	2.0576E-04	2.1014E-04	2.0576E-04	1.9828E-04
N U-Al	4.9442E-02	5.0157E-02	5.0157E-02	5.0020E-02	5.0157E-02	5.0391E-02
Total	5.4024E-02	5.4281E-02	5.4281E-02	5.4232E-02	5.4281E-02	5.4365E-02

Table 6.4-4 – Parametric Analysis Results, Fuel Element

Case ID	Filename	k_{eff}	σ	k_s (k+2σ)	Δ from B1 (mk)
B1	P1	0.46601	0.00096	0.46793	--
B2	P2	0.47015	0.00102	0.47219	4.3
B3	P3	0.46045	0.00102	0.46249	-5.4
B4	P5	0.46403	0.00101	0.46605	-1.9
B5	P4	0.46442	0.00111	0.46664	-1.3
B6	P10	0.46753	0.00105	0.46963	1.7
B7	P9	0.46683	0.00101	0.46885	0.9
B8	P6	0.47528	0.00112	0.47752	9.6
B9	P7	0.47879	0.00100	0.48079	12.9
B10	P8	0.46704	0.00106	0.46916	1.2
B11	P11	0.47123	0.00108	0.47339	5.5
B12	P12	0.48534	0.00104	0.48742	19.5

Table 6.4-5 – HAC Single Package Results, Fuel Element

Case ID	Filename	Water Density Between Plates (g/cm^3)	k_{eff}	σ	k_s (k+2σ)
C1	HS_M100_NOM	1.0	0.42274	0.00095	0.42464
C2	HS_M100_TOL	1.0	0.43639	0.00099	0.43837
C3	HS_M100_TOLW	1.0	0.43991	0.00097	0.44185
C4	HS_M100_TOLW_N1	1.0	0.41002	0.00102	0.41206
C5	HS_M100_TOLW_N2	1.0	0.44040	0.00104	0.44248
C6	HS_M050	0.5	0.35396	0.00088	0.35572
C7	HS_M060	0.6	0.36994	0.00095	0.37184
C8	HS_M070	0.7	0.38607	0.00099	0.38805
C9	HS_M080	0.8	0.40411	0.00102	0.40615
C10	HS_M090	0.9	0.42092	0.00096	0.42284
C11	**HS_M100_TOLW_N2_C89**	**1.0**	**0.45029**	**0.00104**	**0.45237**

Table 6.4-6 – HAC Single Package Results, Loose Plate Basket

Case ID	Filename	Pitch (cm)	k_{eff}	σ	k_s (k+2σ)
LB1	HS_N5P52	1.036	0.43263	0.00097	0.43457
LB2	HS_N5P52A	1.136 (max)	0.43350	0.00092	0.43534
LB3	**HS_N5P52B**	**1.236 (max)**	**0.43443**	**0.00093**	**0.43629**
LB4	HS_N5P52C	1.336 (max)	0.43388	0.00096	0.43580
LB5	HS_N5P52D	1.436 (max)	0.43328	0.00091	0.43510
LB6	HS_N5P52E	1.491 (max)	0.43169	0.00089	0.43347

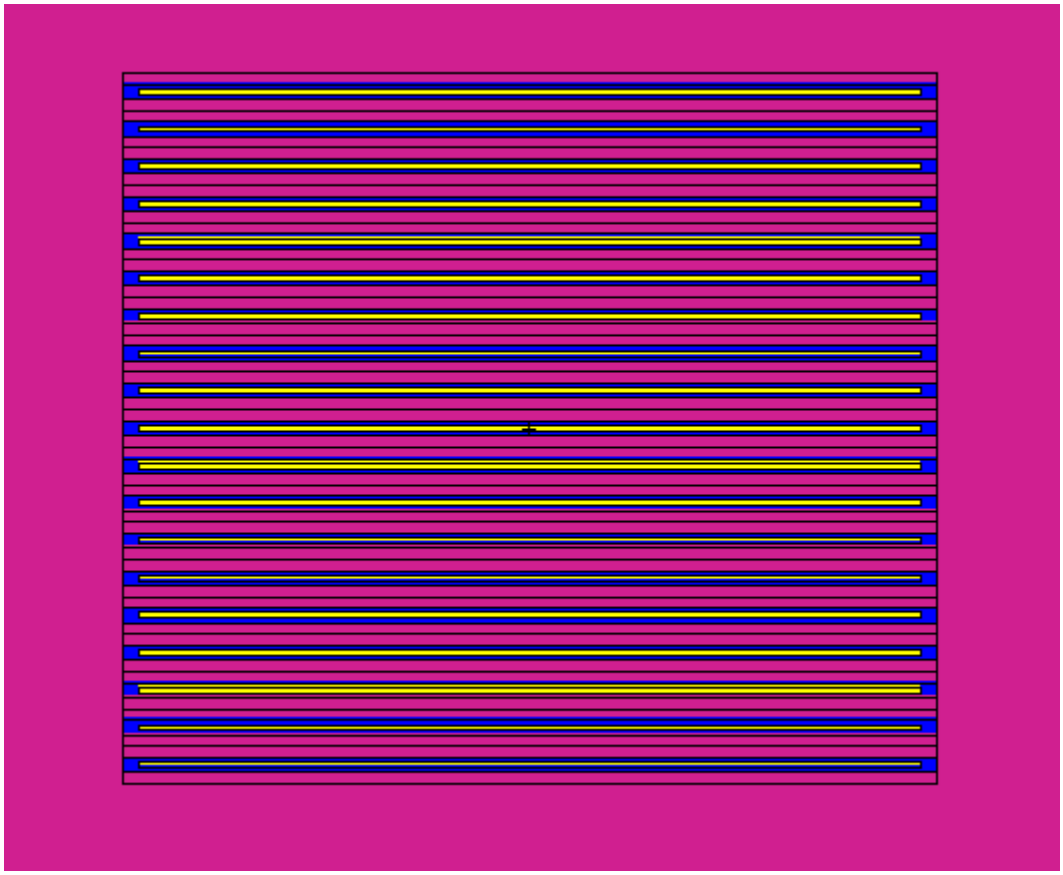

Figure 6.4-1 – Base Parametric Model (Case B1)

6.5 Evaluation of Package Arrays under Normal Conditions of Transport

6.5.1 NCT Array Configuration

6.5.1.1 Fuel Element Payload

The NCT array model is a 9x9x1 array of the NCT single package model, see Figure 6.5-1. Although an 8x8x1 array is of sufficient size to justify a CSI = 4.0, the larger 9x9x1 array is utilized simply for modeling convenience. Neoprene is modeled without chlorine in all models. It is demonstrated in Section 6.6.1.1, *Fuel Element Payload*, that chlorine-free neoprene may have a slight positive effect on the reactivity, although the effect is small. The entire array is reflected with 12-in of full-density water.

The fuel elements are pushed to the center of the array and rotated to minimize the distance between the fuel elements. This geometry is not feasible for NCT, because the FHE would force the fuel elements to remain in the center of the package, although the FHE does allow rotation. Therefore, it is conservative to ignore the FHE to minimize the separation distance. In addition, a small notch is added to the neoprene so that the fuel element may be translated to the maximum extent without interfering with the inner tube geometry. This notch is not present in the single package models.

Three calculational series are developed. In Series 1, the water density is fixed at 1.0 g/cm^3 between the fuel plates and the water density is allowed to vary inside the inner tube. The channel width is modeled at 0.085-in. Series 2 is the same as Series 1, although the density within the fuel plates is at a reduced density of 0.9 g/cm^3. Void is always present between the insulation and the outer tube, as this region is water-tight. Series 3 is a repeat of Series 1, although with the channel width increased to 0.089-in. A channel width of 0.089-in is the maximum local channel width (0.087-in) with an additional margin of 0.002-in. The larger channel width is achieved by reducing the cladding thickness. The results are provided in Table 6.5-1.

Reactivity is at a maximum for Case E23, which has full-density water between the fuel plates, and 0.3 g/cm^3 water inside the inner tube, and a channel width of 0.089-in, with k_s = 0.83616. As expected, the reactivity drops when the water density between the fuel plates is reduced, as the system is under moderated. The maximum result is far below the USL of 0.9209.

As a point of interest, an additional case (Case D12) is developed in which the fuel elements are centered in the cavity and not rotated, using the moderation and channel width assumptions of Case D4 (see the lower figure of Figure 6.5-1). The reactivity drops by 18.5 mk, which essentially represents the additional conservatism of pushing the fuel elements to the center of the array.

6.5.1.2 Loose Plate Basket Payload

The NCT array model is a 9x9x1 array of the NCT single package model. For the NCT single package cases, it was sufficient to laterally center the fuel basket within the inner tube to maximize reflection by the water in the tube. However, in the NCT array configuration, it is expected that reactivity would be maximized by pushing the fuel baskets to the center of the

array, as shown in the top sketch of Figure 6.5-2. The fuel elements may be packed closer by rotating them as shown in the figure. Therefore, unless otherwise noted, all NCT array models have the baskets pushed toward the center of the array. Although this assumption bounds any anticipated basket damage, this arrangement is not credible, because the structural ribs that center the baskets within the inner tube will not deform in this manner.

The loose plate payload consists of 19 different plate types. Each plate type has a different width and uranium mass, although the lengths are the same. Each plate may be either flat or curved, for a total of 19*2 = 38 different variations. However, flat and curved plates will not be mixed in the same basket (to facilitate packaging). Within each loose plate basket, any combination of plate types may be present, with the only limitation that the total U-235 mass present in the basket must not exceed 600 g.

Clearly, there are a large number of possible combinations of plates that may be present within the basket. The objective is to determine a simplified configuration that bounds any random collection of plates. Fortunately, calculations may be performed using only flat plates, because the neutronic behavior of flat and curved plates is demonstrated to be nearly identical. Therefore, the flat plate results also apply to the curved plates. Flat plates allow easy geometry setup using MCNP repeated structures, while curved plates generally cannot be modeled using repeated structures unless the plate pitch is rather large.

Basic data for the 19 plate types are provided in Table 6.2-1. It is not necessary to model each of the 19 different plate types. Rather, from examination of these data, a subset of plates is selected for further analysis. Plates 5 through 15 have a U-235 density of approximately 1.64 g/cm^3, while the remaining plates have a significantly lower U-235 density. Plate 5 is the smallest plate in this range, and Plate 15 is the largest plate in this range; both are selected for further evaluation. Plate 8 is also selected as a representative plate between these two extremes, and should result in reactivity values between Plate 5 and 15. It is demonstrated that the smaller plate configuration (Plate 5) is more reactive than the larger plate configurations (Plates 8 and 15). Plate 3 is also selected for further evaluation because it is smaller than Plate 5, although the reduced U-235 density will result in a larger number of plates.

For simplicity, only one plate type is modeled within each basket. Randomly mixing different plate types would result in a less reactive condition that the most reactive single plate configuration. Also, number densities of the selected plates have been slightly adjusted so that the total mass of U-235 is always 600 g. For plates 5, 8, and 15, the number densities are increased, while for plate 3 the number densities are decreased.

Four initial series of calculations are performed, one series for each of the four plate types under consideration. The goal of these initial calculations is to simply determine the bounding plate type. Once the bounding plate type has been determined, additional series of calculations are performed on the bounding plate type. For all of the initial models, full-density water is modeled between the plates, 0.3 g/cm^3 water is modeled between the plate array and basket (this region is not present once the plate array fills the entire basket area), 0.3 g/cm^3 water is modeled between the basket and inner tube, and insulation/void is modeled between the inner and outer tubes. The water density of 0.3 g/cm^3 is selected based upon the most reactive moderation condition of the ATR fuel element analysis, and will be optimized once the bounding plate is selected.

Fuel Plate 5 Series: Fuel plate 5 is the first plate type examined. Ten plates are required to achieve a mass of 600 g U-235. The plate arrangements for a number of the configurations are

shown in Figure 6.5-3 through Figure 6.5-5. Results are provided in Table 6.5-2. In cases LC1 through LC9, the plates are arranged in a 1x10 array at the center of the basket. Reactivity is low when the pitch is small, and reactivity increases as the pitch increases. In cases LC10 and LC11, the reactivity increases as the plates are alternately shifted to the right and left because moderation increases. In case LC12, plates are alternately shifted up and down until they contact each other.

Because fuel plate 5 is rather narrow, it is possible to further increase the moderation by modeling the plates in a 2x5 array in cases LC13 through LC29. Because the plate is slightly too wide to fit two side-by-side, the two side-by-side plates are modeled as a single plate by doubling the fuel meat width. The reactivity continues to increase with increasing pitch. Case LC19 has the largest reactivity obtained with a constant pitch.

However, moderation can be further increased if a non-regular pitch is utilized. In cases LC20 through LC29, non-regular pitches are examined. In these cases, the plates at the top, center, and bottom of the basket remain fixed, while the two off-center plates are shifted away from the center plate in 0.1-cm increments. Because the pitches in these cases are non-regular, the pitches provided in the results table are noted as "max" values. Case LC21 is the most reactive, with k_s=0.76806, although the reactivity gain resulting from a non-regular pitch is relatively small and within statistical fluctuation. For case LC21, the top, center, and bottom plates are centered in the lattice locations with a base pitch of 1.036 cm, while the off-center plates are shifted 0.2-cm from the center plate (maximum pitch of 1.236 cm).

Fuel Plate 8 Series: Nine plates are required to achieve a mass of 600 g U-235. The plate arrangements for a number of configurations are shown in Figure 6.5-6 and Figure 6.5-7. Results are provided in Table 6.5-3. Considerably fewer cases are generated compared to fuel plate 5 because it has been established that the plates are highly under moderated when packed tightly.

In cases LD1 through LD3, the plates are modeled in a simple 1x9 array. In cases LD4 though LD11, the plates are alternately shifted left and right to increase moderation. In cases LD6 through LD11, the top, bottom, and center plates remain fixed, while the remaining plates are progressively shifted up or down in 0.1-cm increments. Case LD7 is the most reactive, with k_s=0.75241, although the reactivity is less than the most reactive plate 5 case. For case LC7, the base lattice pitch is 0.574-cm, and the off-center plates are shifted 0.2-cm from the center plate.

Fuel Plate 15 Series: Seven plates are required to achieve a mass of 600 g U-235. The plate arrangements for a number of the configurations are shown in Figure 6.5-8. Results are provided in Table 6.5-3. Using the same methodology as plates 5 and 8, case LE8 is the most reactive, with k_s=0.74548. This case also features a non-regular pitch. For case LE8, the base lattice pitch is 0.804 cm, and the off-center plates are shifted 0.1 cm from the center plate.

Comparing the maximum k_s values for plates 5, 8, and 15, plate 5 is the most reactive (k_s=0.76806), plate 15 is the least reactive (k_s=0.74548), and plate 8 falls between the two (k_s=0.75241). In fact, the reactivities of plates 8 and 15 are fairly close, despite the difference in the width and number of plates. Plate 5 is somewhat more reactive than either plate 8 or 15, most likely because its narrow width allows "double stacking" of this plate along the width of the basket, which results in a more advantageous moderation and geometry conditions. Therefore, the trend is that for a fixed U-235 mass per basket, the smaller plates are more reactive than the larger plates.

Of course, plates 1 through 4 are smaller than plate 5. However, these plates have a lower U-235 density so that more plates are required to achieve 600 g U-235. More plates would provide less volume for moderation, so it is expected that plate 5 would bound plates 1 through 4. This is confirmed by running several cases for plate 3.

Fuel Plate 3 Series: Fourteen plates are required to achieve a mass of 600 g U-235. The plate arrangements for the configurations are shown in Figure 6.5-9. Results are provided in Table 6.5-3. All cases are for a 2x7 arrangement and non-regular pitches, as similar arrangements have been shown to be the most reactive for the other plates. Two side-by-side plates are modeled as a single plate with double fuel meat width, consistent with the treatment of the Type 5 plate. Case LF2 is the most reactive, with k_s=0.75904, although this case is less reactive than the Type 5 plate. For case LF2, the pitch is 0.796 cm.

Criticality Analysis Using Plate 5: From the analysis of plate types 3, 5, 8, and 15, Type 5 is shown to be the most reactive. Therefore, the remaining analysis uses only this plate type. An additional two series of cases are performed using fuel plate 5 in which the water densities in the various model regions are allowed to vary. The primary regions of interest are within the basket and between the basket and the inner tube.

In Series 1, full-density water is modeled within the basket, while the water density between the basket and the inner tube is varied from 0 to 1.0 g/cm^3. The results are provided in Table 6.5-4. The maximum reactivity occurs for Case LG5, with k_s = 0.77469. A water density of 0.5 g/cm^3 within the inner tube is utilized in the most reactive case.

In Series 2, the water density inside the basket is reduced to 0.9 g/cm^3, while the water density between the basket and the inner tube is varied from 0 to 1.0 g/cm^3. The reactivity clearly drops when reduced density water is modeled inside the basket.

Several miscellaneous cases are run to validate the assumptions noted above. In Case LJ1, the most reactive case (Case LG5) is run with the fuel baskets centered inside of the tubes (see the lower sketch of Figure 6.5-2). The reactivity drops as the fuel elements are pushed apart, k_s = 0.76237 for Case LJ1, compared to k_s = 0.77469 for Case LG5.

It has been implicitly assumed the maximum reactivity is obtained for the maximum fissile mass of 600 g U-235. In general, the maximum allowable fissile loading is not necessarily the most reactive condition if the volume of fissile material is so large that little volume is available for moderating material. That is not the case for the loose plate analysis, as the fuel plates are thin and only a small number of plates are required to achieve a mass of 600 g U-235. Removing plates might increase moderation slightly as water is added to the system, although reducing the fissile mass more than compensates for the additional moderation and lowers the reactivity. To demonstrate this effect, the arrangement of Case LC9, which has ten type 5 plates in a 1x10 evenly spaced array (see Figure 6.5-3), is repeated with ten, nine, eight, and seven evenly spaced plates (Cases LJ2, LJ3, LJ4, and LJ5, see Figure 6.5-10) with an inner tube water density of 0.5 g/cm^3. The reactivity drops as each successive plate is removed (0.62333 for Case LJ2 to 0.57579 for Case LJ5), despite the fact that the plates are spaced farther and farther apart and moderation is improved. If plates are removed from the most reactive models, for which the pitch is already non-regular to maximize reactivity, the reactivity drop resulting from removing plates would be more pronounced.

It is stated that modeling the plates as flat is neutronically equivalent to modeling the plates as curved. This modeling assumption is verified by modeling both flat and curved plates with a constant pitch of 0.80 cm. This pitch is selected because it is large and constant and the curved plates may be modeled with repeated structures. Case LJ6 is the flat plate model, and Case LJ7 is the curved plate model. Case LJ6 is geometrically identical to case LC13 (see Figure 6.5-4) except the water density inside the basket is 1.0 g/cm^3 between the plate array and the basket. Case LJ7 is shown in Figure 6.5-10. Flat plate Case LJ6 has k_s=0.73021, while curved plate Case LJ7 has k_s=0.73022. The difference between these cases is negligible, and the statement that flat plates are neutronically equivalent to curved plates is verified.

In conclusion, Case LG5 is the most reactive loose plate basket model, with k_s = 0.77469. This result is below the USL of 0.9209. Case LG5 has fully moderated fuel plates, 0.5 g/cm^3 water inside the inner tube, and fuel plate baskets that have been rotated and moved to the center of the array.

6.5.2 NCT Array Results

The results for the NCT array cases are provided in the following table. The most reactive configuration is listed in boldface.

Table 6.5-1 – NCT Array Results, Fuel Element Payload

Case ID	Filename	Water Density Between Tubes (g/cm^3)	Water Density Inside Inner Tube (g/cm^3)	Water Density Between Plates (g/cm^3)	k_{eff}	σ	k_s ($k+2\sigma$)
Series 1: Variable water density inside inner tube, full density water between plates.							
D1	NA_P000	0	0	1.0	0.76716	0.00120	0.76956
D2	NA_P010	0	0.1	1.0	0.80349	0.00123	0.80595
D3	NA_P020	0	0.2	1.0	0.81928	0.00112	0.82152
D4	**NA_P030**	**0**	**0.3**	**1.0**	**0.82605**	**0.00117**	**0.82839**
D5	NA_P040	0	0.4	1.0	0.82149	0.00119	0.82387
D6	NA_P050	0	0.5	1.0	0.81420	0.00118	0.81656
D7	NA_P060	0	0.6	1.0	0.80521	0.00108	0.80737
D8	NA_P070	0	0.7	1.0	0.79216	0.00121	0.79458
D9	NA_P080	0	0.8	1.0	0.78130	0.00132	0.78394
D10	NA_P090	0	0.9	1.0	0.76905	0.00120	0.77145
D11	NA_P100	0	1.0	1.0	0.75603	0.00124	0.75851
D12	NA_P030C	0	0.3	1.0	0.80743	0.00122	0.80987
Series 2: Variable water density inside inner tube, 0.9 g/cm^3 density water between plates.							
E1	NA_M90P000	0	0	0.9	0.72938	0.00111	0.73160
E2	NA_M90P010	0	0.1	0.9	0.77108	0.00120	0.77348
E3	NA_M90P020	0	0.2	0.9	0.79299	0.00116	0.79531
E4	NA_M90P030	0	0.3	0.9	0.79943	0.00123	0.80189
E5	**NA_M90P040**	**0**	**0.4**	**0.9**	**0.80192**	**0.00108**	**0.80408**
E6	NA_M90P050	0	0.5	0.9	0.79378	0.00108	0.79594
E7	NA_M90P060	0	0.6	0.9	0.78539	0.00111	0.78761
E8	NA_M90P070	0	0.7	0.9	0.77658	0.00118	0.77894
E9	NA_M90P080	0	0.8	0.9	0.76496	0.00117	0.76730
E10	NA_M90P090	0	0.9	0.9	0.75315	0.00121	0.75557
E11	NA_M90P100	0	1.0	0.9	0.74334	0.00126	0.74586
Series 3: Variable water density inside inner tube, full density water between plates, channel width increased to 0.089-in							
E20	NA_P000_C89	0	0	1.0	0.78147	0.00115	0.78377
E21	NA_P010_C89	0	0.1	1.0	0.81601	0.00119	0.81839
E22	NA_P020_C89	0	0.2	1.0	0.83027	0.00119	0.83265
E23	**NA_P030_C89**	**0**	**0.3**	**1.0**	**0.83372**	**0.00122**	**0.83616**
E24	NA_P040_C89	0	0.4	1.0	0.82984	0.00118	0.83220
E25	NA_P050_C89	0	0.5	1.0	0.82481	0.00125	0.82731
E26	NA_P060_C89	0	0.6	1.0	0.81462	0.00119	0.81700

Table 6.5-2 – NCT Array Results, Pitch Variations, Plate 5

Case ID	Filename	Pitch (cm)	k_{eff}	σ	k_s (k+2σ)
LC1	NA_N5P08	0.160	0.41955	0.00093	0.42141
LC2	NA_N5P10	0.200	0.44783	0.00091	0.44965
LC3	NA_N5P12	0.240	0.47653	0.00104	0.47861
LC4	NA_N5P14	0.280	0.50372	0.00104	0.50580
LC5	NA_N5P16	0.320	0.53109	0.00103	0.53315
LC6	NA_N5P18	0.360	0.55470	0.00109	0.55688
LC7	NA_N5P20	0.400	0.57669	0.00104	0.57877
LC8	NA_N5P22	0.440	0.59930	0.00111	0.60152
LC9	NA_N5P23	0.460	0.61120	0.00102	0.61324
LC10	NA_N5P23A	0.460	0.69108	0.00118	0.69344
LC11	NA_N5P23B	0.460	0.74866	0.00109	0.75084
LC12	NA_N5P23C	0.460	0.74714	0.00102	0.74918
LC13	NA_N5P40	0.800	0.71462	0.00107	0.71676
LC14	NA_N5P42	0.840	0.72319	0.00108	0.72535
LC15	NA_N5P44	0.880	0.73353	0.00102	0.73557
LC16	NA_N5P46	0.920	0.74169	0.00107	0.74383
LC17	NA_N5P48	0.960	0.74962	0.00112	0.75186
LC18	NA_N5P50	1.000	0.75920	0.00109	0.76138
LC19	NA_N5P52	1.036	0.76423	0.00118	0.76659
LC20	NA_N5P52A	1.136 (max)	0.76520	0.00102	0.76724
LC21	**NA_N5P52B**	**1.236 (max)**	**0.76582**	**0.00112**	**0.76806**
LC22	NA_N5P52C	1.336 (max)	0.76393	0.00107	0.76607
LC23	NA_N5P52D	1.436 (max)	0.76254	0.00096	0.76446
LC24	NA_N5P52E	1.493 (max)	0.75949	0.00093	0.76135
LC25	NA_N5P67	1.540 (max)	0.75942	0.00101	0.76144
LC26	NA_N5P67A	1.640 (max)	0.75508	0.00105	0.75718
LC27	NA_N5P67B	1.740 (max)	0.74803	0.00106	0.75015
LC28	NA_N5P67C	1.840 (max)	0.73839	0.00107	0.74053
LC29	NA_N5P67D	1.940 (max)	0.72412	0.00105	0.72622

Table 6.5-3 – NCT Array Results, Pitch Variations, Plates 8, 15, and 3

Case ID	Filename	Pitch (cm)	k_{eff}	σ	k_s (k+2σ)
Plate 8					
LD1	NA_N8P22	0.440	0.60412	0.00106	0.60624
LD2	NA_N8P24	0.480	0.62588	0.00106	0.62800
LD3	NA_N8P26	0.518	0.64309	0.00112	0.64533
LD4	NA_N8P26A	0.518	0.74015	0.00102	0.74219
LD5	NA_N8P29	0.574	0.74719	0.00105	0.74929
LD6	NA_N8P29A	0.674 (max)	0.74875	0.00112	0.75099
LD7	**NA_N8P29B**	**0.774 (max)**	**0.75035**	**0.00103**	**0.75241**
LD8	NA_N8P29C	0.874 (max)	0.74896	0.00099	0.75094
LD9	NA_N8P29D	0.974 (max)	0.74574	0.00102	0.74778
LD10	NA_N8P29E	1.074 (max)	0.74373	0.00092	0.74557
LD11	NA_N8P29F	1.174 (max)	0.73494	0.00106	0.73706
Plate 15					
LE1	NA_N15P32	0.640	0.68653	0.00107	0.68867
LE2	NA_N15P34	0.690	0.70200	0.00113	0.70426
LE3	NA_N15P34A	0.690	0.73590	0.00114	0.73818
LE4	NA_N15P34B	0.790 (max)	0.74090	0.00110	0.74310
LE5	NA_N15P34C	0.890 (max)	0.74003	0.00111	0.74225
LE6	NA_N15P34D	0.970 (max)	0.74209	0.00108	0.74425
LE7	NA_N15P40	0.804	0.74153	0.00115	0.74383
LE8	**NA_N15P40A**	**0.904 (max)**	**0.74322**	**0.00113**	**0.74548**
LE9	NA_N15P40B	1.004 (max)	0.74089	0.00118	0.74325
LE10	NA_N15P40C	1.104 (max)	0.73801	0.00100	0.74001
Plate 3					
LF1	NA_N3P40	0.796	0.75062	0.00102	0.75266
LF2	**NA_N3P40A**	**0.796**	**0.75696**	**0.00104**	**0.75904**
LF3	NA_N3P40B	0.896 (max)	0.75655	0.00107	0.75869
LF4	NA_N3P40C	0.996 (max)	0.75365	0.00094	0.75553
LF5	NA_N3P40D	1.096 (max)	0.75155	0.00106	0.75367

Table 6.5-4 – NCT Array Results, Plate 5

Case ID	Filename	Water Density Between Tubes (g/cm^3)	Water Density Inside Inner Tube (g/cm^3)	Water Density Between Plates (g/cm^3)	k_{eff}	σ	k_s (k+2σ)
Series 1: Variable water density inside inner tube, full-density water in basket.							
LG1	NA_N5P000	0	0	1.0	0.66797	0.00097	0.66991
LG2	NA_N5P010	0	0.1	1.0	0.71859	0.00100	0.72059
LG3	NA_N5P020	0	0.2	1.0	0.74925	0.00104	0.75133
LC21	NA_N5P52B	0	0.3	1.0	0.76582	0.00112	0.76806
LG4	NA_N5P040	0	0.4	1.0	0.77225	0.00117	0.77459
LG5	**NA_N5P050**	**0**	**0.5**	**1.0**	**0.77251**	**0.00109**	**0.77469**
LG6	NA_N5P060	0	0.6	1.0	0.76738	0.00099	0.76936
LG7	NA_N5P070	0	0.7	1.0	0.75998	0.00100	0.76198
LG8	NA_N5P080	0	0.8	1.0	0.75086	0.00114	0.75314
LG9	NA_N5P090	0	0.9	1.0	0.74066	0.00111	0.74288
LG10	NA_N5P100	0	1.0	1.0	0.72764	0.00111	0.72986
Series 2: Variable water density inside inner tube, reduced density water in basket.							
LH1	NA_N5M090P000	0	0	0.9	0.63496	0.00098	0.63692
LH2	NA_N5M090P010	0	0.1	0.9	0.69390	0.00093	0.69576
LH3	NA_N5M090P020	0	0.2	0.9	0.72793	0.00095	0.72983
LH4	NA_N5M090P030	0	0.3	0.9	0.74560	0.00108	0.74776
LH5	NA_N5M090P040	0	0.4	0.9	0.75402	0.00108	0.75618
LH6	**NA_N5M090P050**	**0**	**0.5**	**0.9**	**0.75480**	**0.00109**	**0.75698**
LH7	NA_N5M090P060	0	0.6	0.9	0.75429	0.00110	0.75649
LH8	NA_N5M090P070	0	0.7	0.9	0.74414	0.00100	0.74614
LH9	NA_N5M090P080	0	0.8	0.9	0.73639	0.00104	0.73847
LH10	NA_N5M090P090	0	0.9	0.9	0.72573	0.00095	0.72763
LH11	NA_N5M090P100	0	1.0	0.9	0.71549	0.00107	0.71763
Miscellaneous Cases							
LJ1	NA_N5P050C	0	0.5	1.0	0.76003	0.00117	0.76237
LJ2	NA_N5P23_10	0	0.5	1.0	0.62119	0.00107	0.62333
LJ3	NA_N5P23_9	0	0.5	1.0	0.60657	0.00106	0.60869
LJ4	NA_N5P23_8	0	0.5	1.0	0.59251	0.00114	0.59479
LJ5	NA_N5P23_7	0	0.5	1.0	0.57369	0.00105	0.57579
LJ6	NA_N5P40_F	0	0.5	1.0	0.72815	0.00103	0.73021
LJ7	NA_N5P40_C	0	0.5	1.0	0.72810	0.00106	0.73022

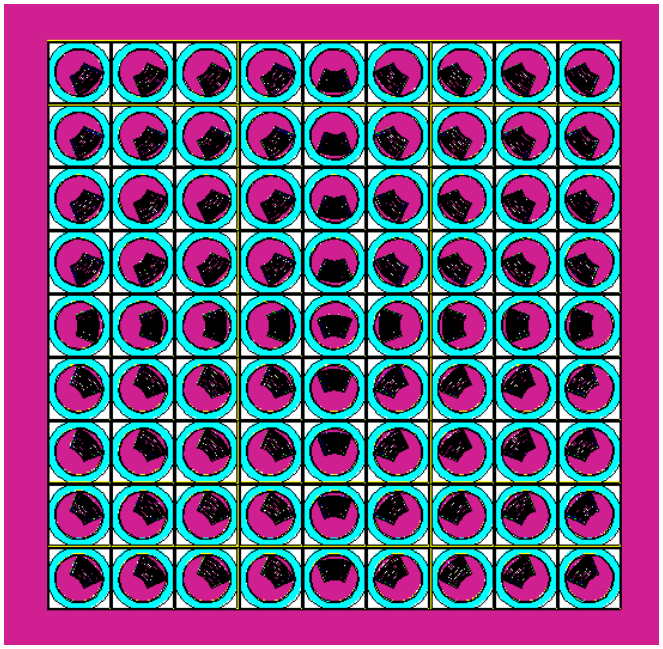

Pushed to center of array

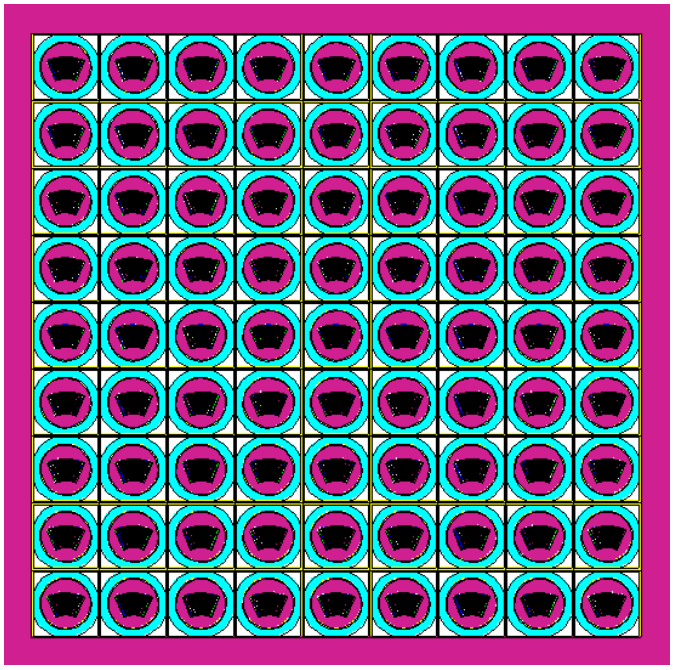

Centered in each tube (D12)

Figure 6.5-1 – NCT Array Geometry, Fuel Element Payload

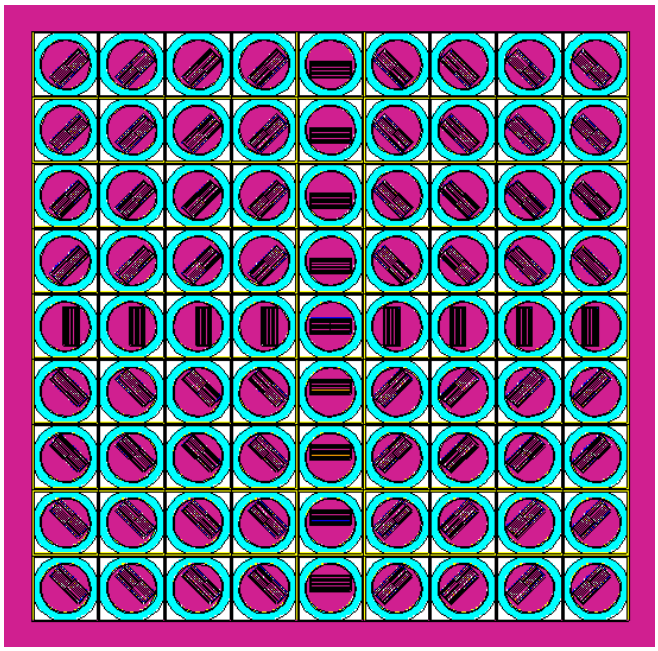

Pushed to center of array

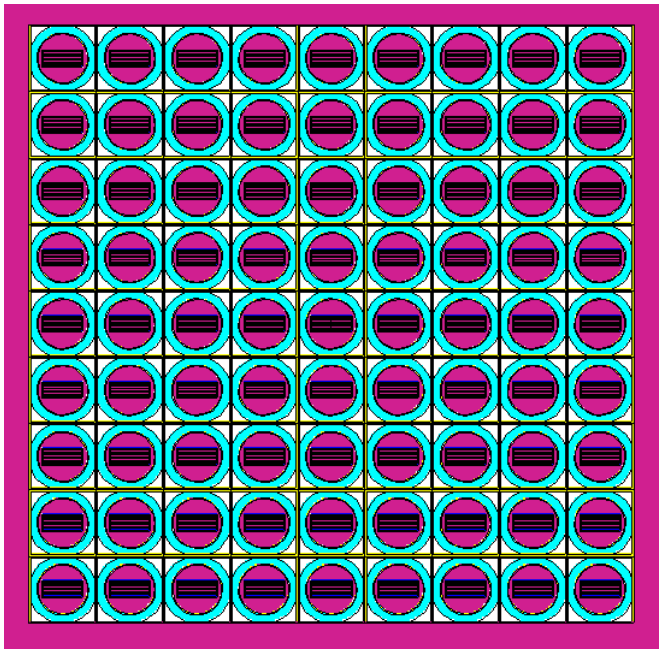

Centered in each tube (LJ1)

Figure 6.5-2 – NCT Array Geometry, Loose Plate Basket Payload

LC1

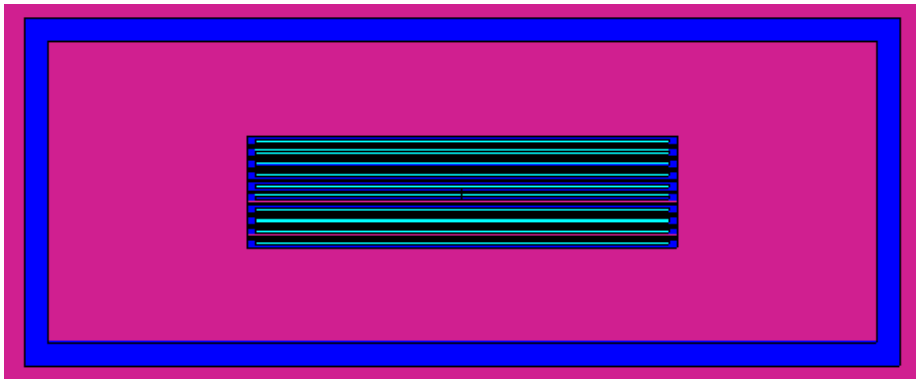

LC9

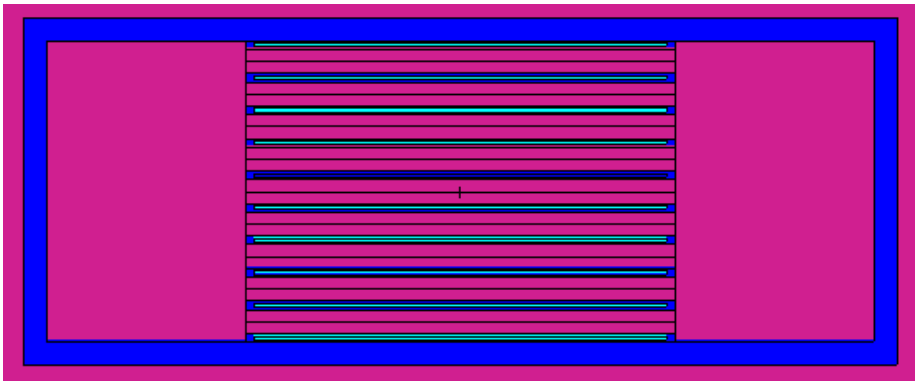

LC10

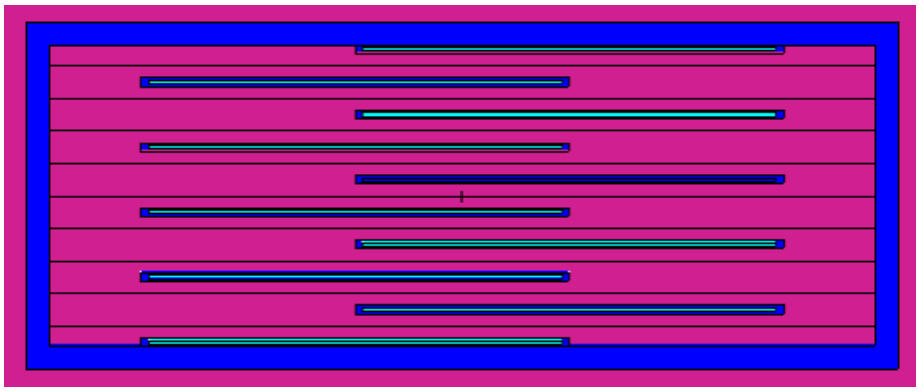

LC11

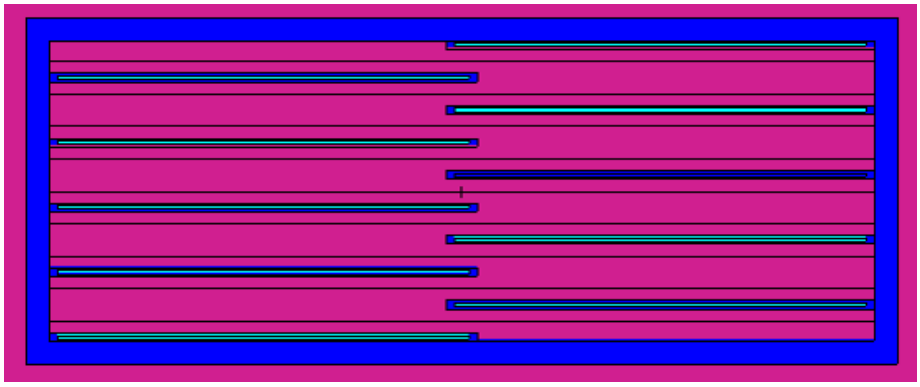

Figure 6.5-3 – NCT Array Geometry, Plate 5 (LC1, LC9, LC10, LC11)

LC12

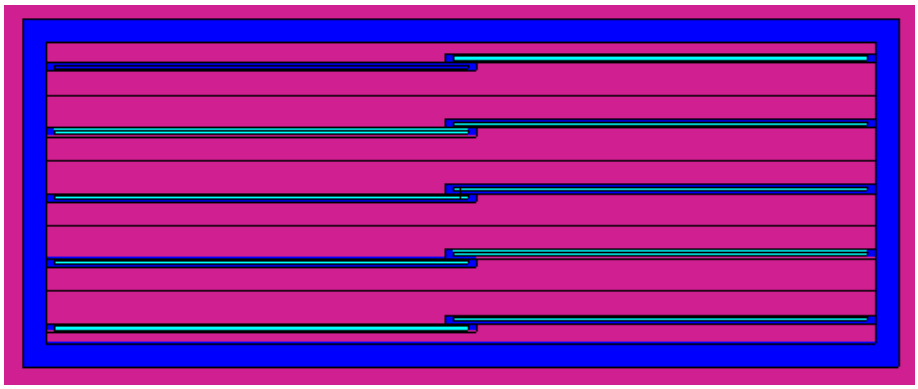

LC13

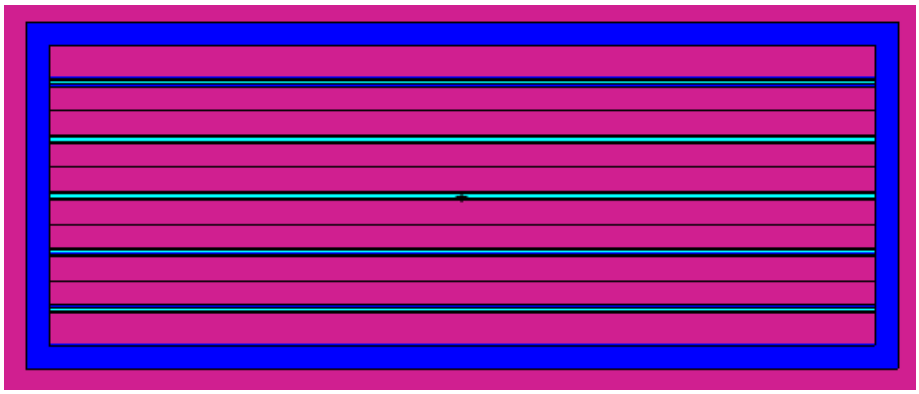

LC19

LC21

Figure 6.5-4 – NCT Array Geometry, Plate 5 (LC12, LC13, LC19, LC21)

LC22

LC24

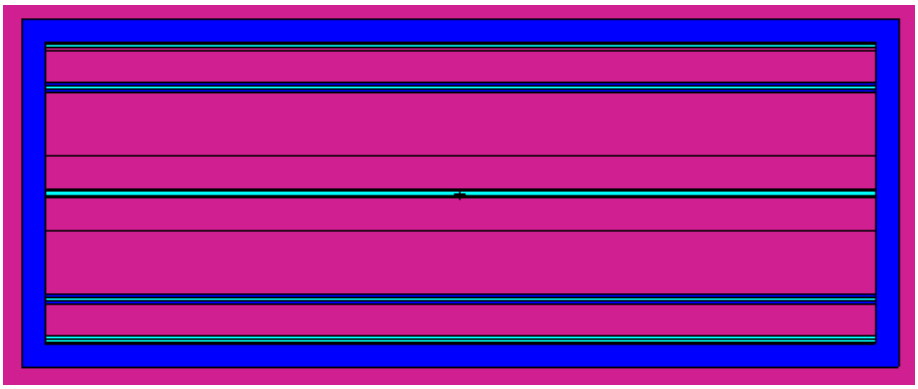

LC26

LC29

Figure 6.5-5 – NCT Array Geometry, Plate 5 (LC22, LC24, LC26, LC29)

LD3

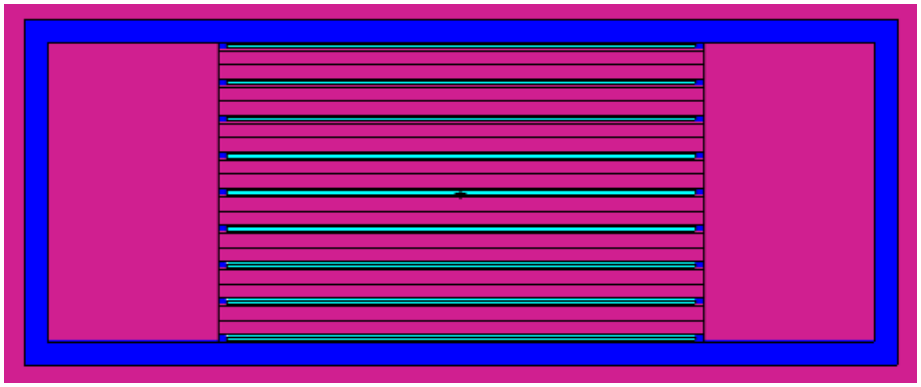

LD4

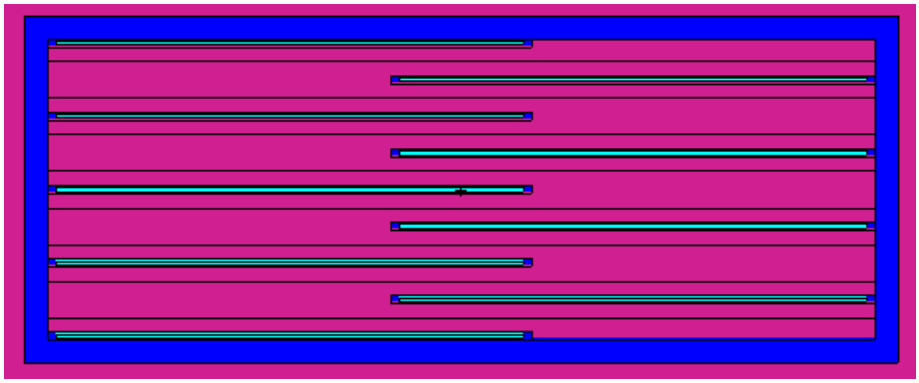

LD5

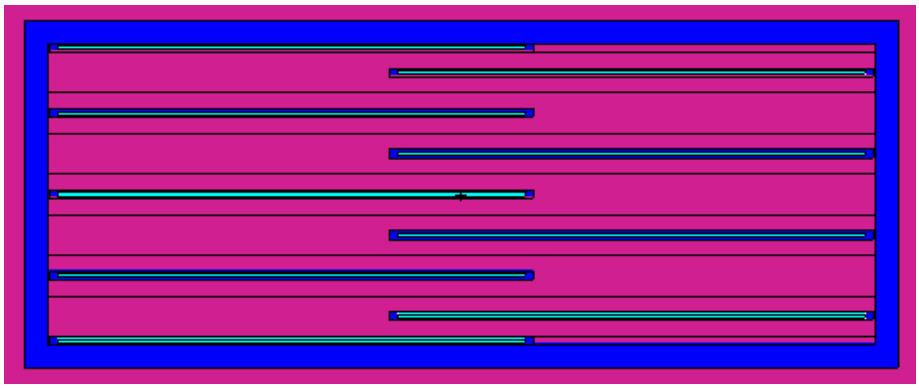

LD7

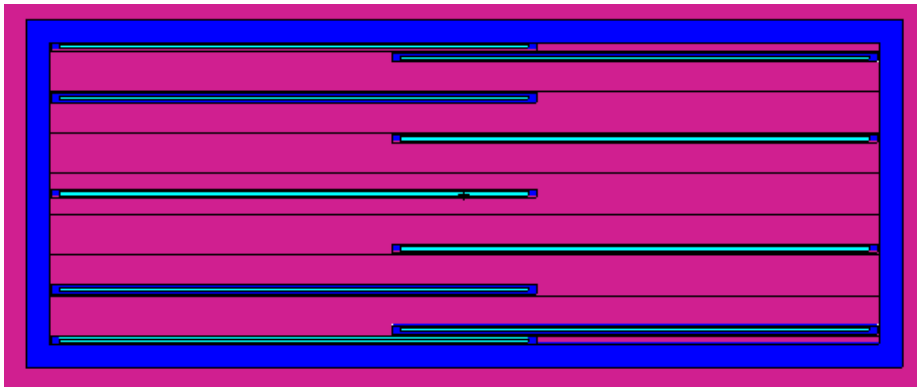

Figure 6.5-6 – NCT Array Geometry, Plate 8 (LD3, LD4, LD5, LD7)

LD8

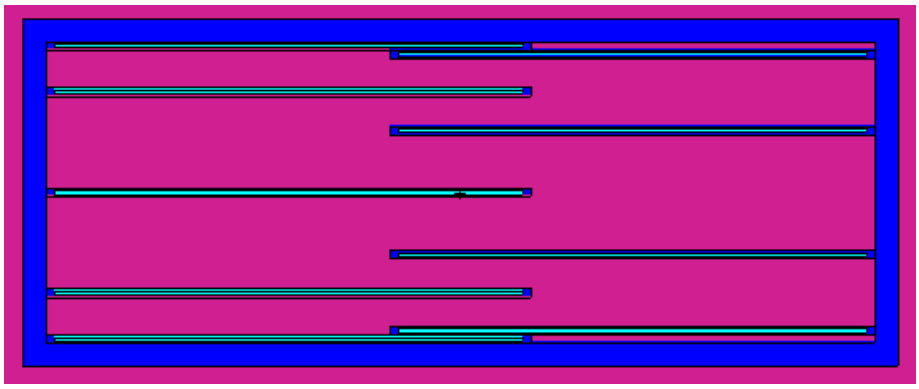

LD9

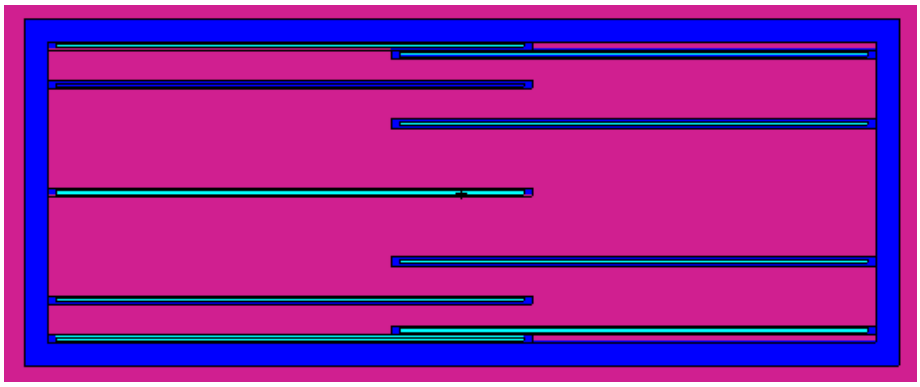

LD10

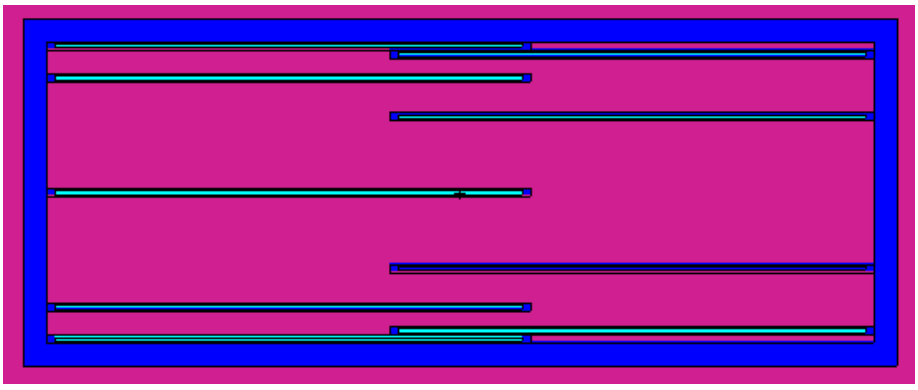

LD11

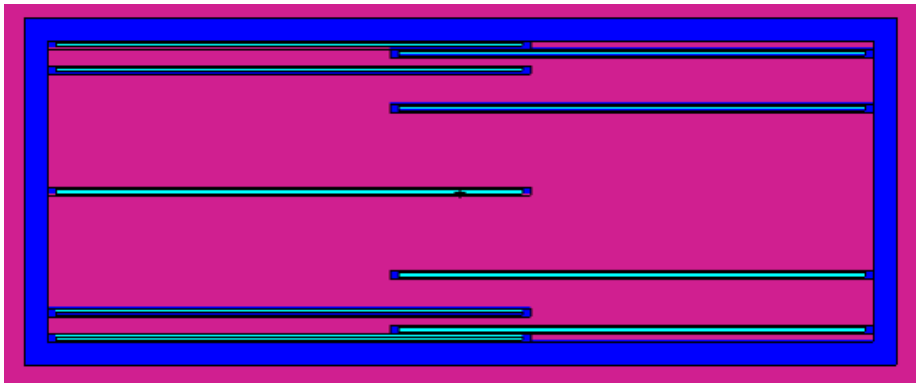

Figure 6.5-7 – NCT Array Geometry, Plate 8 (LD8, LD9, LD10, LD11)

LE2

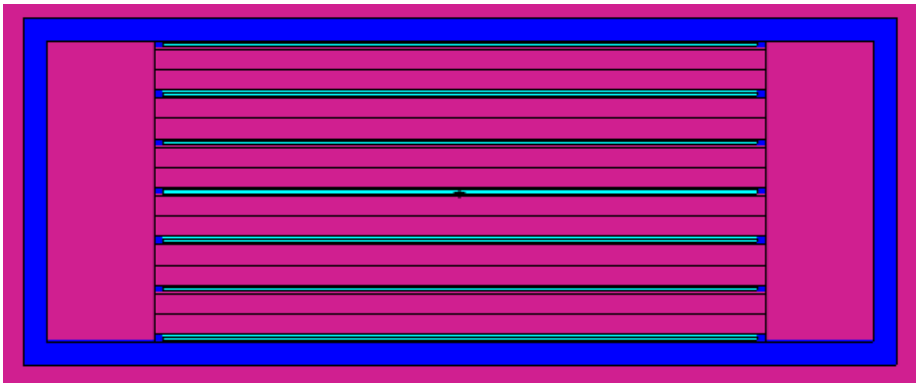

LE3

LE6

LE8

Figure 6.5-8 – NCT Array Geometry, Plate 15 (LE2, LE3, LE6, LE8)

LF1

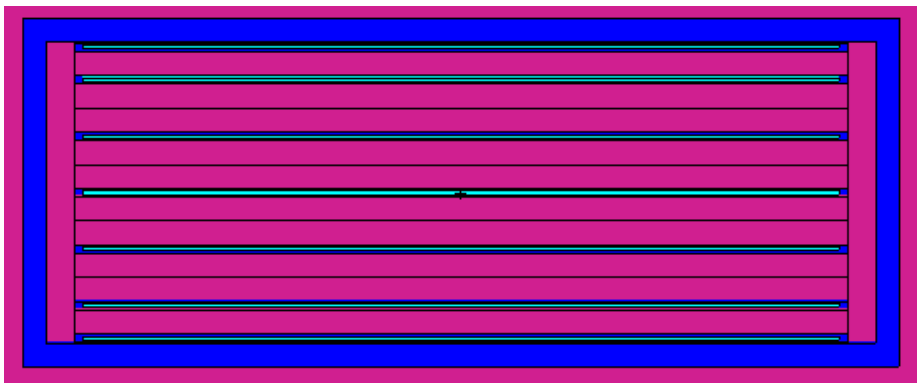

LF2

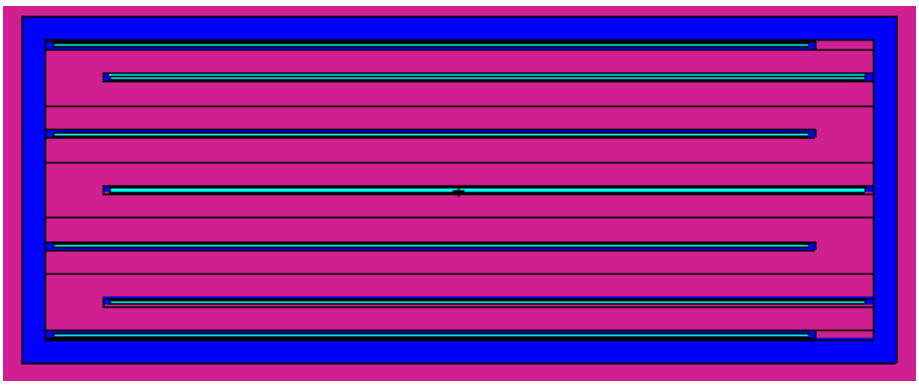

LF4

LF5

Figure 6.5-9 – NCT Array Geometry, Plate 3 (LF1, LF2, LF4, LF5)

LJ3

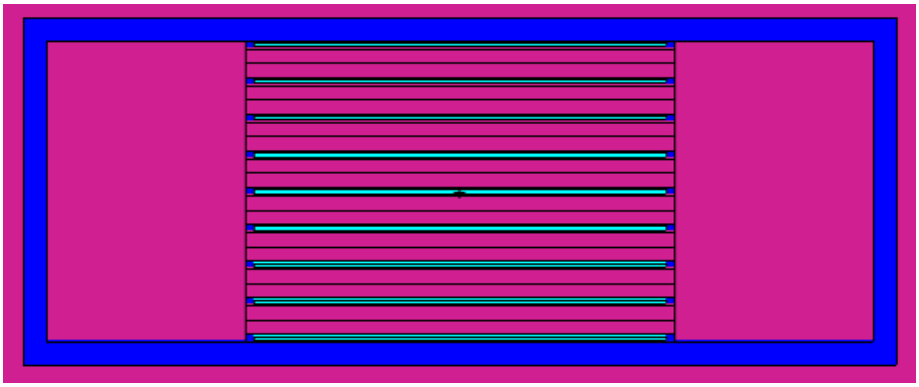

LJ4

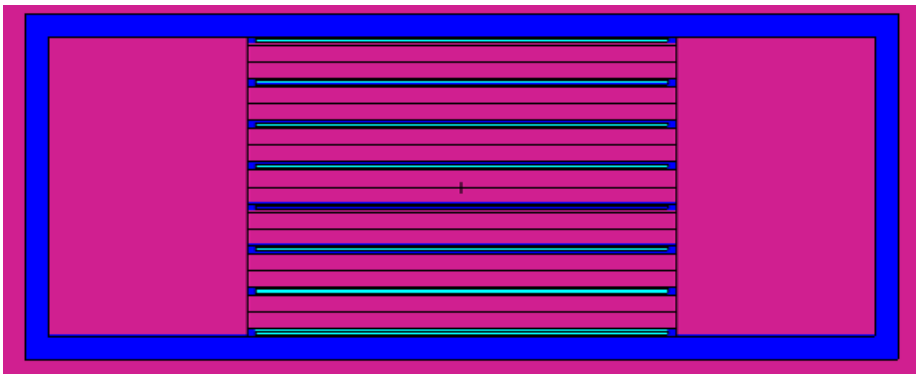

LJ5

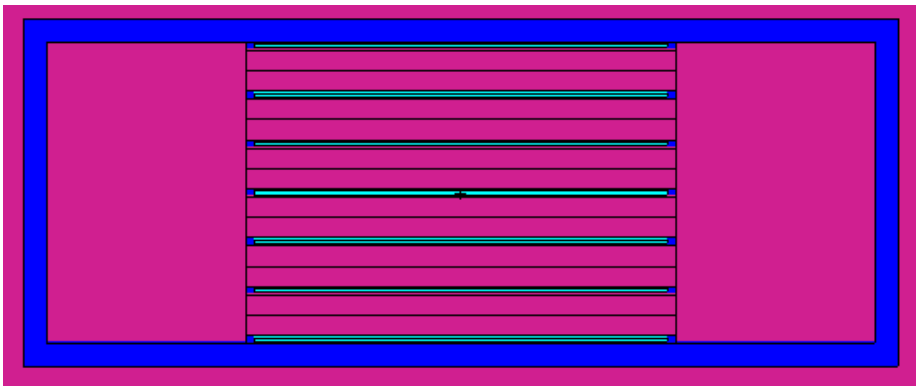

LJ7

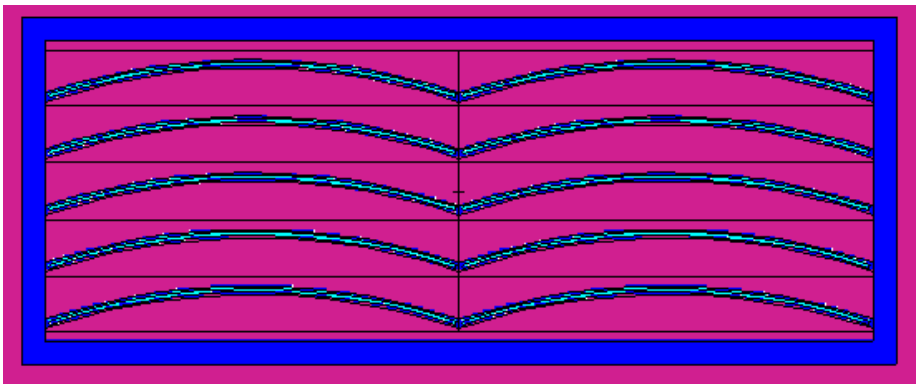

Figure 6.5-10 – NCT Array Geometry, Miscellaneous (LJ3, LJ4, LJ5, LJ7)

6.6 Package Arrays under Hypothetical Accident Conditions

6.6.1 HAC Array Configuration

6.6.1.1 Fuel Element Payload

The HAC array model is a 5x5x1 array of the HAC single package model. As the FHE is assumed to be damaged, the fuel is free to move laterally within the package. To minimize the distance between the fuel elements, in all HAC array models the fuel elements are rotated and moved toward the center of the array, consistent with the NCT array configuration. The FHE is not modeled, because modeling the FHE in any capacity would push the fuel elements apart and lower the reactivity.

From the HAC single package analysis and NCT array analysis, it is known that reactivity is maximized with full-density water between the fuel plates, because the fuel elements are under moderated. Therefore, all HAC array models have full-density water between the fuel plates. Because the fuel elements may be transported in a plastic bag, it is assumed that the water density between the plates may vary independently from the water density inside the inner tube. This partial moderation effect is similar to the partial moderation effect that could be achieved by modeling the FHE explicitly.

Nine computational series are performed. The variables addressed are (1) water density inside inner tube, (2) water density between tubes, (3) presence of insulation, and (4) presence of FHE neoprene. The geometries of two of these series are shown in Figure 6.6-1, and the geometries of the other configurations are similar. These nine computational series are described in the following paragraphs. The full results are provided in Table 6.6-1.

In Series 1, the water density inside the inner tube is varied from 0 to 1.0 g/cm^3, while void is modeled between the tubes. The modeled channel width is 0.085-in. The insulation and FHE neoprene are not modeled. The maximum reactivity occurs for Case F9, with k_s = 0.72933. A water density of 0.8 g/cm^3 within the inner tube is utilized in the most reactive case.

In Series 2, the most reactive case from Series 1 (Case F9) is modified so that the water density between the tubes is varied between 0 and 1.0 g/cm^3, while the water density within the inner tube remains fixed at 0.8 g/cm^3. The reactivity reduces as water is added to this region, indicating that the most reactive condition is with void between the tubes.

In Series 3, the water density both inside and between the tubes is assumed to be exactly the same and varied between 0 and 1.0 g/cm^3. These cases are less reactive than Case F9 in Series 1.

In Series 4, the moderation conditions of Series 1 are repeated except with the insulation modeled. The maximum reactivity occurs for Case J7 for a water density of 0.6 g/cm^3, with a maximum k_s = 0.73476. This case is slightly more reactive than Case F9, in which no insulation was modeled.

In Series 5, the most reactive case from Series 4 (Case J7) is modified so that the water density between the insulation and the outer tube is varied between 0 and 1.0 g/cm^3, while the water density within the inner tube remains fixed at 0.6 g/cm^3. The reactivity decreases as water is added to this region.

In Series 6, the moderation conditions of Series 1 are repeated except with the FHE neoprene modeled. It was determined in the HAC single package analysis that neoprene will lower the reactivity due to absorption in the chlorine. Therefore, the neoprene is conservatively modeled without chlorine. The maximum reactivity occurs for Case L8, with k_s = 0.73297, an increase of 3.6 mk when compared to Case F9. This increase is only slightly above statistical fluctuation, so it may be concluded that the presence of neoprene has at most a small effect on the reactivity. A water density of 0.7 g/cm^3 within the inner tube is utilized in the most reactive case. No cases are performed with the neoprene homogeneously mixed into the water because this scenario is already implicitly considered using the variable water density search within the inner tube.

In Series 7, insulation and neoprene are combined in the same model with variable density water inside the inner pipe, as the presence of both insulation and neoprene slightly increased the reactivity when treated separately. The maximum reactivity occurs for Case M8, with k_s = 0.73599. This case is slightly more reactive than the cases in which insulation and neoprene are addressed separately.

In Series 8, for completeness, void is modeled in the inner tube, while the water density is allowed to vary between the tubes. Chlorine-free neoprene is utilized to increase moderation in the inner tube, but insulation is ignored to maximize the amount of water between the tubes. The peak reactivity for Series 8 is the lowest of all nine series of calculations.

In Series 9, Series 7 is repeated with the channel width increased to 0.089-in. A channel width of 0.089-in is the maximum local channel width (0.087-in) with an additional margin of 0.002-in. The larger channel width is achieved by reducing the cladding thickness. Case O5 is the most reactive of all computational series.

In conclusion, Case O5 is the most reactive, with k_s = 0.74531. This result is below the USL of 0.9209. Case O5 has fully moderated fuel elements, 0.7 g/cm^3 water in the inner tube, insulation and chlorine-free neoprene, void between the insulation and outer tube, fuel elements that have been rotated and moved to the center of the array, and a channel width of 0.089-in. Note that this result is lower than the maximum NCT array case because the HAC and NCT array models are quite similar, except the NCT array uses a much larger 9x9x1 configuration.

6.6.1.2 Loose Plate Basket Payload

It was established in the criticality analysis for the ATR fuel element that the NCT array calculations bound the HAC array calculations. This result is obtained because a 9x9x1 array is utilized in the NCT calculations, while a smaller 5x5x1 array is utilized in the HAC array calculations. Water moderation is modeled in both the NCT and HAC array calculations within the inner tube, although additional moderation is allowed in the HAC cases between the inner and outer tubes. Therefore, the HAC array calculations are performed only for completeness, as these calculations will not be bounding.

In all the HAC array models, the loose plate basket is filled with full-density water, as it has been established in the NCT array analysis that full-density water moderation within the basket maximizes the reactivity. The internal plate arrangement determined in the NCT array calculations to be the most reactive (Case LC21 for plate type 5) is used in all HAC array models. Also, the loose plate basket is modeled pushed to the center of the array to maximize reactivity, as shown in Figure 6.6-2.

Four series of calculations are performed that utilize different moderations conditions. Results for all cases are provided in Table 6.6-2.

Series 1: In Series 1, the insulation is modeled, and void is modeled between the insulation and the outer tube. The water density between the basket and the inner tube is varied between 0 and 1.0 g/cm^3. The maximum reactivity is achieved for Case LK9, with k_s = 0.69792. The water density for this case is 0.8 g/cm^3.

Series 2: In Series 2, the most reactive case from Series 1 (Case LK9) is run with variable density water between the insulation and the outer tube. The reactivity decreases when water is added to this region.

Series 3: In Series 3, Series 1 is repeated, except the insulation is replaced with void. The maximum reactivity is close to but bounded by the maximum reactivity from Series 1.

Series 4: In Series 4, the insulation is not modeled, and the same water density is modeled both between the inner and outer tubes, and between the basket and inner tube. The maximum reactivity is significantly less than the maximum reactivity from Series 1.

In conclusion, the maximum reactivity is from Case LK9, with k_s = 0.69792, in which full-density water is modeled within the basket, 0.8 g/cm^3 water is modeled between the basket and the inner tube, and void between the insulation and the outer tube. This value is less than the USL of 0.9209.

6.6.2 HAC Array Results

Following are the tabulated results for the HAC array cases. The most reactive configuration in each series is listed in boldface.

Table 6.6-1 – HAC Array Results, Fuel Element

Case ID	Filename	Water Density Between Tubes (g/cm^3)	Water Density Inside Inner Tube (g/cm^3)	Water Density Between Plates (g/cm^3)	k_{eff}	σ	k_s (k+2σ)
Series 1: Variable water density in inner tube (no insulation, no neoprene)							
F1	HA_S0P000	0	0	1.0	0.57908	0.00102	0.58112
F2	HA_S0P010	0	0.1	1.0	0.63182	0.00112	0.63406
F3	HA_S0P020	0	0.2	1.0	0.66922	0.00124	0.67170
F4	HA_S0P030	0	0.3	1.0	0.69357	0.00121	0.69599
F5	HA_S0P040	0	0.4	1.0	0.71180	0.00116	0.71412
F6	HA_S0P050	0	0.5	1.0	0.72106	0.00120	0.72346
F7	HA_S0P060	0	0.6	1.0	0.72553	0.00122	0.72797
F8	HA_S0P070	0	0.7	1.0	0.72706	0.00112	0.72930
F9	**HA_S0P080**	**0**	**0.8**	**1.0**	**0.72695**	**0.00119**	**0.72933**
F10	HA_S0P090	0	0.9	1.0	0.72116	0.00110	0.72336
F11	HA_S0P100	0	1.0	1.0	0.71826	0.00123	0.72072
Series 2: Case F9 with variable density water between tubes							
F9	**HA_S0P080**	**0**	**0.8**	**1.0**	**0.72695**	**0.00119**	**0.72933**
G1	HA_P80S010	0.1	0.8	1.0	0.70205	0.00112	0.70429
G2	HA_P80S020	0.2	0.8	1.0	0.67677	0.00125	0.67927
G3	HA_P80S030	0.3	0.8	1.0	0.65374	0.00113	0.65600
G4	HA_P80S040	0.4	0.8	1.0	0.63121	0.00114	0.63349
G5	HA_P80S050	0.5	0.8	1.0	0.60791	0.00104	0.60999
G6	HA_P80S060	0.6	0.8	1.0	0.59303	0.00111	0.59525
G7	HA_P80S070	0.7	0.8	1.0	0.57461	0.00109	0.57679
G8	HA_P80S080	0.8	0.8	1.0	0.56082	0.00110	0.56302
G9	HA_P80S090	0.9	0.8	1.0	0.54767	0.00102	0.54971
G10	HA_P80S100	1.0	0.8	1.0	0.53613	0.00108	0.53829
Series 3: Matching water density inside and between tubes							
F1	HA_S0P000	0	0	1.0	0.57908	0.00102	0.58112
H1	HA_SP010	0.1	0.1	1.0	0.64719	0.00115	0.64949
H2	**HA_SP020**	**0.2**	**0.2**	**1.0**	**0.66047**	**0.00115**	**0.66277**
H3	HA_SP030	0.3	0.3	1.0	0.64457	0.00112	0.64681
H4	HA_SP040	0.4	0.4	1.0	0.62648	0.00117	0.62882
H5	HA_SP050	0.5	0.5	1.0	0.60286	0.00112	0.60510
H6	HA_SP060	0.6	0.6	1.0	0.58814	0.00116	0.59046
H7	HA_SP070	0.7	0.7	1.0	0.57337	0.00106	0.57549
H8	HA_SP080	0.8	0.8	1.0	0.56082	0.00110	0.56302
H9	HA_SP090	0.9	0.9	1.0	0.55245	0.00122	0.55489
H10	HA_SP100	1.0	1.0	1.0	0.54360	0.00100	0.54560

(continued)

Table 6.6-1 – HAC Array Results, Fuel Element (continued)

Case ID	Filename	Water Density Between Tubes (g/cm^3)	Water Density Inside Inner Tube (g/cm^3)	Water Density Between Plates (g/cm^3)	k_{eff}	σ	k_s (k+2σ)
Series 4: Repeat of Series 1 with insulation							
J1	HA_DS0P000	0	0	1.0	0.58824	0.00116	0.59056
J2	HA_DS0P010	0	0.1	1.0	0.63716	0.00111	0.63938
J3	HA_DS0P020	0	0.2	1.0	0.67403	0.00118	0.67639
J4	HA_DS0P030	0	0.3	1.0	0.69920	0.00130	0.70180
J5	HA_DS0P040	0	0.4	1.0	0.71665	0.00116	0.71897
J6	HA_DS0P050	0	0.5	1.0	0.72388	0.00117	0.72622
J7	**HA_DS0P060**	**0**	**0.6**	**1.0**	**0.73230**	**0.00123**	**0.73476**
J8	HA_DS0P070	0	0.7	1.0	0.73178	0.00112	0.73402
J9	HA_DS0P080	0	0.8	1.0	0.72965	0.00124	0.73213
J10	HA_DS0P090	0	0.9	1.0	0.72638	0.00107	0.72852
J11	HA_DS0P100	0	1.0	1.0	0.71985	0.00113	0.72211
Series 5: Case J7 with variable density water between insulation and outer tube							
J7	**HA_DS0P090**	**0**	**0.6**	**1.0**	**0.73230**	**0.00123**	**0.73476**
K1	HA_DP60S010	0.1	0.6	1.0	0.72284	0.00123	0.72530
K2	HA_DP60S020	0.2	0.6	1.0	0.71587	0.00120	0.71827
K3	HA_DP60S030	0.3	0.6	1.0	0.71029	0.00118	0.71265
K4	HA_DP60S040	0.4	0.6	1.0	0.70002	0.00117	0.70236
K5	HA_DP60S050	0.5	0.6	1.0	0.69370	0.00122	0.69614
K6	HA_DP60S060	0.6	0.6	1.0	0.68266	0.00111	0.68488
K7	HA_DP60S070	0.7	0.6	1.0	0.67122	0.00112	0.67346
K8	HA_DP60S080	0.8	0.6	1.0	0.66359	0.00115	0.66589
K9	HA_DP60S090	0.9	0.6	1.0	0.65393	0.00111	0.65615
K10	HA_DP60S100	1.0	0.6	1.0	0.64595	0.00116	0.64827
Series 6: Repeat of Series 1 with neoprene							
L1	HA_N2S0P000	0	0	1.0	0.60058	0.00113	0.60284
L2	HA_N2S0P010	0	0.1	1.0	0.64323	0.00119	0.64561
L3	HA_N2S0P020	0	0.2	1.0	0.68153	0.00118	0.68389
L4	HA_N2S0P030	0	0.3	1.0	0.70640	0.00120	0.70880
L5	HA_N2S0P040	0	0.4	1.0	0.71669	0.00124	0.71917
L6	HA_N2S0P050	0	0.5	1.0	0.72733	0.00117	0.72967
L7	HA_N2S0P060	0	0.6	1.0	0.72872	0.00122	0.73116
L8	**HA_N2S0P070**	**0**	**0.7**	**1.0**	**0.73069**	**0.00114**	**0.73297**
L9	HA_N2S0P080	0	0.8	1.0	0.73081	0.00107	0.73295
L10	HA_N2S0P090	0	0.9	1.0	0.72692	0.00129	0.72950
L11	HA_N2S0P100	0	1.0	1.0	0.72371	0.00122	0.72615

(continued)

Table 6.6-1 – HAC Array Results, Fuel Element (concluded)

Case ID	Filename	Water Density Between Tubes (g/cm^3)	Water Density Inside Inner Tube (g/cm^3)	Water Density Between Plates (g/cm^3)	k_{eff}	σ	k_s (k+2σ)
Series 7: Repeat of Series 1 with insulation and neoprene							
M1	HA_DNS0P000	0	0	1.0	0.60377	0.00107	0.60591
M2	HA_DNS0P010	0	0.1	1.0	0.64940	0.00107	0.65154
M3	HA_DNS0P020	0	0.2	1.0	0.68596	0.00110	0.68816
M4	HA_DNS0P030	0	0.3	1.0	0.70846	0.00115	0.71076
M5	HA_DNS0P040	0	0.4	1.0	0.72168	0.00122	0.72412
M6	HA_DNS0P050	0	0.5	1.0	0.73000	0.00124	0.73248
M7	HA_DNS0P060	0	0.6	1.0	0.73182	0.00122	0.73426
M8	**HA_DNS0P070**	**0**	**0.7**	**1.0**	**0.73365**	**0.00117**	**0.73599**
M9	HA_DNS0P080	0	0.8	1.0	0.73187	0.00127	0.73441
M10	HA_DNS0P090	0	0.9	1.0	0.73006	0.00112	0.73230
M11	HA_DNS0P100	0	1.0	1.0	0.72332	0.00122	0.72576
Series 8: Case L1 with variable density water between tubes							
L1	HA_N2S0P000	0	0	1.0	0.60058	0.00113	0.60284
N1	**HA_N2P0S010**	**0.1**	**0**	**1.0**	**0.63054**	**0.00107**	**0.63268**
N2	HA_N2P0S020	0.2	0	1.0	0.62961	0.00118	0.63197
N3	HA_N2P0S030	0.3	0	1.0	0.61939	0.00113	0.62165
N4	HA_N2P0S040	0.4	0	1.0	0.60776	0.00108	0.60992
N5	HA_N2P0S050	0.5	0	1.0	0.58874	0.00108	0.59090
N6	HA_N2P0S060	0.6	0	1.0	0.57308	0.00109	0.57526
N7	HA_N2P0S070	0.7	0	1.0	0.55837	0.00107	0.56051
N8	HA_N2P0S080	0.8	0	1.0	0.54139	0.00101	0.54341
N9	HA_N2P0S090	0.9	0	1.0	0.52714	0.00106	0.52926
N10	HA_N2P0S100	1.0	0	1.0	0.51600	0.00114	0.51828
Series 9: Repeat of Series 7 with a channel width of 0.089-in							
O1	HA_DNS0P030_C89	0	0.3	1.0	0.71885	0.00118	0.72121
O2	HA_DNS0P040_C89	0	0.4	1.0	0.73301	0.00114	0.73529
O3	HA_DNS0P050_C89	0	0.5	1.0	0.73889	0.00124	0.74137
O4	HA_DNS0P060_C89	0	0.6	1.0	0.74172	0.00121	0.74414
O5	**HA_DNS0P070_C89**	**0**	**0.7**	**1.0**	**0.74299**	**0.00116**	**0.74531**
O6	HA_DNS0P080_C89	0	0.8	1.0	0.74192	0.00125	0.74442
O7	HA_DNS0P090_C89	0	0.9	1.0	0.73527	0.00105	0.73737
O8	HA_DNS0P100_C89	0	1.0	1.0	0.73282	0.00110	0.73502

Table 6.6-2 – HAC Array Results, Plate 5

Case ID	Filename	Water Density Between Tubes (g/cm^3)	Water Density Inside Inner Tube (g/cm^3)	Water Density Between Plates (g/cm^3)	k_{eff}	σ	k_s (k+2σ)
Series 1: Variable water density in inner tube, with insulation							
LK1	HA_N5DS0P000	0	0	1.0	0.53784	0.00096	0.53976
LK2	HA_N5DS0P010	0	0.1	1.0	0.58878	0.00098	0.59074
LK3	HA_N5DS0P020	0	0.2	1.0	0.62946	0.00101	0.63148
LK4	HA_N5DS0P030	0	0.3	1.0	0.65858	0.00102	0.66062
LK5	HA_N5DS0P040	0	0.4	1.0	0.67685	0.00100	0.67885
LK6	HA_N5DS0P050	0	0.5	1.0	0.68901	0.00102	0.69105
LK7	HA_N5DS0P060	0	0.6	1.0	0.69483	0.00107	0.69697
LK8	HA_N5DS0P070	0	0.7	1.0	0.69266	0.00120	0.69506
LK9	**HA_N5DS0P080**	**0**	**0.8**	**1.0**	**0.69576**	**0.00108**	**0.69792**
LK10	HA_N5DS0P090	0	0.9	1.0	0.69250	0.00105	0.69460
LK11	HA_N5DS0P100	0	1.0	1.0	0.68585	0.00104	0.68793
Series 2: Case LK9 with variable density water between tubes.							
LK9	**HA_N5DS0P080**	**0**	**0.8**	**1.0**	**0.69576**	**0.00108**	**0.69792**
LM1	HA_N5DP80S010	0.1	0.8	1.0	0.68989	0.00106	0.69201
LM2	HA_N5DP80S020	0.2	0.8	1.0	0.67989	0.00107	0.68203
LM3	HA_N5DP80S030	0.3	0.8	1.0	0.67352	0.00098	0.67548
LM4	HA_N5DP80S040	0.4	0.8	1.0	0.66658	0.00105	0.66868
LM5	HA_N5DP80S050	0.5	0.8	1.0	0.65700	0.00105	0.65910
LM6	HA_N5DP80S060	0.6	0.8	1.0	0.64893	0.00118	0.65129
LM7	HA_N5DP80S070	0.7	0.8	1.0	0.64141	0.00106	0.64353
LM8	HA_N5DP80S080	0.8	0.8	1.0	0.63415	0.00099	0.63613
LM9	HA_N5DP80S090	0.9	0.8	1.0	0.62748	0.00103	0.62954
LM10	HA_N5DP80S100	1.0	0.8	1.0	0.62100	0.00094	0.62288
Series 3: Repeat of Series 1, no insulation							
LN1	HA_N5S0P000	0	0	1.0	0.53334	0.00092	0.53518
LN2	HA_N5S0P010	0	0.1	1.0	0.58456	0.00091	0.58638
LN3	HA_N5S0P020	0	0.2	1.0	0.62421	0.00108	0.62637
LN4	HA_N5S0P030	0	0.3	1.0	0.65402	0.00109	0.65620
LN5	HA_N5S0P040	0	0.4	1.0	0.67129	0.00108	0.67345
LN6	HA_N5S0P050	0	0.5	1.0	0.68550	0.00108	0.68766
LN7	HA_N5S0P060	0	0.6	1.0	0.69042	0.00106	0.69254
LN8	**HA_N5S0P070**	**0**	**0.7**	**1.0**	**0.69145**	**0.00104**	**0.69353**
LN9	HA_N5S0P080	0	0.8	1.0	0.69071	0.00101	0.69273
LN10	HA_N5S0P090	0	0.9	1.0	0.68925	0.00102	0.69129
LN11	HA_N5S0P100	0	1.0	1.0	0.68493	0.00116	0.68725

(continued)

Table 6.6-2 – HAC Array Results, Plate 5 (concluded)

Case ID	Filename	Water Density Between Packages (g/cm^3)	Water Density Inside Pipe (g/cm^3)	Water Density Between Plates (g/cm^3)	k_{eff}	σ	k_s (k+2σ)
Series 4: No insulation, matching water densities inside and between tubes							
LN1	HA_N5S0P000	0	0	1.0	0.53334	0.00092	0.53518
LO1	HA_N5SP010	0.1	0.1	1.0	0.59685	0.00097	0.59879
LO2	**HA_N5SP020**	**0.2**	**0.2**	**1.0**	**0.61533**	**0.00096**	**0.61725**
LO3	HA_N5SP030	0.3	0.3	1.0	0.60844	0.00108	0.61060
LO4	HA_N5SP040	0.4	0.4	1.0	0.59462	0.00099	0.59660
LO5	HA_N5SP050	0.5	0.5	1.0	0.57802	0.00107	0.58016
LO6	HA_N5SP060	0.6	0.6	1.0	0.56514	0.00107	0.56728
LO7	HA_N5SP070	0.7	0.7	1.0	0.55116	0.00106	0.55328
LO8	HA_N5SP080	0.8	0.8	1.0	0.54262	0.00093	0.54448
LO9	HA_N5SP090	0.9	0.9	1.0	0.53400	0.00102	0.53604
LO10	HA_N5SP100	1.0	1.0	1.0	0.52785	0.00106	0.52997

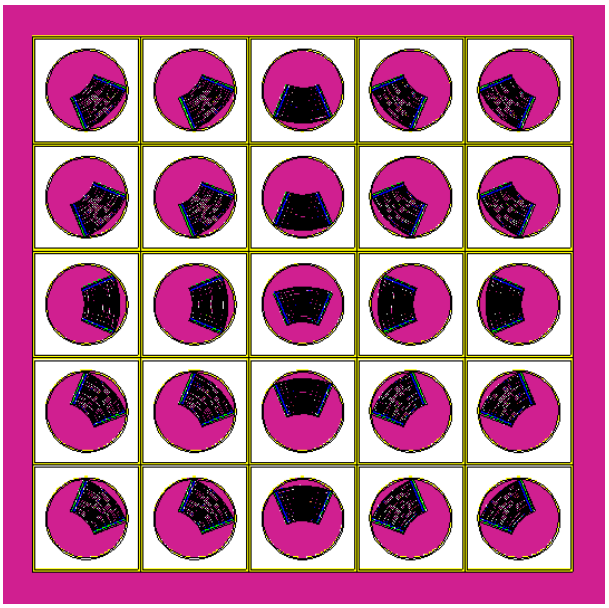

Series 1: Array with variable density water in inner tube, and void between tubes. No insulation modeled.

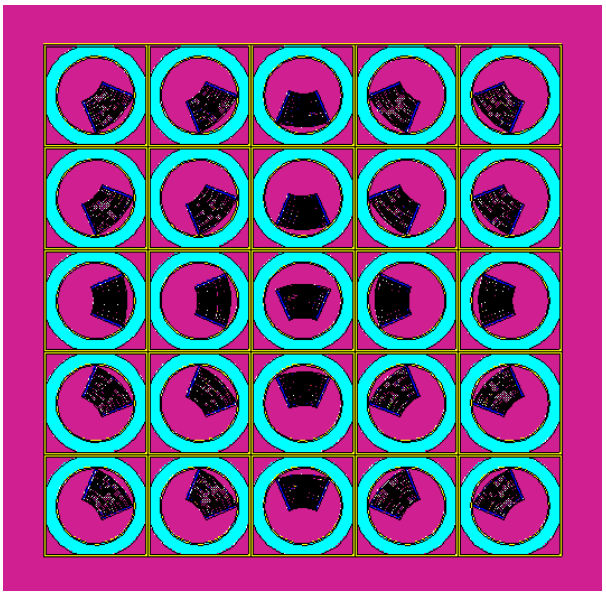

Series 5: Array with 0.6 g/cm^3 water in inner tube and variable density water between tubes. Insulation is modeled.

Figure 6.6-1 – HAC Array Geometry Examples, Fuel Element

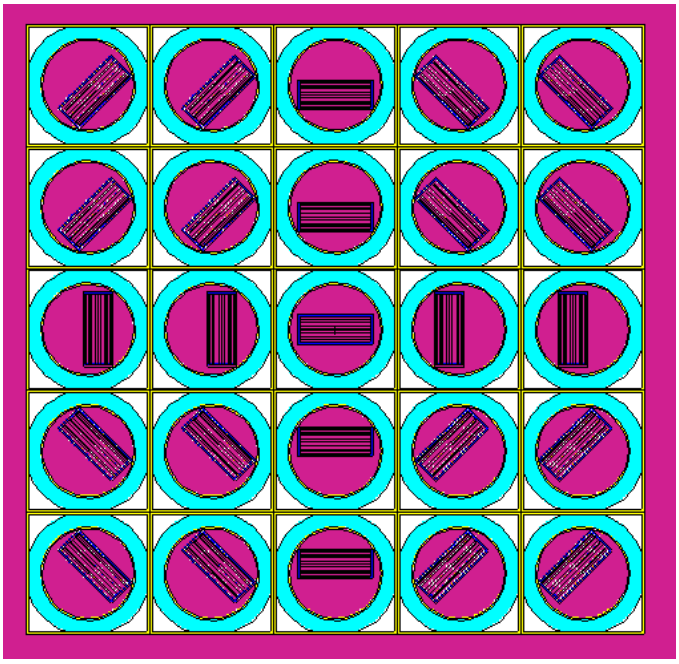

Series 1: Array with variable density water in inner tube, and void between tubes. Insulation is modeled.

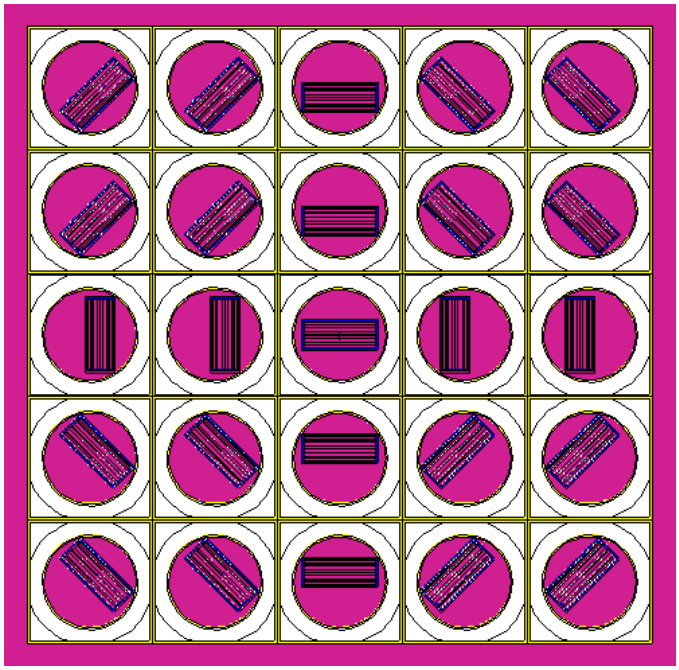

Series 3: Array with variable density water in inner tube, and void between tubes. No insulation modeled.

Figure 6.6-2 – HAC Array Geometry Examples, Loose Plate Basket

6.7 Fissile Material Packages for Air Transport

The applicable licensing requirements for air transport of fissile material are contained in 10 CFR 71.55(f) and IAEA Safety Standard SSR-6, paragraph 683. For air transport, no structural integrity is credited for the hypothetical accident conditions. Rather, the fissile material from a single package is modeled as a sphere that is optimally moderated and reflected by the packaging materials. The sphere is reflected with 20 cm of water. Per the licensing requirements of 10 CFR 71.55(f) and IAEA Safety Standard SSR-6, paragraph 683, environmental water is not included in the fissile sphere.

The air transport analysis is intended to bound all current and projected future payloads. 2000 g U-235 in HEU is conservatively modeled. The non-uranium elements that may be present in the fuel matrix (e.g., aluminum, silicon, molybdenum), and structural materials of the fuel elements and package (e.g., aluminum, steel) are conservatively neglected within the fissile mixture, which minimizes parasitic neutron absorption. Omitting these materials from the fissile sphere also minimizes the size of the fissile sphere, which minimizes neutron leakage. Both of these effects conservatively maximize the reactivity. The U-235 weight percent is modeled at the maximum value of 94%. Consistent with the ATR fuel element analysis, representative weight percents of 0.6% and 0.35% are utilized for U-234 and U-236, respectively, and the balance (5.05%) is modeled as U-238.

The package contains up to 100 g polyethylene (CH_2), and the sum of neoprene (C_4H_5Cl) and cellulosic material ($C_6H_{10}O_5$) (such as kraft paper and cardboard) is limited to 4000 g. Because polyethylene, neoprene, and cellulosic material contain hydrogen, these materials act as a moderator and are explicitly addressed in the analysis.

The fissile sphere is modeled as a mixture of uranium, polyethylene, neoprene and/or cellulosic material. For an air transport analysis, environmental water is not included. The total mass of uranium based on 94% enrichment is 2000 g U-235 / 0.94 = 2127.7 g uranium. The theoretical material densities are 19.0 g/cm^3 uranium metal, 0.92 g/cm^3 polyethylene, 1.23 g/cm^3 neoprene, and 0.44 g/cm^3 for cellulosic material (density of kraft paper). Based upon the mass inputs and the material densities, the volume of uranium, polyethylene, neoprene, and cellulosic material are summed to create the total volume for the fissile sphere, which is used to compute atom densities for each isotope.

The atom densities for several different example mixtures are provided in Table 6.7-1. The total volume V is computed as $V = V_U + V_{poly} + V_{cellulosic} + V_{neoprene}$, and the radius R of the fissile material is then:

$$R = \sqrt[3]{\frac{3V}{4\pi}}$$

The gram density for each material within the sphere is computed as the mass of the material divided by the total volume (V), which is then used to compute the atom density of each material. These atom densities are then summed to create the overall mixture atom densities presented in Table 6.7-1.

In the first series of cases, the uranium is homogeneously mixed with various quantities of polyethylene, neoprene, and cellulosic material in a single fissile sphere reflected with 20 cm of

water, see Figure 6.7-1. These results are summarized in Table 6.7-2. Case AIR01 is pure uranium with no hydrogenous material, with k_s = 0.51683. Cases AIR02 through AIR06 include increasing amounts of polyethylene (no neoprene or cellulosic material) up to the maximum value of 100 g polyethylene. The reactivity decreases compared to Case AIR01 when < 80 g polyethylene is added, but reactivity is maximized with the full 100 g polyethylene, with k_s = 0.52233.

Cases AIR07 through AIR14 include increasing amounts of neoprene (no polyethylene or cellulosic material) up to the maximum value of 4000 g neoprene. The reactivity decreases compared to Case AIR01 when < 1500 g of neoprene is added, but reactivity is maximized with the full 4000 g neoprene, with k_s = 0.57035.

Cases AIR15 through AIR22 include increasing amounts of cellulosic material (no polyethylene or neoprene) up to the maximum value of 4000 g cellulosic material. The reactivity decreases compared to Case AIR01 when < 3000 g of cellulosic material is added, but reactivity is maximized with the full 4000 g cellulosic material, with k_s = 0.55065.

For all three hydrogenous materials, reactivity initially decreases for smaller amounts of moderating material. The most likely reason that reactivity initially decreases when small amounts of hydrogenous material are added is that adding moderator greatly enlarges the volume of the fissile sphere. For small amounts of moderator, the increase in neutron leakage due to the larger sphere results in a net reduction in reactivity despite the increase in moderation. For larger quantities of moderator, the enhanced moderation increases the reactivity despite the increased leakage.

The sum of neoprene and cellulosic material is limited to 4000 g. Comparing Cases AIR14 and AIR22, it is concluded that neoprene is a superior moderator than cellulosic material. Therefore, it is conservative to model the 4000 g of neoprene/cellulosic material as 4000 g neoprene. In Case AIR23, both 100 g polyethylene and 4000 g neoprene are included in the fissile sphere, with k_s = 0.58222. This is the most reactive single fissile sphere case.

The above models do not include the packaging structural materials, which may also act as a reflector. The maximum weight of a loaded package is 290 lbs (see Section 1.2.1.2). This weight includes the fuel, stainless steel structural members, aluminum fuel support structures, insulation, etc. Therefore, 300 lbs (136 kg) bounds the total mass of stainless steel in the package by a large margin and is used as a reflector outside the fissile sphere. The stainless steel density is 7.94 g/cm^3, resulting in a steel reflector thickness of 7.61 cm (see Figure 6.7-2) if added to the most reactive single fissile sphere model (Case AIR23). A 20 cm water reflector is modeled outside the steel reflector. When the steel reflector is added (Case AIR24), k_s = 0.55311, which is less reactive than without the steel reflector. Therefore, the reflection provided by the structural materials of the packaging may be neglected.

The single fissile sphere is undermoderated with 4000 g neoprene and 100 g polyethylene. Moderation may be further enhanced by modeling the fissile material in two regions, an inner sphere and outer shell, with all of the moderating material in the inner sphere (see Figure 6.7-3). The inner sphere contains a mass “M” grams U-235, 4000 g neoprene, and 100 g polyethylene. The outer shell contains (2000 – M) grams U-235 with no moderating material. Therefore, the system always contains 2000 g U-235. The inner sphere in the two region model achieves greater moderation than the single sphere model because less U-235 is moderated with the full mass of moderating material.

The atom densities are computed using the same method developed for the single region model, although the mass of U-235 is now varied. Sample atom densities for the moderated inner sphere for several different U-235 masses are summarized in Table 6.7-3, as well as the outer shell composition.

The two-region model results are summarized in Table 6.7-4. The two-region model achieves a higher reactivity than the single-region model. The reactivity is maximized with 1500 g U-235 in the inner sphere and 500 g U-235 in the outer shell (Case AIR40), with k_s = 0.60739. The most reactive air transport case is far below the USL.

Table 6.7-1 – Example Atom Densities, Single Fissile Sphere

Isotope	2000 g U-235 0 g polyethylene 0 g neoprene 0 g cellulosic (atom/b-cm)	2000 g U-235 100 g polyethylene 0 g neoprene 0 g cellulosic (atom/b-cm)	2000 g U-235 0 g polyethylene 4000 g neoprene 0 g cellulosic (atom/b-cm)	2000 g U-235 0 g polyethylene 0 g neoprene 4000 g cellulosic (atom/b-cm)
U-234	2.9333E-04	1.4885E-04	9.7644E-06	3.5650E-06
U-235	4.5759E-02	2.3220E-02	1.5232E-03	5.5614E-04
U-236	1.6965E-04	8.6091E-05	5.6475E-06	2.0619E-06
U-238	2.4273E-03	1.2317E-03	8.0799E-05	2.9500E-05
H	-	3.8910E-02	4.0439E-02	1.6124E-02
C	-	1.9455E-02	3.2351E-02	9.6743E-03
O	-	-	-	8.0619E-03
Cl	-	-	8.0877E-03	-
Total	4.8649E-02	8.3052E-02	8.2497E-02	3.4451E-02

Table 6.7-2 – Air Transport Results, Single Fissile Sphere

Case ID	Filename	Radius (cm)	Poly-ethylene Mass (g)	Neoprene Mass (g)	Cellulosic Mass (g)	k	σ	k_s (k+2σ)
AIR01	AIR_P0_N0_K0	2.9901	0	0	0	0.51621	0.00031	0.51683
AIR02	AIR_P020	3.1723	20	0	0	0.50988	0.00031	0.51050
AIR03	AIR_P040	3.3356	40	0	0	0.50946	0.00032	0.51010
AIR04	AIR_P060	3.4844	60	0	0	0.51250	0.00033	0.51316
AIR05	AIR_P080	3.6214	80	0	0	0.51649	0.00033	0.51715
AIR06	AIR_P100	3.7488	100	0	0	0.52167	0.00033	0.52233
AIR07	AIR_N0500	4.9837	0	500	0	0.48059	0.00034	0.48127
AIR08	AIR_N1000	6.0443	0	1000	0	0.50801	0.00035	0.50871
AIR09	AIR_N1500	6.8247	0	1500	0	0.52854	0.00036	0.52926
AIR10	AIR_N2000	7.4585	0	2000	0	0.54342	0.00038	0.54418
AIR11	AIR_N2500	7.9998	0	2500	0	0.55460	0.00036	0.55532
AIR12	AIR_N3000	8.4763	0	3000	0	0.56208	0.00036	0.56280
AIR13	AIR_N3500	8.9046	0	3500	0	0.56762	0.00035	0.56832
AIR14	AIR_N4000	9.2952	0	4000	0	0.56965	0.00035	0.57035
Note: All models reflected with 20 cm water.								

(continued)

Table 6.7-2 – Air Transport Results, Single Fissile Sphere (concluded)

Case ID	Filename	Radius (cm)	Poly-ethylene Mass (g)	Neoprene Mass (g)	Cellulosic Mass (g)	k	σ	k_s (k+2σ)
AIR15	AIR_K0500	6.6820	0	0	500	0.43112	0.00034	0.43180
AIR16	AIR_K1000	8.2912	0	0	1000	0.45924	0.00036	0.45996
AIR17	AIR_K1500	9.4413	0	0	1500	0.48136	0.00036	0.48208
AIR18	AIR_K2000	10.3639	0	0	2000	0.49829	0.00037	0.49903
AIR19	AIR_K2500	11.1463	0	0	2500	0.51439	0.00038	0.51515
AIR20	AIR_K3000	11.8319	0	0	3000	0.52755	0.00039	0.52833
AIR21	AIR_K3500	12.4462	0	0	3500	0.53825	0.0004	0.53905
AIR22	AIR_K4000	13.0052	0	0	4000	0.54989	0.00038	0.55065
AIR23	**AIR_NP**	**9.3942**	**100**	**4000**	**0**	**0.58148**	**0.00037**	**0.58222**
Case AIR24 features a steel reflector between the fissile sphere and outer water reflector								
AIR24	AIR_NP_RSS	9.3942	100	4000	0	0.55239	0.00036	0.55311
Note: All models reflected with 20 cm water.								

Table 6.7-3 – Example Atom Densities, Two-Region Model

	Inner Region			Outer Region
Isotope	**500 g U-235 100 g polyethylene 4000 g neoprene (atom/b-cm)**	**1000 g U-235 100 g polyethylene 4000 g neoprene (atom/b-cm)**	**1500 g U-235 100 g polyethylene 4000 g neoprene (atom/b-cm)**	**Uranium Metal**
U-234	2.4233E-06	4.8069E-06	7.1517E-06	2.9333E-04
U-235	3.7803E-04	7.4986E-04	1.1157E-03	4.5759E-02
U-236	1.4016E-06	2.7802E-06	4.1364E-06	1.6965E-04
U-238	2.0052E-05	3.9776E-05	5.9180E-05	2.4273E-03
H	4.2678E-02	4.2328E-02	4.1984E-02	-
C	3.3382E-02	3.3108E-02	3.2839E-02	-
Cl	8.0288E-03	7.9630E-03	7.8983E-03	-
Total	8.4490E-02	8.4197E-02	8.3908E-02	4.8649E-02

Table 6.7-4 – Air Transport Results, Two-Region Model

Case ID	Filename	Radius Inner (cm)	U-235 Mass Inner (g)	U-235 Mass Outer (g)	k	σ	k_s (k+2σ)
AIR30	AIR_MI0500	9.3179	500	1500	0.55303	0.00035	0.55373
AIR31	AIR_MI0600	9.3230	600	1400	0.56436	0.00035	0.56506
AIR32	AIR_MI0700	9.3281	700	1300	0.57413	0.00035	0.57483
AIR33	AIR_MI0800	9.3332	800	1200	0.58213	0.00037	0.58287
AIR34	AIR_MI0900	9.3383	900	1100	0.58823	0.00036	0.58895
AIR35	AIR_MI1000	9.3434	1000	1000	0.59313	0.00036	0.59385
AIR36	AIR_MI1100	9.3485	1100	900	0.59856	0.00037	0.59930
AIR37	AIR_MI1200	9.3536	1200	800	0.60211	0.00038	0.60287
AIR38	AIR_MI1300	9.3587	1300	700	0.60424	0.00038	0.60500
AIR39	AIR_MI1400	9.3638	1400	600	0.60641	0.00038	0.60717
AIR40	**AIR_MI1500**	**9.3689**	**1500**	**500**	**0.60663**	**0.00038**	**0.60739**
AIR41	AIR_MI1600	9.3740	1600	400	0.60610	0.00035	0.60680
AIR42	AIR_MI1700	9.3790	1700	300	0.60433	0.00037	0.60507
AIR43	AIR_MI1800	9.3841	1800	200	0.60075	0.00039	0.60153
AIR44	AIR_MI1900	9.3892	1900	100	0.59442	0.00039	0.59520
AIR45	AIR_MI1995	9.3940	1995	5	0.58274	0.00036	0.58346

Notes:
(1) The total U-235 mass is 2000 g in all models.
(2) All models contain 4000 g neoprene and 100 g polyethylene in the inner sphere. The outer shell is uranium metal.
(3) The outer radius of the outer fissile shell is 9.3942 cm in all models.
(4) All cases reflected with 20 cm water.

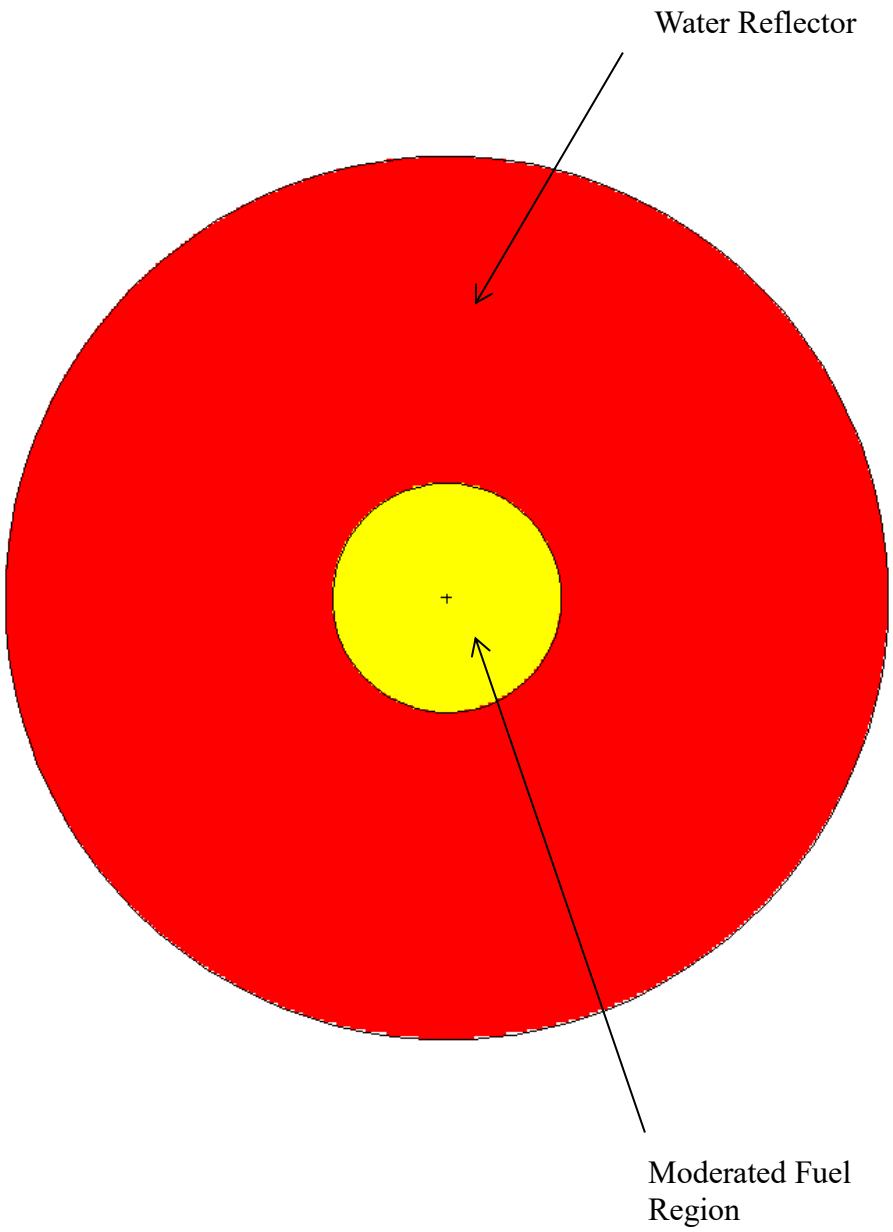

Figure 6.7-1 – Air Transport Model, Single Region Model

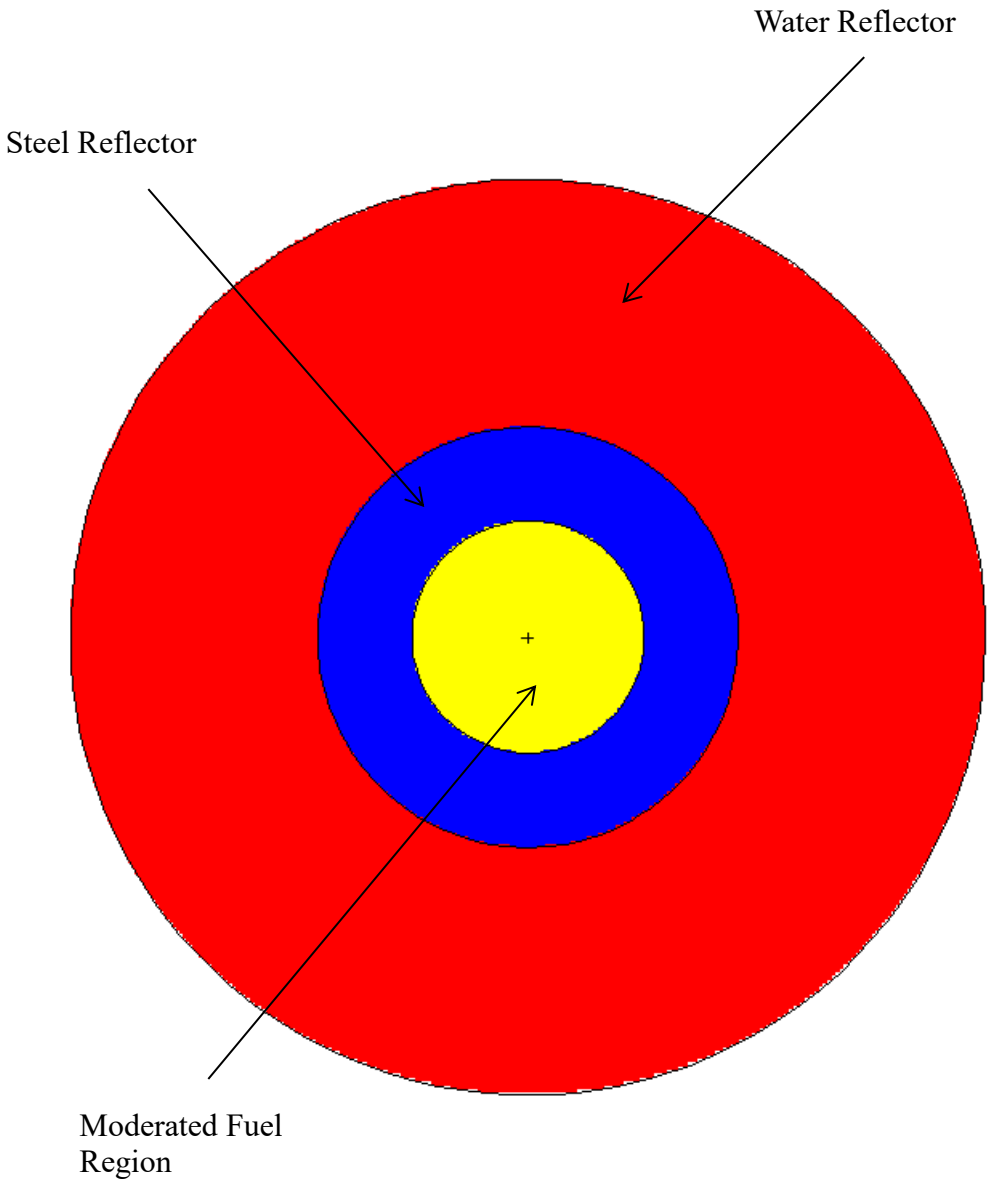

Figure 6.7-2 – Air Transport Model with Steel Reflector

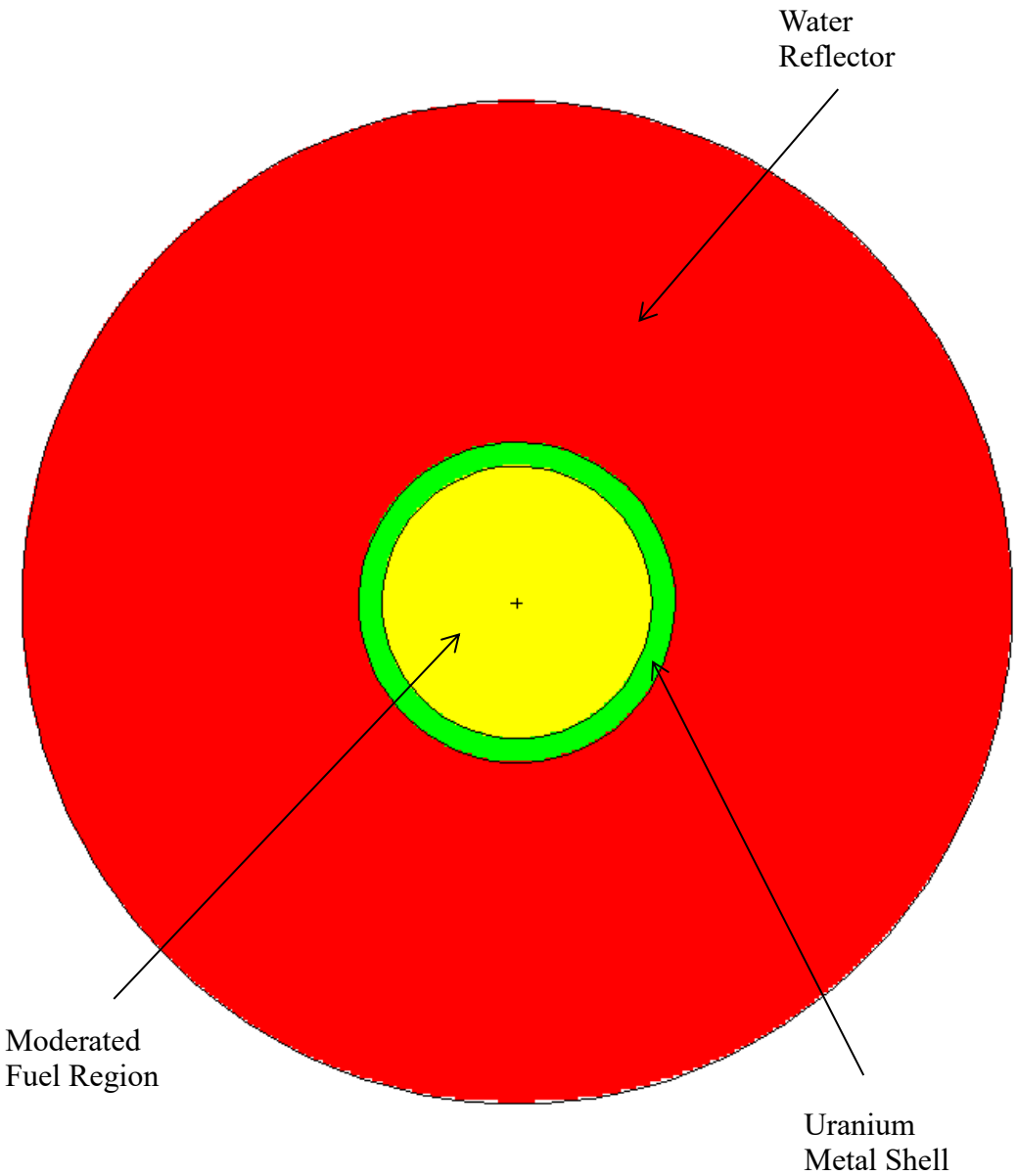

Note: This figure is not to scale. The thickness of the uranium metal shell has been exaggerated for illustrative purposes.

Figure 6.7-3 – Air Transport Model, Two-Region Model

6.8 Benchmark Evaluations

The MCNP, Version 5, Monte Carlo computer code[8] with point-wise ENDF/B-V, -VI, and -VII cross sections has been used extensively in criticality evaluations. The uranium isotopes utilize preliminary ENDF/B-VII cross section data that are considered by Los Alamos National Laboratory to be more accurate than ENDF/B-VI cross sections. ENDF/B-V cross sections are utilized for chromium, nickel, and iron because natural composition ENDF/B-VI cross sections are not available for these elements. The remaining isotopes utilize ENDF/B-VI cross sections. This section justifies the validity of this computation tool and data library combination for application to the ATR FFSC criticality analysis and a bias factor is obtained from these calculations of the critical experiments.

The MCNP code uses room temperature continuous-energy (point-wise) cross sections that are thoroughly documented in Appendix G of the manual. These cross sections are defined with a high-energy resolution that describes each resolved cross section resonance for the isotope. All of the cross-sections used for these analyses were generated from the U.S. Evaluated Nuclear Data Files (ENDF/B).

The validation of the point-wise cross sections is conducted using 35 experimental criticality benchmarks applicable to ATR plate fuels transported in the ATR FFSC. These experiments are supplemented with 21 fast and intermediate spectrum experiments to bound the parameters of the air transport analysis. The statistical analysis of the benchmark experiments results in a USL of 0.9209.

6.8.1 Applicability of Benchmark Experiments

Plate Fuel Analysis

The experimental benchmarks are summarized in the OECD Nuclear Energy Agency's *International Handbook of Evaluated Criticality Safety Benchmark Experiments*[9]. Each experiment is discussed in detail in the *Handbook*. It includes estimates of the uncertainty in the measurements, detailed information regarding dimensions and material compositions, comparisons between the multiplication factor calculated by various computer codes, and a list of input files that were used in their calculations.

The critical experiment benchmarks are selected based upon their similarity to the ATR FFSC and contents. The important selection parameters are high-enriched uranium plate-type fuel with a thermal spectrum. Thirty-five (35) benchmarks that meet these criteria are selected from the *Handbook*. The titles for all utilized experiments are listed in Table 6.8-1. Note that the benchmark from HEU-MET-THERM-022 is for the Advanced Test Reactor itself, so the fuel configuration in this benchmark is essentially the same as the fuel modeled in the packaging analysis.

Ideally, benchmarks would be limited to those with a fuel matrix of UAl_x and aluminum, aluminum cladding, and no absorbers, consistent with the ATR criticality models. Experiment

[8] MCNP5, "*MCNP – A General Monte Carlo N-Particle Transport Code, Version 5; Volume II: User's Guide*," LA-CP-03-0245, Los Alamos National Laboratory, April, 2003.

[9] OECD Nuclear Energy Agency, *International Handbook of Evaluated Criticality Safety Benchmark Experiments*, NEA/NSC/DOC(95)03, September, 2006.

set HEU-MET-THERM-006 consists of 23 benchmark experiments. The first 16 experiments are directly applicable, although experiments 17 and 18 utilize thin cadmium sheets, and experiments 19 through 23 utilize uranium in solution in addition to the fuel plates. Experiment set HEU-COMP-THERM-022 consists of 11 benchmark experiments that utilize UO_2 powder sintered with stainless steel, and stainless steel cladding. Experiments 1 through 5 do not utilize control rods, while experiments 6 through 11 utilize boron control rods. HEU-MET-THERM-022 is a detailed model of the ATR core using explicit ATR fuel elements very similar to the ATR fuel element model utilized in the criticality analysis. However, this full-core model necessarily contains absorber materials. Despite the presence of absorbers, because this benchmark utilizes ATR fuel, it is considered directly applicable to the ATR criticality analysis.

Therefore, of these 35 benchmarks, 17 benchmarks are directly applicable, while 18 benchmarks are applicable to a lesser degree. To compensate for the benchmarks that are not directly applicable, trending will be performed both on all 35 benchmark experiments (Set 1) and on the subset of 17 directly applicable benchmark experiments (Set 2). The USL selected is the minimum of both experimental sets.

Benchmark input files are either obtained from the *Handbook* or directly from Idaho National Laboratory (INL). The only changes made to the input files involve changing to a consistent set of cross section libraries, as needed. Review of the input files indicates that standard MCNP modeling techniques are employed. All but one of the input files consists of simple flat plates in various arrangements. The only benchmark that deviates from simple flat plates is the Advanced Test Reactor full-core model, which is directly applicable to the current analysis. These benchmark input files were developed by INL and have been used extensively for their internal criticality evaluations and are considered to be acceptable. Because the geometry and materials are modeled explicitly, any analyst properly modeling the experimental configuration in MCNP5 would obtain the same result within statistical fluctuation.

Air Transport Analysis

A limited quantity of moderating material is used in the air transport analysis. As a result, the air transport models are closer to an intermediate or fast system and are generally outside the bounds of the plate fuel benchmark experiments described in the preceding paragraphs. Therefore, an additional 21 fast and intermediate benchmark experiments are used to supplement the plate-fuel benchmark experiments. The fast and intermediate benchmark experiments are primarily HEU, consistent with the air transport models.

The fast/intermediate spectrum experiments are summarized in Table 6.8-1. These fast/intermediate spectrum experiments are based upon the OECD Nuclear Energy Agency's *International Handbook of Evaluated Criticality Safety Benchmark Experiments*.

6.8.2 Bias Determination for Plate Fuels

The USL is calculated by application of the USLSTATS computer program[10]. USLSTATS receives as input the k_{eff} as calculated by MCNP, the total 1-σ uncertainty (combined benchmark and MCNP uncertainties), and a trending parameter. Five trending parameters have been selected: (1) Energy of the Average neutron Lethargy causing Fission (EALF), (2) U-235

[10] USLSTATS, "*USLSTATS: A Utility To Calculate Upper Subcritical Limits For Criticality Safety Applications,*" Version 1.4.2, Oak Ridge National Laboratory, April 23, 2003.

number density, (3) channel width, (4) ratio of the number of hydrogen atoms in a unit cell to the number of U-235 atoms in a unit cell (H/U-235), and (5) plate pitch.

The uncertainty value, σ_{total}, assigned to each case is a combination of the benchmark uncertainty for each experiment, σ_{bench}, and the Monte Carlo uncertainty associated with the particular computational evaluation of the case, σ_{MCNP}, or:

$$\sigma_{total} = (\sigma_{bench}^2 + \sigma_{MCNP}^2)^{½}$$

These values are input into the USLSTATS program in addition to the following parameters, which are the values recommended by the USLSTATS user's manual:

- P, proportion of population falling above lower tolerance level = 0.995 (note that this parameter is required input but is not utilized in the calculation of USL Method 1)
- 1-γ, confidence on fit = 0.95
- α, confidence on proportion P = 0.95 (note that this parameter is required input but is not utilized in the calculation of USL Method 1)
- Δk_m, administrative margin used to ensure subcriticality = 0.05.

These data are followed by triplets of trending parameter value, computed k_{eff}, and uncertainty for each case. A confidence band analysis is performed on the data for each trending parameter using USL Method 1. The USL generated for each of the trending parameters utilized is provided in Table 6.8-2. All benchmark data used as input to USLSTATS are reported in Table 6.8-3.

In the following sections, the minimum USL computed for each parameter is identified, and the range of applicability is compared to the fuel element and loose plate models.

6.8.2.1 Energy of the Average neutron Lethargy causing Fission (EALF)

The EALF is used as the first trending parameter for the benchmark cases. The EALF comparison provides a means to observe neutron spectral dependencies or trends. The data for all 35 experiments of Set 1 are plotted in Figure 6.8-1. Over the range of applicability, the minimum USL is 0.9254 for Set 1 and 0.9212 for Set 2.

Range of Applicability, Fuel element models: All of the single package models and most of the NCT and HAC array models fall within the range of the applicability. The EALF of the most reactive fuel element model (Case E23) has an EALF of 1.39E-07 MeV, which is within the range of applicability. Models with significantly more void spaces or low water densities sometimes exceed the range of applicability (maximum EALF = 2.73E-07 MeV for Case E1), although these cases are not the most reactive. Therefore, the EALF of the most reactive models is acceptably within the range of applicability of the benchmarks.

Range of Applicability, Loose plate models: The loose plate analysis is highly moderated, and the EALF of the models fall within the range of applicability of the benchmark experiments with few exceptions. The only cases that fall outside the range of applicability are the very-small pitch cases for Plate 5, because these cases are insufficiently moderated and also thus have low reactivity. Therefore, the EALF is acceptably within the range of applicability of the benchmarks.

6.8.2.2 U-235 Number Density

The U-235 number density is used as the second trending parameter for the benchmark cases. The data for all 35 experiments of Set 1 are plotted in Figure 6.8-2. Over the range of applicability, the minimum USL is 0.9240 for Set 1, and 0.9209 for Set 2.

Range of Applicability, Fuel element models: For the optimized fuel element model, the U-235 number densities for plates 1 through 4 and 16 through 19 fall within the range of applicability, while the number densities for plates 5 through 15 exceed the range of applicability (maximum value = 4.22E-03 atom/b-cm). The maximum range of applicability is 3.92E-03 atom/b-cm, so range is exceeded only slightly. If the minimum USL is extrapolated to this larger number density, the minimum USL of 0.9209 does not change. Also, the average U-235 number density for the fuel element is 3.73E-03 atom/b-cm, which is within the allowable range. Therefore, application of this USL to the fuel element criticality models is considered acceptable.

Range of Applicability, Loose plate models: Of the four plate types modeled, the U-235 number densities for plate type 3 fall within the range of applicability, while the number densities for plate types 5, 8, and 15 exceed the range of applicability (maximum value = 4.29E-03 atom/b-cm). The maximum range of applicability is 3.92E-03 atom/b-cm, so the range is exceeded only slightly. If the minimum USL is extrapolated to this larger number density, the minimum USL of 0.9209 does not change. Therefore, application of this USL to the loose plate basket criticality models is considered acceptable.

6.8.2.3 Channel Width

The channel width is used as the third trending parameter for the benchmark cases. The data for all 35 experiments of Set 1 are plotted in Figure 6.8-3. Over the range of applicability, the minimum USL is 0.9225 for Set 1 and 0.9209 for Set 2.

Range of Applicability, Fuel element models: The channel width is fixed at 0.089-in for the most reactive fuel element models, which exceeds the maximum channel width of 0.078-in of the benchmark experiments. However, this parameter is only slightly larger than the maximum benchmark experiment channel width, and was maximized in order to maximize model reactivity. Extrapolation of the USL to the channel width of 0.089-in yields a USL of 0.9208, which is essentially the same as the minimum USL of 0.9209 over the range of applicability. Therefore, application of this USL to the fuel element criticality models is considered acceptable.

Range of Applicability, Loose plate models: The maximum channel width of the benchmark models is 0.078-in, while the channel width of the most reactive loose plate model is 0.439-in. Clearly, the loose plate models are well outside the bounds of the benchmark models and extrapolation of the USL would not be appropriate over such a wide range. However, the channel width is directly related to system moderation, and the acceptability of the EALF indicator demonstrates that MCNP is performing acceptably for thermal conditions.

6.8.2.4 H/U-235 Atom Ratio

The H/U-235 atom ratio is used as the fourth trending parameter for the benchmark cases. The H/U-235 atom ratio is defined here as the ratio of hydrogen atoms to U-235 atoms in a unit cell. This parameter is computed by the following equation:

NH*C/(NU235*M)

where,

NH is the hydrogen number density

C is the channel width

NU235 is the U-235 number density

M is the fuel meat width

The data for all 35 experiments of Set 1 are plotted in Figure 6.8-4. Over the range of applicability, the minimum USL is 0.9257 for Set 1 and 0.9209 for Set 2.

Range of Applicability, Fuel element models: Using the maximum fuel element plate U-235 number density for the optimized fuel element model, the H/U-235 value may be computed as:

6.687E-02*0.089/(4.224E-03*0.02) = 70.4

Therefore, H/U-235 of the models is acceptably within the range of applicability of the benchmarks.

Range of Applicability, Loose plate models: The H/U-235 atom ratio for the most reactive model may be computed as:

6.687E-02*0.439/(4.2887E-03*0.02) = 342

The maximum H/U-235 atom ratio of the benchmark models is 116.5. Clearly, the loose plate models are well outside the bounds of the benchmark models and extrapolation of the USL would not be appropriate over such a wide range. However, the H/U-235 atom ratio is directly related to system moderation, and the acceptability of the EALF indicator demonstrates that MCNP is performing acceptably for thermal conditions.

6.8.2.5 Pitch

The fuel plate pitch is used as the fifth trending parameter for the benchmark cases. The data for all 35 experiments of Set 1 is plotted in Figure 6.8-5. Over the range of applicability, the minimum USL is 0.9225 for Set 1 and 0.9209 for Set 2.

Range of Applicability, Fuel element models: The fuel plate pitch is fixed at 0.128-in for all fuel element models (excluding the pitch for plates 1 and 19, which is slightly bigger because these plates are thicker). This pitch falls within the range of the benchmark experiments.

Range of Applicability, Loose plate models: The maximum pitch of the benchmark models is 0.128-in, while the pitch of the most reactive loose plate model is 0.487-in (1.236 cm). Clearly, the loose plate models are well outside the bounds of the benchmark models and extrapolation of the USL would not be appropriate over such a wide range. However, the pitch is directly related to system moderation, and the acceptability of the EALF indicator demonstrates that MCNP is performing acceptably for thermal conditions.

6.8.2.6 Recommended USL

For Set 1, the minimum USL is 0.9225, while for Set 2, the minimum USL is 0.9209. Therefore, the USL is trending lower for Set 2. Note, however, that the average k_{eff} = 0.992 for both Set 1 and Set 2. The USL could likely be improved by development of additional benchmark models,

but given the large margins to the most reactive case, the lower value (0.9209) is conservatively selected as the USL for the plate fuel analysis.

6.8.3 Bias Determination for Air Transport Analysis

Only the EALF parameter is considered for the air transport benchmark analysis because the other trending parameters used in the plate fuel analysis are generally not applicable to either fast/intermediate systems or the air transport models.

Corresponding data for the fast/intermediate spectrum experiments are summarized in Table 6.8-4. In the plate-fuel benchmarks, the experiments are divided into two sets, a total set of 35 benchmarks (Set 1) and a subset of 17 directly applicable benchmarks (Set 2). These groupings are continued when the fast/intermediate experiments are added:

1. Set 3: All 56 experiments (35 plate-fuel benchmark experiments and 21 fast/intermediate benchmark experiments)
2. Set 4: 17 directly applicable plate-fuel benchmarks experiments and 21 fast/intermediate benchmark experiments.
3. Set 5: 21 fast/intermediate benchmark experiments.

The USL is computed for each of the three sets of experiments, and the results are summarized in Table 6.8-2. When the fast/intermediate spectrum experiments are included, the minimum USL over the range of applicability is 0.9260, 0.9254, and 0.9248 for the three sets considered. These USLs are larger than the minimum USL when the fast/intermediate spectrum experiments are not included (0.9209). Therefore, it is conservative to use a USL of 0.9209 for the air transport analysis.

The range of applicability for EALF over all benchmark experiments is 5.2221×10^{-8} MeV $\leq$ EALF $\leq$ 0.83695 MeV. The EALF values extracted from the air transport output files are in the range 2.43×10^{-7} MeV $\leq$ EALF $\leq$ 8.08×10^{-3} MeV. Therefore, all air transport cases are within the range of applicability of the benchmark experiments for the EALF parameter.

Table 6.8-1 – Benchmark Experiments Utilized

Series	Title
Thermal Plate Fuel Benchmarks	
HEU-COMP-THERM-022	SPERT III Stainless-Steel-Clad Plate-Type Fuel in Water
HEU-MET-THERM-006	SPERT-D Aluminum-Clad Plate-Type Fuel in Water, Dilute Uranyl Nitrate, or Borated Uranyl Nitrate
HEU-MET-THERM-022	Advanced Test Reactor: Serpentine Arrangement of Highly Enriched Water-Moderated Uranium-Aluminide Fuel Plates Reflected by Beryllium
Intermediate and Fast Benchmarks	
HEU-MET-FAST-023 (case 16)	Tinkertoy: Unmoderated Uranium Metal (93.2) Arrays With Cylinders of 10.5 Kg Mass
HEU-MET-FAST-032 (case 1)	^{235}U(94%) Spheres Surrounded by Natural-Uranium Reflectors
HEU-MET-FAST-043 (case 1)	HEU Cylinders Axially Reflected by Steel
HEU-MET-FAST-072 (first configuration)	Zeus: Fast-Spectrum Critical Assemblies With An Iron - HEU Core Surrounded By A Copper Reflector
HEU-MET-FAST-076 (cases 5, 8, 12, 16)	Uranium (93.14 ^{235}U) Metal Annuli and Cylinders With Thick Polyethylene Reflectors and/or Internal Polyethylene Moderator
HEU-MET-FAST-078 (case 1, 41)	HEU Metal Cylinders, Partially Reflected by Water, Polyethylene, Lucite, and Paraffin
HEU-MET-FAST-084 (case 7, 19)	HEU Metal Cylinders With Magnesium, Titanium, Aluminum, Graphite, Mild Steel, Nickel, Copper, Cobalt, Molybdenum, Natural Uranium, Tungsten, Beryllium, Aluminum Oxide, Molybdenum Carbide, and Polyethylene Reflectors
HEU-MET-FAST-087 (case 1)	Heterogeneous Iron-Diluted HEU Cylinder
HEU-MET-INTER-001 (case 1)	The Uranium/Iron Benchmark Assembly: A ^{235}U(93%)/Iron Cylinder Reflected by Stainless Steel
HEU-MET-MIXED-010 (case 3)	Lattices of Oralloy Cubes In Water
HEU-MET-MIXED-011 (case 4, 5)	Oil-Reflected Spheres and Hemispheres of Highly Enriched Uranium (93.1% ^{235}U) Metal with Oil or Steel Moderator
HEU-MET-MIXED-015 (case 1)	Heterogeneous Cylinder of Highly Enriched Uranium, Polyethylene, and Titanium With Polyethylene Reflector
HEU-MET-THERM-025 (case CA-1)	Beryllium Moderated Critical Assemblies of Highly Enriched Uranium (ORNL CA-1 and CA-18)
IEU-MET-FAST-005 (case 1)	Steel-Reflected Spherical Assembly of ^{235}U(36%)
IEU-MET-FAST-021 (case 1)	The FR0 Series 4: 20% Enriched "Cylindrical" Uranium Metal Reflected by Natural Uranium

Table 6.8-2 – USL Results

Trending Parameter (X)	Minimum USL Over Range of Applicability	Range of Applicability
Set 1: 35 Thermal Plate-Fuel Experiments		
EALF (MeV)	0.9254	5.22210E-08 <= X <= 1.58510E-07
U-235 Number Density (atom/b-cm)	0.9240	1.84900E-03 <= X <= 3.92600E-03
Channel width (in)	0.9225	6.45700E-02 <= X <= 7.80000E-02
H/U-235	0.9257	65.100 <= X <= 116.50
Pitch (in)	0.9225	0.12457 <= X <= 0.12800
Set 2: 17 Directly Applicable Thermal Plate-Fuel Experiments		
EALF (MeV)	0.9212	5.22210E-08 <= X <= 1.58510E-07
U-235 Number Density (atom/b-cm)	0.9209	1.84900E-03 <= X <= 3.92600E-03
Channel width (in)	0.9209	6.45700E-02 <= X <= 7.80000E-02
H/U-235	0.9209	66.0 <= X <= 116.50
Pitch (in)	0.9209	0.12457 <= X <= 0.12800
Set 3: 35 Thermal Plate-Fuel Experiments plus 21 Fast/Intermediate Experiments		
EALF (MeV)	0.9260	5.2221E-08 <= X <= 0.83695
Set 4: 17 Directly Applicable Thermal Plate-Fuel Experiments plus 21 Fast/Intermediate Experiments		
EALF (MeV)	0.9254	5.2221E-08 <= X <= 0.83695
Set 5: 21 Fast/Intermediate Experiments		
EALF (MeV)	0.9248	2.8058E-06 <= X <= 0.83695

Table 6.8-3 – Benchmark Experiment Data, Plate Fuels

No	Case	k	σ_{mcnp}	σ_{bench}	σ_{total}	EALF (MeV)	U-235 (atom/b-cm)	Chanel Width (in)	H/U-235	Pitch (in)
1	hct022_c01	0.98895	0.00060	0.0081	0.0081	9.528E-08	3.3155E-03	0.06457	65.1	0.12457
2	hct022_c02	0.98980	0.00061	0.0081	0.0081	9.665E-08	3.3155E-03	0.06457	65.1	0.12457
3	hct022_c03	0.98985	0.00063	0.0081	0.0081	9.809E-08	3.3155E-03	0.06457	65.1	0.12457
4	hct022_c04	0.98856	0.00060	0.0081	0.0081	9.917E-08	3.3155E-03	0.06457	65.1	0.12457
5	hct022_c05	0.98909	0.00063	0.0081	0.0081	9.587E-08	3.3155E-03	0.06457	65.1	0.12457
6	hct022_c06	0.98902	0.00059	0.0081	0.0081	9.840E-08	3.3155E-03	0.06457	65.1	0.12457
7	hct022_c07	0.98963	0.00056	0.0081	0.0081	9.890E-08	3.3155E-03	0.06457	65.1	0.12457
8	hct022_c08	0.98908	0.00057	0.0081	0.0081	9.951E-08	3.3155E-03	0.06457	65.1	0.12457
9	hct022_c09	0.98840	0.00056	0.0081	0.0081	9.589E-08	3.3155E-03	0.06457	65.1	0.12457
10	hct022_c10	0.98845	0.00060	0.0081	0.0081	9.963E-08	3.3155E-03	0.06457	65.1	0.12457
11	hct022_c11	0.98930	0.00060	0.0081	0.0081	1.001E-07	3.3155E-03	0.06457	65.1	0.12457
12	hmt006_c01	0.99240	0.00082	0.0044	0.0045	8.481E-08	1.8490E-03	0.06457	116.5	0.12457
13	hmt006_c02	0.99331	0.00088	0.0040	0.0041	7.044E-08	1.8490E-03	0.06457	116.5	0.12457
14	hmt006_c03	0.99740	0.00072	0.0040	0.0041	6.338E-08	1.8490E-03	0.06457	116.5	0.12457
15	hmt006_c04	0.99282	0.00081	0.0040	0.0041	6.185E-08	1.8490E-03	0.06457	116.5	0.12457
16	hmt006_c05	0.99230	0.00079	0.0040	0.0041	5.852E-08	1.8490E-03	0.06457	116.5	0.12457
17	hmt006_c06	0.99010	0.00071	0.0040	0.0041	5.615E-08	1.8490E-03	0.06457	116.5	0.12457
18	hmt006_c07	0.98783	0.00073	0.0040	0.0041	5.432E-08	1.8490E-03	0.06457	116.5	0.12457
19	hmt006_c08	0.98428	0.00076	0.0040	0.0041	5.245E-08	1.8490E-03	0.06457	116.5	0.12457
20	hmt006_c09	0.98657	0.00072	0.0040	0.0041	5.222E-08	1.8490E-03	0.06457	116.5	0.12457
21	hmt006_c10	0.99885	0.00085	0.0040	0.0041	8.220E-08	1.8490E-03	0.06457	116.5	0.12457
22	hmt006_c11	0.98965	0.00081	0.0040	0.0041	6.236E-08	1.8490E-03	0.06457	116.5	0.12457
23	hmt006_c12	0.99403	0.00070	0.0040	0.0041	5.415E-08	1.8490E-03	0.06457	116.5	0.12457
24	hmt006_c13	1.01283	0.00086	0.0061	0.0062	8.231E-08	1.8490E-03	0.06457	116.5	0.12457
25	hmt006_c14	0.98495	0.00071	0.0040	0.0041	5.715E-08	1.8490E-03	0.06457	116.5	0.12457

(continued)

Table 6.8-3 – Benchmark Experiment Data, Plate Fuels (concluded)

No	Case	k	σ_{mcnp}	σ_{bench}	σ_{total}	EALF (MeV)	U-235 (atom/b-cm)	Chanel Width (in)	H/U-235	Pitch (in)
26	hmt006_c15	0.98128	0.00077	0.0040	0.0041	5.654E-08	1.8490E-03	0.06457	116.5	0.12457
27	hmt006_c16	0.99241	0.00078	0.0040	0.0041	6.330E-08	1.8490E-03	0.06457	116.5	0.12457
28	hmt006_c17	0.98934	0.00082	0.0040	0.0041	7.405E-08	1.8490E-03	0.06457	116.5	0.12457
29	hmt006_c18	0.99282	0.00087	0.0040	0.0041	8.003E-08	1.8490E-03	0.06457	116.5	0.12457
30	hmt006_c19	0.99360	0.00068	0.0040	0.0041	5.243E-08	1.8490E-03	0.06457	113.9	0.12457
31	hmt006_c20	0.99275	0.00076	0.0040	0.0041	6.471E-08	1.8490E-03	0.06457	113.7	0.12457
32	hmt006_c21	0.99469	0.00077	0.0040	0.0041	6.917E-08	1.8490E-03	0.06457	113.7	0.12457
33	hmt006_c22	0.99670	0.00080	0.0040	0.0041	7.407E-08	1.8490E-03	0.06457	113.6	0.12457
34	hmt006_c23	1.00132	0.00080	0.0040	0.0041	7.670E-08	1.8490E-03	0.06457	113.5	0.12457
35	hmt022_c01	0.99179	0.00013	0.0035	0.0035	1.585E-07	3.9260E-03	0.078	66.0	0.12800

Table 6.8-4 – Benchmark Experiment Data, Fast/Intermediate

No	Case	k	σ_{mcnp}	σ_{bench}	σ_{total}	EALF (MeV)
1	HEU-MET-FAST-023, case 16	0.99687	0.00056	0.0052	0.0052	8.113E-01
2	HEU-MET-FAST-032 case 1	1.00427	0.00064	0.0016	0.0017	7.736E-01
3	HEU-MET-FAST-043, case 1	1.00096	0.00059	0.0018	0.0019	7.940E-01
4	HEU-MET-FAST-072, configuration 1	1.00516	0.00065	0.0024	0.0025	4.280E-02
5	HEU-MET-FAST-076, case 5	0.99978	0.00084	0.0006	0.0010	2.560E-03
6	HEU-MET-FAST-076, case 8	0.99814	0.00078	0.0004	0.0009	1.010E-02
7	HEU-MET-FAST-076, case 12	0.99627	0.00076	0.0002	0.0008	5.805E-03
8	HEU-MET-FAST-076, case 16	0.99948	0.00077	0.0005	0.0009	5.410E-03
9	HEU-MET-FAST-078, case 1	0.99209	0.00082	0.0018	0.0020	8.613E-02
10	HEU-MET-FAST-078, case 41	0.99627	0.00061	0.0025	0.0026	8.370E-01
11	HEU-MET-FAST-084, case 19	0.99849	0.00060	0.0019	0.0020	8.016E-01
12	HEU-MET-FAST-084, case 7	1.01966	0.00060	0.0020	0.0021	7.736E-01
13	HEU-MET-FAST-087, case 1	0.99887	0.00060	0.0013	0.0014	7.515E-01
14	HEU-MET-INTER-001, case 1	0.96645	0.00055	0.0026	0.0027	3.908E-02
15	HEU-MET-MIXED-010, case 3	0.97677	0.00072	0.0060	0.0060	1.964E-04
16	HEU-MET-MIXED-011, case 4	1.00179	0.00076	0.0030	0.0031	6.898E-04
17	HEU-MET-MIXED-011, case 5	0.99317	0.00074	0.0041	0.0042	3.530E-04
18	HEU-MET-MIXED-015, case 1	0.99920	0.00080	0.0008	0.0011	9.683E-05
19	HEU-MET-THERM-025, case CA-1	1.01340	0.00109	0.0047	0.0048	2.806E-06
20	IEU-MET-FAST-005, case 1	1.00822	0.00062	0.0023	0.0024	5.738E-01
21	IEU-MET-FAST-021, case 1	1.00471	0.00060	0.00145	0.0016	4.800E-01

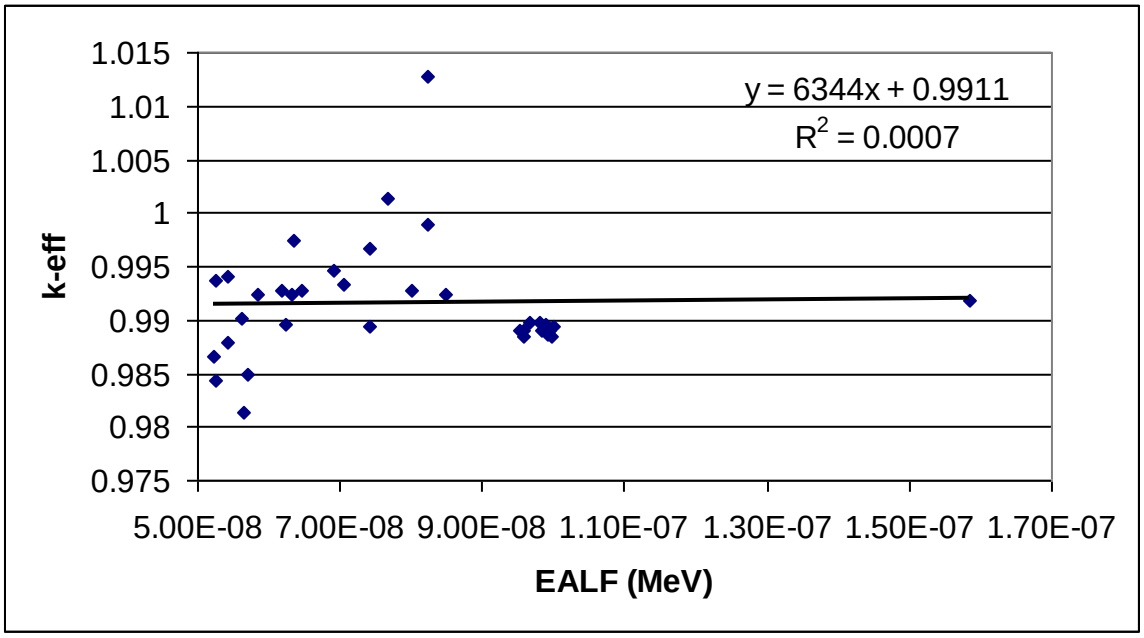

Figure 6.8-1 – Benchmark Data Trend for EALF, Set 1

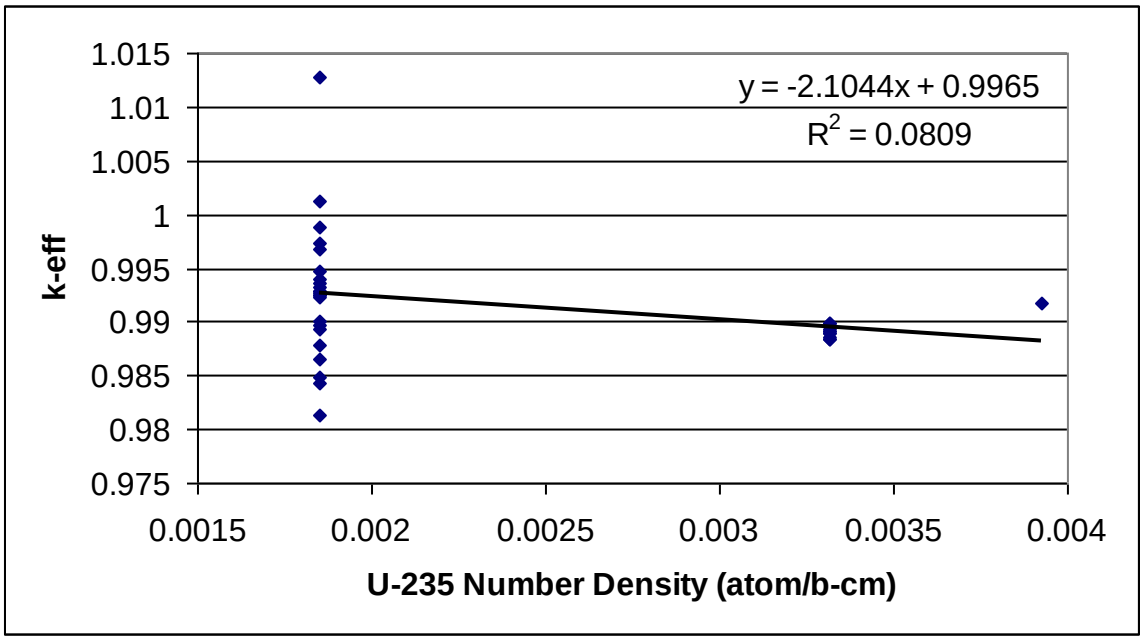

Figure 6.8-2 – Benchmark Data Trend for U-235 Number Density, Set 1

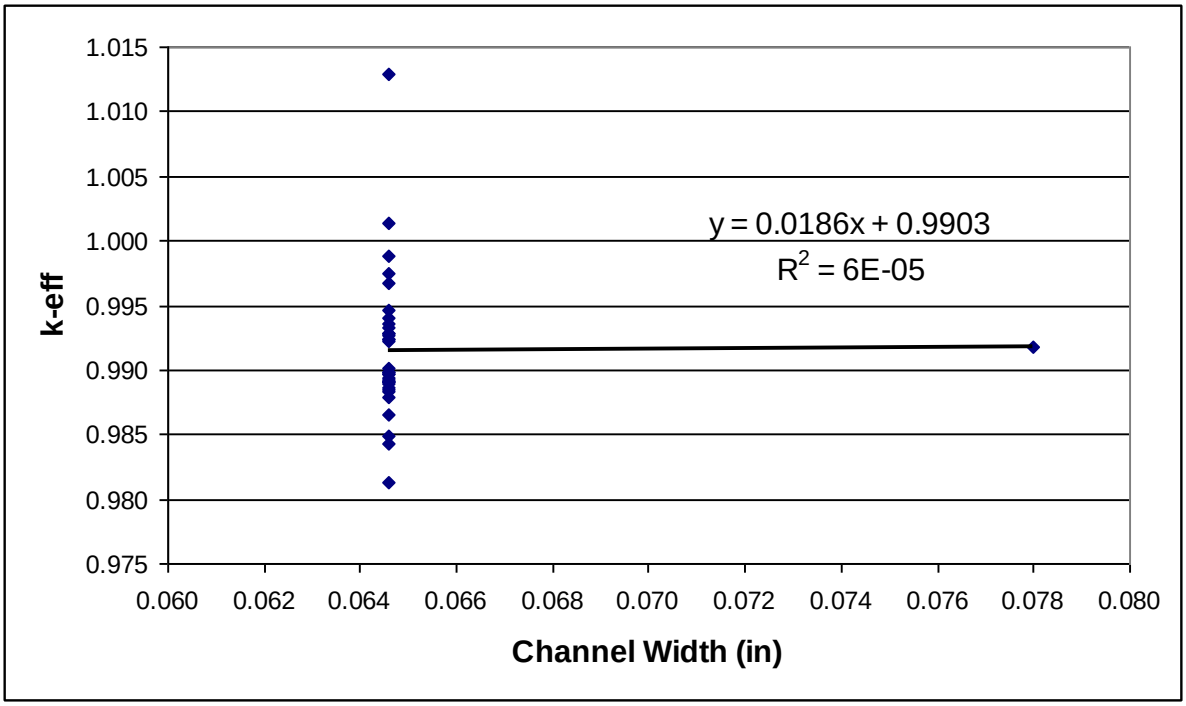

Figure 6.8-3 – Benchmark Data Trend for Channel Width, Set 1

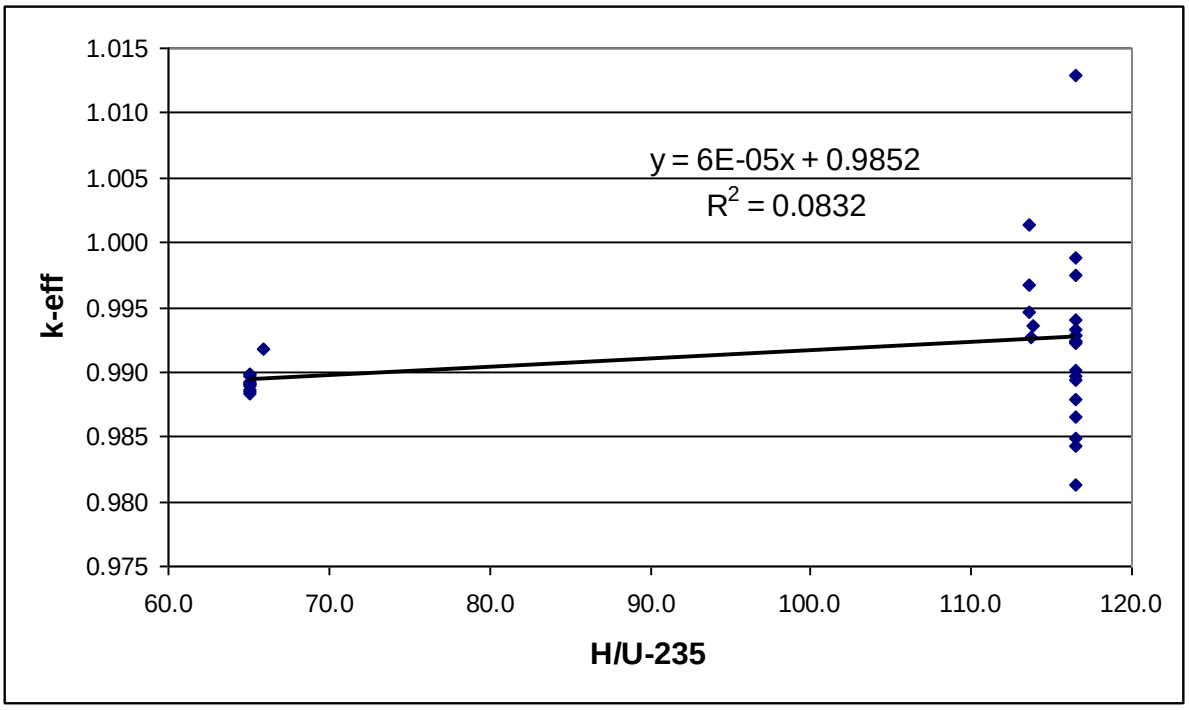

Figure 6.8-4 – Benchmark Data Trend for H/U-235, Set 1

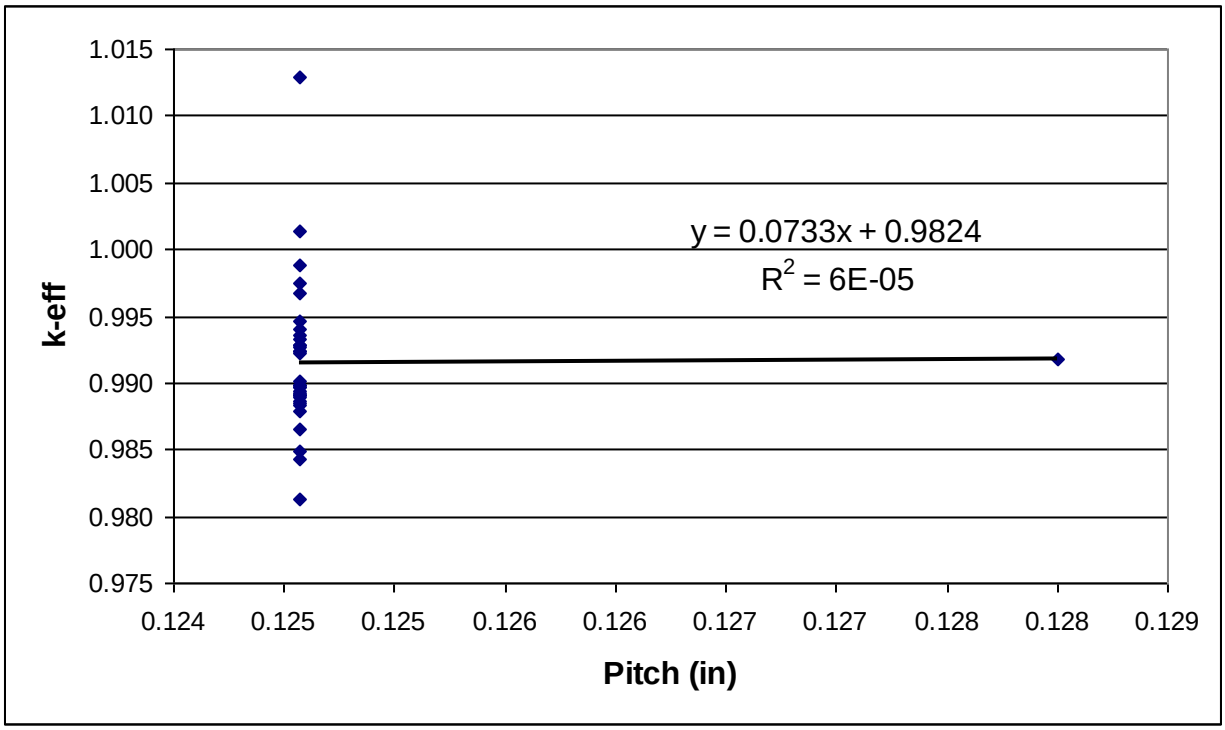

Figure 6.8-5 – Benchmark Data Trend for Pitch, Set 1

6.9 Appendix A: Sample Input Files

Sample input files are provided for the most reactive NCT array case for both the fuel element payload (Case E23) and the loose plate basket payload (Case LG5).

Case E23 (NA_P030_C89)

```
ATR
999     0      -320:321:-322:323:-324:325                imp:n=0
900     0      310 -311 312 -313 24 -25     fill=3       imp:n=1
901     2 -1.0 (311:-310:313:-312:-24:25) 320 -321 322 -323 324 -325  imp:n=1
c
c       Universe 1: ATR Fuel Element (infinitely long)
c
2       3 -2.7         -6 8 9 -10                u=1 imp:n=1 $ left Al piece
4       3 -2.7         -5 7 9 -10                u=1 imp:n=1 $ right Al piece
6       10 5.5010E-02  52 -53 -14 -13            u=1 imp:n=1 $ plate 1
8       3 -2.7         51 -54   -7 -8       #6   u=1 imp:n=1
10      2 -1.00        54 -55   -7 -8            u=1 imp:n=1
12      11 5.4998E-02  56 -57 -16 -15            u=1 imp:n=1 $ plate 2
14      3 -2.7         55 -58   -7 -8       #12  u=1 imp:n=1
16      2 -1.00        58 -59   -7 -8            u=1 imp:n=1
18      12 5.4574E-02  60 -61 -16 -15            u=1 imp:n=1 $ plate 3
20      3 -2.7         59 -62   -7 -8       #18  u=1 imp:n=1
22      2 -1.00        62 -63   -7 -8            u=1 imp:n=1
24      13 5.4583E-02  64 -65 -16 -15            u=1 imp:n=1 $ plate 4
26      3 -2.7         63 -66   -7 -8       #24  u=1 imp:n=1
28      2 -1.00        66 -67   -7 -8            u=1 imp:n=1
30      14 5.4115E-02  68 -69 -16 -15            u=1 imp:n=1 $ plate 5
32      3 -2.7         67 -70   -7 -8       #30  u=1 imp:n=1
34      2 -1.00        70 -71   -7 -8            u=1 imp:n=1
36      15 5.4106E-02  72 -73 -16 -15            u=1 imp:n=1 $ plate 6
38      3 -2.7         71 -74   -7 -8       #36  u=1 imp:n=1
40      2 -1.00        74 -75   -7 -8            u=1 imp:n=1
42      16 5.4102E-02  76 -77 -16 -15            u=1 imp:n=1 $ plate 7
44      3 -2.7         75 -78   -7 -8       #42  u=1 imp:n=1
46      2 -1.00        78 -79   -7 -8            u=1 imp:n=1
48      17 5.4098E-02  80 -81 -16 -15            u=1 imp:n=1 $ plate 8
50      3 -2.7         79 -82   -7 -8       #48  u=1 imp:n=1
52      2 -1.00        82 -83   -7 -8            u=1 imp:n=1
54      18 5.4095E-02  84 -85 -16 -15            u=1 imp:n=1 $ plate 9
56      3 -2.7         83 -86   -7 -8       #54  u=1 imp:n=1
58      2 -1.00        86 -87   -7 -8            u=1 imp:n=1
60      19 5.4092E-02  88 -89 -16 -15            u=1 imp:n=1 $ plate 10
62      3 -2.7         87 -90   -7 -8       #60  u=1 imp:n=1
64      2 -1.00        90 -91   -7 -8            u=1 imp:n=1
66      20 5.4089E-02  92 -93 -16 -15            u=1 imp:n=1 $ plate 11
68      3 -2.7         91 -94   -7 -8       #66  u=1 imp:n=1
70      2 -1.00        94 -95   -7 -8            u=1 imp:n=1
72      21 5.4086E-02  96 -97 -16 -15            u=1 imp:n=1 $ plate 12
74      3 -2.7         95 -98   -7 -8       #72  u=1 imp:n=1
76      2 -1.00        98 -99   -7 -8            u=1 imp:n=1
78      22 5.4083E-02  100 -101 -16 -15          u=1 imp:n=1 $ plate 13
80      3 -2.7          99 -102   -7 -8     #78  u=1 imp:n=1
82      2 -1.00        102 -103   -7 -8          u=1 imp:n=1
84      23 5.4081E-02  104 -105 -16 -15          u=1 imp:n=1 $ plate 14
```

```
86      3 -2.7         103 -106   -7 -8     #84  u=1 imp:n=1
88      2 -1.00        106 -107   -7 -8          u=1 imp:n=1
90      24 5.4075E-02  108 -109 -16 -15          u=1 imp:n=1 $ plate 15
92      3 -2.7         107 -110   -7 -8     #90  u=1 imp:n=1
94      2 -1.00        110 -111   -7 -8          u=1 imp:n=1
96      25 5.4544E-02  112 -113 -16 -15          u=1 imp:n=1 $ plate 16
98      3 -2.7         111 -114   -7 -8     #96  u=1 imp:n=1
100     2 -1.00        114 -115   -7 -8          u=1 imp:n=1
102     26 5.4544E-02  116 -117 -16 -15          u=1 imp:n=1 $ plate 17
104     3 -2.7         115 -118   -7 -8     #102 u=1 imp:n=1
106     2 -1.00        118 -119   -7 -8          u=1 imp:n=1
108     27 5.4949E-02  120 -121 -18 -17          u=1 imp:n=1 $ plate 18
110     3 -2.7         119 -122   -7 -8     #108 u=1 imp:n=1
112     2 -1.00        122 -123   -7 -8          u=1 imp:n=1
114     28 5.4967E-02  124 -125 -14 -13          u=1 imp:n=1 $ plate 19
116     3 -2.7         123 -126   -7 -8     #114 u=1 imp:n=1
c 122     2 -1.00       6:5:-9:10:9 -51 -8 -7:126 -10 -8 -7 u=1 imp:n=1
120     2 -1.00        126 -10 -8 -7             u=1 imp:n=1 $ above 19
121     2 -1.00        9 -51 -8 -7               u=1 imp:n=1 $ below 1
122     5 -0.737       5 -11 9 -10               u=1 imp:n=1 $ right neoprene
123     5 -0.737     -12 6 9 -10                 u=1 imp:n=1 $ left neoprene
125     2 -1.0        12:11:-9:10                u=1 imp:n=1
c
c       Universe 20: ATR with pipe (center)
c
200     0  -27 -26 22 -23:26 -20 22 -28:27 -21 22 -28  trcl=1
             fill=1  u=20 imp:n=1
201     2 -0.3     #200 -200                   u=20 imp:n=1 $ between
ATR/pipe
202     4 -7.94     200 -201                   u=20 imp:n=1 $ pipe
203     6 -0.096    201 -203 250 -251 252 -253 u=20 imp:n=1 $ insulation
204     0           203 250 -251 252 -253      u=20 imp:n=1 $ insulation to
tube
205     4 -7.94     -250:251:-252:253          u=20 imp:n=1 $ tube to inf
c
c       Universe 21: ATR with pipe (down)
c
210     0  -27 -26 22 -23:26 -20 22 -28:27 -21 22 -28  trcl=2
             fill=1  u=21 imp:n=1
211     2 -0.3     #210 -200                   u=21 imp:n=1 $ between
ATR/pipe
212     4 -7.94     200 -201                   u=21 imp:n=1 $ pipe
213     6 -0.096    201 -203 250 -251 252 -253 u=21 imp:n=1 $ insulation
214     0           203 250 -251 252 -253      u=21 imp:n=1 $ insulation to
tube
215     4 -7.94     -250:251:-252:253          u=21 imp:n=1 $ tube to inf
c
c       Universe 22: ATR with pipe (up)
c
220     0  -27 -26 22 -23:26 -20 22 -28:27 -21 22 -28  trcl=3
             fill=1  u=22 imp:n=1
221     2 -0.3     #220 -200                   u=22 imp:n=1 $ between
ATR/pipe
222     4 -7.94     200 -201                   u=22 imp:n=1 $ pipe
223     6 -0.096    201 -203 250 -251 252 -253 u=22 imp:n=1 $ insulation
224     0           203 250 -251 252 -253      u=22 imp:n=1 $ insulation to
tube
```

```
225     4 -7.94     -250:251:-252:253          u=22 imp:n=1 $ tube to inf
c
c       Universe 23: ATR with pipe (right)
c
230     0  -27 -26 22 -23:26 -20 22 -28:27 -21 22 -28  trcl=4
             fill=1  u=23 imp:n=1
231     2 -0.3     #230 -200                   u=23 imp:n=1 $ between
ATR/pipe
232     4 -7.94     200 -201                   u=23 imp:n=1 $ pipe
233     6 -0.096    201 -203 250 -251 252 -253 u=23 imp:n=1 $ insulation
234     0           203 250 -251 252 -253      u=23 imp:n=1 $ insulation to
tube
235     4 -7.94     -250:251:-252:253          u=23 imp:n=1 $ tube to inf
c
c       Universe 24: ATR with pipe (left)
c
240     0  -27 -26 22 -23:26 -20 22 -28:27 -21 22 -28  trcl=5
             fill=1  u=24 imp:n=1
241     2 -0.3     #240 -200                   u=24 imp:n=1 $ between
ATR/pipe
242     4 -7.94     200 -201                   u=24 imp:n=1 $ pipe
243     6 -0.096    201 -203 250 -251 252 -253 u=24 imp:n=1 $ insulation
244     0           203 250 -251 252 -253      u=24 imp:n=1 $ insulation to
tube
245     4 -7.94     -250:251:-252:253          u=24 imp:n=1 $ tube to inf
c
c       Universe 25: ATR with pipe (up right)
c
250     0  -27 -26 22 -23:26 -20 22 -28:27 -21 22 -28  trcl=6
             fill=1  u=25 imp:n=1
251     2 -0.3     #250 -200                   u=25 imp:n=1 $ between
ATR/pipe
252     4 -7.94     200 -201                   u=25 imp:n=1 $ pipe
253     6 -0.096    201 -203 250 -251 252 -253 u=25 imp:n=1 $ insulation
254     0           203 250 -251 252 -253      u=25 imp:n=1 $ insulation to
tube
255     4 -7.94     -250:251:-252:253          u=25 imp:n=1 $ tube to inf
c
c       Universe 26: ATR with pipe (up left)
c
260     0  -27 -26 22 -23:26 -20 22 -28:27 -21 22 -28  trcl=7
             fill=1  u=26 imp:n=1
261     2 -0.3     #260 -200                   u=26 imp:n=1 $ between
ATR/pipe
262     4 -7.94     200 -201                   u=26 imp:n=1 $ pipe
263     6 -0.096    201 -203 250 -251 252 -253 u=26 imp:n=1 $ insulation
264     0           203 250 -251 252 -253      u=26 imp:n=1 $ insulation to
tube
265     4 -7.94     -250:251:-252:253          u=26 imp:n=1 $ tube to inf
c
c       Universe 27: ATR with pipe (down right)
c
270     0  -27 -26 22 -23:26 -20 22 -28:27 -21 22 -28  trcl=8
             fill=1  u=27 imp:n=1
271     2 -0.3     #270 -200                   u=27 imp:n=1 $ between
ATR/pipe
272     4 -7.94     200 -201                   u=27 imp:n=1 $ pipe
```

```
273     6 -0.096    201 -203 250 -251 252 -253 u=27 imp:n=1 $ insulation
274     0           203 250 -251 252 -253      u=27 imp:n=1 $ insulation to
tube
275     4 -7.94     -250:251:-252:253          u=27 imp:n=1 $ tube to inf
c
c       Universe 28: ATR with pipe (down left)
c
280     0  -27 -26 22 -23:26 -20 22 -28:27 -21 22 -28  trcl=9
             fill=1  u=28 imp:n=1
281     2 -0.3     #280 -200                   u=28 imp:n=1 $ between
ATR/pipe
282     4 -7.94     200 -201                   u=28 imp:n=1 $ pipe
283     6 -0.096    201 -203 250 -251 252 -253 u=28 imp:n=1 $ insulation
284     0           203 250 -251 252 -253      u=28 imp:n=1 $ insulation to
tube
285     4 -7.94     -250:251:-252:253          u=28 imp:n=1 $ tube to inf
c
c       Universe 3: Array of Packages
c
300   0    -300 301 -302 303 imp:n=1 u=3 lat=1 fill=-4:4 -4:4 0:0
             25 25 25 25 22 26 26 26 26
             25 25 25 25 22 26 26 26 26
             25 25 25 25 22 26 26 26 26
             25 25 25 25 22 26 26 26 26
             23 23 23 23 20 24 24 24 24
             27 27 27 27 21 28 28 28 28
             27 27 27 27 21 28 28 28 28
             27 27 27 27 21 28 28 28 28
             27 27 27 27 21 28 28 28 28

5       p  2.4142136 -1 0 -0.2665911 $ right Al outer
6       p -2.4142136 -1 0 -0.2665911 $ left Al outer
7       p  2.4142136 -1 0 -1.474587  $ right Al inner
8       p -2.4142136 -1 0 -1.474587  $ left Al inner
9       cz 7.52856                   $ Al boundary
10      cz 14.015466                 $ Al boundary
11      p  2.4142136 -1 0  0.563076  $ right neoprene
12      p -2.4142136 -1 0  0.563076  $ left neoprene
c
13      p  2.4142136 -1 0 -2.4370013 $ plate 1 & 19 meat
14      p -2.4142136 -1 0 -2.4370013 $ plate 1 & 19 meat
15      p  2.4142136 -1 0 -1.7732672 $ plate 2-17 meat
16      p -2.4142136 -1 0 -1.7732672 $ plate 2-17 meat
17      p  2.4142136 -1 0 -1.9060140 $ plate 18 meat
18      p -2.4142136 -1 0 -1.9060140 $ plate 18 meat
c
20      p  2.4142136 -1 0   0.6      $ right u0 boundary
21      p -2.4142136 -1 0   0.6      $ left u0 boundary
22      cz 7.51                      $ u0 boundary
23      cz 14.02                     $ u0 boundary
24      pz -60.96                    $ bottom of fuel
25      pz  60.96                    $ top of fuel (48")
26      p  2.4142136 -1 0  0.0       $ neoprene notch
27      p -2.4142136 -1 0  0.0       $ neoprene notch
28      cz 13.9                      $ neoprene notch
c
51      cz 7.67207  $ fuel plate 1 (0.089)
```

```
52      cz 7.7343
53      cz 7.7851
54      cz 7.84733
c
55      cz 8.07339  $ fuel plate 2
56      cz 8.09752
57      cz 8.14832
58      cz 8.17245
c
59      cz 8.39851  $ fuel plate 3
60      cz 8.42264
61      cz 8.47344
62      cz 8.49757
c
63      cz 8.72363  $ fuel plate 4
64      cz 8.74776
65      cz 8.79856
66      cz 8.82269
c
67      cz 9.04875  $ fuel plate 5
68      cz 9.07288
69      cz 9.12368
70      cz 9.14781
c
71      cz 9.37387  $ fuel plate 6
72      cz 9.398
73      cz 9.4488
74      cz 9.47293
c
75      cz 9.69899  $ fuel plate 7
76      cz 9.72312
77      cz 9.77392
78      cz 9.79805
c
79      cz 10.02411  $ fuel plate 8
80      cz 10.04824
81      cz 10.09904
82      cz 10.12317
c
83      cz 10.34923  $ fuel plate 9
84      cz 10.37336
85      cz 10.42416
86      cz 10.44829
c
87      cz 10.67435  $ fuel plate 10
88      cz 10.69848
89      cz 10.74928
90      cz 10.77341
c
91      cz 10.99947  $ fuel plate 11
92      cz 11.0236
93      cz 11.0744
94      cz 11.09853
c
95      cz 11.32459  $ fuel plate 12
96      cz 11.34872
97      cz 11.39952
```

```
98      cz 11.42365
c
99       cz 11.64971  $ fuel plate 13
100      cz 11.67384
101      cz 11.72464
102      cz 11.74877
c
103      cz 11.97483  $ fuel plate 14
104      cz 11.99896
105      cz 12.04976
106      cz 12.07389
c
107      cz 12.29995  $ fuel plate 15
108      cz 12.32408
109      cz 12.37488
110      cz 12.39901
c
111      cz 12.62507  $ fuel plate 16
112      cz 12.6492
113      cz 12.7
114      cz 12.72413
c
115      cz 12.95019  $ fuel plate 17
116      cz 12.97432
117      cz 13.02512
118      cz 13.04925
c
119      cz 13.27531  $ fuel plate 18
120      cz 13.29944
121      cz 13.35024
122      cz 13.37437
c
123      cz 13.60043  $ fuel plate 19 (0.089)
124      cz 13.68806
125      cz 13.73886
126      cz 13.82649
c
200      cz 7.3838 $ IR pipe
201      cz 7.6581 $ OR pipe
202      cz 38.1   $ 12" water
203      cz 10.1981 $ 1" insulation
c
250      px  -9.6032 $ square tube
251      px   9.6032
252      py  -9.6032
253      py   9.6032
c
300      px  10.033 $ lattice surfaces/sq. tube
301      px -10.033
302      py  10.033
303      py -10.033
310      px -90.297 $ 9x9 bounds
311      px  90.297
312      py -90.297
313      py  90.297
320      px -120.777 $ outer bounds
321      px  120.777
```

```
322      py -120.777
323      py  120.777
324      pz -91.44
325      pz  91.44

m2      1001.62c  2          $ water
        8016.62c  1
mt2     lwtr.60t
m3      13027.62c 1          $ Al
m4      6000.66c   -0.08     $ SS-304
        14000.60c  -1.0
        15031.66c  -0.045
        24000.50c  -19.0
        25055.62c  -2.0
        26000.55c  -68.375
        28000.50c  -9.5
m5      1001.62c  -0.056920  $ neoprene
        6000.66c  -0.542646
c        17000.66c -0.400434
m6      13027.62c  -26.5     $ insulation material
        14000.60c  -23.4
        8016.62c   -50.2
m10     92234.69c 1.7026E-05 $ fuel plate 1
        92235.69c 2.6560E-03
        92236.69c 9.8475E-06
        92238.69c 1.4089E-04
        13027.62c 5.2187E-02
c       total     5.5010E-02
m11     92234.69c 1.7156E-05 $ fuel plate 2
        92235.69c 2.6763E-03
        92236.69c 9.9226E-06
        92238.69c 1.4196E-04
        13027.62c 5.2153E-02
c       total     5.4998E-02
m12     92234.69c 2.1711E-05 $ fuel plate 3
        92235.69c 3.3869E-03
        92236.69c 1.2557E-05
        92238.69c 1.7966E-04
        13027.62c 5.0974E-02
c       total     5.4574E-02
m13     92234.69c 2.1618E-05 $ fuel plate 4
        92235.69c 3.3724E-03
        92236.69c 1.2503E-05
        92238.69c 1.7889E-04
        13027.62c 5.0998E-02
c       total     5.4583E-02
m14     92234.69c 2.6648E-05 $ fuel plate 5
        92235.69c 4.1571E-03
        92236.69c 1.5413E-05
        92238.69c 2.2051E-04
        13027.62c 4.9696E-02
c       total     5.4115E-02
m15     92234.69c 2.6746E-05 $ fuel plate 6
        92235.69c 4.1724E-03
        92236.69c 1.5470E-05
        92238.69c 2.2132E-04
        13027.62c 4.9670E-02
```

```
c       total     5.4106E-02
m16     92234.69c 2.6790E-05 $ fuel plate 7
        92235.69c 4.1791E-03
        92236.69c 1.5495E-05
        92238.69c 2.2168E-04
        13027.62c 4.9659E-02
c       total     5.4102E-02
m17     92234.69c 2.6830E-05 $ fuel plate 8
        92235.69c 4.1854E-03
        92236.69c 1.5518E-05
        92238.69c 2.2201E-04
        13027.62c 4.9649E-02
c       total     5.4098E-02
m18     92234.69c 2.6867E-05 $ fuel plate 9
        92235.69c 4.1911E-03
        92236.69c 1.5539E-05
        92238.69c 2.2232E-04
        13027.62c 4.9639E-02
c       total     5.4095E-02
m19     92234.69c 2.6901E-05 $ fuel plate 10
        92235.69c 4.1965E-03
        92236.69c 1.5559E-05
        92238.69c 2.2260E-04
        13027.62c 4.9630E-02
c       total     5.4092E-02
m20     92234.69c 2.6933E-05 $ fuel plate 11
        92235.69c 4.2015E-03
        92236.69c 1.5577E-05
        92238.69c 2.2287E-04
        13027.62c 4.9622E-02
c       total     5.4089E-02
m21     92234.69c 2.6963E-05 $ fuel plate 12
        92235.69c 4.2061E-03
        92236.69c 1.5595E-05
        92238.69c 2.2311E-04
        13027.62c 4.9614E-02
c       total     5.4086E-02
m22     92234.69c 2.6990E-05 $ fuel plate 13
        92235.69c 4.2105E-03
        92236.69c 1.5611E-05
        92238.69c 2.2334E-04
        13027.62c 4.9607E-02
c       total     5.4083E-02
m23     92234.69c 2.7017E-05 $ fuel plate 14
        92235.69c 4.2145E-03
        92236.69c 1.5626E-05
        92238.69c 2.2356E-04
        13027.62c 4.9600E-02
c       total     5.4081E-02
m24     92234.69c 2.7077E-05 $ fuel plate 15
        92235.69c 4.2239E-03
        92236.69c 1.5661E-05
        92238.69c 2.2406E-04
        13027.62c 4.9585E-02
c       total     5.4075E-02
m25     92234.69c 2.2037E-05 $ fuel plate 16
        92235.69c 3.4377E-03
```

```
        92236.69c 1.2746E-05
        92238.69c 1.8235E-04
        13027.62c 5.0889E-02
c       total     5.4544E-02
m26     92234.69c 2.2037E-05 $ fuel plate 17
        92235.69c 3.4377E-03
        92236.69c 1.2745E-05
        92238.69c 1.8235E-04
        13027.62c 5.0889E-02
c       total     5.4544E-02
m27     92234.69c 1.7683E-05 $ fuel plate 18
        92235.69c 2.7586E-03
        92236.69c 1.0228E-05
        92238.69c 1.4633E-04
        13027.62c 5.2016E-02
c       total     5.4949E-02
m28     92234.69c 1.7487E-05 $ fuel plate 19
        92235.69c 2.7279E-03
        92236.69c 1.0114E-05
        92238.69c 1.4470E-04
        13027.62c 5.2067E-02
c       total     5.4967E-02
c
*tr1     0 -10.8 0                        $ base to center
*tr2     0 7.9 0    180 90 90 90 180 90   $ down
*tr3     0 -7.9 0                         $ up
*tr4    -7.9 0 0    90 180 90 0 90 90     $ right
*tr5     7.9 0 0    90 0 90 180 90 90     $ left
*tr6    -5.6  -5.6 0 45 135 90 45 45 90   $ up/right
*tr7     5.6  -5.6 0 45 45 90 135 45 90   $ up/left
*tr8    -5.6   5.6 0 135 135 90 45 135 90 $ down/right
*tr9     5.6   5.6 0 135 45 90 135 135 90 $ down/left
c
mode   n
kcode  2500 1.0 50 250
sdef    x=d1 y=d2 z=d3
si1     -90 90
sp1     0 1
si2     -90 90
sp2     0 1
si3     -60 60
sp3     0 1
```

Case LG5 (NA_N5P050)

```
ATR
999     0      -320:321:-322:323:-324:325                imp:n=0
900     0      310 -311 312 -313 24 -25     fill=3       imp:n=1
901     2 -1.0 (311:-310:313:-312:-24:25) 320 -321 322 -323 324 -325  imp:n=1
c
c       Universe 5: Plate 5
c
500     14 5.4037E-02   500 -501 502 -503            u=5 imp:n=1 $ fuel meat
501     3 -2.7         (-500:501:-502:503) 510 -511 512 -513  u=5 imp:n=1 $
cladding
502     2 -1.0         -510:511:-512:513                      u=5 imp:n=1 $
water
```

```
c
c       Universe 6: Lattice
c
600     0  -531 530  lat=1 fill=-2:2 0:0 0:0
           5
           5(0 -0.2 0)
           5
           5(0 0.2 0)
           5
                            imp:n=1 u=6
c
c       Universe 4: Plates and basket (no pipe)
c
400     0          520 -521 522 -523   fill=6(0 0 0)     imp:n=1 u=4 $ fuel
lattice
401     2 -0.5     (-520:521:-522:523) 400 -401 402 -403 imp:n=1 u=4 $ water
between fuel and basket
402     3 -2.7    -400:401:-402:403        imp:n=1 u=4 $ basket (to infinity)
c
c       Universe 20: Plates with pipe (center)
c
200     0         410 -411 412 -413        fill=4 imp:n=1 u=20 $ fuel/basket
201     2 -0.5    #200 -200            imp:n=1 u=20 $ water between basket
and tube
202     4 -7.94   200 -201                        imp:n=1 u=20 $ tube
203     6 -0.096    201 -203 250 -251 252 -253    imp:n=1 u=20 $ insulation
204     0           203 250 -251 252 -253         imp:n=1 u=20 $ insulation
to tube
205     4 -7.94     -250:251:-252:253             imp:n=1 u=20 $ tube to inf
c
c       Universe 21: Plates with pipe (down)
c
210     0         410 -411 412 -413 trcl=2 fill=4 imp:n=1 u=21 $ fuel/basket
211     2 -0.5    #210 -200            imp:n=1 u=21 $ water between basket
and tube
212     4 -7.94   200 -201                        imp:n=1 u=21 $ tube
213     6 -0.096    201 -203 250 -251 252 -253    imp:n=1 u=21 $ insulation
214     0           203 250 -251 252 -253         imp:n=1 u=21 $ insulation
to tube
215     4 -7.94     -250:251:-252:253             imp:n=1 u=21 $ tube to inf
c
c       Universe 22: Plates with pipe (up)
c
220     0         410 -411 412 -413 trcl=3 fill=4 imp:n=1 u=22 $ fuel/basket
221     2 -0.5    #220 -200            imp:n=1 u=22 $ water between basket
and tube
222     4 -7.94   200 -201                        imp:n=1 u=22 $ tube
223     6 -0.096    201 -203 250 -251 252 -253    imp:n=1 u=22 $ insulation
224     0           203 250 -251 252 -253         imp:n=1 u=22 $ insulation
to tube
225     4 -7.94     -250:251:-252:253             imp:n=1 u=22 $ tube to inf
c
c       Universe 23: Plates with pipe (right)
c
230     0         410 -411 412 -413 trcl=4 fill=4 imp:n=1 u=23 $ fuel/basket
231     2 -0.5    #230 -200            imp:n=1 u=23 $ water between basket
and tube
```

```
232     4 -7.94   200 -201                        imp:n=1 u=23 $ tube
233     6 -0.096    201 -203 250 -251 252 -253    imp:n=1 u=23 $ insulation
234     0           203 250 -251 252 -253         imp:n=1 u=23 $ insulation
to tube
235     4 -7.94     -250:251:-252:253             imp:n=1 u=23 $ tube to inf
c
c       Universe 24: Plates with pipe (left)
c
240     0         410 -411 412 -413 trcl=5 fill=4 imp:n=1 u=24 $ fuel/basket
241     2 -0.5    #240 -200             imp:n=1 u=24 $ water between basket
and tube
242     4 -7.94   200 -201                        imp:n=1 u=24 $ tube
243     6 -0.096    201 -203 250 -251 252 -253    imp:n=1 u=24 $ insulation
244     0           203 250 -251 252 -253         imp:n=1 u=24 $ insulation
to tube
245     4 -7.94     -250:251:-252:253             imp:n=1 u=24 $ tube to inf
c
c       Universe 25: Plates with pipe (up right)
c
250     0         410 -411 412 -413 trcl=6 fill=4 imp:n=1 u=25 $ fuel/basket
251     2 -0.5    #250 -200            imp:n=1 u=25 $ water between basket
and tube
252     4 -7.94   200 -201                        imp:n=1 u=25 $ tube
253     6 -0.096    201 -203 250 -251 252 -253    imp:n=1 u=25 $ insulation
254     0           203 250 -251 252 -253         imp:n=1 u=25 $ insulation
to tube
255     4 -7.94     -250:251:-252:253             imp:n=1 u=25 $ tube to inf
c
c       Universe 26: Plates with pipe (up left)
c
260     0         410 -411 412 -413 trcl=7 fill=4 imp:n=1 u=26 $ fuel/basket
261     2 -0.5    #260 -200           imp:n=1 u=26 $ water between basket and
tube
262     4 -7.94   200 -201                        imp:n=1 u=26 $ tube
263     6 -0.096    201 -203 250 -251 252 -253    imp:n=1 u=26 $ insulation
264     0           203 250 -251 252 -253         imp:n=1 u=26 $ insulation
to tube
265     4 -7.94     -250:251:-252:253             imp:n=1 u=26 $ tube to inf
c
c       Universe 27: Plates with pipe (down right)
c
270     0         410 -411 412 -413 trcl=8 fill=4 imp:n=1 u=27 $ fuel/basket
271     2 -0.5    #270 -200            imp:n=1 u=27 $ water between basket
and tube
272     4 -7.94   200 -201                        imp:n=1 u=27 $ tube
273     6 -0.096    201 -203 250 -251 252 -253    imp:n=1 u=27 $ insulation
274     0           203 250 -251 252 -253         imp:n=1 u=27 $ insulation
to tube
275     4 -7.94     -250:251:-252:253             imp:n=1 u=27 $ tube to inf
c
c       Universe 28: Plates with pipe (down left)
c
280     0         410 -411 412 -413 trcl=9 fill=4 imp:n=1 u=28 $ fuel/basket
281     2 -0.5    #280 -200            imp:n=1 u=28 $ water between basket
and tube
282     4 -7.94   200 -201                        imp:n=1 u=28 $ tube
283     6 -0.096    201 -203 250 -251 252 -253    imp:n=1 u=28 $ insulation
```

```
284     0           203 250 -251 252 -253         imp:n=1 u=28 $ insulation
to tube
285     4 -7.94     -250:251:-252:253             imp:n=1 u=28 $ tube to inf
c
c       Universe 3: Array of Packages
c
300   0    -300 301 -302 303 imp:n=1 u=3 lat=1 fill=-4:4 -4:4 0:0
             25 25 25 25 22 26 26 26 26
             25 25 25 25 22 26 26 26 26
             25 25 25 25 22 26 26 26 26
             25 25 25 25 22 26 26 26 26
             23 23 23 23 20 24 24 24 24
             27 27 27 27 21 28 28 28 28
             27 27 27 27 21 28 28 28 28
             27 27 27 27 21 28 28 28 28
             27 27 27 27 21 28 28 28 28

24      pz -60.96                    $ bottom of fuel
25      pz  60.96                    $ top of fuel (48")
c
200      cz 7.3838 $ IR pipe
201      cz 7.6581 $ OR pipe
203      cz 10.1981 $ 1" insulation
c
250      px  -9.6032 $ square tube
251      px   9.6032
252      py  -9.6032
253      py   9.6032
c
300      px  10.033 $ lattice surfaces/sq. tube
301      px -10.033
302      py  10.033
303      py -10.033
310      px -90.297 $ 9x9 bounds
311      px  90.297
312      py -90.297
313      py  90.297
320      px -120.777 $ outer bounds
321      px  120.777
322      py -120.777
323      py  120.777
324      pz -91.44
325      pz  91.44
c
400      px -5.7912  $ inner basket surfaces
401      px  5.7912
402      py -2.1336
403      py  2.1336
410      px -6.1214  $ outer basket surfaces
411      px  6.1214
412      py -2.4638
413      py  2.4638
c
500      px -5.7873 $ fuel meat
501      px  5.7873
502      py -0.0254
503      py  0.0254
```

```
510      px -5.79   $ fuel cladding
511      px  5.79
512      py -0.06096
513      py  0.06096
520      px -5.791  $ array boundary
521      px  5.791
522      py -2.13296
523      py  2.13296
530      py -0.518    $ lattice bounds
531      py  0.518

m2      1001.62c  2          $ water
        8016.62c  1
mt2     lwtr.60t
m3      13027.62c 1          $ Al
m4      6000.66c   -0.08     $ SS-304
        14000.60c  -1.0
        15031.66c  -0.045
        24000.50c  -19.0
        25055.62c  -2.0
        26000.55c  -68.375
        28000.50c  -9.5
m6      13027.62c  -26.5     $ insulation material
        14000.60c  -23.4
        8016.62c   -50.2
m14     92234.69c 2.7492E-05 $ plate 5
        92235.69c 4.2887E-03
        92236.69c 1.5901E-05
        92238.69c 2.2749E-04
        13027.62c 4.9477E-02
c       total     5.4037E-02
c
*tr2     0  -1.6 0                            $ down
*tr3     0   1.6 0                            $ up
*tr4     1.6 0   0       90 180 90 0 90 90    $ right
*tr5    -1.6 0   0       90 0 90 180 90 90    $ left
*tr6     1.13  1.13 0    45 135 90 45 45 90   $ up/right
*tr7    -1.13  1.13 0    45 45 90 135 45 90   $ up/left
*tr8     1.13 -1.13 0    135 135 90 45 135 90 $ down/right
*tr9    -1.13 -1.13 0    135 45 90 135 135 90 $ down/left
c
mode   n
kcode  2500 1.0 50 250
sdef    x=d1 y=d2 z=d3
si1     -90 90
sp1     0 1
si2     -90 90
sp2     0 1
si3     -60 60
sp3     0 1
```

6.10 Appendix B: Criticality Analysis for MIT and MURR Fuel

The ATR FFSC may be utilized to transport MIT fuel and MURR fuel. Both of these fuels are high-enriched plate-type fuels similar to the ATR fuel analyzed in this chapter, although the fuel geometries are different. The following analyses demonstrate that the ATR FFSC with the MIT and MURR fuel complies with the requirements of 10 CFR §71.55 and §71.59. Based on a 5x5 array of damaged packages, the Criticality Safety Index (CSI), per 10 CFR §71.59, is 4.0.

6.10.1 Description of Criticality Design

6.10.1.1 Design Features Important for Criticality

No special design features are required to maintain criticality safety. No poisons are utilized in the package. The MURR and MIT fuel handling enclosures (FHEs) restrict postulated fuel element pitch expansion under hypothetical accident conditions. In addition, the separation provided by the packaging (outer flat-to-flat dimension of 7.9-in), along with the limit on the number of packages per shipment, is sufficient to maintain criticality safety.

6.10.1.2 Summary Table of Criticality Evaluation

The upper subcritical limit (USL) for ensuring that the ATR FFSC (single package or package array) is acceptably subcritical, is:

$$USL = 0.9209$$

The package is considered to be acceptably subcritical if the computed k_{safe} (k_s), which is defined as $k_{effective}$ (k_{eff}) plus twice the statistical uncertainty (σ), is less than or equal to the USL, or:

$$k_s = k_{eff} + 2\sigma \leq USL$$

The USL is determined on the basis of a benchmark analysis and incorporates the combined effects of code computational bias, the uncertainty in the bias based on both benchmark-model and computational uncertainties, and an administrative margin. The results of the benchmark analysis indicate that the USL is adequate to ensure subcriticality of the package.

The packaging design is shown to meet the requirements of 10 CFR 71.55(b). Moderation by water in the most reactive credible extent is utilized in both the normal conditions of transport (NCT) and hypothetical accident conditions of transport (HAC) analyses. In the single package NCT models, full-density water fills the accessible cavity, while in the single package HAC models, full-density water fills all cavities. In the NCT fuel element models, the fuel element is modeled as undamaged, although the most reactive credible configuration is utilized by maximizing the gap between the fuel plates. Maximizing this gap maximizes the moderation and hence the reactivity because the system is undermoderated. In the HAC fuel element models, a damaged fuel element is assumed, and the fuel element pitch is allowed to expand until constrained by the FHE, which maximizes moderation. In all single package models, 12-in of water reflection is utilized.

In the NCT and HAC array cases, partial moderation is considered to maximize array interaction effects. A 9x9x1 array is utilized for the NCT array, while a 5x5x1 array is utilized in the HAC array. In all array models, 12-in of water reflection are utilized.

The maximum results of the criticality calculations are summarized in Table 6.10-1. The MURR fuel is significantly more reactive than the MIT fuel. The maximum calculated k_s is 0.85881, which occurs for the optimally moderated MURR HAC array case. In this case, the FHE is moderated with full-density water, the inner tube (outside the FHE) is moderated with 0.8 g/cm^3 water, and void is modeled between the insulation and outer tube.

6.10.1.3 Criticality Safety Index

The criticality safety index of 4.0 for MIT and MURR fuel is unchanged from the value provided in Section 6.1.3, *Criticality Safety Index*.

Table 6.10-1 – Summary of Criticality Evaluation

	MURR	**MIT**
Normal Conditions of Transport (NCT)		
Case	k_s	k_s
Single Unit Maximum	0.44807	0.36978
9x9 Array Maximum	0.85643	0.65658
Hypothetical Accident Conditions (HAC)		
Case	k_s	k_s
Single Unit Maximum	0.54584	0.43666
5x5 Array Maximum	0.85881	0.67309
USL = 0.9209		

6.10.2 Fissile Material Contents

The package can accommodate either one MURR or one MIT fuel element. The geometry and composition of these fuel elements are described in the following sections.

6.10.2.1 MURR Fuel Element

Each MURR element contains up to 785 g U-235, enriched up to 94 wt.%. The weight percents of the remaining uranium isotopes are 1.2 wt.% U-234, 0.7 wt.% U-236, and 5.0-7.0 wt.% U-238. Each fuel element contains 24 curved fuel plates. Fuel plate 1 has the smallest radius, while fuel plate 24 has the largest radius, as shown in Figure 6.10-1 and Figure 6.10-3. The fuel "meat" is a mixture of uranium metal and aluminum, while the cladding and structural materials are an aluminum alloy.

The geometry of the fuel element is defined in Figure 6.10-1. Each fuel plate is nominally 0.05-in thick, with a thickness tolerance of ±0.002-in. The fuel meat is nominally 0.02-in thick, and the cladding is nominally 0.015-in thick. The plate cladding material is aluminum. Fuel element side plates are fabricated of ASTM B 209, aluminum alloy 6061-T6 or 6061-T651. These fuel element side plates have a minimum thickness of 0.145-in. The channel width between the plates is 0.080 ± 0.008-in. This tolerance represents average and not localized channel width.

For an actual fuel element, the channel width may exceed this tolerance in localized areas. The maximum local channel width is 0.090-in.

The arc length of the fuel meat changes from plate to plate. Reference fuel meat arc length and inner radius dimensions for each plate are provided in Table 6.10-2. The active fuel length ranges from 23.25-in to 24.75-in as illustrated in Figure 6.10-1.

It is necessary to determine the number densities of the fuel meat, which are the same for all fuel plates. To determine the number densities of the fuel meat, it is first necessary to compute the volume of the fuel meat. The volume of the fuel meat for each plate is the arc length of the meat (nominal + 0.065-in) multiplied by the active fuel length (24.0-in) and meat thickness (0.02-in). The active fuel length and meat thickness are modeled at nominal values in all final (i.e., non-parametric) fuel element models, and the use of these dimensions is justified in Section 6.10.4.1.2, *HAC Single Package Configuration*. It is demonstrated that reactivity increases with increasing meat arc length. The results of the fuel meat volume computations for all 24 plates are provided in Table 6.10-2 for maximum fuel arc length.

The midpoint radii of the fuel plates are treated as fixed quantities in the NCT models, and are computed based on nominal dimensions. However, the channel width is modeled at the maximum value of 0.088-in between all plates in most NCT fuel element models. To achieve this channel width between all fuel plates, the cladding is artificially reduced to a thickness of 0.011-in, or a total plate thickness of 0.042-in. In the most reactive NCT models, a channel width of 0.092-in is modeled between all fuel plates. This value represents the maximum local channel width (0.090-in) plus an additional 0.002-in. To achieve this channel width between all fuel plates, the cladding is artificially reduced to a thickness of 0.009-in, or a total plate thickness of 0.038-in. These plate thicknesses are impossible to achieve in actual practice because they are below the allowable minimum plate thickness of 0.048-in.

The U-235 gram density for each fuel plate is computed by dividing the U-235 mass by the total volume, or 785 g/556.4 cm^3 = 1.41 g/cm^3. The fuel itself is a mixture of UAl_x and aluminum. The density of this mixture for ATR fuel is proportional to the U-235 gram density, as shown in Table 6.2-2. Because ATR and MURR fuel are of the same type, this equation is also used to develop the MURR fuel matrix density. These data are perfectly linear, and a linear fit of the data is $\rho_2 = 0.8733\rho_1 + 2.5357$, where ρ_2 is the total gram density of the mixture, and ρ_1 is the gram density of the U-235 in the mixture. Therefore, using this equation, the total density of the fuel matrix is computed to be approximately 3.77 g/cm^3.

From the fuel volumes, U-235 gram densities, and total mixture densities provided, the number densities for the fuel region may be computed. These number densities are provided in Table 6.10-3. The U-235 weight percent is modeled at the maximum value of 94%. Representative weight percents of 0.6% and 0.35% are utilized for U-234 and U-236, respectively, and the balance (5.05%) is modeled as U-238.

6.10.2.2 MIT Fuel Element

Each MIT element contains up to 515 g U-235, enriched up to 94 wt.%. The weight percents of the remaining uranium isotopes are 1.2 wt.% U-234, 0.7 wt.% U-236, and 5.0-7.0 wt.% U-238. Each fuel element contains 15 flat fuel plates, as shown in Figure 6.10-2 and Figure 6.10-4. The fuel "meat" is a mixture of uranium metal and aluminum, while the cladding and structural materials are an aluminum alloy.

The geometry of the fuel element is defined in Figure 6.10-2. Each fuel plate is nominally 0.08-in thick, with a thickness tolerance of ±0.003-in. The fuel meat is nominally 0.03-in thick, and the cladding is nominally 0.025-in thick. The plate cladding material is aluminum. Fuel element side plates are fabricated of ASTM B 209, aluminum alloy 6061-T6. These fuel element side plates have a nominal thickness of 0.188-in. The channel width between the plates is 0.078 ± 0.004-in (excluding the thermal grooves). This tolerance represents average and not localized channel width. For an actual fuel element, the channel width may exceed this tolerance in localized areas. The maximum local channel width is 0.090-in (excluding the thermal grooves).

The maximum and minimum active fuel lengths and maximum and minimum active fuel widths may be computed based on Figure 6.10-2:

- Maximum active fuel length = (23.0+0.01)-2(0.125) = 22.76-in
- Minimum active fuel length = (23.0-0.01)-2(0.5) = 21.99-in
- Maximum active fuel width = 2.531 – 2(0.18) = 2.171-in
- Minimum active fuel width = 2.521 – 2(0.27) = 1.981-in.

The nominal active fuel length may be estimated as the average of the maximum and minimum values, or 22.375-in.

It is necessary to determine the number densities of the fuel meat, which are the same for all fuel plates. To determine the number densities of the fuel meat, it is first necessary to compute the volume of the fuel meat. The volume of the fuel meat for each plate is the maximum width of the meat (2.171-in) multiplied by the active fuel length (22.375-in) and meat thickness (0.03-in). The active fuel length and meat thickness are modeled at nominal values in all final (i.e., non-parametric) fuel element models, and the use of these dimensions is justified in Section 6.10.4.1.2, *HAC Single Package Configuration*. It is demonstrated that reactivity increases with increasing meat width. The total meat volume is therefore $(15)(0.03)(22.375)(2.171)(2.54^3)$ = 358.2 cm^3.

The centerlines of the fuel plates are treated as fixed quantities in the NCT models, and are computed based on nominal dimensions. However, the channel width is modeled at 0.094-in between all plates in most NCT fuel element models. This modeled channel width includes half of the thermal groove depth on each cladding plate. The fuel plates have grooves a maximum of 0.012-in deep cut into the surface of the fuel plates to increase heat transfer. Because the grooves cover approximately half the surface area of the cladding, half of the groove depth (i.e., 0.006-in) is removed from each cladding plate, so that a channel width of 0.082+2*0.006 = 0.094-in is modeled. To achieve this channel width between all fuel plates, the cladding is artificially reduced to a thickness of 0.017-in, or a total plate thickness of 0.064-in.

Additional NCT models are developed in which the channel width is modeled at 0.116-in. This value is based upon the local maximum channel width (0.090-in) with an additional margin of 0.002-in, and the full thermal groove depth (0.012-in) removed from each plate (0.090-in + 0.002-in + 2*0.012-in = 0.116-in). To achieve this channel width between all fuel plates, the cladding is artificially reduced to a thickness of 0.006-in, or a total plate thickness of 0.042-in.

The U-235 gram density for each fuel plate is computed by dividing the U-235 mass by the total volume, or 515 g/358.2 cm^3 = 1.44 g/cm^3. The fuel itself is a mixture of UAl_x and aluminum. The density of this mixture for ATR fuel is proportional to the U-235 gram density, as shown in

Table 6.2-2. Because ATR and MIT fuel are of the same type, this equation is also used to develop the MIT fuel matrix density. These data are perfectly linear, and a linear fit of the data is $\rho_2 = 0.8733\rho_1 + 2.5357$, where ρ_2 is the total gram density of the mixture, and ρ_1 is the gram density of the U-235 in the mixture. Therefore, using this equation, the total density of the fuel matrix is computed to be approximately 3.79 g/cm^3.

From the fuel volumes, U-235 gram densities, and total mixture densities provided, the number densities for the fuel region may be computed. These number densities are provided in Table 6.10-4. The U-235 weight percent is modeled at the maximum value of 94%. Representative weight percents of 0.6% and 0.35% are utilized for U-234 and U-236, respectively, and the balance (5.05%) is modeled as U-238.

Table 6.10-2 – MURR Fuel Volume Computation (maximum arc length)

Plate	Midpoint Radius (cm)	Fuel Arc (cm)	Volume (cm^3)
1	7.0993	4.5034	13.9460
2	7.4295	4.7625	14.7484
3	7.7597	5.0216	15.5507
4	8.0899	5.2832	16.3608
5	8.4201	5.5423	17.1632
6	8.7503	5.8014	17.9655
7	9.0805	6.0604	18.7678
8	9.4107	6.3195	19.5701
9	9.7409	6.5786	20.3724
10	10.0711	6.8377	21.1747
11	10.4013	7.0968	21.9770
12	10.7315	7.3558	22.7793
13	11.0617	7.6149	23.5816
14	11.3919	7.8765	24.3918
15	11.7221	8.1356	25.1941
16	12.0523	8.3947	25.9964
17	12.3825	8.6538	26.7987
18	12.7127	8.9129	27.6011
19	13.0429	9.1719	28.4034
20	13.3731	9.4310	29.2057
21	13.7033	9.6901	30.0080
22	14.0335	9.9492	30.8103
23	14.3637	10.2083	31.6126
24	14.6939	10.4699	32.4228
Total			556.4024

Table 6.10-3 – MURR Fuel Number Densities (maximum arc length)

Isotope	Number Density (atom/b-cm)
U-234	2.3171E-05
U-235	3.6147E-03
U-236	1.3402E-05
U-238	1.9174E-04
Al	5.0596E-02
Total	5.4439E-02

Table 6.10-4 – MIT Fuel Number Densities (maximum fuel width)

Isotope	Number Density (atom/b-cm)
U-234	2.3613E-05
U-235	3.6835E-03
U-236	1.3657E-05
U-238	1.9539E-04
Al	5.0481E-02
Total	5.4398E-02

PLATE NO.	DIM A REF	DIM B REF MIN	DIM C ± 0.01
1	2.770	1.643	1.993
2	2.990	1.745	2.095
3	3.030	1.847	2.197
4	3.160	1.950	2.300
5	3.290	2.052	2.402
6	3.420	2.154	2.504
7	3.550	2.256	2.606
8	3.680	2.358	2.708
9	3.810	2.460	2.810
10	3.940	2.562	2.912
11	4.070	2.664	3.014
12	4.200	2.766	3.116
13	4.330	2.868	3.218
14	4.460	2.971	3.321
15	4.590	3.073	3.423
16	4.720	3.175	3.525
17	4.850	3.277	3.627
18	4.980	3.379	3.729
19	5.110	3.481	3.831
20	5.240	3.583	3.933
21	5.370	3.685	4.035
22	5.500	3.787	4.137
23	5.630	3.889	4.239
24	5.760	3.992	4.342

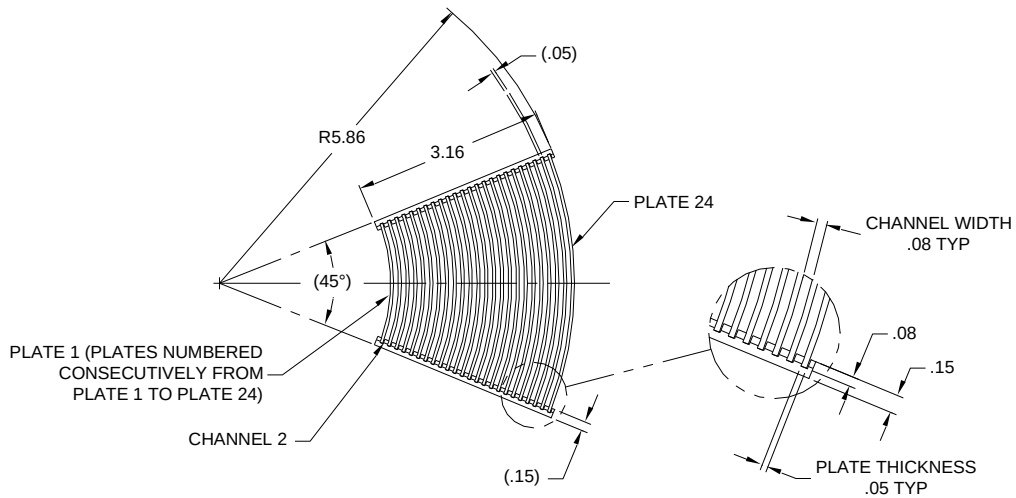

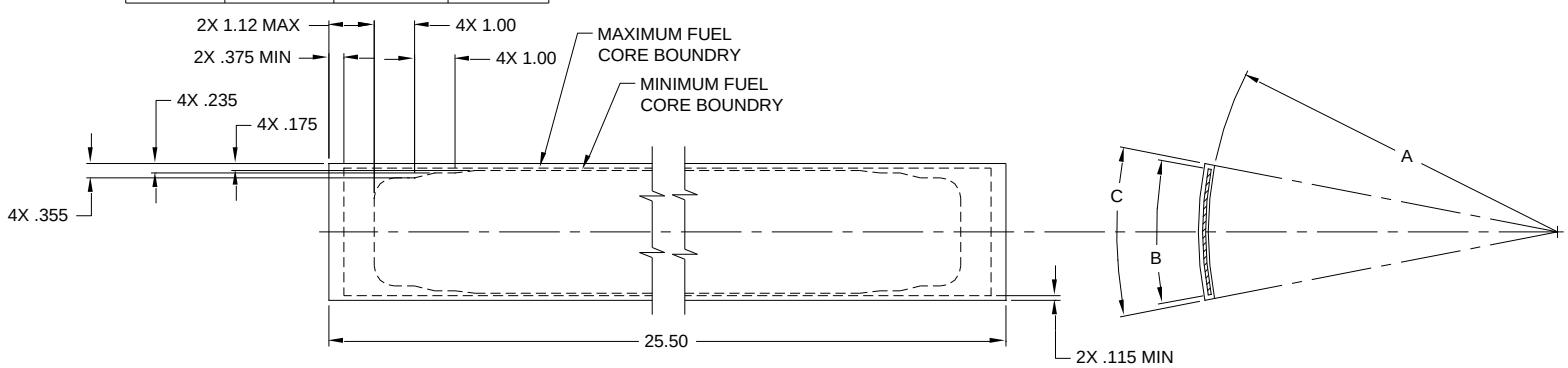

FUEL PLATE DETAIL

Figure 6.10-1 – MURR Fuel Element Dimensions

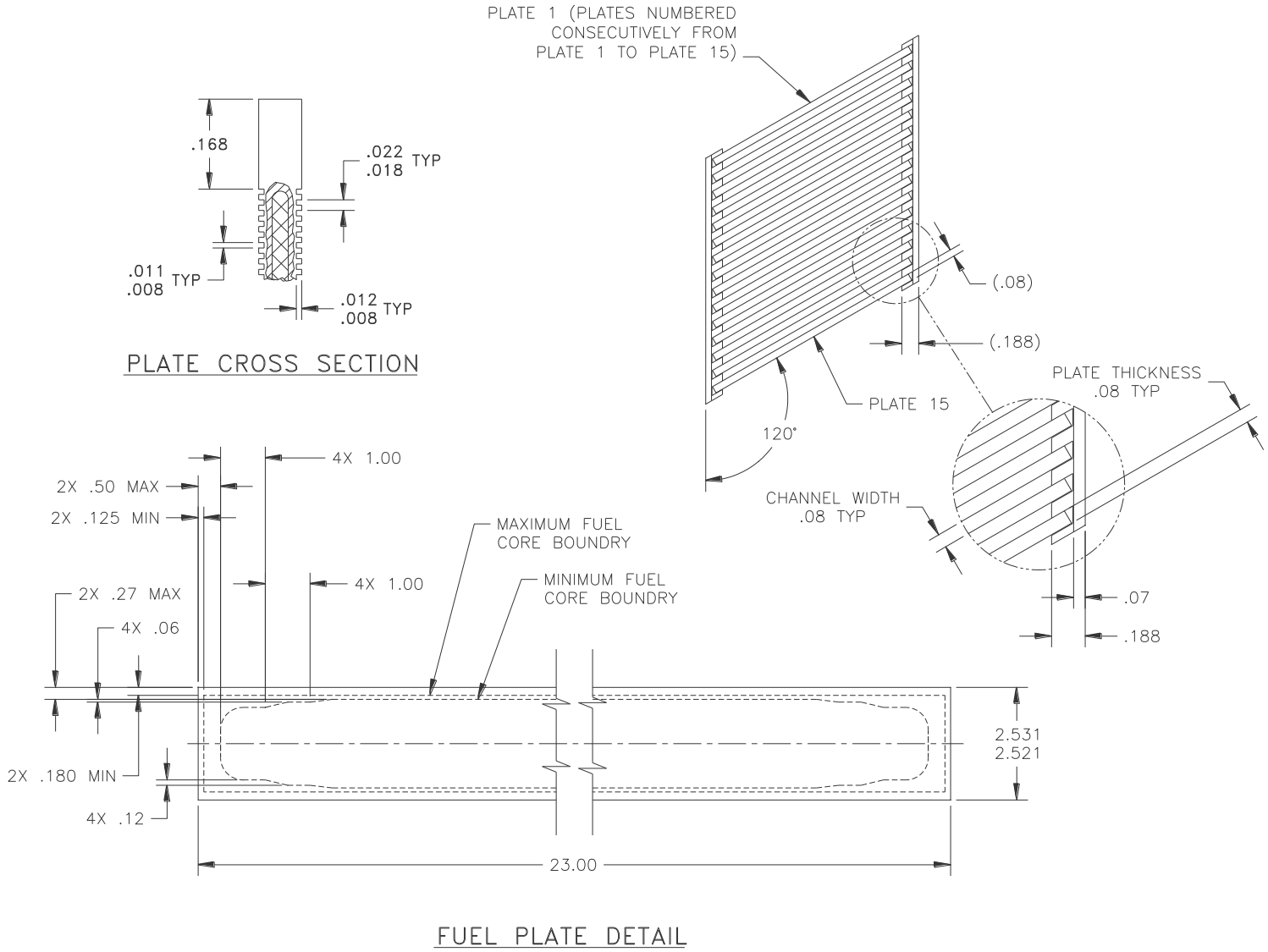

Figure 6.10-2 – MIT Fuel Element Dimensions

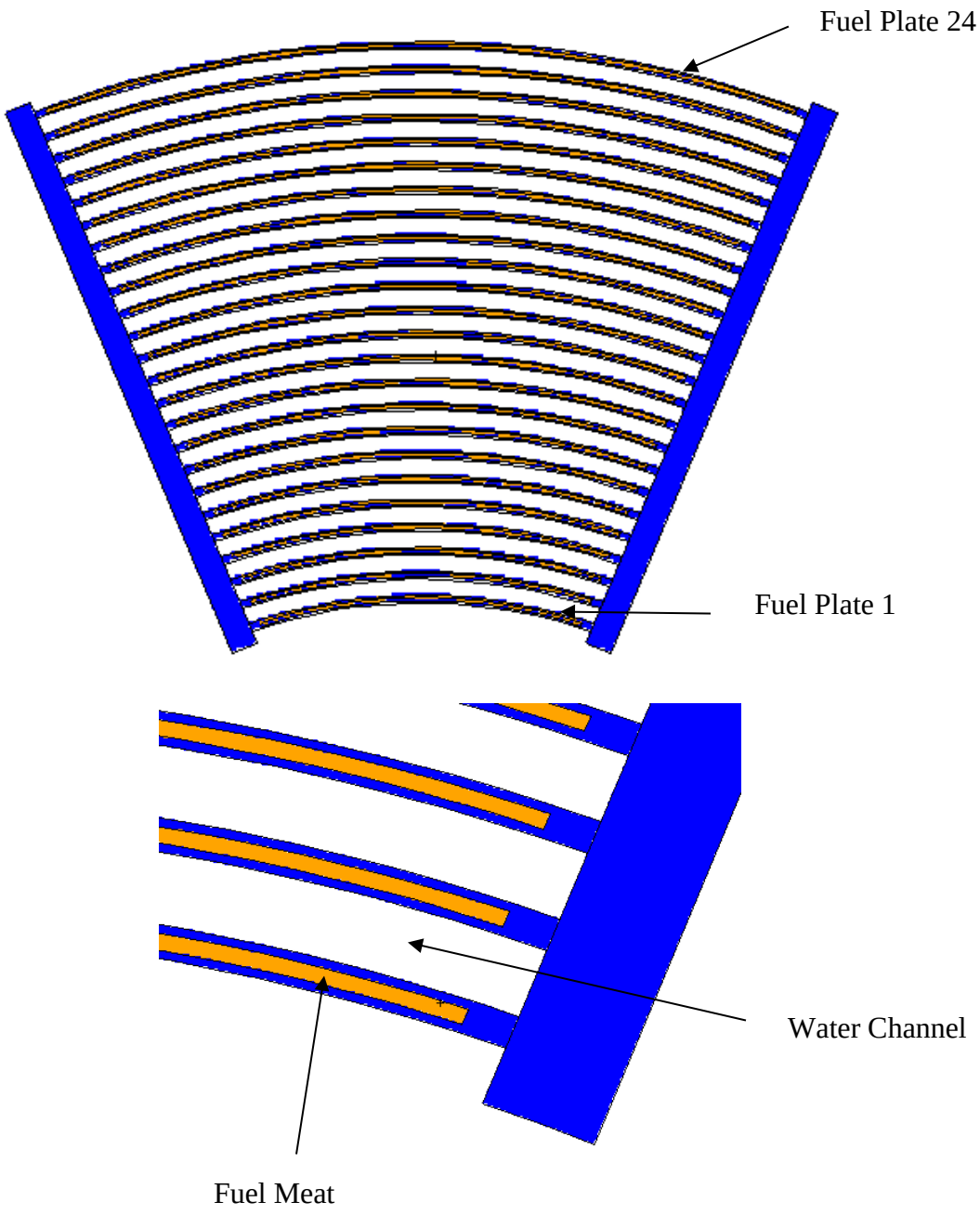

Figure 6.10-3 – MURR Fuel Element Model

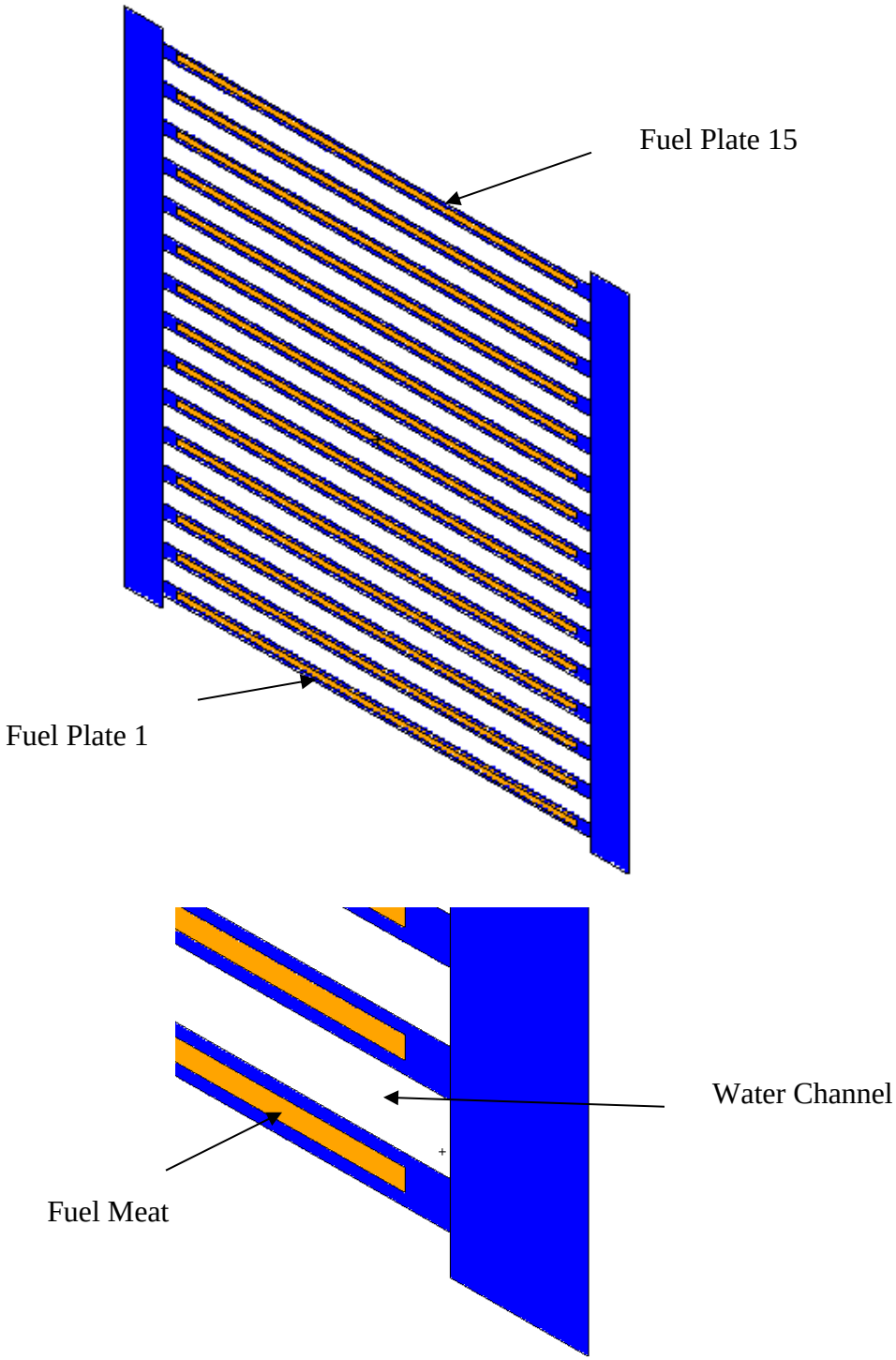

Figure 6.10-4 – MIT Fuel Element Model

6.10.3 General Considerations

6.10.3.1 Model Configuration

The packaging is modeled essentially the same as described in Section 6.3.1, *Model Configuration*, including the number of packages utilized in the NCT and HAC array cases. The only difference is the FHE is modeled explicitly, and the contents are different.

The MURR and MIT FHEs are modeled explicitly over the active fuel length. The FHEs are constructed of aluminum. Maximum dimensional tolerances are selected so that the FHEs are as large as possible, which results in the largest possible pitch expansion in the HAC models. For the MURR FHE, these dimensions are 2.00+0.06-in, 3.56+0.06-in, 1.85+0.06-in, and 22.5°+2° (see the packaging general arrangement drawings for dimension placement). For the MIT FHE, these dimensions are 1.62+0.06-in and 2.82+0.06-in (see the packaging general arrangement drawings for dimension placement). The wall thickness is 0.19 ± 0.06-in for each FHE. The array cases are run with both minimum and maximum wall thickness to determine the most reactive condition. All of the figures in this chapter show minimum wall thickness models. Each FHE is comprised of two pieces held together by ball lock pins. Under NCT, the two FHE halves do not separate.

In the NCT single package models, the inner tube, FHE, insulation, and outer tube are modeled explicitly, as shown in Figure 6.10-5 and Figure 6.10-6 for MURR and MIT, respectively. An axial view is shown in Figure 6.10-7. Note that the thin steel sheet that encases the insulation has been conservatively neglected (the steel sheet would absorb neutrons and lower the reactivity). Although negligible water ingress is expected during NCT, the inner cavity of the package is assumed to be flooded with water because the package lid does not contain a seal. However, the region between the insulation and the outer tube will remain dry because water cannot enter this region. In the models, the fuel element is conservatively positioned at the radial center of the FHE to maximize neutron reflection. The package is reflected with 12-in of full-density water.

The neoprene along the sides of the FHEs is modeled in an approximate manner using a thickness of 1/8-in. In both cases, the neoprene is modeled continuously along two sides for simplicity, rather than modeling the neoprene in detail as narrow strips. Because it was determined in the ATR fuel criticality analysis that neoprene will reduce the reactivity due to parasitic absorption in chlorine, the neoprene is modeled without chlorine, and the density is reduced accordingly.

The HAC single package model is similar to the NCT single package model. Damage in the drop tests was shown to be negligible and concentrated at the ends of the package (See Section 2.12.1, *Certification Tests on CTU-1*). As the ends of the package are not modeled, this end damage does not affect the modeling. The various side drops resulted in only minor localized damage to the outer tube, and no observable bulk deformation of the package. Therefore, the minor damage observed will not impact the reactivity. The insulation is replaced with full-density water, and the region between the insulation and outer tube is also filled with full-density water (see Figure 6.10-8 and Figure 6.10-9 for the MURR and MIT model geometry, respectively). The treatment of the fuel enclosure is the same as the NCT single package models. Cases are developed both with and without the neoprene.

No MURR or MIT fuels were included in the drop tests. Therefore, the damage to the MURR or MIT fuel under HAC is not known precisely. To conservatively bound the potential fuel damage in the HAC models, the fuel plate pitch is allowed to expand uniformly until constrained by the FHE. In addition, the FHEs, which are composed of two halves pinned together, are assumed to separate in a manner that maximizes the space available for pitch expansion. For simplicity, the gap between the two halves is not modeled explicitly in the HAC models. This pitch expansion increases the moderation and the reactivity. In actuality, such a large uniform expansion of the fuel element pitch is not credible, and in the worst case scenario would be localized at one end of the fuel element. Drop tests performed with ATR fuel, which is similar to MURR and MIT fuel, showed no damage that would affect the criticality analysis [See Section 2.12.1, *Certification Tests on CTU-1*]. The modeled damage is intended to bound a damaged fuel element that is otherwise intact.

In the NCT array models, a 9x9x1 array is utilized. To increase the reactivity, fuel elements are pushed toward the center of the array. Because the fuel elements are transported in a thin (~0.01-in) plastic bag, this plastic bag is allowed to act as a boundary for partial moderation effects. The plastic bag is not modeled explicitly, because it is too thin to have an appreciable effect on the reactivity. Therefore, it is postulated that the fuel element channels may fill with full-density water, while the region between the fuel element and FHE fills with variable density water. Different water densities inside and outside the FHE are also addressed. Axial movement of the fuel elements is not considered because axial movement would increase the effective active height of the system (i.e., if some fuel elements shift and others remain in place) and reduce the reactivity due to increased leakage. The presence of chlorine-free neoprene is also considered in the array cases.

In the HAC array models, a 5x5x1 array is utilized, although the moderation conditions considered are similar to the NCT array analysis. Cases in which the insulation is replaced with water are also investigated. The fuel elements are modeled at the maximum pitch, consistent with the most reactive single package models.

The detailed moderation assumptions for these cases are discussed more fully in Section 6.10.5, *Evaluation of Package Arrays under Normal Conditions of Transport*, and Section 6.10.6, *Package Arrays under Hypothetical Accident Conditions*.

6.10.3.2 Material Properties

The fuel meat compositions are provided in Table 6.10-3 and Table 6.10-4 for MURR and MIT fuel, respectively. The material properties of the packaging materials are provided in Section 6.3.2, *Material Properties*. The aluminum of the FHE is modeled as pure with a density of 2.7 g/cm^3.

6.10.3.3 Computer Codes and Cross-Section Libraries

The computer code and cross section libraries utilized are provided in Section 6.3.3, *Computer Codes and Cross-Section Libraries*.

6.10.3.4 Demonstration of Maximum Reactivity

The reactivities of the NCT and HAC single package cases are small, with $k_s < 0.6$.

For the NCT array, a 9x9x1 array is utilized, while for the HAC array, a smaller 5x5x1 array is utilized. Because negligible packaging damage was observed in the drop tests, the package dimensions are the same between the NCT and HAC models. However, the fuel elements are modeled differently between the NCT and HAC models. In the NCT models, the fuel elements are modeled as intact, although with dimensions optimized to maximize the reactivity. In the HAC models, the fuel is assumed to be damaged, and the pitch is allowed to expand until constrained by the FHE. In the HAC cases, the pins connecting the two halves of the FHE are assumed to break, and the two halves are pushed apart to the maximum extent to maximize the available space for pitch expansion. The FHEs and fuel elements are pushed toward the center of the array.

In both NCT and HAC array cases, flooding with partial moderation is allowed in the fuel element itself, between the fuel element and the FHE, and between the FHE and the inner tube. A number of different partial moderation scenarios are considered.

In the NCT array models, insulation is modeled between the inner and outer tubes. In the HAC array models, it is demonstrated that modeling the insulation is more reactive than replacing the insulation with variable density water. In both sets of models, chlorine-free neoprene that is attached to the FHE is modeled, although the effect on the reactivity is small. No models in which the neoprene is allowed to decompose and homogeneously mix with the water are developed, as this scenario is already implicitly included in the search for optimum reactivity using various water densities.

Tolerances of the packaging materials are selected to maximize the reactivity. Both maximum and minimum wall thicknesses for the FHE are modeled to determine the most reactive condition, although the effect on the reactivity of this parameter is not significant.

The MURR fuel is significantly more reactive than the MIT fuel in all scenarios, a difference in k_s of 0.186 comparing the most reactive models. The most reactive case occurs for the HAC array (Case XN9), and results in a k_s = 0.85881, which is below the USL of 0.9209. For this case, full-density water is modeled between the fuel plates and inside the FHE, 0.8 g/cm^3 water is modeled between the FHE and inner tube, the FHE is modeled with a thick wall, and insulation is modeled.

When comparing the reactivities of the three fuel types (ATR, MURR, MIT), MURR is the most reactive, MIT is the least reactive.

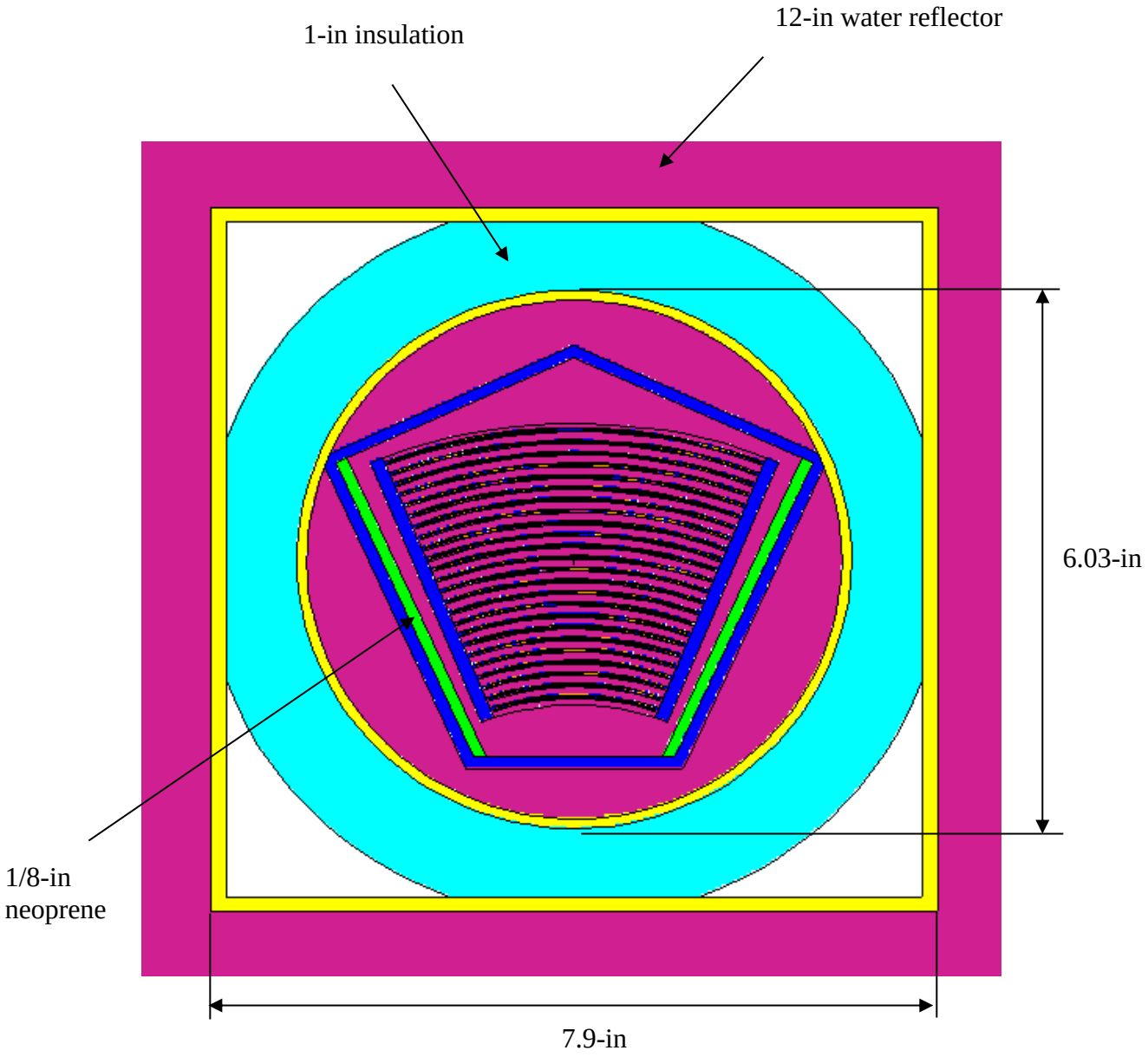

Figure 6.10-5 – MURR NCT Single Package Model (planar view)

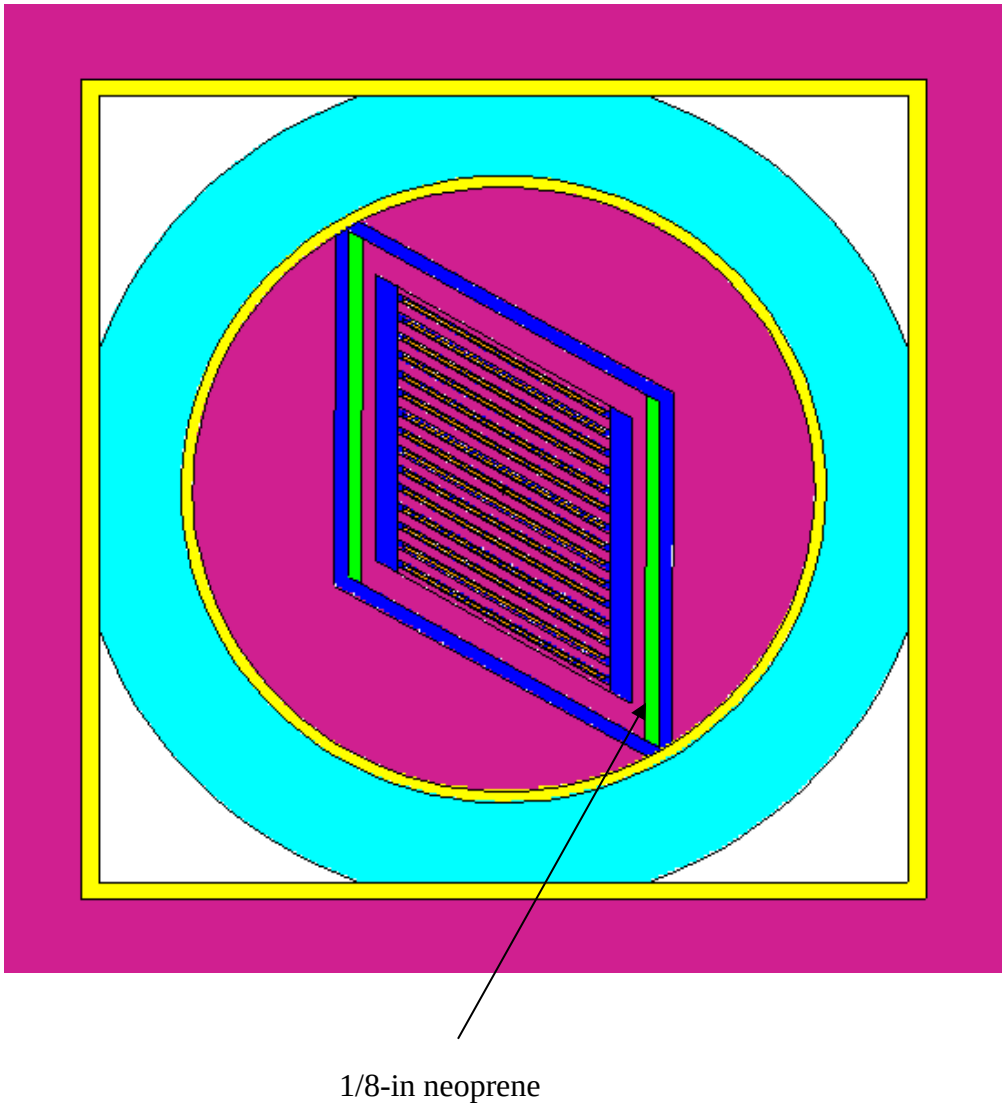

Figure 6.10-6 – MIT NCT Single Package Model (planar view)

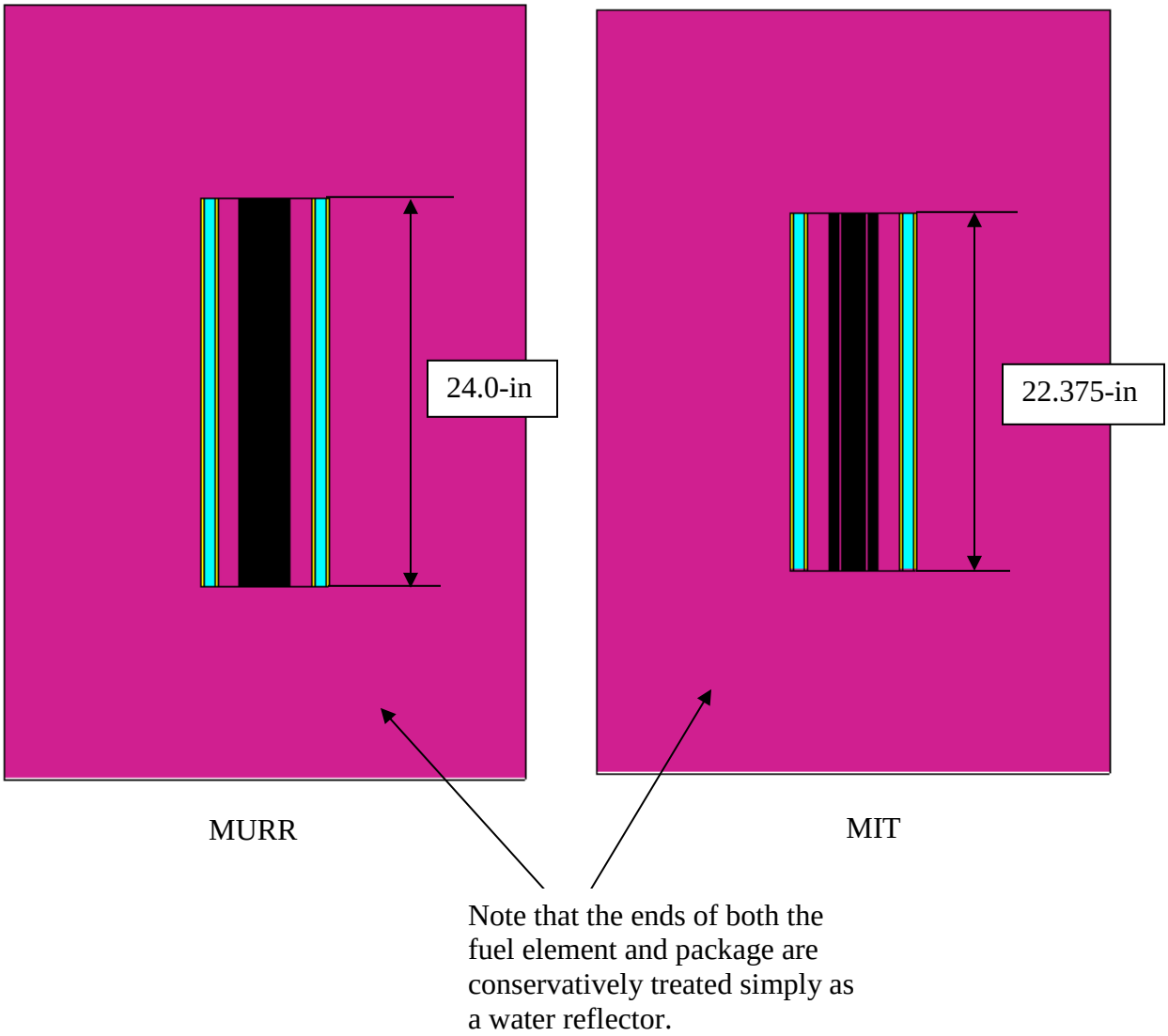

Figure 6.10-7 – MURR/MIT NCT Single Package Models (axial view)

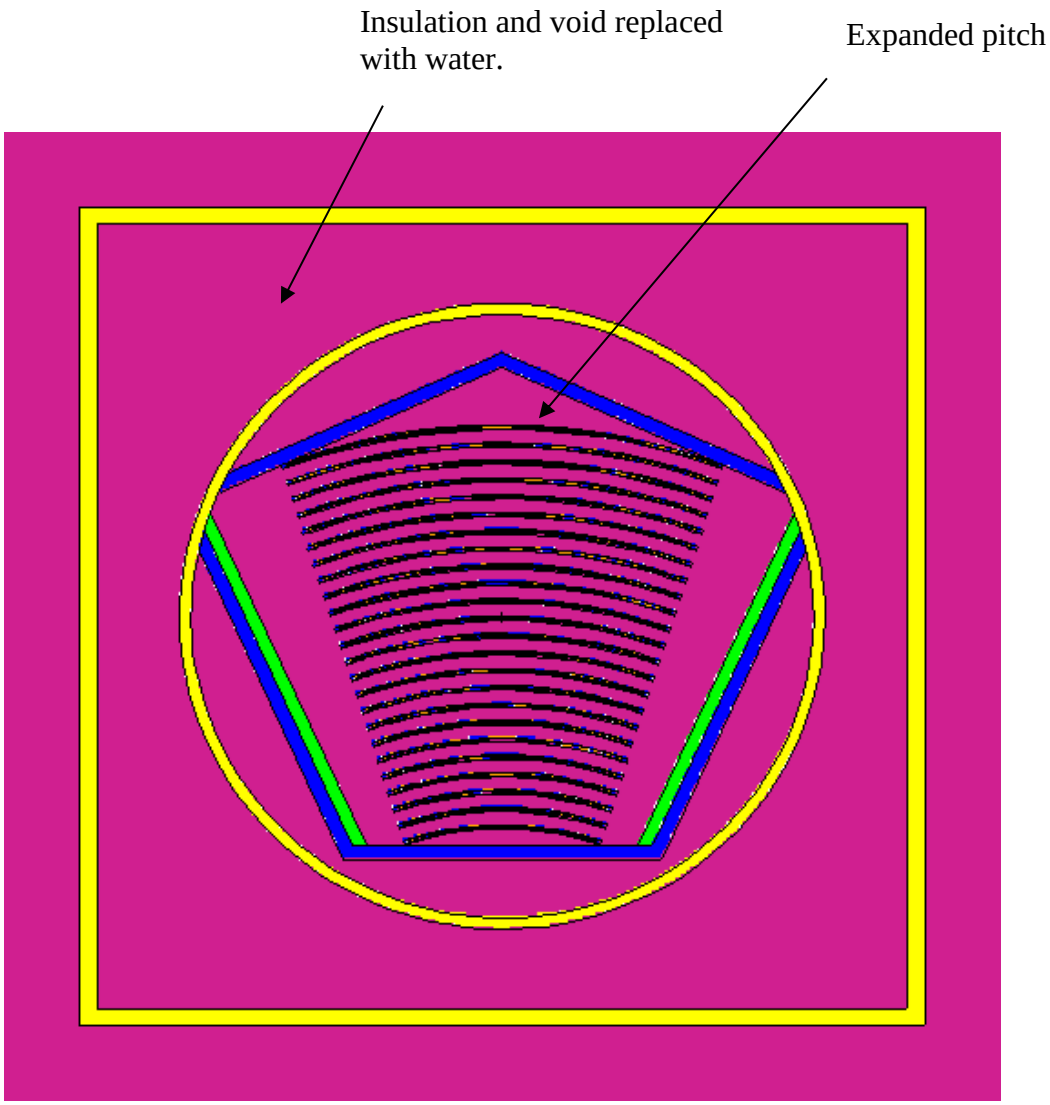

Figure 6.10-8 – MURR HAC Single Package Model (planar view)

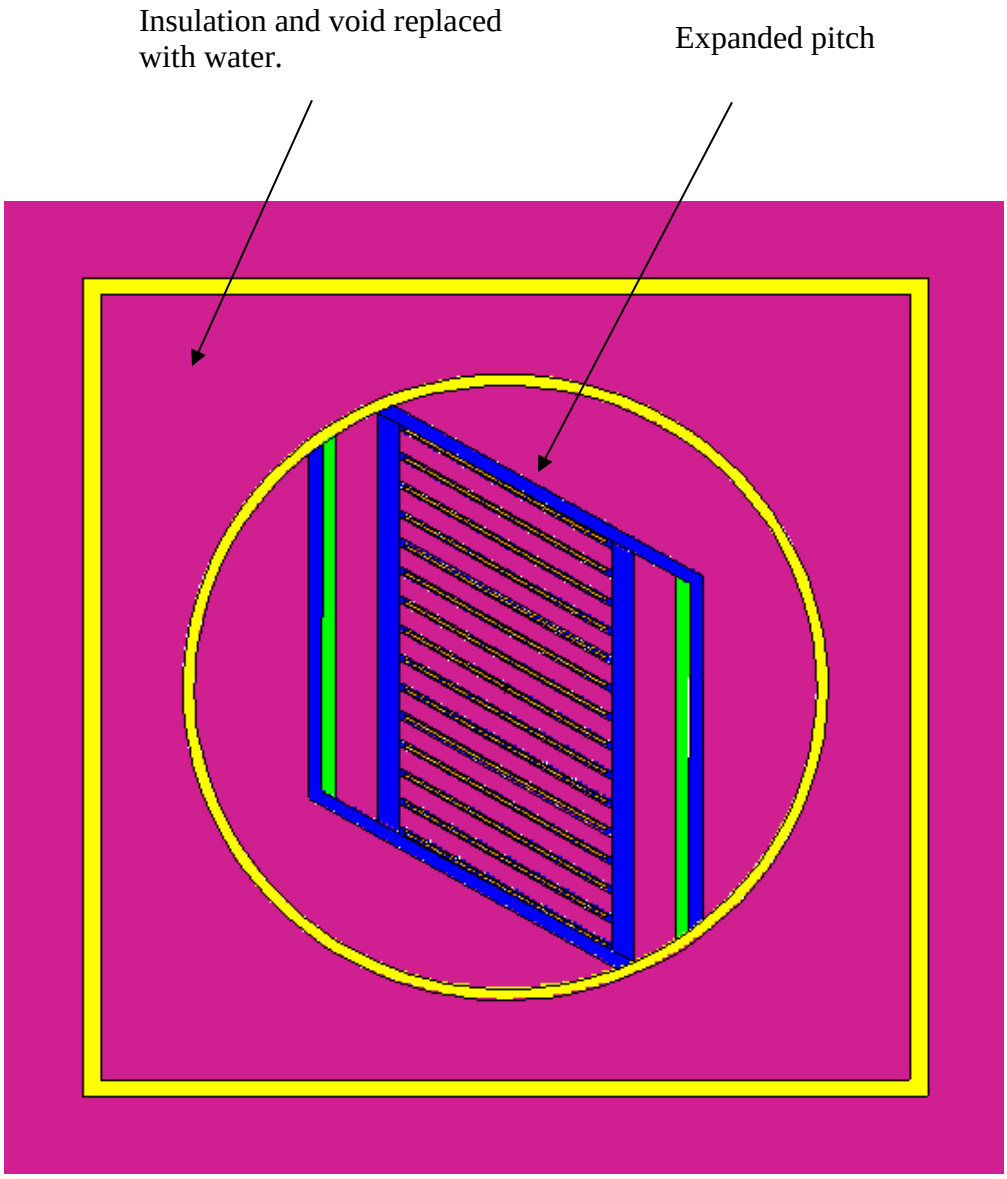

Figure 6.10-9 – MIT HAC Single Package Model (planar view)

6.10.4 Single Package Evaluation

6.10.4.1 Single Package Configuration

Prior to development of a single package model, a parametric analysis is performed to determine the impacts of various fuel element tolerances on the reactivity. In the criticality analysis for ATR fuel (see Section 6.4.1.2.1, *Fuel Element Payload Parametric Evaluation*), it was determined that reactivity was maximized by maximizing the arc length of the fuel meat and the channel thickness. Because ATR, MURR, and MIT fuel are all plate-type and utilize similar enrichments, it is expected that MURR and MIT fuel will also experience maximum reactivity with these parameters maximized. Therefore, the parametric analysis considers the effects of only the following parameters: fuel meat arc length/width, channel width, and active fuel length.

The base configuration for both MURR and MIT consists of plates with a nominal meat arc length/width, nominal active fuel length, and nominal channel width. The minimum, nominal, and maximum meat arc lengths for MURR fuel are provided in Table 6.10-5. The minimum meat arc lengths are obtained directly from Figure 6.10-1 (see dimension B). The maximum meat arc lengths are computed by subtracting twice the fuel-free width (2*0.115-in) from the maximum plate width (dimension C of Figure 6.10-1 + 0.010-in). The nominal value is computed as the average of the minimum and maximum values.

A total of 14 parametric models are developed (7 for each fuel type), as listed in the following table. The detailed model descriptions of the parametric cases are summarized in Table 6.10-6. In each parametric case, the indicated parameter is modified in comparison with the base case. In all parametric models, the fuel element is modeled in the center of an ATR FFSC with the inner tube flooded, and the insulation replaced with full density water. The FHEs are neglected for simplicity.

Case ID	Case Description
XB1	Base MURR case
XB2	Decrease active fuel length to minimum value
XB3	Increase active fuel length to maximum value
XB4	Increase channel width to 0.088-in
XB5	Decrease width of fuel meat to minimum value
XB6	Increase width of fuel meat to maximum value
XB7	Combine cases XB4 and XB6
Case ID	**Case Description**
YB1	Base MIT case
YB2	Decrease active fuel length to minimum value
YB3	Increase active fuel length to maximum value
YB4	Increase channel width to 0.094-in
YB5	Decrease width of fuel meat to minimum value
YB6	Increase width of fuel meat to maximum value
YB7	Combine cases YB4 and YB6

The results of the parametric analysis are summarized in Table 6.10-7. Because the uncertainty in the calculation is ~0.001, a difference of at least 0.002 (2 milli-k, abbreviated mk) between the

various cases is required in order to distinguish a real effect from statistical fluctuation. For both MURR and MIT fuel, the variation of the active fuel length has a negligible effect on the results. Also, both MURR and MIT fuel show a positive reactivity increase when the fuel meat is widened and the channel width is increased. For MURR fuel, the increase is 23.5 mk (compare Case XB7 with Case XB1), and for MIT fuel, the increase is 8.8 mk (compare Case YB7 with Case YB1). This result is consistent with the results obtained in the ATR fuel analysis. Therefore, in all subsequent NCT MURR and MIT fuel models, the fuel is modeled with nominal active fuel length and maximum fuel width. Also, in subsequent models, maximizing the channel width is achieved by either reducing the cladding thickness (if the fuel is undamaged) or increasing the plate pitch (if the fuel is damaged).

6.10.4.1.1 NCT Single Package Configuration

The geometry of the NCT single package configuration is discussed in Section 6.10.3.1, *Model Configuration*. In the NCT single package models, the FHEs are modeled explicitly, and the neoprene is modeled in an approximate manner (see Figure 6.10-5 and Figure 6.10-6 for the NCT single package MURR and MIT models, respectively). The inner tube is flooded with full-density water. The fuel element geometry for both MURR and MIT is consistent with the most reactive fuel element model, including tolerances, as determined in the previous section. Neoprene from the FHEs is modeled at the sides of the fuel element. Chlorine is conservatively removed from the neoprene because chlorine acts as a poison. The package is reflected with 12-in of water.

Results are provided in Table 6.10-8 for both MURR and MIT fuel. For MURR, Case XA1 is for a modeled channel width of 0.088-in, and Case XA2 is for a modeled channel width of 0.092-in. The channel width of 0.088-in represents the maximum average channel width, while the channel width of 0.092-in is the local maximum channel width of 0.090-in with an additional 0.002-in of margin. For MIT, Case YA1 is for a modeled channel width of 0.094-in, and Case YA2 is for a modeled channel width of 0.116-in. The channel width of 0.094-in represents the maximum average channel width (0.082-in) plus half of the thermal groove (0.006-in) on each cladding plate. The channel width of 0.116-in represents the local maximum channel width of 0.090-in plus the full thermal groove (0.012-in) on each cladding plate, plus an additional 0.002-in margin.

For both MURR and MIT, reactivity increases with increased channel width. The reactivity is low, with k_s = 0.44807 for MURR and k_s = 0.36978 for MIT. These results are below the USL of 0.9209.

6.10.4.1.2 HAC Single Package Configuration

The geometry of the HAC single package configuration is discussed in Section 6.10.3.1, *Model Configuration*. In the HAC single package models, the FHEs are modeled explicitly, and the neoprene is modeled in an approximate manner (see Figure 6.10-8 and Figure 6.10-9 for the HAC single package MURR and MIT models, respectively). Chlorine is conservatively removed from the neoprene because chlorine acts as a poison. Eliminating the chlorine from the neoprene may be postulated to be a result of decomposition during a fire, although such a scenario is not credible.

The results are summarized in Table 6.10-9. In both the MURR and MIT models, the pitch is varied from the nominal value to the maximum value allowed by the FHE (Cases XC1 through

XC6 for MURR and YC1 through YC10 for MIT). For both fuel types, the reactivity increases as the plate pitch increases, reaching the maximum reactivity at the maximum pitch. For MURR, the maximum pitch is 0.167-in, which corresponds to a modeled channel spacing of 0.125-in. For MIT, the maximum pitch is 0.240-in, which corresponds to a modeled channel spacing of 0.176-in. Neoprene is included in the variable pitch models. Note that the aluminum fuel element side plates are omitted from the MURR model for simplicity. In the MIT models, the aluminum fuel element side plates are allowed to "stretch" with the model for simplicity.

In Cases XC7 and YC11, the maximum-pitch MURR and MIT cases are repeated without neoprene. In both instances, the reactivity increases slightly when neoprene is modeled as water.

Because the fuel may be transported inside of a plastic bag, it is conservatively assumed that the water density inside of the FHE may vary independently of the water density inside of the fuel element. Note that additional surfaces are added to the MURR model to isolate the water between the fuel plates from the water inside the FHE (in Figure 6.10-8 these regions are combined). To maximize neutron reflection, full-density water is always modeled inside and outside the FHE, and the fuel element is centered laterally within the FHE.

In MURR Cases XC8 and XC9, Case XC7 is run with reduced water densities of 0.8 and 0.9 g/cm^3 between the fuel plates, but maximum water density in all other regions of the model. MIT Cases YC12 and YC13 are similar, except the Case YC11 is used as the base case. In both cases, reactivity drops as the water density is reduced between the fuel plates, indicating that the system is undermoderated.

The results are summarized in Table 6.10-9. Case XC7 is the most reactive MURR model, with k_s = 0.54584, while Case YC11 is the most reactive MIT model, with k_s = 0.43666. Both results are below the USL of 0.9209.

6.10.4.2 Single Package Results

Following are the tabulated results for the single package cases. The most reactive configurations are listed in boldface.

Table 6.10-5 – MURR Meat Arc Lengths

Plate	Minimum (in)	Nominal (in)	Maximum (in)
1	1.643	1.708	1.773
2	1.745	1.810	1.875
3	1.847	1.912	1.977
4	1.950	2.015	2.080
5	2.052	2.117	2.182
6	2.154	2.219	2.284
7	2.256	2.321	2.386
8	2.358	2.423	2.488
9	2.460	2.525	2.590
10	2.562	2.627	2.692
11	2.664	2.729	2.794
12	2.766	2.831	2.896
13	2.868	2.933	2.998
14	2.971	3.036	3.101
15	3.073	3.138	3.203
16	3.175	3.240	3.305
17	3.277	3.342	3.407
18	3.379	3.444	3.509
19	3.481	3.546	3.611
20	3.583	3.648	3.713
21	3.685	3.750	3.815
22	3.787	3.852	3.917
23	3.889	3.954	4.019
24	3.992	4.057	4.122

Table 6.10-6 – Parametric Analysis Input Data

MURR					
Parameter	**XB1/XB4**	**XB2**	**XB3**	**XB5**	**XB6/XB7**
Fuel width (in)	nominal	nominal	nominal	nominal-0.065	nominal+0.065
Meat thickness (in)	0.02	0.02	0.02	0.02	0.02
Active fuel height (in)	24	23.25	24.75	24	24
Channel (in)	0.08/0.088	0.08	0.08	0.08	0.08/0.088
Cladding (in)	0.015/0.011	0.015	0.015	0.015	0.015/0.011
Total plate (in)	0.050/0.042	0.050	0.050	0.050	0.050/0.042
Pitch (in)	0.13	0.13	0.13	0.13	0.13
Meat volume (cm3)	544.13	527.13	561.14	531.86	556.40
U-235 mass (g)	785	785	785	785	785
U-235 den (g/cm3)	1.44	1.49	1.40	1.48	1.41
UAlx+Al den (g/cm3)	3.80	3.84	3.76	3.82	3.77
N-234 (atom/b-cm)	2.3694E-05	2.4458E-05	2.2976E-05	2.4241E-05	2.3171E-05
N-235 (atom/b-cm)	3.6962E-03	3.8154E-03	3.5842E-03	3.7815E-03	3.6147E-03
N-236 (atom/b-cm)	1.3704E-05	1.4146E-05	1.3289E-05	1.4020E-05	1.3402E-05
N-238 (atom/b-cm)	1.9607E-04	2.0239E-04	1.9012E-04	2.0059E-04	1.9174E-04
N-Al (atom/b-cm)	5.0460E-02	5.0262E-02	5.0646E-02	5.0319E-02	5.0596E-02
Total (atom/b-cm)	5.4390E-02	5.4319E-02	5.4457E-02	5.4339E-02	5.4439E-02
MIT					
Parameter	**YB1/YB4**	**YB2**	**YB3**	**YB5**	**YB6/YB7**
Fuel width (in)	2.076	2.076	2.076	1.981	2.171
Meat thickness (in)	0.03	0.03	0.03	0.03	0.03
Active fuel height (in)	22.375	21.99	22.76	22.375	22.375
Channel (in)	0.090/0.094	0.090	0.090	0.090	0.090/0.094
Cladding (in)	0.019/0.017	0.019	0.019	0.019	0.019/0.017
Total plate (in)	0.068/0.064	0.068	0.068	0.068	0.068/0.064
Pitch (in)	0.158	0.158	0.158	0.158	0.158
Meat volume (cm^3)	342.53	336.64	348.43	326.86	358.21
U-235 mass (g)	515	515	515	515	515
U-235 den (g/cm3)	1.503	1.530	1.478	1.576	1.438
UAlx+Al den (g/cm3)	3.85	3.87	3.83	3.91	3.79
N-234 (atom/b-cm)	2.4693E-05	2.5125E-05	2.4275E-05	2.5877E-05	2.3613E-05
N-235 (atom/b-cm)	3.8521E-03	3.9195E-03	3.7869E-03	4.0368E-03	3.6835E-03
N-236 (atom/b-cm)	1.4282E-05	1.4532E-05	1.4040E-05	1.4967E-05	1.3657E-05
N-238 (atom/b-cm)	2.0433E-04	2.0791E-04	2.0088E-04	2.1413E-04	1.9539E-04
N-Al (atom/b-cm)	5.0202E-02	5.0090E-02	5.0310E-02	4.9895E-02	5.0481E-02
Total (atom/b-cm)	5.4297E-02	5.4257E-02	5.4336E-02	5.4187E-02	5.4398E-02

Table 6.10-7 – Parametric Analysis Results

Case ID	Filename	k_{eff}	σ	k_s (k+2σ)	Δ from XB1 (mk)
MURR					
XB1	HS_MURR2_P1	0.47068	0.00109	0.47286	--
XB2	HS_MURR2_P2	0.47199	0.00114	0.47427	1.4
XB3	HS_MURR2_P3	0.47075	0.00114	0.47303	0.2
XB4	HS_MURR2_P4	0.49257	0.00101	0.49459	21.7
XB5	HS_MURR2_P5	0.46808	0.00116	0.47040	-2.5
XB6	HS_MURR2_P6	0.47465	0.00097	0.47659	3.7
XB7	**HS_MURR2_P7**	**0.49432**	**0.00102**	**0.49636**	**23.5**
MIT					
Case ID	**Filename**	**k_{eff}**	**σ**	**k_s (k+2σ)**	**Δ from YB1 (mk)**
YB1	HS_MIT_P1	0.37801	0.00089	0.37979	--
YB2	HS_MIT_P2	0.37683	0.00093	0.37869	-1.1
YB3	HS_MIT_P3	0.37722	0.00091	0.37904	-0.8
YB4	HS_MIT_P4	0.38179	0.00095	0.38369	3.9
YB5	HS_MIT_P5	0.37018	0.00087	0.37192	-7.9
YB6	HS_MIT_P6	0.38064	0.00088	0.38240	2.6
YB7	**HS_MIT_P7**	**0.38664**	**0.00097**	**0.38858**	**8.8**

Table 6.10-8 – NCT Single Package Results

Case ID	Filename	Moderator Density (g/cm^3)	k_{eff}	σ	k_s (k+2σ)
MURR					
XA1	NS_MURR	1.0	0.43268	0.00107	0.43482
XA2	**NS_MURR2C**	**1.0**	**0.44597**	**0.00105**	**0.44807**
MIT					
YA1	NS_MIT	1.0	0.33434	0.00086	0.33606
YA2	**NS_MITC**	**1.0**	**0.36788**	**0.00095**	**0.36978**

Table 6.10-9 – HAC Single Package Results

Case ID	Filename	Pitch (in)	Water Density Between Plates (g/cm^3)	k	σ	k_s (k+2σ)
MURR						
XC1	HS_MURR2_NP00	0.130	1.0	0.48916	0.00107	0.49130
XC2	HS_MURR2_NP02	0.138	1.0	0.50506	0.00111	0.50728
XC3	HS_MURR2_NP04	0.146	1.0	0.51620	0.00116	0.51852
XC4	HS_MURR2_NP06	0.154	1.0	0.52285	0.00113	0.52511
XC5	HS_MURR2_NP08	0.161	1.0	0.53481	0.00104	0.53689
XC6	HS_MURR2_NP09	0.167	1.0	0.53887	0.00103	0.54093
XC7	**HS_MURR2_P09**	**0.167**	**1.0**	**0.54374**	**0.00105**	**0.54584**
XC8	HS_MURR2_P09_M080	0.167	0.8	0.47997	0.00111	0.48219
XC9	HS_MURR2_P09_M090	0.167	0.9	0.51244	0.00106	0.51456
MIT						
YC1	HS_MIT_NP158	0.158	1.0	0.37316	0.00090	0.37496
YC2	HS_MIT_NP16	0.160	1.0	0.37349	0.00095	0.37539
YC3	HS_MIT_NP17	0.170	1.0	0.38238	0.00088	0.38414
YC4	HS_MIT_NP18	0.180	1.0	0.38957	0.00098	0.39153
YC5	HS_MIT_NP19	0.190	1.0	0.39967	0.00105	0.40177
YC6	HS_MIT_NP20	0.200	1.0	0.40825	0.00095	0.41015
YC7	HS_MIT_NP21	0.210	1.0	0.41309	0.00104	0.41517
YC8	HS_MIT_NP22	0.220	1.0	0.41701	0.00100	0.41901
YC9	HS_MIT_NP23	0.230	1.0	0.42605	0.00093	0.42791
YC10	HS_MIT_NP24	0.240	1.0	0.43051	0.00105	0.43261
YC11	**HS_MIT_P24**	**0.240**	**1.0**	**0.43474**	**0.00096**	**0.43666**
YC12	HS_MIT_P24_M080	0.240	0.8	0.39439	0.00098	0.39635
YC13	HS_MIT_P24_M090	0.240	0.9	0.41226	0.00095	0.41416

6.10.5 Evaluation of Package Arrays under Normal Conditions of Transport

6.10.5.1 NCT Array Configuration

6.10.5.1.1 MURR Fuel Element Models

The NCT array model is a 9x9x1 array of the NCT single package model. Although an 8x8x1 array is of sufficient size to justify a CSI = 4.0, the larger 9x9x1 array is utilized simply for modeling convenience. Void is always present between the insulation and the outer tube, as this region is water-tight. The entire array is reflected with 12-in of full-density water.

The FHEs are pushed to the center of the array and rotated to minimize the distance between the fuel elements, see Figure 6.10-10. The modeled lateral shifting of the FHE inside of the tube is computed assuming the maximum inner diameter of the inner tube (5.814-in, see Section 6.3.1, *Model Configuration*) and minimum outer radius of the FHE (2.8-0.2 = 2.6-in, from the packaging general arrangement drawings), or 0.307-in. The fuel element is also modeled at the lateral "top" of the FHE to minimize the distance between the fuel elements.

Six calculational series are developed, as described below. Results are summarized in Table 6.10-10.

Series 1 (Cases XD1 through XD12): In Series 1, the water density is fixed at 1.0 g/cm^3 between the fuel plates, and the water density inside and outside the FHE is modeled at the same density, which is allowed to vary between 0 and 1.0 g/cm^3. This moderation condition simulates the partial moderation effect of assuming the plastic bag that surrounds the fuel element retains water. The neoprene (without chlorine) from the FHEs is modeled in an approximate manner. The modeled channel width is 0.088-in. Also, the FHE is modeled with the minimum wall thickness.

As a point of interest, an additional case (Case XD12) is developed in which the fuel elements are centered in the cavity and not rotated, using the moderation assumptions of the most reactive case (Case XD7). The reactivity drops by 18.5 mk, which essentially represents the additional conservatism of pushing the fuel elements to the center of the array.

Series 2 (Cases XE1 through XE11): Series 2 is the same as Series 1, although the FHE neoprene is not modeled. The results in Table 6.10-10 indicate that the maximum reactivity occurs when chlorine-free neoprene is modeled (compare Cases XD7 and XE7), although the difference is within statistical fluctuation.

Series 3 (Cases XF1 through XF10): In Series 3, the water density inside the FHE is fixed at 1.0 g/cm^3, while the water density outside the FHE is allowed to vary between 0 and 1.0 g/cm^3. This moderation condition simulates the partial moderation effect of assuming the FHE retains water. The maximum reactivity increases slightly compared to Series 1.

Series 4 (Cases XG1 through XG11): Series 4 is the same as Series 3, although the FHE is modeled with the maximum wall thickness. The reactivity increases slightly, although the difference is within statistical fluctuation.

Series 5 (Cases XH1 through XH11): Series 5 is the same as Series 3, although the density within the fuel plates is modeled at a reduced density of 0.9 g/cm^3. The reactivity drops sharply as the water density between the plates is reduced.

Series 6 (Cases XI1 through XI11) is the same as Series 4, except the channel width is increased from 0.088-in to 0.092-in. The reactivity increases with increasing channel width, consistent with the single package models. Reactivity is at a maximum for Case XI5, with k_s = 0.85643. In this case, the fuel elements are pushed to the center of the array, full-density water is modeled between the plates and inside the FHE, 0.4 g/cm^3 water is modeled outside the FHE, chlorine-free neoprene is included, the FHE is modeled with maximum wall thickness, and the channel width is modeled at 0.092-in. The maximum result is below the USL of 0.9209.

6.10.5.1.2 MIT Fuel Element Models

The NCT array model is a 9x9x1 array of the NCT single package model. Although an 8x8x1 array is of sufficient size to justify a CSI = 4.0, the larger 9x9x1 array is utilized simply for modeling convenience. Void is always present between the insulation and the outer tube, as this region is water-tight. The entire array is reflected with 12-in of full-density water.

The FHEs are pushed to the center of the array and rotated to minimize the distance between the fuel elements, see Figure 6.10-10. The modeled lateral shifting of the FHE inside of the tube is computed assuming the maximum inner diameter of the inner tube (5.814-in, see Section 6.3.1, *Model Configuration*) and minimum outer radius of the FHE (2.8-0.2 = 2.6-in, from the packaging general arrangement drawings), or 0.307-in.

In addition to the lateral shifting of the FHE within the tube, the MIT fuel element is free to move laterally within the FHE. To simplify the model geometry, rather than modeling each fuel element shifted within each FHE, the fuel elements are modeled in the center of the FHE, and the FHE is shifted toward the center of the array an additional 0.13-in (the approximate as-modeled distance between the fuel element and neoprene).

Six calculational series are developed, as described below. Results are summarized in Table 6.10-11.

Series 1 (Cases YD1 through YD12): In Series 1, the water density is fixed at 1.0 g/cm^3 between the fuel plates, and the water density inside and outside the FHE is modeled at the same density, which is allowed to vary between 0 and 1.0 g/cm^3. This moderation condition simulates the partial moderation effect of assuming the plastic bag that surrounds the fuel element retains water. The neoprene (without chlorine) from the FHE is modeled in an approximate manner. The modeled channel width is 0.094-in. Also, the FHE is modeled with the minimum wall thickness.

As a point of interest, an additional case (Case YD12) is developed in which the fuel elements are centered in the cavity and not rotated, using the moderation assumptions of the most reactive case (Case YD7). The reactivity drops by 12.5 mk, which essentially represents the additional conservatism of pushing the fuel elements to the center of the array.

Series 2 (Cases YE1 through YE11): Series 2 is the same as Series 1, although the FHE neoprene is not modeled. Comparing Series 1 to Series 2, the reactivity is slightly higher when chlorine-free neoprene is modeled (compare Cases YD7 and YE7), although the difference is within statistical fluctuation.

Series 3 (Cases YF1 through YF10): In Series 3, the water density inside the FHE is fixed at 1.0 g/cm^3, while the water density outside the FHE is allowed to vary between 0 and 1.0 g/cm^3. This moderation condition simulates the partial moderation effect of assuming the FHE retains water. The maximum reactivity increases slightly compared to Series 1, although the effect is well within statistical fluctuation.

Series 4 (Cases YG1 through YG11): Series 4 is the same as Series 3, although the FHE is modeled with the maximum wall thickness. The reactivity decreases slightly, although the difference may be statistical fluctuation. Note that reactivity increased slightly with the thicker walled FHE in the MURR models.

Series 5 (Cases YH1 through YH11): Series 5 is the same as Series 3, although the density within the fuel plates is modeled at a reduced density of 0.9 g/cm^3. The reactivity drops sharply as the water density between the plates is reduced.

Series 6 (Cases YI1 through YI11): Series 6 is the same as Series 3, although the modeled channel width is increased from 0.094-in to 0.116-in. Reactivity is at a maximum for Case YI6, with k_s = 0.65658. In this case, the fuel elements are pushed to the center of the array, full-density water is modeled between the plates and inside the FHE, 0.5 g/cm^3 water is modeled outside the FHE, chlorine-free neoprene is included, the FHE is modeled with minimum wall thickness, and the modeled channel width is 0.116-in. The maximum result is far below the USL of 0.9209.

6.10.5.2 NCT Array Results

The results for the NCT array cases are provided in the following tables. The most reactive configuration in each series is listed in boldface.

Table 6.10-10 – MURR NCT Array Results

Case ID	Filename	Water Density Inside FHE (g/cm^3)	Water Density Outside FHE (g/cm^3)	Water Density Between Plates (g/cm^3)	k_{eff}	σ	k_s (k+2σ)
Series 1: Variable water density inside and outside FHE, with neoprene.							
XD1	NA_MURR2_NW000	0	0	1.0	0.76937	0.00121	0.77179
XD2	NA_MURR2_NW010	0.1	0.1	1.0	0.79729	0.00123	0.79975
XD3	NA_MURR2_NW020	0.2	0.2	1.0	0.81129	0.00129	0.81387
XD4	NA_MURR2_NW030	0.3	0.3	1.0	0.82519	0.00129	0.82777
XD5	NA_MURR2_NW040	0.4	0.4	1.0	0.83449	0.00130	0.83709
XD6	NA_MURR2_NW050	0.5	0.5	1.0	0.83502	0.00123	0.83748
XD7	**NA_MURR2_NW060**	**0.6**	**0.6**	**1.0**	**0.83801**	**0.00124**	**0.84049**
XD8	NA_MURR2_NW070	0.7	0.7	1.0	0.83447	0.00111	0.83669
XD9	NA_MURR2_NW080	0.8	0.8	1.0	0.83185	0.00119	0.83423
XD10	NA_MURR2_NW090	0.9	0.9	1.0	0.82537	0.00123	0.82783
XD11	NA_MURR2_NW100	1.0	1.0	1.0	0.81935	0.00120	0.82175
XD12	NA_MURR2_NW060C	0.6	0.6	1.0	0.81957	0.00123	0.82203
Series 2: Repeat of Series 1 without neoprene							
XE1	NA_MURR2_W000	0	0	1.0	0.75717	0.00117	0.75951
XE2	NA_MURR2_W010	0.1	0.1	1.0	0.78680	0.00103	0.78886
XE3	NA_MURR2_W020	0.2	0.2	1.0	0.80910	0.00116	0.81142
XE4	NA_MURR2_W030	0.3	0.3	1.0	0.82154	0.00114	0.82382
XE5	NA_MURR2_W040	0.4	0.4	1.0	0.83148	0.00129	0.83406
XE6	NA_MURR2_W050	0.5	0.5	1.0	0.83479	0.00111	0.83701
XE7	**NA_MURR2_W060**	**0.6**	**0.6**	**1.0**	**0.83681**	**0.00115**	**0.83911**
XE8	NA_MURR2_W070	0.7	0.7	1.0	0.83504	0.00126	0.83756
XE9	NA_MURR2_W080	0.8	0.8	1.0	0.83138	0.00116	0.83370
XE10	NA_MURR2_W090	0.9	0.9	1.0	0.82487	0.00122	0.82731
XE11	NA_MURR2_W100	1.0	1.0	1.0	0.81734	0.00128	0.81990
Series 3: Variable water density outside FHE, with neoprene.							
XF1	NA_MURR2_FNW000	1.0	0	1.0	0.83204	0.00135	0.83474
XF2	NA_MURR2_FNW010	1.0	0.1	1.0	0.83421	0.00118	0.83657
XF3	NA_MURR2_FNW020	1.0	0.2	1.0	0.84008	0.00131	0.84270
XF4	**NA_MURR2_FNW030**	**1.0**	**0.3**	**1.0**	**0.84082**	**0.00132**	**0.84346**
XF5	NA_MURR2_FNW040	1.0	0.4	1.0	0.84055	0.00120	0.84295
XF6	NA_MURR2_FNW050	1.0	0.5	1.0	0.83832	0.00116	0.84064
XF7	NA_MURR2_FNW060	1.0	0.6	1.0	0.83730	0.00118	0.83966
XF8	NA_MURR2_FNW070	1.0	0.7	1.0	0.83373	0.00130	0.83633
XF9	NA_MURR2_FNW080	1.0	0.8	1.0	0.83100	0.00124	0.83348
XF10	NA_MURR2_FNW090	1.0	0.9	1.0	0.82544	0.00129	0.82802
XD11	NA_MURR2_NW100	1.0	1.0	1.0	0.81935	0.00120	0.82175

(continued)

Table 6.10-10 – MURR NCT Array Results (concluded)

Case ID	Filename	Water Density Inside FHE (g/cm^3)	Water Density Outside FHE (g/cm^3)	Water Density Between Plates (g/cm^3)	k_{eff}	σ	k_s (k+2σ)
Series 4: Same as Series 3 but with maximum thickness FHE.							
XG1	NA_MURR2_TFNW000	1.0	0	1.0	0.83659	0.00121	0.83901
XG2	NA_MURR2_TFNW010	1.0	0.1	1.0	0.83959	0.00114	0.84187
XG3	NA_MURR2_TFNW020	1.0	0.2	1.0	0.84116	0.00126	0.84368
XG4	NA_MURR2_TFNW030	1.0	0.3	1.0	0.84029	0.00128	0.84285
XG5	**NA_MURR2_TFNW040**	**1.0**	**0.4**	**1.0**	**0.84340**	**0.00128**	**0.84596**
XG6	NA_MURR2_TFNW050	1.0	0.5	1.0	0.83927	0.00116	0.84159
XG7	NA_MURR2_TFNW060	1.0	0.6	1.0	0.83816	0.00117	0.84050
XG8	NA_MURR2_TFNW070	1.0	0.7	1.0	0.83704	0.00131	0.83966
XG9	NA_MURR2_TFNW080	1.0	0.8	1.0	0.83199	0.00118	0.83435
XG10	NA_MURR2_TFNW090	1.0	0.9	1.0	0.82930	0.00116	0.83162
XG11	NA_MURR2_TFNW100	1.0	1.0	1.0	0.82461	0.00129	0.82719
Series 5: Same as Series 3 with 0.9 g/cm^3 water between fuel plates.							
XH1	NA_MURR2_M90FNW000	1.0	0	0.9	0.80160	0.00132	0.80424
XH2	NA_MURR2_M90FNW010	1.0	0.1	0.9	0.80747	0.00120	0.80987
XH3	NA_MURR2_M90FNW020	1.0	0.2	0.9	0.81288	0.00127	0.81542
XH4	**NA_MURR2_M90FNW030**	**1.0**	**0.3**	**0.9**	**0.81512**	**0.00127**	**0.81766**
XH5	NA_MURR2_M90FNW040	1.0	0.4	0.9	0.81504	0.00120	0.81744
XH6	NA_MURR2_M90FNW050	1.0	0.5	0.9	0.81382	0.00112	0.81606
XH7	NA_MURR2_M90FNW060	1.0	0.6	0.9	0.81369	0.00121	0.81611
XH8	NA_MURR2_M90FNW070	1.0	0.7	0.9	0.81165	0.00129	0.81423
XH9	NA_MURR2_M90FNW080	1.0	0.8	0.9	0.80950	0.00122	0.81194
XH10	NA_MURR2_M90FNW090	1.0	0.9	0.9	0.80311	0.00124	0.80559
XH11	NA_MURR2_M90FNW100	1.0	1.0	0.9	0.79735	0.00117	0.79969
Series 6: Same as Series 4 but with a modeled channel width of 0.092-in.							
XI1	NA_MURR2_TFNW000C	1.0	0	1.0	0.84994	0.00110	0.85214
XI2	NA_MURR2_TFNW010C	1.0	0.1	1.0	0.85141	0.00120	0.85381
XI3	NA_MURR2_TFNW020C	1.0	0.2	1.0	0.85273	0.00124	0.85521
XI4	NA_MURR2_TFNW030C	1.0	0.3	1.0	0.85209	0.00124	0.85457
XI5	**NA_MURR2_TFNW040C**	**1.0**	**0.4**	**1.0**	**0.85405**	**0.00119**	**0.85643**
XI6	NA_MURR2_TFNW050C	1.0	0.5	1.0	0.84925	0.00127	0.85179
XI7	NA_MURR2_TFNW060C	1.0	0.6	1.0	0.84912	0.00124	0.85160
XI8	NA_MURR2_TFNW070C	1.0	0.7	1.0	0.84584	0.00115	0.84814
XI9	NA_MURR2_TFNW080C	1.0	0.8	1.0	0.84296	0.00127	0.84550
XI10	NA_MURR2_TFNW090C	1.0	0.9	1.0	0.83957	0.00115	0.84187
XI11	NA_MURR2_TFNW100C	1.0	1.0	1.0	0.83490	0.00123	0.83736

Table 6.10-11 – MIT NCT Array Results

Case ID	Filename	Water Density Inside FHE (g/cm^3)	Water Density Outside FHE (g/cm^3)	Water Density Between Plates (g/cm^3)	k_{eff}	σ	k_s (k+2σ)
Series 1: Variable water density and outside FHE, with neoprene							
YD1	NA_MIT_NW000	0	0	1.0	0.48041	0.00096	0.48233
YD2	NA_MIT_NW010	0.1	0.1	1.0	0.52918	0.00105	0.53128
YD3	NA_MIT_NW020	0.2	0.2	1.0	0.56301	0.00103	0.56507
YD4	NA_MIT_NW030	0.3	0.3	1.0	0.59062	0.00105	0.59272
YD5	NA_MIT_NW040	0.4	0.4	1.0	0.60722	0.00122	0.60966
YD6	NA_MIT_NW050	0.5	0.5	1.0	0.61575	0.00118	0.61811
YD7	**NA_MIT_NW060**	**0.6**	**0.6**	**1.0**	**0.61989**	**0.00114**	**0.62217**
YD8	NA_MIT_NW070	0.7	0.7	1.0	0.61723	0.00110	0.61943
YD9	NA_MIT_NW080	0.8	0.8	1.0	0.61618	0.00116	0.61850
YD10	NA_MIT_NW090	0.9	0.9	1.0	0.61352	0.00112	0.61576
YD11	NA_MIT_NW100	1.0	1.0	1.0	0.60885	0.00112	0.61109
YD12	NA_MIT_CNW060	0.6	0.6	1.0	0.60764	0.00103	0.60970
Series 2: Repeat of Series 1 without neoprene							
YE1	NA_MIT_W000	0	0	1.0	0.46154	0.00093	0.46340
YE2	NA_MIT_W010	0.1	0.1	1.0	0.51291	0.00095	0.51481
YE3	NA_MIT_W020	0.2	0.2	1.0	0.55394	0.00103	0.55600
YE4	NA_MIT_W030	0.3	0.3	1.0	0.58160	0.00113	0.58386
YE5	NA_MIT_W040	0.4	0.4	1.0	0.60184	0.00111	0.60406
YE6	NA_MIT_W050	0.5	0.5	1.0	0.61163	0.00119	0.61401
YE7	**NA_MIT_W060**	**0.6**	**0.6**	**1.0**	**0.61746**	**0.00117**	**0.61980**
YE8	NA_MIT_W070	0.7	0.7	1.0	0.61518	0.00116	0.61750
YE9	NA_MIT_W080	0.8	0.8	1.0	0.61215	0.00106	0.61427
YE10	NA_MIT_W090	0.9	0.9	1.0	0.61082	0.00111	0.61304
YE11	NA_MIT_W100	1.0	1.0	1.0	0.60324	0.00110	0.60544
Series 3: Variable water density outside FHE, with neoprene.							
YF1	NA_MIT_FNW000	1.0	0	1.0	0.55417	0.00118	0.55653
YF2	NA_MIT_FNW010	1.0	0.1	1.0	0.57731	0.00104	0.57939
YF3	NA_MIT_FNW020	1.0	0.2	1.0	0.59825	0.00117	0.60059
YF4	NA_MIT_FNW030	1.0	0.3	1.0	0.60830	0.00119	0.61068
YF5	NA_MIT_FNW040	1.0	0.4	1.0	0.61581	0.00116	0.61813
YF6	NA_MIT_FNW050	1.0	0.5	1.0	0.61968	0.00107	0.62182
YF7	**NA_MIT_FNW060**	**1.0**	**0.6**	**1.0**	**0.62059**	**0.00113**	**0.62285**
YF8	NA_MIT_FNW070	1.0	0.7	1.0	0.62035	0.00110	0.62255
YF9	NA_MIT_FNW080	1.0	0.8	1.0	0.61650	0.00110	0.61870
YF10	NA_MIT_FNW090	1.0	0.9	1.0	0.61120	0.00105	0.61330
YD11	NA_MIT_NW100	1.0	1.0	1.0	0.60885	0.00112	0.61109

(continued)

Table 6.10-11 – MIT NCT Array Results (concluded)

Case ID	Filename	Water Density Inside FHE (g/cm^3)	Water Density Outside FHE (g/cm^3)	Water Density Between Plates (g/cm^3)	k_{eff}	σ	k_s (k+2σ)
Series 4: Same as Series 3 but with maximum thickness FHE.							
YG1	NA_MIT_TFNW000	1.0	0	1.0	0.55951	0.00106	0.56163
YG2	NA_MIT_TFNW010	1.0	0.1	1.0	0.58058	0.00105	0.58268
YG3	NA_MIT_TFNW020	1.0	0.2	1.0	0.59653	0.00105	0.59863
YG4	NA_MIT_TFNW030	1.0	0.3	1.0	0.60581	0.00118	0.60817
YG5	NA_MIT_TFNW040	1.0	0.4	1.0	0.61242	0.00110	0.61462
YG6	NA_MIT_TFNW050	1.0	0.5	1.0	0.61318	0.00104	0.61526
YG7	NA_MIT_TFNW060	1.0	0.6	1.0	0.61463	0.00120	0.61703
YG8	**NA_MIT_TFNW070**	**1.0**	**0.7**	**1.0**	**0.61501**	**0.00111**	**0.61723**
YG9	NA_MIT_TFNW080	1.0	0.8	1.0	0.61394	0.00114	0.61622
YG10	NA_MIT_TFNW090	1.0	0.9	1.0	0.60894	0.00113	0.61120
YG11	NA_MIT_TFNW100	1.0	1.0	1.0	0.60456	0.00120	0.60696
Series 5: Same as Series 3 with 0.9 g/cm^3 water between fuel plates.							
YH1	NA_MIT_M90FNW000	1.0	0	0.9	0.53177	0.00107	0.53391
YH2	NA_MIT_M90FNW010	1.0	0.1	0.9	0.55655	0.00108	0.55871
YH3	NA_MIT_M90FNW020	1.0	0.2	0.9	0.57776	0.00122	0.58020
YH4	NA_MIT_M90FNW030	1.0	0.3	0.9	0.59349	0.00102	0.59553
YH5	NA_MIT_M90FNW040	1.0	0.4	0.9	0.60205	0.00103	0.60411
YH6	NA_MIT_M90FNW050	1.0	0.5	0.9	0.60659	0.00102	0.60863
YH7	NA_MIT_M90FNW060	1.0	0.6	0.9	0.60651	0.00119	0.60889
YH8	**NA_MIT_M90FNW070**	**1.0**	**0.7**	**0.9**	**0.60753**	**0.00121**	**0.60995**
YH9	NA_MIT_M90FNW080	1.0	0.8	0.9	0.60615	0.00112	0.60839
YH10	NA_MIT_M90FNW090	1.0	0.9	0.9	0.60192	0.00100	0.60392
YH11	NA_MIT_M90FNW100	1.0	1.0	0.9	0.59396	0.00111	0.59618
Series 6: Same as Series 3 but with modeled channel width of 0.116-in.							
YI1	NA_MIT_FNW000C	1.0	0	1.0	0.60247	0.00113	0.60473
YI2	NA_MIT_FNW010C	1.0	0.1	1.0	0.62391	0.00116	0.62623
YI3	NA_MIT_FNW020C	1.0	0.2	1.0	0.63710	0.00115	0.63940
YI4	NA_MIT_FNW030C	1.0	0.3	1.0	0.64617	0.00129	0.64875
YI5	NA_MIT_FNW040C	1.0	0.4	1.0	0.65160	0.00119	0.65398
YI6	**NA_MIT_FNW050C**	**1.0**	**0.5**	**1.0**	**0.65414**	**0.00122**	**0.65658**
YI7	NA_MIT_FNW060C	1.0	0.6	1.0	0.65181	0.00119	0.65419
YI8	NA_MIT_FNW070C	1.0	0.7	1.0	0.65016	0.00109	0.65234
YI9	NA_MIT_FNW080C	1.0	0.8	1.0	0.64541	0.00118	0.64777
YI10	NA_MIT_FNW090C	1.0	0.9	1.0	0.64029	0.00106	0.64241
YI11	NA_MIT_FNW100C	1.0	1.0	1.0	0.63436	0.00114	0.63664

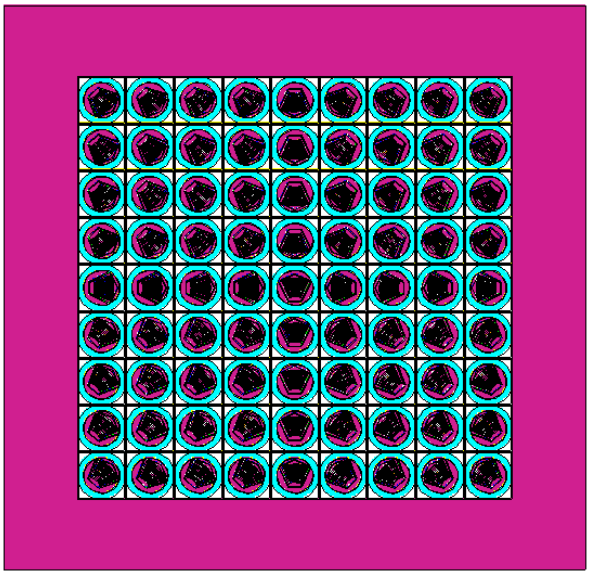

MURR Full view

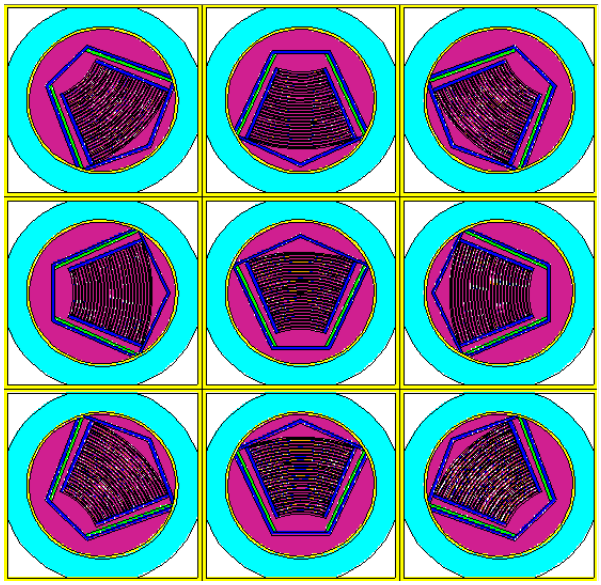

MURR Close-up

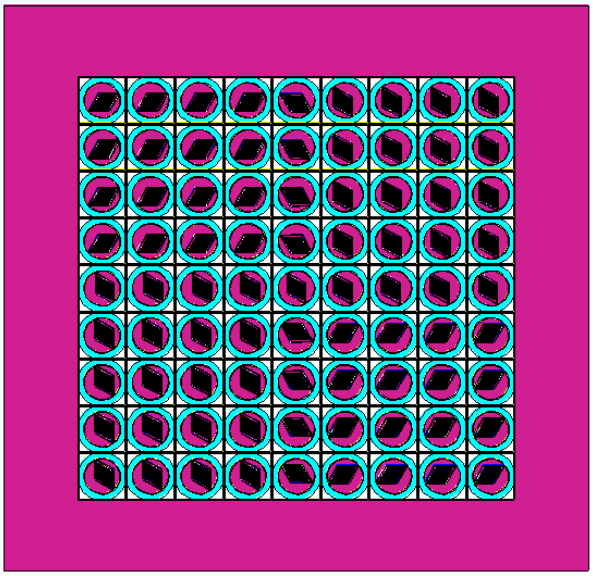

MIT Full view

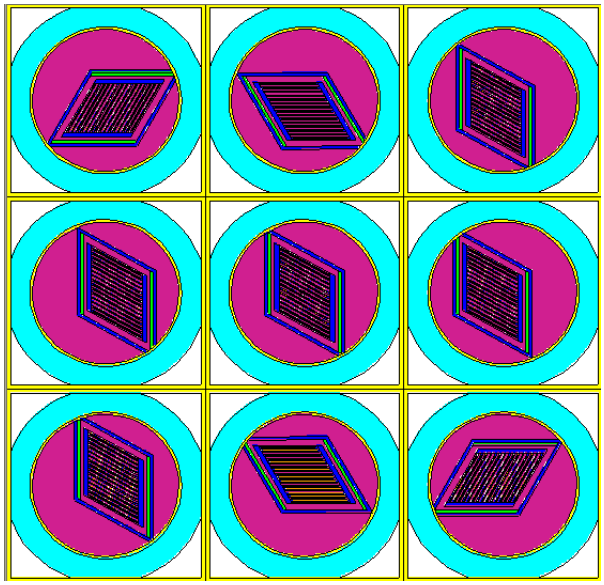

MIT Close-up

Figure 6.10-10 – MURR/MIT NCT Array Geometry

6.10.6 Package Arrays under Hypothetical Accident Conditions

6.10.6.1 HAC Array Condition

The HAC array model is a 5x5x1 array of packages. The primary difference comparing NCT to HAC is the modeled fuel damage, and separation of the FHE halves. Consistent with the HAC single package models, the two FHE halves are allowed to separate to the maximum possible extent, and the fuel element pitch is allowed to increase to the maximum possible value until constrained by the FHE. It is established in the HAC single package analysis that the reactivity is maximized with the maximum pitch, so all HAC array calculations utilize the maximum pitch.

The moderation conditions for the HAC array cases are largely the same as the NCT array moderation conditions, with the exception of the insulation region. In the HAC models, this region may be filled with variable density water. From the NCT array calculations, it was determined that the neoprene has a statistically insignificant effect on the reactivity, although the results showed a negligible increase. Therefore, neoprene is included in all HAC array models. Also, it has also been established in the HAC single package and NCT array cases that reducing the water density between the fuel plates reduces the reactivity. Therefore, the water between the fuel plates is always modeled at full density.

Although it is not feasible in actual practice to push the FHEs to the center of the array if the two FHE halves are already pushed apart, both the MURR and MIT models are shifted by 0.307-in towards the center of the array, as determined in Section 6.10.5.1, *NCT Array Configuration*. Note in Figure 6.10-11 that the FHEs for both MURR and MIT are “sliced off” in the corners because such a translation is not possible without interference, and the aluminum corners of the MIT element are also “sliced off” slightly for the same reason.

6.10.6.1.1 MURR Fuel Element Models

Five calculational series are developed, as described below. Results are summarized in Table 6.10-12.

Series 1 (Cases XJ1 through XJ11): In Series 1, the water density inside and outside the FHE is modeled at the same density, which is allowed to vary between 0 and 1.0 g/cm^3. This moderation condition simulates the partial moderation effect of assuming the plastic bag that surrounds the fuel element retains water. The region between the circular and square tubes is modeled as insulation/void, and the FHE is modeled with the minimum wall thickness.

Series 2 (Cases XK1 through XK11): In Series 2, the water density inside the FHE is fixed at 1.0 g/cm^3, while the water density outside the FHE is allowed to vary between 0 and 1.0 g/cm^3. This moderation condition simulates the partial moderation effect of assuming the FHE retains water. The region between the circular and square tubes is modeled as insulation/void, and the FHE is modeled with a minimum wall thickness. The maximum reactivity increases slightly compared to Series 1, although the effect is well within statistical fluctuation.

An additional case (Case XK11) is developed in which the insulation is replaced with void for the most reactive Series 2 case (Case XK10). Comparing Cases XK10 and XK11, it is slightly more reactive to model the insulation, which is consistent with the trend in the ATR fuel analysis.

Series 3 (Cases XL1 through XL11): In Series 3, the outer insulation/void region is replaced with variable density water. There are now three regions that contain water: (1) between the circular and square tubes, (2) between FHE and circular tube, and (3) between fuel element and FHE. In this series, each of these regions is modeled with the same water density, which is allowed to vary between 0 and 1.0 g/cm^3. Reactivity is significantly lower in Series 3 compared with either Series 1 or 2.

Series 4 (Cases XM1 through XM10): In Series 4, full-density water is modeled inside the FHE, while variable density water between 0 and 1.0 g/cm^3 is modeled outside the FHE and between the inner and outer tubes. This series is less reactive than either Series 1 or 2.

Series 5 (Cases XN1 through XN11): Series 5 is a repeat of Series 2 except using a thick-walled FHE. The reactivity increases slightly when the thick-walled FHE is used.

Series 1, 2 and 5 result in similar reactivities within the statistical uncertainty of the method. Case XN9 is the most reactive MURR case, with k_s = 0.85881. In this case, the fuel elements are pushed to the center of the array, full-density water is modeled between the plates and inside the FHE, 0.8 g/cm^3 water is modeled outside the FHE, insulation/void is modeled between the inner and outer tubes, chlorine-free neoprene is included, and the FHE is modeled with maximum wall thickness. The maximum result is below the USL of 0.9209.

6.10.6.1.2 MIT Fuel Element Models

Five calculational series are developed, as described below. Results are summarized in Table 6.10-13.

Series 1 (Cases YJ1 through YJ11): In Series 1, the water density inside and outside the FHE is modeled at the same density, which is allowed to vary between 0 and 1.0 g/cm^3. This moderation condition simulates the partial moderation effect of assuming the plastic bag that surrounds the fuel element retains water. The region between the circular and square tubes is modeled as insulation/void, and the FHE is modeled with the minimum wall thickness.

Series 2 (Cases YK1 through YK11): In Series 2, the water density inside the FHE is fixed at 1.0 g/cm^3, while the water density outside the FHE is allowed to vary between 0 and 1.0 g/cm^3. This moderation condition simulates the partial moderation effect of assuming the FHE retains water. The region between the circular and square tubes is modeled as insulation/void, and the FHE is modeled with a minimum wall thickness. The maximum reactivity increases slightly compared to Series 1, although the effect is well within statistical fluctuation.

An additional case (Case YK11) is developed in which the insulation is replaced with void for the most reactive Series 2 case (Case YK9). Comparing Cases YK9 and YK11, it is slightly more reactive to model the insulation, which is consistent with the trend in the ATR fuel analysis.

Series 3 (Cases YL1 through YL11): In Series 3, the outer insulation/void region is replaced with variable density water. There are now three regions that contain water: (1) between the circular and square tubes, (2) between FHE and circular tube, and (3) between fuel element and FHE. In this series, each of these regions is modeled with the same water density, which is allowed to vary between 0 and 1.0 g/cm^3. Reactivity is significantly lower in Series 3 compared with either Series 1 or 2.

Series 4 (Cases YM1 through YM10): In Series 4, full-density water is modeled inside the FHE, while variable density water between 0 and 1.0 g/cm^3 is modeled outside the FHE and between the inner and outer tubes. This series is less reactive than either Series 1 or 2.

Series 5 (Cases YN1 through YN11): Series 5 is a repeat of Series 2 except using a thick-walled FHE. The reactivity decreases slightly when the thick-walled FHE is used, although the decrease is within statistical fluctuation.

Series 1, 2 and 5 result in similar reactivities within the statistical uncertainty of the method. Case YK9 is the most reactive MIT case, with k_s = 0.67309. In this case, the fuel elements are pushed to the center of the array, full-density water is modeled between the plates and inside the FHE, 0.8 g/cm^3 water is modeled outside the FHE, insulation/void is modeled between the inner and outer tubes, chlorine-free neoprene is included, and the FHE is modeled with minimum wall thickness. The maximum result is below the USL of 0.9209.

6.10.6.2 HAC Array Results

Following are the tabulated results for the HAC array cases. The most reactive configuration in each series is listed in boldface.

Table 6.10-12 – MURR HAC Array Results

Case ID	Filename	Water Density Between Tubes (g/cm^3)	Water Density Inside FHE (g/cm^3)	Water Density Outside FHE (g/cm^3)	k_{eff}	σ	k_s (k+2σ)
Series 1: Insulation modeled, full-density water between plates, variable density water as indicated.							
XJ1	HA_MURR2_NW000	0	0	0	0.76355	0.00115	0.76585
XJ2	HA_MURR2_NW010	0	0.1	0.1	0.78430	0.00122	0.78674
XJ3	HA_MURR2_NW020	0	0.2	0.2	0.80290	0.00111	0.80512
XJ4	HA_MURR2_NW030	0	0.3	0.3	0.81874	0.00124	0.82122
XJ5	HA_MURR2_NW040	0	0.4	0.4	0.83311	0.00127	0.83565
XJ6	HA_MURR2_NW050	0	0.5	0.5	0.84140	0.00122	0.84384
XJ7	HA_MURR2_NW060	0	0.6	0.6	0.84544	0.00124	0.84792
XJ8	HA_MURR2_NW070	0	0.7	0.7	0.85035	0.00118	0.85271
XJ9	HA_MURR2_NW080	0	0.8	0.8	0.84998	0.00127	0.85252
XJ10	**HA_MURR2_NW090**	**0**	**0.9**	**0.9**	**0.85379**	**0.00128**	**0.85635**
XJ11	HA_MURR2_NW100	0	1.0	1.0	0.84975	0.00120	0.85215
Series 2: Insulation modeled, full-density water between plates and inside FHE, variable density water as indicated.							
XK1	HA_MURR2_FNW000	0	1.0	0	0.83610	0.00115	0.83840
XK2	HA_MURR2_FNW010	0	1.0	0.1	0.84001	0.00125	0.84251
XK3	HA_MURR2_FNW020	0	1.0	0.2	0.84152	0.00115	0.84382
XK4	HA_MURR2_FNW030	0	1.0	0.3	0.84875	0.00130	0.85135
XK5	HA_MURR2_FNW040	0	1.0	0.4	0.84946	0.00127	0.85200
XK6	HA_MURR2_FNW050	0	1.0	0.5	0.84850	0.00119	0.85088
XK7	HA_MURR2_FNW060	0	1.0	0.6	0.85141	0.00118	0.85377
XK8	HA_MURR2_FNW070	0	1.0	0.7	0.85076	0.00117	0.85310
XK9	HA_MURR2_FNW080	0	1.0	0.8	0.85054	0.00127	0.85308
XK10	**HA_MURR2_FNW090**	**0**	**1.0**	**0.9**	**0.85391**	**0.00125**	**0.85641**
XJ11	HA_MURR2_NW100	0	1.0	1.0	0.84975	0.0012	0.85215
XK11	HA_MURR2_FNW090X	0	1.0	0.9	0.84922	0.00132	0.85186
Series 3: Insulation not modeled, variable density water as indicated.							
XL1	HA_MURR2_ANW000	0	0	0	0.75710	0.00115	0.75940
XL2	HA_MURR2_ANW010	0.1	0.1	0.1	0.78773	0.00117	0.79007
XL3	**HA_MURR2_ANW020**	**0.2**	**0.2**	**0.2**	**0.78883**	**0.00124**	**0.79131**
XL4	HA_MURR2_ANW030	0.3	0.3	0.3	0.77894	0.00115	0.78124
XL5	HA_MURR2_ANW040	0.4	0.4	0.4	0.75950	0.00114	0.76178
XL6	HA_MURR2_ANW050	0.5	0.5	0.5	0.74010	0.00119	0.74248
XL7	HA_MURR2_ANW060	0.6	0.6	0.6	0.72381	0.00113	0.72607
XL8	HA_MURR2_ANW070	0.7	0.7	0.7	0.70323	0.00130	0.70583
XL9	HA_MURR2_ANW080	0.8	0.8	0.8	0.69154	0.00108	0.69370
XL10	HA_MURR2_ANW090	0.9	0.9	0.9	0.67881	0.00115	0.68111
XL11	HA_MURR2_ANW100	1.0	1.0	1.0	0.67207	0.00113	0.67433

(continued)

Table 6.10-12 – MURR HAC Array Results (concluded)

Case ID	Filename	Water Density Between Tubes (g/cm^3)	Water Density Inside FHE (g/cm^3)	Water Density Outside FHE (g/cm^3)	k_{eff}	σ	k_s (k+2σ)
Series 4: Insulation not modeled, variable density water as indicated.							
XM1	**HA_MURR2_IFNW000**	**0**	**1.0**	**0**	**0.83196**	**0.00121**	**0.83438**
XM2	HA_MURR2_IFNW010	0.1	1.0	0.1	0.82347	0.00123	0.82593
XM3	HA_MURR2_IFNW020	0.2	1.0	0.2	0.80575	0.00127	0.80829
XM4	HA_MURR2_IFNW030	0.3	1.0	0.3	0.78652	0.00109	0.78870
XM5	HA_MURR2_IFNW040	0.4	1.0	0.4	0.76597	0.00108	0.76813
XM6	HA_MURR2_IFNW050	0.5	1.0	0.5	0.74360	0.00124	0.74608
XM7	HA_MURR2_IFNW060	0.6	1.0	0.6	0.72740	0.00119	0.72978
XM8	HA_MURR2_IFNW070	0.7	1.0	0.7	0.70952	0.00112	0.71176
XM9	HA_MURR2_IFNW080	0.8	1.0	0.8	0.69669	0.00115	0.69899
XM10	HA_MURR2_IFNW090	0.9	1.0	0.9	0.68144	0.00119	0.68382
XL11	HA_MURR2_ANW100	1.0	1.0	1.0	0.67207	0.00113	0.67433
Series 5: Repeat of Series 2 with thick-walled FHE.							
XN1	HA_MURR2_TFNW000	0	1.0	0	0.83999	0.00136	0.84271
XN2	HA_MURR2_TFNW010	0	1.0	0.1	0.84169	0.00120	0.84409
XN3	HA_MURR2_TFNW020	0	1.0	0.2	0.84521	0.00115	0.84751
XN4	HA_MURR2_TFNW030	0	1.0	0.3	0.84875	0.00131	0.85137
XN5	HA_MURR2_TFNW040	0	1.0	0.4	0.84997	0.00117	0.85231
XN6	HA_MURR2_TFNW050	0	1.0	0.5	0.85368	0.00128	0.85624
XN7	HA_MURR2_TFNW060	0	1.0	0.6	0.85219	0.00115	0.85449
XN8	HA_MURR2_TFNW070	0	1.0	0.7	0.85204	0.00121	0.85446
XN9	**HA_MURR2_TFNW080**	**0**	**1.0**	**0.8**	**0.85621**	**0.00130**	**0.85881**
XN10	HA_MURR2_TFNW090	0	1.0	0.9	0.85319	0.00126	0.85571
XN11	HA_MURR2_TFNW100	0	1.0	1.0	0.85277	0.00121	0.85519

Table 6.10-13 – MIT HAC Array Results

Case ID	Filename	Water Density Between Tubes (g/cm^3)	Water Density Inside FHE (g/cm^3)	Water Density Outside FHE (g/cm^3)	k_{eff}	σ	k_s (k+2σ)
Series 1: Insulation modeled, full-density water between plates, variable density water as indicated.							
YJ1	HA_MIT_NW000	0	0	0	0.53667	0.00092	0.53851
YJ2	HA_MIT_NW010	0	0.1	0.1	0.56904	0.00111	0.57126
YJ3	HA_MIT_NW020	0	0.2	0.2	0.59837	0.00116	0.60069
YJ4	HA_MIT_NW030	0	0.3	0.3	0.62139	0.00122	0.62383
YJ5	HA_MIT_NW040	0	0.4	0.4	0.63737	0.00108	0.63953
YJ6	HA_MIT_NW050	0	0.5	0.5	0.65014	0.00109	0.65232
YJ7	HA_MIT_NW060	0	0.6	0.6	0.65850	0.00122	0.66094
YJ8	HA_MIT_NW070	0	0.7	0.7	0.66668	0.00115	0.66898
YJ9	**HA_MIT_NW080**	**0**	**0.8**	**0.8**	**0.67043**	**0.00121**	**0.67285**
YJ10	HA_MIT_NW090	0	0.9	0.9	0.67026	0.00112	0.67250
YJ11	HA_MIT_NW100	0	1.0	1.0	0.67058	0.00104	0.67266
Series 2: Insulation modeled, full-density water between plates and inside FHE, variable density water as indicated.							
YK1	HA_MIT_FNW000	0	1.0	0	0.60486	0.00110	0.60706
YK2	HA_MIT_FNW010	0	1.0	0.1	0.62101	0.00117	0.62335
YK3	HA_MIT_FNW020	0	1.0	0.2	0.63436	0.00121	0.63678
YK4	HA_MIT_FNW030	0	1.0	0.3	0.64759	0.00106	0.64971
YK5	HA_MIT_FNW040	0	1.0	0.4	0.65646	0.00117	0.65880
YK6	HA_MIT_FNW050	0	1.0	0.5	0.66078	0.00117	0.66312
YK7	HA_MIT_FNW060	0	1.0	0.6	0.66656	0.00107	0.66870
YK8	HA_MIT_FNW070	0	1.0	0.7	0.67022	0.00114	0.67250
YK9	**HA_MIT_FNW080**	**0**	**1.0**	**0.8**	**0.67105**	**0.00102**	**0.67309**
YK10	HA_MIT_FNW090	0	1.0	0.9	0.66898	0.00113	0.67124
YJ11	HA_MIT_NW100	0	1.0	1.0	0.67058	0.00104	0.67266
YK11	HA_MIT_FNW080X	0	1.0	0.9	0.66684	0.00110	0.66904
Series 3: Insulation not modeled, variable density water as indicated.							
YL1	HA_MIT_ANW000	0	0	0	0.53173	0.00103	0.53379
YL2	HA_MIT_ANW010	0.1	0.1	0.1	0.58121	0.00100	0.58321
YL3	HA_MIT_ANW020	0.2	0.2	0.2	0.59902	0.00119	0.60140
YL4	**HA_MIT_ANW030**	**0.3**	**0.3**	**0.3**	**0.60054**	**0.00105**	**0.60264**
YL5	HA_MIT_ANW040	0.4	0.4	0.4	0.59003	0.00116	0.59235
YL6	HA_MIT_ANW050	0.5	0.5	0.5	0.57811	0.00109	0.58029
YL7	HA_MIT_ANW060	0.6	0.6	0.6	0.56624	0.00114	0.56852
YL8	HA_MIT_ANW070	0.7	0.7	0.7	0.55438	0.00107	0.55652
YL9	HA_MIT_ANW080	0.8	0.8	0.8	0.54409	0.00114	0.54637
YL10	HA_MIT_ANW090	0.9	0.9	0.9	0.53935	0.00105	0.54145
YL11	HA_MIT_ANW100	1.0	1.0	1.0	0.53078	0.00104	0.53286

(continued)

Table 6.10-13 – MIT HAC Array Results (concluded)

Case ID	Filename	Water Density Between Tubes (g/cm^3)	Water Density Inside FHE (g/cm^3)	Water Density Outside FHE (g/cm^3)	k_{eff}	σ	k_s ($k+2\sigma$)
Series 4: Insulation not modeled, variable density water as indicated.							
YM1	HA_MIT_IFNW000	0	1.0	0	0.59996	0.00108	0.60212
YM2	**HA_MIT_IFNW010**	**0.1**	**1.0**	**0.1**	**0.61992**	**0.00112**	**0.62216**
YM3	HA_MIT_IFNW020	0.2	1.0	0.2	0.61899	0.00117	0.62133
YM4	HA_MIT_IFNW030	0.3	1.0	0.3	0.61130	0.00107	0.61344
YM5	HA_MIT_IFNW040	0.4	1.0	0.4	0.59725	0.00106	0.59937
YM6	HA_MIT_IFNW050	0.5	1.0	0.5	0.58253	0.00113	0.58479
YM7	HA_MIT_IFNW060	0.6	1.0	0.6	0.56935	0.00115	0.57165
YM8	HA_MIT_IFNW070	0.7	1.0	0.7	0.56002	0.00118	0.56238
YM9	HA_MIT_IFNW080	0.8	1.0	0.8	0.54870	0.00112	0.55094
YM10	HA_MIT_IFNW090	0.9	1.0	0.9	0.54119	0.00095	0.54309
YL11	HA_MIT_ANW100	1.0	1.0	1.0	0.53078	0.00104	0.53286
Series 5: Repeat of Series 2 with thick-walled FHE.							
YN1	HA_MIT_TFNW000	0	1.0	0	0.61405	0.00116	0.61637
YN2	HA_MIT_TFNW010	0	1.0	0.1	0.62418	0.00114	0.62646
YN3	HA_MIT_TFNW020	0	1.0	0.2	0.63652	0.00110	0.63872
YN4	HA_MIT_TFNW030	0	1.0	0.3	0.64631	0.00101	0.64833
YN5	HA_MIT_TFNW040	0	1.0	0.4	0.65197	0.00108	0.65413
YN6	HA_MIT_TFNW050	0	1.0	0.5	0.65994	0.00114	0.66222
YN7	HA_MIT_TFNW060	0	1.0	0.6	0.66467	0.00118	0.66703
YN8	HA_MIT_TFNW070	0	1.0	0.7	0.66785	0.00120	0.67025
YN9	HA_MIT_TFNW080	0	1.0	0.8	0.66872	0.00123	0.67118
YN10	**HA_MIT_TFNW090**	**0**	**1.0**	**0.9**	**0.66920**	**0.00111**	**0.67142**
YN11	HA_MIT_TFNW100	0	1.0	1.0	0.66847	0.00122	0.67091

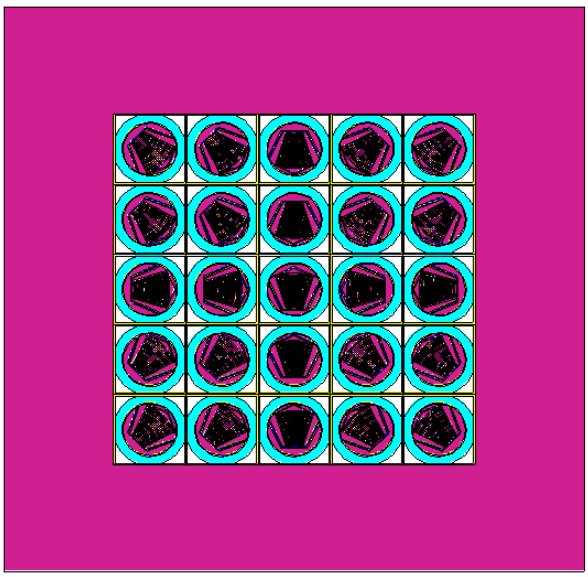

MURR Full view

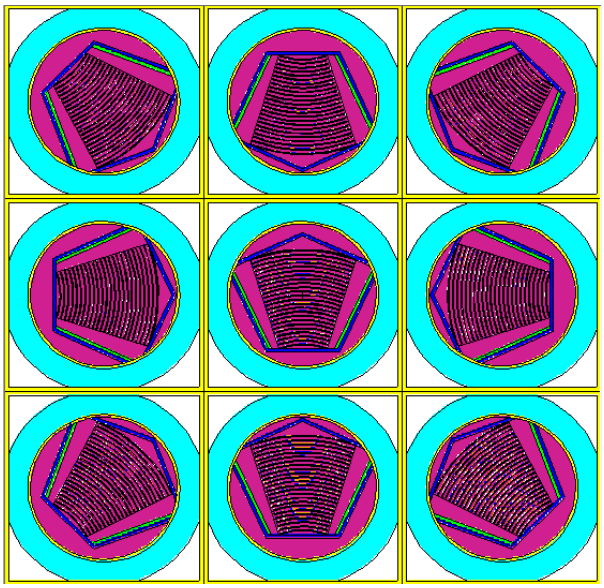

MURR Close-up

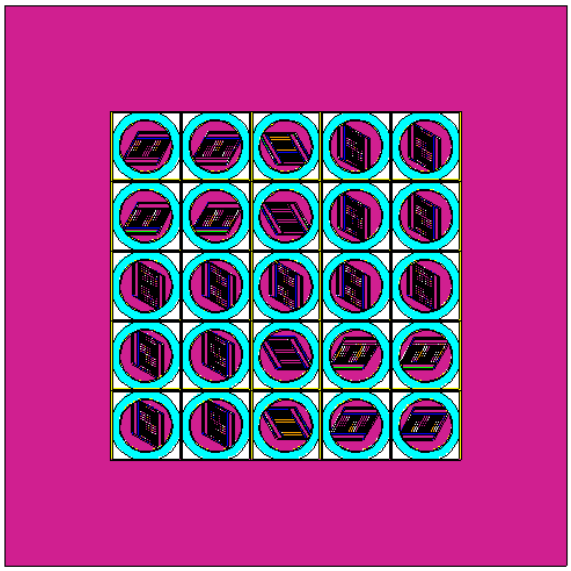

MIT Full view

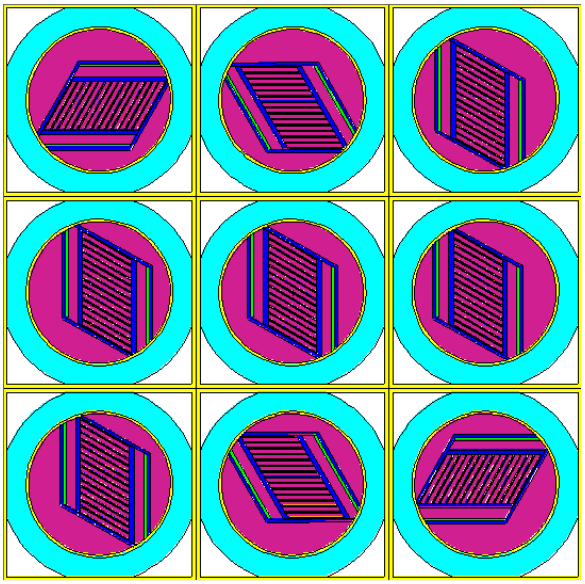

MIT Close-up

Figure 6.10-11 – MURR/MIT HAC Array Geometry

6.10.7 Fissile Material Packages for Air Transport

See Section 6.7, which applies to all contents.

6.10.8 Benchmark Evaluations

MURR and MIT fuel are both high-enriched aluminum plate-type fuel, similar to ATR fuel. Therefore, the benchmarking evaluation performed for the ATR fuel in Section 6.8, *Benchmark Evaluations*, is applicable to the current analysis, and the USL is 0.9209. The Monte Carlo computer program MCNP5 v1.30 was utilized in the benchmark analysis. MCNP has been used extensively in criticality evaluations for several decades and is considered a standard in the industry.

Five parameters were selected for the benchmark evaluation: (1) energy of the average neutron lethargy causing fission (EALF), (2) U-235 number density, (3) channel width, (4) H/U-235 atom ratio, and (5) pitch. The range of applicability of these parameters for the benchmarks utilized is summarized in Table 6.8-2. In the following sections, the range of applicability of the benchmarks is compared with the MURR and MIT criticality analysis.

6.10.8.1 Energy of the Average neutron Lethargy causing Fission (EALF)

Range of Applicability, MURR models: All of the single package models and most of the NCT and HAC array models fall within the range of the applicability. The EALF of the most reactive MURR fuel element model (Case XN9) has an EALF of 9.26E-08 MeV, which is within the range of applicability. Models with significantly more void spaces or low water densities sometimes exceed the range of applicability (maximum EALF = 2.03E-07 MeV for Case XE1), although these cases are not the most reactive. Therefore, the EALF of the most reactive models is acceptably within the range of applicability of the benchmarks.

Range of Applicability, MIT models: All of the single package models and most of the NCT and HAC array models fall within the range of the applicability. The EALF of the most reactive MIT fuel element model (Case YK9) has an EALF of 8.70E-08 MeV, which is within the range of applicability. Models with significantly more void spaces or low water densities sometimes exceed the range of applicability (maximum EALF = 3.30E-07 MeV for Case YE1), although these cases are not the most reactive. Therefore, the EALF of the most reactive models is acceptably within the range of applicability of the benchmarks.

6.10.8.2 U-235 Number Density

The U-235 number density is 3.61E-03 atom/b-cm in the MURR models and 3.68E-03 atom/b-cm in the MIT models. These number densities are within the range of applicability.

6.10.8.3 Channel Width

The maximum modeled NCT channel width is 0.092-in in the MURR models and 0.116-in in the MIT models. In the HAC models, in which the pitch is allowed to expand, the maximum channel width is 0.125-in in the MURR models and 0.176-in in the MIT models. All of these values exceed the maximum channel width of 0.078-in of the benchmark experiments. However, this parameter was artificially maximized in order to maximize model reactivity. As the channel width is directly related to system moderation, the acceptability of the EALF indicator

demonstrates that MCNP is performing acceptably for thermal conditions. Therefore, this parameter is considered to be acceptable.

6.10.8.4 H/U-235 Atom Ratio

The H/U-235 atom ratio is used as the fourth trending parameter for the benchmark cases. The H/U-235 atom ratio is defined here as the ratio of hydrogen atoms to U-235 atoms in a unit cell. This parameter is computed by the following equation:

NH*C/(NU235*M)

where,

NH is the hydrogen number density

C is the channel width

NU235 is the U-235 number density

M is the fuel meat width

Range of Applicability, MURR models: The H/U-235 atom ratio may be computed as:

NCT: 6.687E-02*0.088/(3.6147E-03*0.02) = 81.4

NCT: 6.687E-02*0.092/(3.6147E-03*0.02) = 85.1

HAC: 6.687E-02*0.125/(3.6147E-03*0.02) = 115.6

Therefore, H/U-235 of the MURR cases is acceptably within the range of applicability of the benchmarks.

Range of Applicability, MIT models: The H/U-235 atom ratio may be computed as:

NCT: 6.687E-02*0.094/(3.6835E-03*0.03) = 56.9

NCT: 6.687E-02*0.116/(3.6835E-03*0.03) = 70.2

HAC: 6.687E-02*0.176/(3.6835E-03*0.03) = 106.5

The minimum H/U-235 atom ratio of the benchmark models is 65.1. Therefore, this parameter is slightly outside the range of the benchmark experiments for the 0.094-in channel width NCT cases, although this parameter is in range for the more reactive 0.116-in channel width NCT cases. Therefore, this parameter is considered to be acceptable for the NCT cases. For the HAC cases, which bound the NCT cases, this parameter is acceptably within the range of applicability of the benchmarks.

6.10.8.5 Pitch

The NCT pitch is fixed at 0.13-in in the MURR models and 0.16-in in the MIT models. In the HAC models, in which the pitch is allowed to expand, the maximum pitch is 0.167-in in the MURR models and 0.24-in in the MIT models. The maximum pitch of the benchmark models is 0.128-in, so the pitch in the models exceeds the range of the benchmarks, particularly for the HAC cases. However, this parameter was artificially maximized in order to maximize model reactivity. As the pitch is directly related to system moderation, the acceptability of the EALF indicator demonstrates that MCNP is performing acceptably for thermal conditions. Therefore, this parameter is considered to be acceptable.

6.10.9 Sample Input Files

A sample input file is provided for the most reactive MURR and MIT cases.

MURR Case XN9 (HA_MURR2_TFNW080)

```
MURR
999     0      -320:321:-322:323:-324:325                imp:n=0
900     0      310 -311 312 -313 24 -25     fill=3       imp:n=1
901     2 -1.0 (311:-310:313:-312:-24:25) 320 -321 322 -323 324 -325  imp:n=1
c
c       Universe 1: MURR Fuel Element (infinitely long)
c
10       10 5.4439E-02 52 -53 -16 -15                        u=1 imp:n=1 $
plate 1
11       3 -2.7        (-52:53:16:15) 51 -54 -7 -8           u=1 imp:n=1
12       10 5.4439E-02 401 -402 -406 -407                    u=1 imp:n=1 $
plate 2
13       3 -2.7        (-401:402:406:407) 400 -403 -404 -405 u=1 imp:n=1
14       10 5.4439E-02 411 -412 -416 -417                    u=1 imp:n=1 $
plate 3
15       3 -2.7        (-411:412:416:417) 410 -413 -414 -415 u=1 imp:n=1
16       10 5.4439E-02 421 -422 -426 -427                    u=1 imp:n=1 $
plate 4
17       3 -2.7        (-421:422:426:427) 420 -423 -424 -425 u=1 imp:n=1
18       10 5.4439E-02 431 -432 -436 -437                    u=1 imp:n=1 $
plate 5
19       3 -2.7        (-431:432:436:437) 430 -433 -434 -435 u=1 imp:n=1
20       10 5.4439E-02 441 -442 -446 -447                    u=1 imp:n=1 $
plate 6
21       3 -2.7        (-441:442:446:447) 440 -443 -444 -445 u=1 imp:n=1
22       10 5.4439E-02 451 -452 -456 -457                    u=1 imp:n=1 $
plate 7
23       3 -2.7        (-451:452:456:457) 450 -453 -454 -455 u=1 imp:n=1
24       10 5.4439E-02 461 -462 -466 -467                    u=1 imp:n=1 $
plate 8
25       3 -2.7        (-461:462:466:467) 460 -463 -464 -465 u=1 imp:n=1
26       10 5.4439E-02 471 -472 -476 -477                    u=1 imp:n=1 $
plate 9
27       3 -2.7        (-471:472:476:477) 470 -473 -474 -475 u=1 imp:n=1
28       10 5.4439E-02 481 -482 -486 -487                    u=1 imp:n=1 $
plate 10
29       3 -2.7        (-481:482:486:487) 480 -483 -484 -485 u=1 imp:n=1
30       10 5.4439E-02 491 -492 -496 -497                    u=1 imp:n=1 $
plate 11
31       3 -2.7        (-491:492:496:497) 490 -493 -494 -495 u=1 imp:n=1
32       10 5.4439E-02 501 -502 -506 -507                    u=1 imp:n=1 $
plate 12
33       3 -2.7        (-501:502:506:507) 500 -503 -504 -505 u=1 imp:n=1
34       10 5.4439E-02 511 -512 -516 -517                    u=1 imp:n=1 $
plate 13
35       3 -2.7        (-511:512:516:517) 510 -513 -514 -515 u=1 imp:n=1
36       10 5.4439E-02 521 -522 -526 -527                    u=1 imp:n=1 $
plate 14
37       3 -2.7        (-521:522:526:527) 520 -523 -524 -525 u=1 imp:n=1
38       10 5.4439E-02 531 -532 -536 -537                    u=1 imp:n=1 $
plate 15
```

```
39       3 -2.7        (-531:532:536:537) 530 -533 -534 -535 u=1 imp:n=1
40       10 5.4439E-02 541 -542 -546 -547                    u=1 imp:n=1 $
plate 16
41       3 -2.7        (-541:542:546:547) 540 -543 -544 -545 u=1 imp:n=1
42       10 5.4439E-02 551 -552 -556 -557                    u=1 imp:n=1 $
plate 17
43       3 -2.7        (-551:552:556:557) 550 -553 -554 -555 u=1 imp:n=1
44       10 5.4439E-02 561 -562 -566 -567                    u=1 imp:n=1 $
plate 18
45       3 -2.7        (-561:562:566:567) 560 -563 -564 -565 u=1 imp:n=1
46       10 5.4439E-02 571 -572 -576 -577                    u=1 imp:n=1 $
plate 19
47       3 -2.7        (-571:572:576:577) 570 -573 -574 -575 u=1 imp:n=1
48       10 5.4439E-02 581 -582 -586 -587                    u=1 imp:n=1 $
plate 20
49       3 -2.7        (-581:582:586:587) 580 -583 -584 -585 u=1 imp:n=1
50       10 5.4439E-02 591 -592 -596 -597                    u=1 imp:n=1 $
plate 21
51       3 -2.7        (-591:592:596:597) 590 -593 -594 -595 u=1 imp:n=1
52       10 5.4439E-02 601 -602 -606 -607                    u=1 imp:n=1 $
plate 22
53       3 -2.7        (-601:602:606:607) 600 -603 -604 -605 u=1 imp:n=1
54       10 5.4439E-02 611 -612 -616 -617                    u=1 imp:n=1 $
plate 23
55       3 -2.7        (-611:612:616:617) 610 -613 -614 -615 u=1 imp:n=1
56       10 5.4439E-02 621 -622 -626 -627                    u=1 imp:n=1 $
plate 24
57       3 -2.7        (-621:622:626:627) 620 -623 -624 -625 u=1 imp:n=1
150      2 -1.0  (-51:54:7:8)       (-400:403:404:405) (-410:413:414:415)
                 (-420:423:424:425) (-430:433:434:435) (-440:443:444:445)
                 (-450:453:454:455) (-460:463:464:465) (-470:473:474:475)
                 (-480:483:484:485) (-490:493:494:495) (-500:503:504:505)
                 (-510:513:514:515) (-520:523:524:525) (-530:533:534:535)
                 (-540:543:544:545) (-550:553:554:555) (-560:563:564:565)
                 (-570:573:574:575) (-580:583:584:585) (-590:593:594:595)
                 (-600:603:604:605) (-610:613:614:615) (-620:623:624:625)
                 u=1 imp:n=1
c
c       Universe 19: MURR with FHE
c
200     0         -232 -233 212 213 214 -234 fill=1(1) u=19 imp:n=1
201     5 -0.737  230 -210 212 214                u=19 imp:n=1 $ right
neoprene
202     5 -0.737  231 -211 213 214                u=19 imp:n=1 $ left
neoprene
203     2 -1.0    213 212 234                     u=19 imp:n=1 $ top water
outside bag
204     2 -1.0    -230 232 214 212                u=19 imp:n=1 $ side water
outside bag
205     2 -1.0    -231 233 214 213                u=19 imp:n=1 $ side water
outside bag
206     3 -2.7    (210:211:-212:-213:-214) -220 -221 222 223 224 u=19 imp:n=1
$ FHE
207     2 -0.8     220:221:-222:-223:-224        u=19 imp:n=1 $ water
c
c       Universe 20: MURR with pipe (center)
c
```

```
210     0           -200 fill=19                u=20 imp:n=1
211     4 -7.94     200 -201                    u=20 imp:n=1 $ pipe
212     6 -0.096    201 -203 250 -251 252 -253  u=20 imp:n=1 $ insulation
213     0           203 250 -251 252 -253       u=20 imp:n=1 $ insulation to
tube
214     4 -7.94     -250:251:-252:253           u=20 imp:n=1 $ tube to inf
c
c       Universe 21: MURR with pipe (down)
c
220     0           -200 fill=19(2)             u=21 imp:n=1
221     4 -7.94     200 -201                    u=21 imp:n=1 $ pipe
222     6 -0.096    201 -203 250 -251 252 -253  u=21 imp:n=1 $ insulation
223     0           203 250 -251 252 -253       u=21 imp:n=1 $ insulation to
tube
224     4 -7.94     -250:251:-252:253           u=21 imp:n=1 $ tube to inf
c
c       Universe 22: MURR with pipe (up)
c
230     0           -200 fill=19(3)             u=22 imp:n=1
231     4 -7.94     200 -201                    u=22 imp:n=1 $ pipe
232     6 -0.096    201 -203 250 -251 252 -253  u=22 imp:n=1 $ insulation
233     0           203 250 -251 252 -253       u=22 imp:n=1 $ insulation to
tube
234     4 -7.94     -250:251:-252:253           u=22 imp:n=1 $ tube to inf
c
c       Universe 23: MURR with pipe (right)
c
240     0           -200 fill=19(4)             u=23 imp:n=1
241     4 -7.94     200 -201                    u=23 imp:n=1 $ pipe
242     6 -0.096    201 -203 250 -251 252 -253  u=23 imp:n=1 $ insulation
243     0           203 250 -251 252 -253       u=23 imp:n=1 $ insulation to
tube
244     4 -7.94     -250:251:-252:253           u=23 imp:n=1 $ tube to inf
c
c       Universe 24: MURR with pipe (left)
c
250     0           -200 fill=19(5)             u=24 imp:n=1
251     4 -7.94     200 -201                    u=24 imp:n=1 $ pipe
252     6 -0.096    201 -203 250 -251 252 -253  u=24 imp:n=1 $ insulation
253     0           203 250 -251 252 -253       u=24 imp:n=1 $ insulation to
tube
254     4 -7.94     -250:251:-252:253           u=24 imp:n=1 $ tube to inf
c
c       Universe 25: MURR with pipe (up right)
c
260     0           -200 fill=19(6)             u=25 imp:n=1
261     4 -7.94     200 -201                    u=25 imp:n=1 $ pipe
262     6 -0.096    201 -203 250 -251 252 -253  u=25 imp:n=1 $ insulation
263     0           203 250 -251 252 -253       u=25 imp:n=1 $ insulation to
tube
264     4 -7.94     -250:251:-252:253           u=25 imp:n=1 $ tube to inf
c
c       Universe 26: MURR with pipe (up left)
c
270     0           -200 fill=19(7)             u=26 imp:n=1
271     4 -7.94     200 -201                    u=26 imp:n=1 $ pipe
272     6 -0.096    201 -203 250 -251 252 -253  u=26 imp:n=1 $ insulation
```

```
273     0           203 250 -251 252 -253       u=26 imp:n=1 $ insulation to
tube
274     4 -7.94     -250:251:-252:253           u=26 imp:n=1 $ tube to inf
c
c       Universe 27: MURR with pipe (down right)
c
280     0           -200 fill=19(8)             u=27 imp:n=1
281     4 -7.94     200 -201                    u=27 imp:n=1 $ pipe
282     6 -0.096    201 -203 250 -251 252 -253  u=27 imp:n=1 $ insulation
283     0           203 250 -251 252 -253       u=27 imp:n=1 $ insulation to
tube
284     4 -7.94     -250:251:-252:253           u=27 imp:n=1 $ tube to inf
c
c       Universe 28: MURR with pipe (down left)
c
290     0           -200 fill=19(9)             u=28 imp:n=1
291     4 -7.94     200 -201                    u=28 imp:n=1 $ pipe
292     6 -0.096    201 -203 250 -251 252 -253  u=28 imp:n=1 $ insulation
293     0           203 250 -251 252 -253       u=28 imp:n=1 $ insulation to
tube
294     4 -7.94     -250:251:-252:253           u=28 imp:n=1 $ tube to inf
c
c       Universe 3: Array of Packages
c
300   0    -300 301 -302 303 imp:n=1 u=3 lat=1 fill=-2:2 -2:2 0:0
             25 25 22 26 26
             25 25 22 26 26
             23 23 20 24 24
             27 27 21 28 28
             27 27 21 28 28

c 5       p  2.4142136 -1 0 -0.13275   $ right Al outer
c 6       p -2.4142136 -1 0 -0.13275   $ left Al outer
7       p  2.4142136 -1 0 -1.09516   $ right Al inner
8       p -2.4142136 -1 0 -1.09516   $ left Al inner
c 9       cz 6.858                     $ Al boundary
c 10      cz 14.884                    $ Al boundary
c
15      p  2.4142136 -1 0 -1.39997   $ plate meat boundary
16      p -2.4142136 -1 0 -1.39997   $ plate meat boundary
c
24      pz -30.48                    $ bottom of fuel
25      pz  30.48                    $ top of fuel (24")
c
51      cz 7.0460 $ fuel plate 1
52      cz 7.0739
53      cz 7.1247
54      cz 7.1526
c
400 22    cz 7.3762 $ fuel plate 2
401 22    cz 7.4041
402 22    cz 7.4549
403 22    cz 7.4828
404 22    p  2.4142136 -1 0 -1.09516   $ right Al inner
405 22    p -2.4142136 -1 0 -1.09516   $ left Al inner
406 22    p  2.4142136 -1 0 -1.39997   $ plate meat boundary
407 22    p -2.4142136 -1 0 -1.39997   $ plate meat boundary
```

```
c
410 23  cz 7.7064 $ fuel plate 3
411 23  cz 7.7343
412 23  cz 7.7851
413 23  cz 7.8130
414 23    p  2.4142136 -1 0 -1.09516   $ right Al inner
415 23    p -2.4142136 -1 0 -1.09516   $ left Al inner
416 23    p  2.4142136 -1 0 -1.39997   $ plate meat boundary
417 23    p -2.4142136 -1 0 -1.39997   $ plate meat boundary
c
420 24  cz 8.0366 $ fuel plate 4
421 24  cz 8.0645
422 24  cz 8.1153
423 24  cz 8.1432
424 24    p  2.4142136 -1 0 -1.09516   $ right Al inner
425 24    p -2.4142136 -1 0 -1.09516   $ left Al inner
426 24    p  2.4142136 -1 0 -1.39997   $ plate meat boundary
427 24    p -2.4142136 -1 0 -1.39997   $ plate meat boundary
c
430 25  cz 8.3668 $ fuel plate 5
431 25  cz 8.3947
432 25  cz 8.4455
433 25  cz 8.4734
434 25    p  2.4142136 -1 0 -1.09516   $ right Al inner
435 25    p -2.4142136 -1 0 -1.09516   $ left Al inner
436 25    p  2.4142136 -1 0 -1.39997   $ plate meat boundary
437 25    p -2.4142136 -1 0 -1.39997   $ plate meat boundary
c
440 26  cz 8.6970 $ fuel plate 6
441 26  cz 8.7249
442 26  cz 8.7757
443 26  cz 8.8036
444 26    p  2.4142136 -1 0 -1.09516   $ right Al inner
445 26    p -2.4142136 -1 0 -1.09516   $ left Al inner
446 26    p  2.4142136 -1 0 -1.39997   $ plate meat boundary
447 26    p -2.4142136 -1 0 -1.39997   $ plate meat boundary
c
450 27  cz 9.0272 $ fuel plate 7
451 27  cz 9.0551
452 27  cz 9.1059
453 27  cz 9.1338
454 27    p  2.4142136 -1 0 -1.09516   $ right Al inner
455 27    p -2.4142136 -1 0 -1.09516   $ left Al inner
456 27    p  2.4142136 -1 0 -1.39997   $ plate meat boundary
457 27    p -2.4142136 -1 0 -1.39997   $ plate meat boundary
c
460 28  cz 9.3574 $ fuel plate 8
461 28  cz 9.3853
462 28  cz 9.4361
463 28  cz 9.4640
464 28    p  2.4142136 -1 0 -1.09516   $ right Al inner
465 28    p -2.4142136 -1 0 -1.09516   $ left Al inner
466 28    p  2.4142136 -1 0 -1.39997   $ plate meat boundary
467 28    p -2.4142136 -1 0 -1.39997   $ plate meat boundary
c
470 29  cz 9.6876 $ fuel plate 9
471 29  cz 9.7155
```

```
472 29  cz 9.7663
473 29  cz 9.7942
474 29    p  2.4142136 -1 0 -1.09516   $ right Al inner
475 29    p -2.4142136 -1 0 -1.09516   $ left Al inner
476 29    p  2.4142136 -1 0 -1.39997   $ plate meat boundary
477 29    p -2.4142136 -1 0 -1.39997   $ plate meat boundary
c
480 30  cz 10.0178 $ fuel plate 10
481 30  cz 10.0457
482 30  cz 10.0965
483 30  cz 10.1244
484 30    p  2.4142136 -1 0 -1.09516   $ right Al inner
485 30    p -2.4142136 -1 0 -1.09516   $ left Al inner
486 30    p  2.4142136 -1 0 -1.39997   $ plate meat boundary
487 30    p -2.4142136 -1 0 -1.39997   $ plate meat boundary
c
490 31  cz 10.3480 $ fuel plate 11
491 31  cz 10.3759
492 31  cz 10.4267
493 31  cz 10.4546
494 31    p  2.4142136 -1 0 -1.09516   $ right Al inner
495 31    p -2.4142136 -1 0 -1.09516   $ left Al inner
496 31    p  2.4142136 -1 0 -1.39997   $ plate meat boundary
497 31    p -2.4142136 -1 0 -1.39997   $ plate meat boundary
c
500 32  cz 10.6782 $ fuel plate 12
501 32  cz 10.7061
502 32  cz 10.7569
503 32  cz 10.7848
504 32    p  2.4142136 -1 0 -1.09516   $ right Al inner
505 32    p -2.4142136 -1 0 -1.09516   $ left Al inner
506 32    p  2.4142136 -1 0 -1.39997   $ plate meat boundary
507 32    p -2.4142136 -1 0 -1.39997   $ plate meat boundary
c
510 33  cz 11.0084 $ fuel plate 13
511 33  cz 11.0363
512 33  cz 11.0871
513 33  cz 11.1150
514 33    p  2.4142136 -1 0 -1.09516   $ right Al inner
515 33    p -2.4142136 -1 0 -1.09516   $ left Al inner
516 33    p  2.4142136 -1 0 -1.39997   $ plate meat boundary
517 33    p -2.4142136 -1 0 -1.39997   $ plate meat boundary
c
520 34  cz 11.3386 $ fuel plate 14
521 34  cz 11.3665
522 34  cz 11.4173
523 34  cz 11.4452
524 34    p  2.4142136 -1 0 -1.09516   $ right Al inner
525 34    p -2.4142136 -1 0 -1.09516   $ left Al inner
526 34    p  2.4142136 -1 0 -1.39997   $ plate meat boundary
527 34    p -2.4142136 -1 0 -1.39997   $ plate meat boundary
c
530 35  cz 11.6688 $ fuel plate 15
531 35  cz 11.6967
532 35  cz 11.7475
533 35  cz 11.7754
534 35    p  2.4142136 -1 0 -1.09516   $ right Al inner
```

```
35    p -2.4142136 -1 0 -1.09516   $ left Al inner
35    p  2.4142136 -1 0 -1.39997   $ plate meat boundary
35    p -2.4142136 -1 0 -1.39997   $ plate meat boundary
c
36  cz 11.9990 $ fuel plate 16
36  cz 12.0269
36  cz 12.0777
36  cz 12.1056
36    p  2.4142136 -1 0 -1.09516   $ right Al inner
36    p -2.4142136 -1 0 -1.09516   $ left Al inner
36    p  2.4142136 -1 0 -1.39997   $ plate meat boundary
36    p -2.4142136 -1 0 -1.39997   $ plate meat boundary
c
37  cz 12.3292 $ fuel plate 17
37  cz 12.3571
37  cz 12.4079
37  cz 12.4358
37    p  2.4142136 -1 0 -1.09516   $ right Al inner
37    p -2.4142136 -1 0 -1.09516   $ left Al inner
37    p  2.4142136 -1 0 -1.39997   $ plate meat boundary
37    p -2.4142136 -1 0 -1.39997   $ plate meat boundary
c
38  cz 12.6594 $ fuel plate 18
38  cz 12.6873
38  cz 12.7381
38  cz 12.7660
38    p  2.4142136 -1 0 -1.09516   $ right Al inner
38    p -2.4142136 -1 0 -1.09516   $ left Al inner
38    p  2.4142136 -1 0 -1.39997   $ plate meat boundary
38    p -2.4142136 -1 0 -1.39997   $ plate meat boundary
c
39  cz 12.9896 $ fuel plate 19
39  cz 13.0175
39  cz 13.0683
39  cz 13.0962
39    p  2.4142136 -1 0 -1.09516   $ right Al inner
39    p -2.4142136 -1 0 -1.09516   $ left Al inner
39    p  2.4142136 -1 0 -1.39997   $ plate meat boundary
39    p -2.4142136 -1 0 -1.39997   $ plate meat boundary
c
40  cz 13.3198 $ fuel plate 20
40  cz 13.3477
40  cz 13.3985
40  cz 13.4264
40    p  2.4142136 -1 0 -1.09516   $ right Al inner
40    p -2.4142136 -1 0 -1.09516   $ left Al inner
40    p  2.4142136 -1 0 -1.39997   $ plate meat boundary
40    p -2.4142136 -1 0 -1.39997   $ plate meat boundary
c
41  cz 13.6500 $ fuel plate 21
41  cz 13.6779
41  cz 13.7287
41  cz 13.7566
41    p  2.4142136 -1 0 -1.09516   $ right Al inner
41    p -2.4142136 -1 0 -1.09516   $ left Al inner
41    p  2.4142136 -1 0 -1.39997   $ plate meat boundary
41    p -2.4142136 -1 0 -1.39997   $ plate meat boundary
```

```
c
600 42  cz 13.9802 $ fuel plate 22
601 42  cz 14.0081
602 42  cz 14.0589
603 42  cz 14.0868
604 42    p  2.4142136 -1 0 -1.09516   $ right Al inner
605 42    p -2.4142136 -1 0 -1.09516   $ left Al inner
606 42    p  2.4142136 -1 0 -1.39997   $ plate meat boundary
607 42    p -2.4142136 -1 0 -1.39997   $ plate meat boundary
c
610 43  cz 14.3104 $ fuel plate 23
611 43  cz 14.3383
612 43  cz 14.3891
613 43  cz 14.4170
614 43    p  2.4142136 -1 0 -1.09516   $ right Al inner
615 43    p -2.4142136 -1 0 -1.09516   $ left Al inner
616 43    p  2.4142136 -1 0 -1.39997   $ plate meat boundary
617 43    p -2.4142136 -1 0 -1.39997   $ plate meat boundary
c
620 44  cz 14.6406 $ fuel plate 24
621 44  cz 14.6685
622 44  cz 14.7193
623 44  cz 14.7472
624 44    p  2.4142136 -1 0 -1.09516   $ right Al inner
625 44    p -2.4142136 -1 0 -1.09516   $ left Al inner
626 44    p  2.4142136 -1 0 -1.39997   $ plate meat boundary
627 44    p -2.4142136 -1 0 -1.39997   $ plate meat boundary
c
200      cz 7.3838 $ IR pipe
201      cz 7.6581 $ OR pipe
c 202      cz 38.1   $ 12" water
203      cz 10.1981 $ 1" insulation
c
210 50     p  2.194300 -1 0 11.6987 $ right lower inner
211 51     p -2.194300 -1 0 11.6987 $ left lower inner
212 50     p -0.455726 -1 0 -5.7501 $ right upper inner
213 51     p  0.455726 -1 0 -5.7501 $ left upper inner
214        py -5.6175               $ bottom inner
220 50     p  2.194300 -1 0 13.2300 $ right lower outer
221 51     p -2.194300 -1 0 13.2300 $ left lower outer
222 50     p -0.455726 -1 0 -6.4479 $ right upper outer
223 51     p  0.455726 -1 0 -6.4479 $ left upper outer
224        py -6.2525               $ bottom outer
230 50     p  2.194300 -1 0 10.9331 $ right neoprene
231 51     p -2.194300 -1 0 10.9331 $ left neoprene
232        p  3.1993   -1 0 13.2244 $ right plastic bag
233        p -3.1993   -1 0 13.2244 $ left plastic bag
234        c/z 0 -10.065 14.8       $ top of plastic bag
c
250      px  -9.6032 $ square tube
251      px   9.6032
252      py  -9.6032
253      py   9.6032
c
300      px  10.033 $ lattice surfaces/sq. tube
301      px -10.033
302      py  10.033
```

```
303      py -10.033
310      px -50.165 $ 5x5 bounds
311      px  50.165
312      py -50.165
313      py  50.165
320      px -80.645 $ outer bounds
321      px  80.645
322      py -80.645
323      py  80.645
324      pz -60.96
325      pz  60.96

m2      1001.62c  2          $ water
        8016.62c  1
mt2     lwtr.60t
m3      13027.62c 1          $ Al
m4      6000.66c   -0.08     $ SS-304
        14000.60c  -1.0
        15031.66c  -0.045
        24000.50c  -19.0
        25055.62c  -2.0
        26000.55c  -68.375
        28000.50c  -9.5
m5      1001.62c  -0.056920  $ neoprene (no Cl)
        6000.66c  -0.542646
c        17000.66c -0.400434
m6      13027.62c  -26.5     $ insulation material
        14000.60c  -23.4
        8016.62c   -50.2
m10     92234.69c 2.3171E-05
        92235.69c 3.6147E-03
        92236.69c 1.3402E-05
        92238.69c 1.9174E-04
        13027.62c 5.0596E-02
c           total 5.4439E-02
c
*tr1     0 -12.25 0                        $ base to center
*tr2     0 -0.7798 0  180 90 90 90 180 90  $ down
*tr3     0  0.7798 0                       $ up
*tr4     0.7798 0 0  90 180 90 0 90 90     $ right
*tr5    -0.7798 0 0  90 0 90 180 90 90     $ left
*tr6     0.5514   0.5514  0  45 135 90 45 45 90     $ up/right
*tr7    -0.5514   0.5514  0  45 45 90 135 45 90     $ up/left
*tr8     0.5514  -0.5514  0  135 135 90 45 135 90   $ down/right
*tr9    -0.5514  -0.5514  0  135 45 90 135 135 90   $ down/left
tr22 0 0.095 0 $ plate 2
tr23 0 0.190 0 $ plate 3
tr24 0 0.285 0 $ plate 4
tr25 0 0.380 0 $ plate 5
tr26 0 0.475 0 $ plate 6
tr27 0 0.570 0 $ plate 7
tr28 0 0.665 0 $ plate 8
tr29 0 0.760 0 $ plate 9
tr30 0 0.855 0 $ plate 10
tr31 0 0.950 0 $ plate 11
tr32 0 1.045 0 $ plate 12
tr33 0 1.140 0 $ plate 13
```

```
tr34 0 1.235 0 $ plate 14
tr35 0 1.330 0 $ plate 15
tr36 0 1.425 0 $ plate 16
tr37 0 1.520 0 $ plate 17
tr38 0 1.615 0 $ plate 18
tr39 0 1.710 0 $ plate 19
tr40 0 1.805 0 $ plate 20
tr41 0 1.900 0 $ plate 21
tr42 0 1.995 0 $ plate 22
tr43 0 2.090 0 $ plate 23
tr44 0 2.185 0 $ plate 24
tr50   0.7798 0 0  $ shift FHE right
tr51  -0.7798 0 0  $ shift FHE left
c
mode   n
kcode  2500 1.0 50 250
sdef    x=d1 y=d2 z=d3
si1     -50 50
sp1     0 1
si2     -50 50
sp2     0 1
si3     -31 31
sp3     0 1
```

MIT Case YK9 (HA_MIT_FNW080)

```
MIT
999     0      -320:321:-322:323:-324:325                imp:n=0
900     0      310 -311 312 -313 24 -25     fill=3       imp:n=1
901     2 -1.0 (311:-310:313:-312:-24:25) 320 -321 322 -323 324 -325  imp:n=1
c
c       Universe 1: MIT Fuel Element (infinitely long)
c
10      3 -2.7        10 -11 50 -124            u=1 imp:n=1 $ right Al piece
11      3 -2.7        13 -12 50 -124            u=1 imp:n=1 $ left Al piece
c 12      2 -1.0        12 -10 18 -50             u=1 imp:n=1
20      10 5.4398E-02 40 -41 70 -90             u=1 imp:n=1 $ plate 1
21      3 -2.7        12 -10 50 -110 #20        u=1 imp:n=1
22      2 -1.0        12 -10 110 -51            u=1 imp:n=1
30      10 5.4398E-02 40 -41 71 -91             u=1 imp:n=1 $ plate 2
31      3 -2.7        12 -10 51 -111 #30        u=1 imp:n=1
32      2 -1.0        12 -10 111 -52            u=1 imp:n=1
40      10 5.4398E-02 40 -41 72 -92             u=1 imp:n=1 $ plate 3
41      3 -2.7        12 -10 52 -112 #40        u=1 imp:n=1
42      2 -1.0        12 -10 112 -53            u=1 imp:n=1
50      10 5.4398E-02 40 -41 73 -93             u=1 imp:n=1 $ plate 4
51      3 -2.7        12 -10 53 -113 #50        u=1 imp:n=1
52      2 -1.0        12 -10 113 -54            u=1 imp:n=1
60      10 5.4398E-02 40 -41 74 -94             u=1 imp:n=1 $ plate 5
61      3 -2.7        12 -10 54 -114 #60        u=1 imp:n=1
62      2 -1.0        12 -10 114 -55            u=1 imp:n=1
70      10 5.4398E-02 40 -41 75 -95             u=1 imp:n=1 $ plate 6
71      3 -2.7        12 -10 55 -115 #70        u=1 imp:n=1
72      2 -1.0        12 -10 115 -56            u=1 imp:n=1
80      10 5.4398E-02 40 -41 76 -96             u=1 imp:n=1 $ plate 7
81      3 -2.7        12 -10 56 -116 #80        u=1 imp:n=1
```

```
82      2 -1.0        12 -10 116 -57            u=1 imp:n=1
90      10 5.4398E-02 40 -41 77 -97             u=1 imp:n=1 $ plate 8
91      3 -2.7        12 -10 57 -117 #90        u=1 imp:n=1
92      2 -1.0        12 -10 117 -58            u=1 imp:n=1
100      10 5.4398E-02 40 -41 78 -98             u=1 imp:n=1 $ plate 9
101      3 -2.7        12 -10 58 -118 #100       u=1 imp:n=1
102      2 -1.0        12 -10 118 -59            u=1 imp:n=1
110      10 5.4398E-02 40 -41 79 -99             u=1 imp:n=1 $ plate 10
111      3 -2.7        12 -10 59 -119 #110       u=1 imp:n=1
112      2 -1.0        12 -10 119 -60            u=1 imp:n=1
120      10 5.4398E-02 40 -41 80 -100            u=1 imp:n=1 $ plate 11
121      3 -2.7        12 -10 60 -120 #120       u=1 imp:n=1
122      2 -1.0        12 -10 120 -61            u=1 imp:n=1
130      10 5.4398E-02 40 -41 81 -101            u=1 imp:n=1 $ plate 12
131      3 -2.7        12 -10 61 -121 #130       u=1 imp:n=1
132      2 -1.0        12 -10 121 -62            u=1 imp:n=1
140      10 5.4398E-02 40 -41 82 -102            u=1 imp:n=1 $ plate 13
141      3 -2.7        12 -10 62 -122 #140       u=1 imp:n=1
142      2 -1.0        12 -10 122 -63            u=1 imp:n=1
150      10 5.4398E-02 40 -41 83 -103            u=1 imp:n=1 $ plate 14
151      3 -2.7        12 -10 63 -123 #150       u=1 imp:n=1
152      2 -1.0        12 -10 123 -64            u=1 imp:n=1
160      10 5.4398E-02 40 -41 84 -104            u=1 imp:n=1 $ plate 15
161      3 -2.7        12 -10 64 -124 #160       u=1 imp:n=1
c 162      2 -1.0        12 -10 124 -19            u=1 imp:n=1
170      2 -1.0        -13:11:-50:124            u=1 imp:n=1 $ water between
fuel and enclosure
c
c       Universe 19: MIT with FHE
c
201     0           30 38 -32 -39 fill=1                u=19 imp:n=1
202     5 -0.737    -33 39 -32 30                       u=19 imp:n=1 $ right
neo
203     5 -0.737    31 -38 -32 30                       u=19 imp:n=1 $ left
neo
204     3 -2.7      (-30:-31:32:33) 34 35 -36 -37       u=19 imp:n=1 $
enclosure
205     2 -0.8      -34:-35:36:37                       u=19 imp:n=1 $ water
outside FHE
c
c       Universe 20: FHE in tube (center)
c
210     2 -0.9     -200           fill=19              u=20 imp:n=1 $ inside
pipe
211     4 -7.94     200 -201                            u=20 imp:n=1 $ pipe
212     6 -0.096    201 -203 250 -251 252 -253          u=20 imp:n=1 $
insulation
213     0           203 250 -251 252 -253               u=20 imp:n=1 $ pipe to
tube
214     4 -7.94     -250:251:-252:253                   u=20 imp:n=1 $ tube to
inf
c
c       Universe 21: FHE in tube (down)
c
220     2 -0.9     -200           fill=19(2)           u=21 imp:n=1 $ inside
pipe
221     4 -7.94     200 -201                            u=21 imp:n=1 $ pipe
```

```
222     6 -0.096    201 -203 250 -251 252 -253         u=21 imp:n=1 $
insulation
223     0           203 250 -251 252 -253              u=21 imp:n=1 $ pipe to
tube
224     4 -7.94     -250:251:-252:253                  u=21 imp:n=1 $ tube to
inf
c
c       Universe 22: FHE in tube (up)
c
230     2 -0.9     -200           fill=19(3)           u=22 imp:n=1 $ inside
pipe
231     4 -7.94     200 -201                           u=22 imp:n=1 $ pipe
232     6 -0.096    201 -203 250 -251 252 -253         u=22 imp:n=1 $
insulation
233     0           203 250 -251 252 -253              u=22 imp:n=1 $ pipe to
tube
234     4 -7.94     -250:251:-252:253                  u=22 imp:n=1 $ tube to
inf
c
c       Universe 23: FHE in tube (right)
c
240     2 -0.9     -200           fill=19(4)           u=23 imp:n=1 $ inside
pipe
241     4 -7.94     200 -201                           u=23 imp:n=1 $ pipe
242     6 -0.096    201 -203 250 -251 252 -253         u=23 imp:n=1 $
insulation
243     0           203 250 -251 252 -253              u=23 imp:n=1 $ pipe to
tube
244     4 -7.94     -250:251:-252:253                  u=23 imp:n=1 $ tube to
inf
c
c       Universe 24: FHE in tube (left)
c
250     2 -0.9     -200           fill=19(5)           u=24 imp:n=1 $ inside
pipe
251     4 -7.94     200 -201                           u=24 imp:n=1 $ pipe
252     6 -0.096    201 -203 250 -251 252 -253         u=24 imp:n=1 $
insulation
253     0           203 250 -251 252 -253              u=24 imp:n=1 $ pipe to
tube
254     4 -7.94     -250:251:-252:253                  u=24 imp:n=1 $ tube to
inf
c
c       Universe 25: FHE in tube (up/right)
c
260     2 -0.9     -200           fill=19(6)           u=25 imp:n=1 $ inside
pipe
261     4 -7.94     200 -201                           u=25 imp:n=1 $ pipe
262     6 -0.096    201 -203 250 -251 252 -253         u=25 imp:n=1 $
insulation
263     0           203 250 -251 252 -253              u=25 imp:n=1 $ pipe to
tube
264     4 -7.94     -250:251:-252:253                  u=25 imp:n=1 $ tube to
inf
c
c       Universe 26: FHE in tube (up/left)
c
```

```
270     2 -0.9     -200           fill=19(7)           u=26 imp:n=1 $ inside
pipe
271     4 -7.94     200 -201                           u=26 imp:n=1 $ pipe
272     6 -0.096    201 -203 250 -251 252 -253         u=26 imp:n=1 $
insulation
273     0           203 250 -251 252 -253              u=26 imp:n=1 $ pipe to
tube
274     4 -7.94     -250:251:-252:253                  u=26 imp:n=1 $ tube to
inf
c
c       Universe 27: FHE in tube (down/right)
c
280     2 -0.9     -200           fill=19(8)           u=27 imp:n=1 $ inside
pipe
281     4 -7.94     200 -201                           u=27 imp:n=1 $ pipe
282     6 -0.096    201 -203 250 -251 252 -253         u=27 imp:n=1 $
insulation
283     0           203 250 -251 252 -253              u=27 imp:n=1 $ pipe to
tube
284     4 -7.94     -250:251:-252:253                  u=27 imp:n=1 $ tube to
inf
c
c       Universe 28: FHE in tube (down/left)
c
290     2 -0.9     -200           fill=19(9)           u=28 imp:n=1 $ inside
pipe
291     4 -7.94     200 -201                           u=28 imp:n=1 $ pipe
292     6 -0.096    201 -203 250 -251 252 -253         u=28 imp:n=1 $
insulation
293     0           203 250 -251 252 -253              u=28 imp:n=1 $ pipe to
tube
294     4 -7.94     -250:251:-252:253                  u=28 imp:n=1 $ tube to
inf
c
c       Universe 3: Array of Packages
c
300   0    -300 301 -302 303 imp:n=1 u=3 lat=1 fill=-2:2 -2:2 0:0
             25 25 22 26 26
             25 25 22 26 26
             23 23 20 24 24
             27 27 21 28 28
             27 27 21 28 28

10      px  2.5451   $ Al side
11      px  3.0226   $ Al side
12      px -2.5451   $ Al side
13      px -3.0226   $ Al side
18  10  py -3.02768  $ Al bottom
19  10  py 3.02768   $ Al top
20  10  py -3.34518  $ neoprene
21  10  py  3.34518  $ neoprene
c
24      pz -28.41625  $ bottom of fuel
25      pz  28.41625  $ top of fuel (22.375")
30 20   p -1.71429 -1 0 -7.3152 $ inner FHE
31 21   p  1.71429 -1 0 -7.3152 $ inner FHE
32 21   p -1.71429 -1 0  7.3152 $ inner FHE
```

```
33 20   p  1.71429 -1 0  7.3152 $ inner FHE
34 20   p -1.71429 -1 0 -7.9697 $ outer FHE
35 21   p  1.71429 -1 0 -7.9697 $ outer FHE
36 21   p -1.71429 -1 0  7.9697 $ outer FHE
37 20   p  1.71429 -1 0  7.9697 $ outer FHE
38 21   p  1.71429 -1 0 -6.6859 $ left neo
39 20   p  1.71429 -1 0  6.6859 $ right neo
c
40      px -2.3878 $ meat width (w/2*cos(30))
41      px  2.3878 $ meat width
c
50 10   py -4.34848
51 10   py -3.73888
52 10   py -3.12928
53 10   py -2.51968
54 10   py -1.91008
55 10   py -1.30048
56 10   py -0.69088
57 10   py -0.08128
58 10   py 0.52832
59 10   py 1.13792
60 10   py 1.74752
61 10   py 2.35712
62 10   py 2.96672
63 10   py 3.57632
64 10   py 4.18592
c
70 10   py -4.30530
71 10   py -3.69570
72 10   py -3.08610
73 10   py -2.47650
74 10   py -1.86690
75 10   py -1.25730
76 10   py -0.64770
77 10   py -0.03810
78 10   py 0.57150
79 10   py 1.18110
80 10   py 1.79070
81 10   py 2.40030
82 10   py 3.00990
83 10   py 3.61950
84 10   py 4.22910
c
90 10   py -4.22910
91 10   py -3.61950
92 10   py -3.00990
93 10   py -2.40030
94 10   py -1.79070
95 10   py -1.18110
96 10   py -0.57150
97 10   py 0.03810
98 10   py 0.64770
99 10   py 1.25730
100 10   py 1.86690
101 10   py 2.47650
102 10   py 3.08610
103 10   py 3.69570
```

```
104 10   py 4.30530
c
110 10   py -4.18592
111 10   py -3.57632
112 10   py -2.96672
113 10   py -2.35712
114 10   py -1.74752
115 10   py -1.13792
116 10   py -0.52832
117 10   py 0.08128
118 10   py 0.69088
119 10   py 1.30048
120 10   py 1.91008
121 10   py 2.51968
122 10   py 3.12928
123 10   py 3.73888
124 10   py 4.34848
c
199      cz 6.9012 $ Al
200      cz 7.3838 $ IR pipe
201      cz 7.6581 $ OR pipe
203      cz 10.1981 $ 1" insulation
c
250      px  -9.6032 $ square tube
251      px   9.6032
252      py  -9.6032
253      py   9.6032
c
300      px  10.033 $ lattice surfaces/sq. tube
301      px -10.033
302      py  10.033
303      py -10.033
310      px -50.165 $ 5x5 bounds
311      px  50.165
312      py -50.165
313      py  50.165
320      px -80.645 $ outer bounds
321      px  80.645
322      py -80.645
323      py  80.645
324      pz -58.8963
325      pz  58.8963

m2      1001.62c  2          $ water
        8016.62c  1
mt2     lwtr.60t
m3      13027.62c 1          $ Al
m4      6000.66c   -0.08     $ SS-304
        14000.60c  -1.0
        15031.66c  -0.045
        24000.50c  -19.0
        25055.62c  -2.0
        26000.55c  -68.375
        28000.50c  -9.5
m5      1001.62c  -0.056920  $ neoprene (no Cl)
        6000.66c  -0.542646
c        17000.66c -0.400434
```

```
m6      13027.62c  -26.5     $ insulation material
        14000.60c  -23.4
        8016.62c   -50.2
m10     92234.69c 2.3613E-05 $ fuel
        92235.69c 3.6835E-03
        92236.69c 1.3657E-05
        92238.69c 1.9539E-04
        13027.62c 5.0481E-02
c           total 5.4398E-02
c
*tr2     0 -0.7798 0  30 60 90 120 30 90   $ down
*tr3     0  0.7798 0  30 60 90 120 30 90   $ up
*tr4     0.7798 0 0                        $ right
*tr5    -0.7798 0 0                        $ left
*tr6     0.5514    0.5514  0                      $ up/right
*tr7    -0.5514    0.5514  0  90 0 90 180 90 90   $ up/left
*tr8     0.5514   -0.5514  0  90 0 90 180 90 90   $ down/right
*tr9    -0.5514   -0.5514  0                      $ down/left
*tr10    0 0 0  30 120 90 60 30 90 $ rotate fuel surfaces 30 deg CCW
*tr20    -0.7798 0 0  30.2 59.8 90 120.2 30.2 90 j j j -1 $ rotate right FHE
30.2 deg CCW
*tr21     0.7798 0 0  30.2 59.8 90 120.2 30.2 90 j j j -1 $ rotate left FHE
30.2 deg CCW
c
mode   n
kcode  2500 1.0 50 250
sdef    x=d1 y=d2 z=d3
si1     -50 50
sp1     0 1
si2     -50 50
sp2     0 1
si3     -31 31
sp3     0 1
```

6.11 Appendix C: Criticality Analysis for Small Quantity Payloads

The ATR FFSC may be utilized to transport fuel with a small U-235 fissile loading (≤ 400 g U-235). This fuel may be enriched up to 94% U-235. The intent is to bound in a generic manner several classes of research and development fuel types, as the geometry and fissile loading of such fuels is subject to change. These fuel types include those described in Section 1.2.2.4, *Small Quantity Payload*. In addition, some standard fuel elements, such as RINSC, classify for transport as a small quantity payload, as well as individual plates used to fabricate MURR, MIT, and Cobra fuel. The following analysis demonstrates that the ATR FFSC with small quantity payload fuel complies with the requirements of 10 CFR 71.55 and 71.59. Based on a 3x4 array of 10 undamaged packages and a 2x2 array of four damaged packages, the Criticality Safety Index (CSI), per 10 CFR 71.59, is 25.0.

6.11.1 Description of Criticality Design

6.11.1.1 Design Features Important for Criticality

No special design features are required to maintain criticality safety. No poisons are utilized in the package. The separation provided by the packaging (outer flat-to-flat dimension of 7.9-in), along with the limit on the number of packages per shipment, is sufficient to maintain criticality safety.

6.11.1.2 Summary Table of Criticality Evaluation

The upper subcritical limit (USL) for ensuring that the ATR FFSC (single package or package array) is acceptably subcritical, as determined in Section 6.11.8, *Benchmark Evaluations*, is:

$$USL = 0.9209$$

The package is considered to be acceptably subcritical if the computed k_{safe} (k_s), which is defined as $k_{effective}$ (k_{eff}) plus twice the statistical uncertainty (σ), is less than or equal to the USL, or:

$$k_s = k_{eff} + 2\sigma \leq USL$$

The USL is determined on the basis of a benchmark analysis and incorporates the combined effects of code computational bias, the uncertainty in the bias based on both benchmark-model and computational uncertainties, and an administrative margin. The results of the benchmark analysis indicate that the USL is adequate to ensure subcriticality of the package.

The packaging design is shown to meet the requirements of 10 CFR 71.55(b). Moderation by water in the most reactive credible extent is utilized in both the normal conditions of transport (NCT) and hypothetical accident conditions of transport (HAC) analyses. In the single package NCT models, full-density water fills the accessible cavity, while in the single package HAC models, full-density water fills all cavities. In all single package models, 12-in of water reflection is utilized.

A 3x4x1 array of 10 packages (2 empty locations) is utilized for the NCT array, while a 2x2x1 array of 4 packages is utilized in the HAC array. In the HAC array cases, partial moderation is considered to maximize array interaction effects. In all array models, 12-in of water reflection is utilized external to the array.

The maximum results of the criticality calculations are summarized in Table 6.11-1. The maximum calculated k_s is 0.8943, which occurs for the optimally moderated NCT array case. The NCT array is more reactive than the HAC array because the NCT array is larger, and moderation is allowed in both conditions. In this case, the fuel mixture is modeled with a height of 32.5 cm, and void is modeled between the insulation and outer tube.

6.11.1.3 Criticality Safety Index

The criticality safety index is defined in 10 CFR 71.59 as 50/N, where 5N packages are used in the NCT array configuration, and 2N packages are used in the HAC array configuration. A 2x2 array (2N = 4, or N = 2) is utilized for the HAC array calculations, while a 3x4 array of 10 packages (5N = 10, or N = 2) is utilized for the NCT array calculations. Therefore, the criticality safety index is 50/N = 50/2 = 25.0. With a CSI = 25.0, a maximum of four packages is allowed per exclusive use shipment.

Table 6.11-1 – Summary of Small Quantity Payloads Criticality Evaluation

Normal Conditions of Transport (NCT)	
Case	k_s
Single Unit Maximum	0.6478
Array Maximum	0.8943
Hypothetical Accident Conditions (HAC)	
Case	k_s
Single Unit Maximum	0.7244
Array Maximum	0.8222
USL = 0.9209	

6.11.2 Fissile Material Contents

The fissile material content is up to 400 g U-235 enriched up to 94% as a general payload material. Because HEU is modeled in the analysis, the results also apply to medium enriched uranium (MEU) and low enriched uranium (LEU) fuels. The analysis also applies to any generic fuel with U-235 as the fissile isotope. The objective is to bound research and development fuels with designs that are subject to change. The full list of anticipated contents bounded by this analysis is summarized in Section 1.2.2.4, *Small Quantity Payload*.

In general, for enrichments greater than 5% U-235, a system is more reactive using a homogenized mixture rather than an explicit heterogeneous representation[11]. Therefore, to simplify the modeling approach, the fuel is modeled as a homogenized mixture of uranium and water. Note that the homogenized representation is simply a conservative representation, and it is not implied that the actual fuel would behave in this manner. The fuel, even in accident conditions, would remain largely intact.

[11] JJ Duderstadt and LJ Hamilton, *Nuclear Reactor Analysis*, p. 405, John Wiley & Sons, Inc., 1976.

This fuel mixture is assumed to conform to the cylindrical geometry constraint of the inner circular tube of the ATR FFSC. The fuel element structural materials (i.e., aluminum, silicon, etc.) are conservatively ignored, as well as the fuel handling enclosure (FHE) that supports the fuel element (either the RINSC FHE for RINSC fuel, or the small payload FHE for the remaining fuels). Modeling the structural materials would increase parasitic neutron absorption, as well as enlarge the size of the fissile volume to achieve the same hydrogen/U-235 ratio, and both effects would decrease the reactivity. A polyethylene limit of 100 g is justified in the analysis.

The contents may contain burnable absorbers, such as gadolinium, samarium, or boron. All burnable absorbers are conservatively neglected in the analysis.

The isotopic distribution of HEU fuel used in the analysis is listed in Table 6.11-2. The U-235 enrichment is conservatively modeled at 94%, which bounds the approximately 20% enrichment of LEU fuel, and 40-80% enrichment of MEU fuel. The remaining uranium isotopic values are representative and are consistent with the values used in the ATR criticality analysis (see Section 6.2, *Fissile Material Contents*). The fuel is modeled as homogenized mixture of uranium and water. Optimum reactivity is achieved by varying the height of the fissile mixture. A useful index of moderation for homogeneous systems is the hydrogen to U-235 ratio, abbreviated as H/U-235. This parameter is adjusted by varying the height of the fissile mixture. Increasing the height of the fissile mixture increases H/U-235.

The number densities of the homogenized mixture are computed in the following manner. A U-235 mass of 400 g is modeled, which bounds the masses of the small quantity payload items. The weight percent of U-235 is 94.0%. Therefore, the total mass of uranium M_U for 400 g U-235 is 400/0.94 = 425.5 g U. The theoretical density of uranium is 19.0 g/cm^3, so the solid-volume V_U of 425.5 g U is 425.5/19.0 = 22.4 cm^3. The homogenized volume V is $\pi R^2 H$, where R is the inner radius of the ATR FFSC circular tube (7.3838 cm) and H is the height of the fissile mixture. The gram density of uranium in the mixture is then M_U/V, and if water of density 1.0 g/cm^3 fills the remaining volume, the water density in the mixture is $(V- V_U)/V$. The number densities of uranium and water may then be computed from the mixture densities. An example set of fuel mixture number densities for a height of 40 cm is provided in Table 6.11-3.

The ATR FFSC may contain hydrogenous materials. Fuel elements may be transported in a polyethylene (CH_2) bag with a mass of approximately 3 oz, or 85 g. Neoprene (C_4H_5Cl) is used as a padding material in the fuel holders, and cellulosic material ($C_6H_{10}O_5$) (e.g., kraft paper, cardboard) may be used as a cushioning material. The total mass of neoprene and cellulosic material is limited to a sum of 4000 g. Fiberglass reinforced tape may also be used to secure bundles of loose plates, and the mass of tape is conservatively treated as polyethylene. Homogenized mixtures are developed that include either polyethylene, neoprene, cellulosic material, or structural material (such as aluminum) using the same method described above. For these computations, the density of polyethylene is 0.92 g/cm^3, the density of neoprene is 1.23 g/cm^3, the density of cellulosic material is 0.44 g/cm^3, and the density of aluminum is 2.6989 g/cm^3. As an example, fuel mixture number densities are provided in Table 6.11-3 for a height of 40 cm. Mixture number densities for other heights may be computed using the methodology described above.

Table 6.11-2 – Uranium Isotopics

Isotope	Modeled HEU Isotopics (Wt. %)
U-234	0.60
U-235	94.0
U-236	0.35
U-238	5.05

This page left intentionally blank.

Table 6.11-3 – Example Fissile Mixture Number Densities for Height = 40 cm

Isotope	Fuel/Water Number Densities (atom/b-cm)	Fuel/Water Number Densities (atom/b-cm) with 100 g of Polyethylene	Fuel/Water Number Densities (atom/b-cm) with 1500 g of Neoprene	Fuel/Water Number Densities (atom/b-cm) with 1500 g of Cellulosic Material	Fuel/Water Number Densities (atom/b-cm) with 1500 g of Aluminum
U-234	9.5888E-07	9.5888E-07	9.5888E-07	9.5888E-07	9.5888E-07
U-235	1.4958E-04	1.4958E-04	1.4958E-04	1.4958E-04	1.4958E-04
U-236	5.5459E-07	5.5459E-07	5.5459E-07	5.5459E-07	5.5459E-07
U-238	7.9346E-06	7.9346E-06	7.9346E-06	7.9346E-06	7.9346E-06
H	6.6636E-02	6.6828E-02	6.2182E-02	4.1461E-02	6.1213E-02
O	3.3318E-02	3.2788E-02	2.7368E-02	2.0731E-02	3.0606E-02
C	-	6.2664E-04	5.9567E-03	4.8789E-03	-
Cl	-	-	1.4892E-03	-	-
Al	-	-	-	-	4.8865E-03
Total	1.0011E-01	1.0040E-01	9.7155E-02	6.7230E-02	9.6864E-02

This page left intentionally blank.

6.11.3 General Considerations

6.11.3.1 Model Configuration

The packaging is modeled essentially the same as described in Section 6.3.1, *Model Configuration*. Refer to that section for details of the packaging model. The package length is modeled as 48-in long to be consistent with the original criticality models using ATR fuel (which has an active length of 48-in), although this length is somewhat arbitrary and is conservatively shorter than the actual inner cavity length of 67.88-in. The package is reflected with 12-in of full-density water.

In the NCT single package models, the inner tube, insulation, and outer tube are modeled explicitly, as shown in Figure 6.11-1 and Figure 6.11-2. Although negligible water ingress is expected during NCT, the inner cavity of the package is assumed to be flooded with water because the package lid does not contain a seal. However, the region between the insulation and the outer tube will remain dry because water cannot enter this region. The fuel is transported in a Fuel Handling Enclosure (FHE), which is conservatively ignored because the fuel is homogenized with water. Modeling the FHE would decrease the reactivity significantly if it is assumed that the fuel is homogenized within the constraint of the FHE. If it is assumed that the homogenized mixture could flow out of the FHE, modeling the FHE would still be less reactive than ignoring it because it would displace fissile material and increase the size of the fissile cylinder.

Although the FHE is not modeled, hydrogenous neoprene cushioning material along the sides of the enclosure is included in the fissile mixture in the NCT array models to demonstrate the poisoning effect of neoprene. The combined mass of neoprene and cellulosic material is limited to 4000 g.

The fuel elements may be transported in a polyethylene bag with an approximate mass of 3 oz, or 85 g. A polyethylene mass of 100 g is conservatively homogenized with the fuel/water mixture when indicated. The mass of fiberglass reinforced tape, which may be used to bind loose plates, shall be included in the polyethylene mass.

The HAC single package model is essentially the same as the NCT single package model. Damage in the drop tests was shown to be negligible and concentrated at the ends of the package [See Section 2.12.1, *Certification Tests on CTU-1*]. As the ends of the package are not modeled, this end damage does not affect the modeling. The various side drops resulted in only minor localized damage to the outer tube, and no observable bulk deformation of the package. Therefore, the minor damage observed will not impact the reactivity. The insulation is replaced with full-density water, and the region between the insulation and outer tube is also filled with full-density water (see Figure 6.11-3). The treatment of the FHE is the same as the NCT single package model.

In the NCT array models, a 3x4x1 array is utilized, although two array positions are empty, for a total of 10 packages. The geometry of a package in the NCT array is the same as the NCT single package models. In the HAC array models, a 2x2x1 array is utilized. The HAC array models are essentially the same as the NCT array models, except additional cases are developed to determine the reactivity effect of allowing variable density water in the region between the inner and outer tubes. Cases are also developed with and without the insulation. The FHE is

conservatively ignored for the reasons stated in the previous paragraphs. Because the NCT and HAC models are very similar and the NCT models utilize a larger array, the NCT array models are more reactive than the HAC array models.

The detailed moderation assumptions for these cases are discussed more fully in Section 6.11.5, *Evaluation of Package Arrays under Normal Conditions of Transport*, and Section 6.11.6, *Package Arrays under Hypothetical Accident Conditions*.

6.11.3.2 Material Properties

An example fissile material composition is provided in Table 6.11-3. The material properties of the packaging materials are provided in Section 6.3.2, *Material Properties*.

6.11.3.3 Computer Codes and Cross-Section Libraries

The computer codes and cross-section libraries utilized are provided in Section 6.3.3, *Computer Codes and Cross-Section Libraries*.

6.11.3.4 Demonstration of Maximum Reactivity

A number of conservative assumptions are utilized to obtain the maximum reactivity:

- The fuel is modeled as a homogeneous mixture of uranium and water, which is a significantly more reactive configuration than modeling the fuel explicitly. Fuel element structural materials are ignored in the most reactive case.
- 400 g of U-235 is modeled, which bounds the U-235 loading of the proposed contents.
- The U-235 enrichment is modeled as 94%, which bounds the enrichment of the proposed contents.

The fissile mixture is assumed to fill the inner tube of the ATR FFSC, and moderation is varied by running cases with different fissile mixture heights. No credit is taken for fuel handling enclosures that would maintain the fuel in a more favorable geometry. Note that the homogenized representation is simply a conservative representation, and it is not implied that the actual fuel would behave in this manner. The fuel, even in accident conditions, would remain largely intact.

In the NCT cases, water fills only the inner tube, because water would not enter the region between the inner circular tube and outer square tube. In the HAC cases, water is allowed in the region between the inner circular tube and outer square tube. Also, insulation may be replaced with water in the HAC cases. All single package cases are reflected with 12-in of water.

For the NCT array, 10 packages are modeled in a 3x4x1 array (with 2 empty locations), while in the HAC array, a smaller 2x2x1 array is utilized. Because negligible damage was observed in the drop tests, the package dimensions are the same between the NCT and HAC models. Dimensions of the packaging are selected to maximize reactivity, and 12-in of close-water reflection is utilized.

The NCT array analysis is rather straightforward, because the only variable is the height of the fissile mixture. In the HAC array analysis, variables include the height of the fissile mixture, the presence or absence of insulation, and the water density of the region between the circular and square tubes. These parameters are varied to find the most reactive HAC condition.

Because fuel elements may be transported in polyethylene bags, 100 g of polyethylene is included in the fissile mixture. Polyethylene has a small, but positive, effect on the reactivity. The hydrogenous materials neoprene and cellulosic material are shown to have a negative effect on reactivity because they are less effective at moderating the fissile mixture than the water that is displaced. Therefore, it is conservative to ignore neoprene and cellulosic material in the models. It is also explicitly demonstrated that modeling inert structural materials, such as aluminum, has a negative effect on the reactivity.

The NCT array is more reactive than the HAC array, primarily because the NCT array is significantly larger, and both cases use a homogenized fuel assumption. The most reactive NCT array case (Case HC16) has a fissile mixture height of 32.5 cm and results in a k_s = 0.89427, which is below the USL of 0.9209. The most reactive HAC array case (Case HD34) results in a k_s = 0.82217.

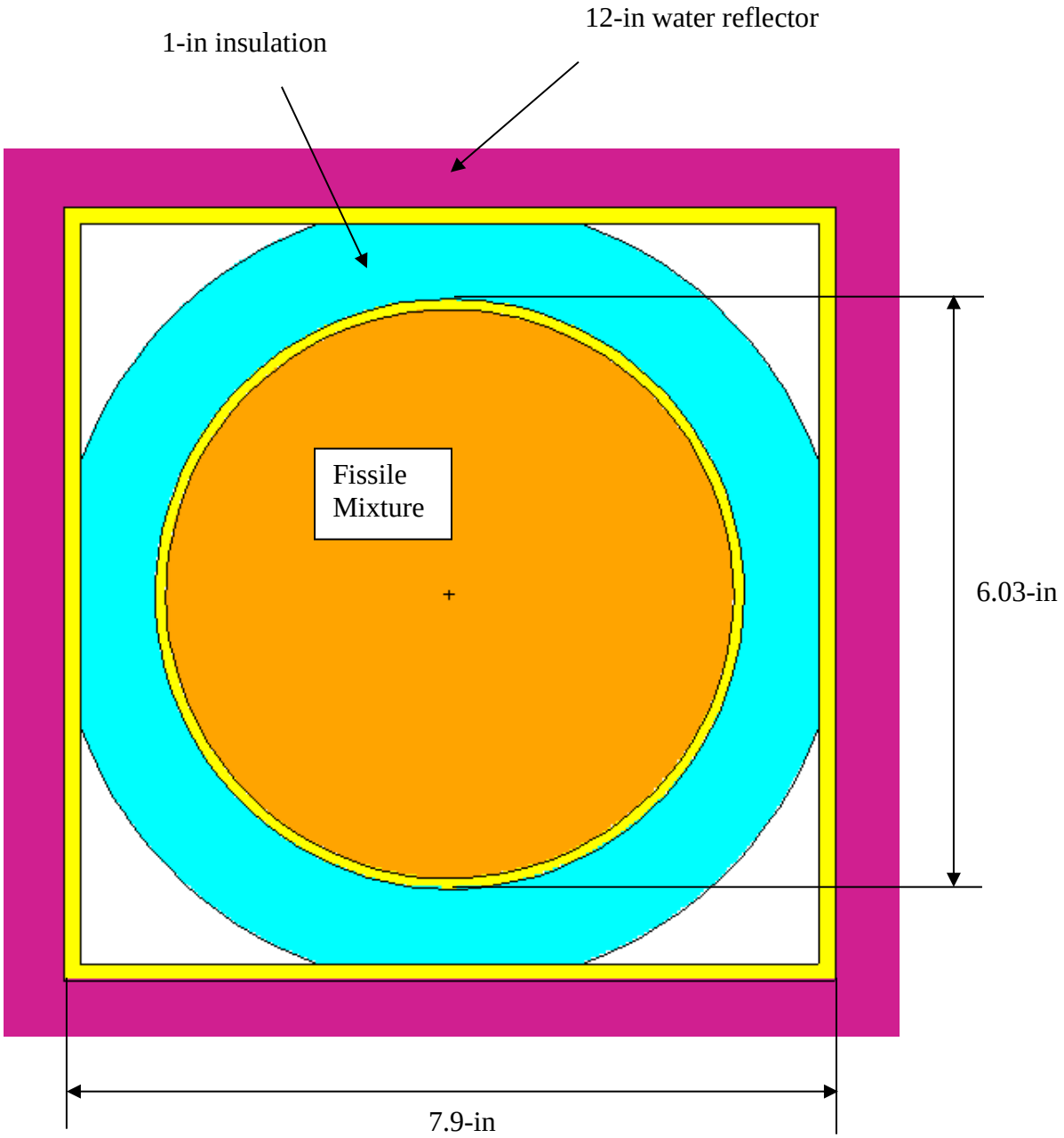

Figure 6.11-1 – NCT Single Package Model (planar view)

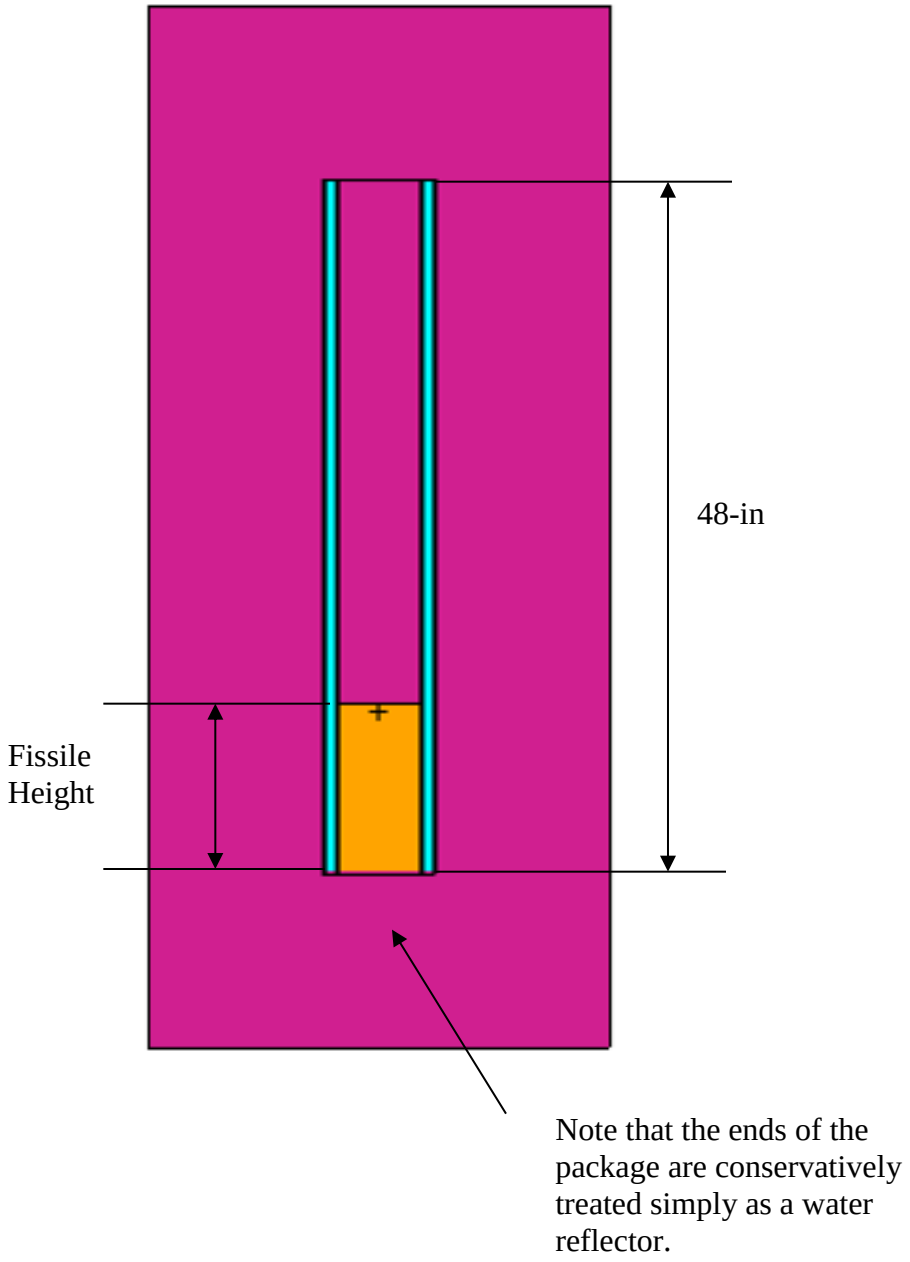

Figure 6.11-2 – NCT Single Package Model (axial view)

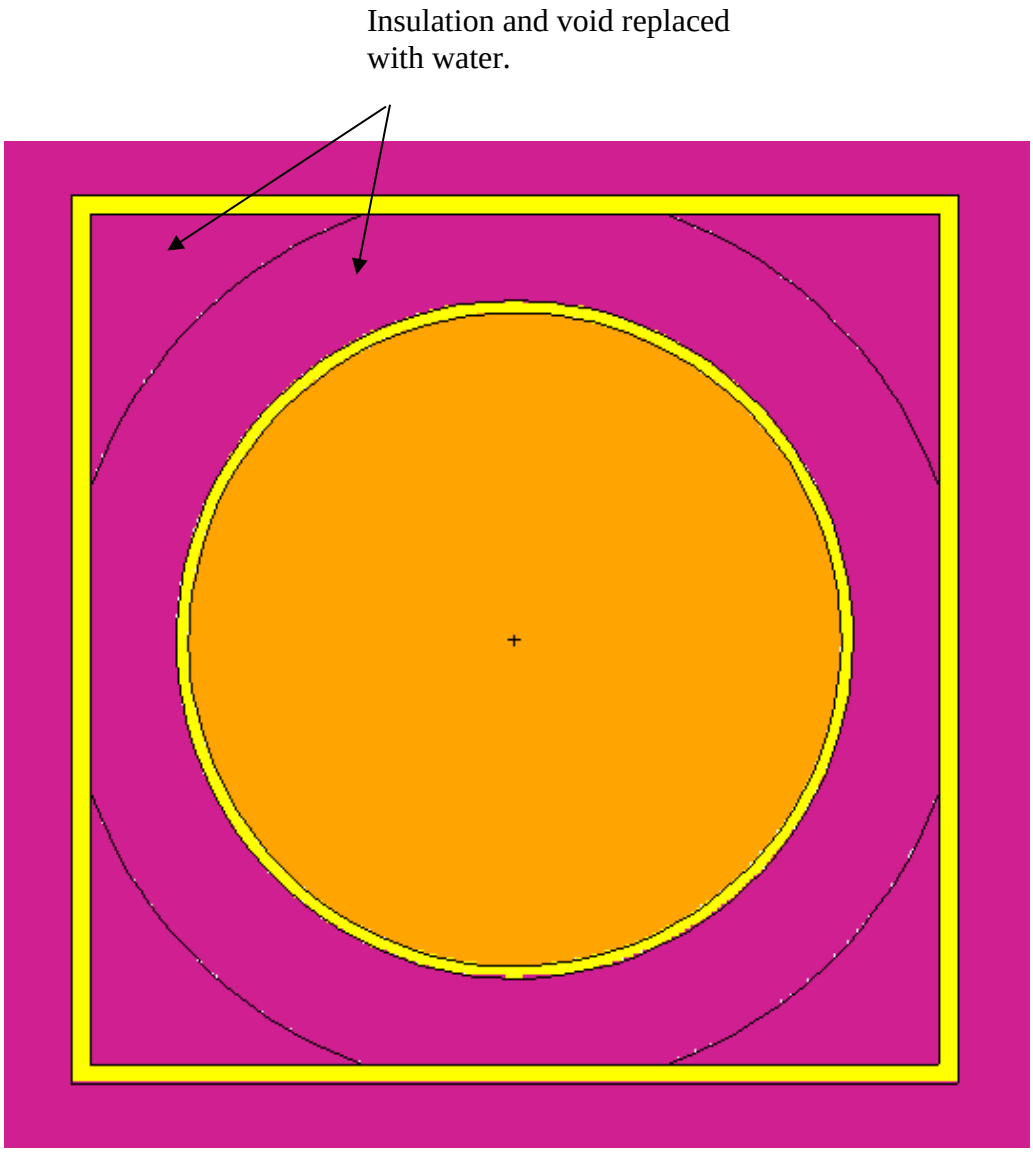

Figure 6.11-3 – HAC Single Package Model (planar view)

6.11.4 Single Package Evaluation

6.11.4.1 Single Package Configuration

6.11.4.1.1 NCT Single Package Configuration

The geometry of the NCT single package configuration is discussed in Section 6.11.3.1, *Model Configuration*. The fissile material is homogenized with water for a variety of fissile mixture heights. The water above the fissile mixture is modeled at full-density to maximize reflection. The package is reflected with 12-in of water.

It is demonstrated in Section 6.11.5 that including neoprene, cellulosic material, or structural materials in the fissile mixture reduces the reactivity, so these materials are conservatively neglected in the NCT single package configuration.

Results are provided in Table 6.11-4. Cases HA1 through HA10 are without polyethylene, and Cases HA11 through HA20 include 100 g of polyethylene. The cases with polyethylene are slightly more reactive, although the effect is small. Maximum reactivity is achieved for Case HA13, with a fissile mixture height of 25.0 cm. The reactivity of this case is low, with k_s = 0.64775. This result is below the USL of 0.9209.

6.11.4.1.2 HAC Singe Package Configuration

The geometry of the HAC single package configuration is discussed in Section 6.11.3.1, *Model Configuration*. The fissile material is homogenized with water for a variety of fissile mixture heights. The water above the fissile mixture is modeled at full-density to maximize reflection. The insulation is replaced with full-density water, and full-density water is also modeled between the inner and outer tubes. The package is reflected with 12-in of water.

It is demonstrated in Section 6.11.5 that including neoprene, cellulosic material, or structural materials in the fissile mixture reduces the reactivity, so these materials are conservatively neglected in the HAC single package configuration.

Results are provided in Table 6.11-5. Cases HB1 through HB10 are without polyethylene, and Cases HB11 through HB20 include 100 g of polyethylene. The cases with polyethylene are slightly more reactive, although the effect is small. Maximum reactivity is achieved for Case HB15, with a fissile mixture height of 27.5 cm. The reactivity of this case is low, with k_s = 0.72441. This result is below the USL of 0.9209.

6.11.4.2 Single Package Results

Following are the tabulated results for the single package cases. The most reactive configurations are listed in boldface.

Table 6.11-4 – NCT Single Package Results

Case ID	Filename	Fissile Mixture Height (cm)	k_{eff}	σ	k_s (k+2σ)
No Polyethylene					
HA1	NS_HEU_H15	15.0	0.61609	0.00130	0.61869
HA2	NS_HEU_H20	20.0	0.63614	0.00115	0.63844
HA3	NS_HEU_H25	25.0	0.64046	0.00116	0.64278
HA4	**NS_HEU_H275**	**27.5**	**0.64251**	**0.00114**	**0.64479**
HA5	NS_HEU_H30	30.0	0.64189	0.00116	0.64421
HA6	NS_HEU_H325	32.5	0.63773	0.00111	0.63995
HA7	NS_HEU_H35	35.0	0.62944	0.00106	0.63156
HA8	NS_HEU_H40	40.0	0.62060	0.00105	0.62270
HA9	NS_HEU_H45	45.0	0.60913	0.00110	0.61133
HA10	NS_HEU_H50	50.0	0.59328	0.00104	0.59536
With 100 g Polyethylene					
HA11	NS_HEUP_H15	15.0	0.62298	0.00128	0.62554
HA12	NS_HEUP_H20	20.0	0.64179	0.00112	0.64403
HA13	**NS_HEUP_H25**	**25.0**	**0.64531**	**0.00122**	**0.64775**
HA14	NS_HEUP_H275	27.5	0.64503	0.00114	0.64731
HA15	NS_HEUP_H30	30.0	0.64193	0.00113	0.64419
HA16	NS_HEUP_H325	32.5	0.63741	0.00116	0.63973
HA17	NS_HEUP_H35	35.0	0.63154	0.00113	0.63380
HA18	NS_HEUP_H40	40.0	0.62058	0.00108	0.62274
HA19	NS_HEUP_H45	45.0	0.60798	0.00109	0.61016
HA20	NS_HEUP_H50	50.0	0.59553	0.00101	0.59755

Table 6.11-5 – HAC Single Package Results

Case ID	Filename	Fissile Mixture Height (cm)	k_{eff}	σ	k_s (k+2σ)
No Polyethylene					
HB1	HS_HEU_H15	15.0	0.69170	0.00124	0.69418
HB2	HS_HEU_H20	20.0	0.71519	0.00122	0.71763
HB3	HS_HEU_H225	22.5	0.72038	0.00131	0.72300
HB4	**HS_HEU_H25**	**25.0**	**0.72067**	**0.00126**	**0.72319**
HB5	HS_HEU_H275	27.5	0.71817	0.00114	0.72045
HB6	HS_HEU_H30	30.0	0.71422	0.00120	0.71662
HB7	HS_HEU_H325	32.5	0.70809	0.00116	0.71041
HB8	HS_HEU_H35	35.0	0.70653	0.00121	0.70895
HB9	HS_HEU_H40	40.0	0.69450	0.00111	0.69672
HB10	HS_HEU_H45	45.0	0.67855	0.00120	0.68095
With 100 g Polyethylene					
HB11	HS_HEUP_H15	15.0	0.69905	0.00128	0.70161
HB12	HS_HEUP_H20	20.0	0.71848	0.00128	0.72104
HB13	HS_HEUP_H225	22.5	0.72122	0.00125	0.72372
HB14	HS_HEUP_H25	25.0	0.72136	0.00120	0.72376
HB15	**HS_HEUP_H275**	**27.5**	**0.72189**	**0.00126**	**0.72441**
HB16	HS_HEUP_H30	30.0	0.71679	0.00130	0.71939
HB17	HS_HEUP_H325	32.5	0.71212	0.00123	0.71458
HB18	HS_HEUP_H35	35.0	0.70759	0.00119	0.70997
HB19	HS_HEUP_H40	40.0	0.69424	0.00111	0.69646
HB20	HS_HEUP_H45	45.0	0.67857	0.00112	0.68081

6.11.5 Evaluation of Package Arrays under Normal Conditions of Transport

6.11.5.1 NCT Array Configuration

The NCT array model is a 3x4x1 array with two empty locations, for a total of 10 packages. The array configuration utilized is the most reactive 10 package configuration, with 9 packages in a 3x3 configuration, and one package at the center of a side, see Figure 6.11-4. Axial stacking configurations, such as 2x3x2 with two empty locations, would lower the reactivity and are not investigated. The geometry of the individual packages is the same as the NCT single package model. The entire array is reflected with 12-in of full-density water. Moderation is varied by adjusting the height of the fissile mixture. The region above the fissile mixture is filled with full density water to maximize reflection.

The following series of cases are run:

- Table 6.11-6: Moderator as pure water or water with 100 g polyethylene
- Table 6.11-7: Moderator as water with 100 g, 1500 g, or 4000 g neoprene
- Table 6.11-8: Moderator as water with 100 g, 1500 g, or 4000 g cellulosic material
- Table 6.11-9: Moderator as water with 100 g or 1500 g aluminum

The results for pure water and water with 100 g polyethylene are provided in Table 6.11-6. For a pure water moderator, k_s = 0.89381 at a fissile mixture height of 30 cm (Case HC5). When 100 g of polyethylene is added, k_s = 0.89427 at a fissile mixture height of 32.5 cm (Case HC16). While polyethylene is a superior moderator than water, the results with polyethylene are statistically identical to the results with pure water because the mass of added polyethylene is small.

While neoprene and cellulosic material both contain hydrogen, these materials are less effective moderators than pure water and the reactivity decreases when these materials are added to the fissile mixture, as shown in Table 6.11-7 and Table 6.11-8. The chlorine in the neoprene also acts as a poison. Therefore, it is conservative to neglect neoprene and cellulosic material in the models. A combined mass limit for neoprene plus cellulosic material of 4000 g is therefore justified.

When aluminum is added to the fissile mixture, the reactivity also decreases, as shown in Table 6.11-9. There is a sizable quantity of aluminum within the package cavity due to both the fuel cladding and FHE structural materials. Therefore, the modeling approach is inherently conservative because all metallic structural materials are neglected. Inert materials in the fuel meat, such as molybdenum or silicon, are also conservatively neglected.

The most reactive condition is Case HC16, which includes 100 g polyethylene and has a fissile height of 32.5 cm. For this case, k_s = 0.89427, which is below the USL of 0.9209.

6.11.5.2 NCT Array Results

The results for the NCT array cases are provided in the following tables. The most reactive configurations are listed in boldface.

Table 6.11-6 – NCT Array Results with Polyethylene

Case ID	Filename	Fissile Mixture Height (cm)	k_{eff}	σ	k_s (k+2σ)
Moderator: Water					
HC1	NA_HEU_H15	15.0	0.81375	0.00130	0.81635
HC2	NA_HEU_H20	20.0	0.86031	0.00130	0.86291
HC3	NA_HEU_H25	25.0	0.88140	0.00120	0.88380
HC4	NA_HEU_H275	27.5	0.88591	0.00129	0.88849
HC5	**NA_HEU_H30**	**30.0**	**0.89141**	**0.00120**	**0.89381**
HC6	NA_HEU_H325	32.5	0.89089	0.00123	0.89335
HC7	NA_HEU_H35	35.0	0.89028	0.00114	0.89256
HC8	NA_HEU_H40	40.0	0.88126	0.00116	0.88358
HC9	NA_HEU_H45	45.0	0.87387	0.00116	0.87619
HC10	NA_HEU_H50	50.0	0.85981	0.00104	0.86189
Moderator: Water with 100 g Polyethylene					
HC11	NA_HEUP_H15	15.0	0.81856	0.00130	0.82116
HC12	NA_HEUP_H20	20.0	0.86138	0.00129	0.86396
HC13	NA_HEUP_H25	25.0	0.88386	0.00119	0.88624
HC14	NA_HEUP_H275	27.5	0.88818	0.00113	0.89044
HC15	NA_HEUP_H30	30.0	0.88873	0.00122	0.89117
HC16	**NA_HEUP_H325**	**32.5**	**0.89207**	**0.00110**	**0.89427**
HC17	NA_HEUP_H35	35.0	0.88988	0.00113	0.89214
HC18	NA_HEUP_H40	40.0	0.88439	0.00110	0.88659
HC19	NA_HEUP_H45	45.0	0.87352	0.00106	0.87564
HC20	NA_HEUP_H50	50.0	0.86011	0.00110	0.86231

Table 6.11-7 – NCT Array Results with Neoprene

Case ID	Filename	Fissile Mixture Height (cm)	k_{eff}	σ	k_s (k+2σ)
Moderator: Water with 100 g Neoprene					
HC30	NA_N100_H15	15.0	0.78812	0.00045	0.78902
HC31	NA_N100_H20	20.0	0.83258	0.00043	0.83344
HC32	NA_N100_H25	25.0	0.85690	0.00044	0.85778
HC33	NA_N100_H30	30.0	0.86748	0.00042	0.86832
HC34	**NA_N100_H35**	**35.0**	**0.86790**	**0.00040**	**0.86870**
HC35	NA_N100_H40	40.0	0.86268	0.00039	0.86346
HC36	NA_N100_H45	45.0	0.85398	0.00040	0.85478
HC37	NA_N100_H50	50.0	0.84194	0.00039	0.84272
Moderator: Water with 1500 g Neoprene					
HC40	NA_HEUN_H30	30.0	0.62595	0.00096	0.62787
HC41	NA_HEUN_H35	35.0	0.63410	0.00092	0.63594
HC42	NA_HEUN_H40	40.0	0.63992	0.00099	0.64190
HC43	**NA_HEUN_H45**	**45.0**	**0.64188**	**0.00091**	**0.64370**
HC44	NA_HEUN_H50	50.0	0.63611	0.00086	0.63783
HC45	NA_HEUN_H55	55.0	0.63358	0.00079	0.63516
HC46	NA_HEUN_H60	60.0	0.62747	0.00087	0.62921
Moderator: Water with 4000 g Neoprene					
HC90	NA_N4000_H40	40.0	0.42787	0.00023	0.42833
HC91	NA_N4000_H45	45.0	0.43470	0.00023	0.43516
HC92	NA_N4000_H50	50.0	0.43803	0.00024	0.43851
HC93	**NA_N4000_H55**	**55.0**	**0.44046**	**0.00023**	**0.44092**
HC94	NA_N4000_H60	60.0	0.44040	0.00023	0.44086
HC95	NA_N4000_H65	65.0	0.43867	0.00022	0.43911
HC96	NA_N4000_H70	70.0	0.43710	0.00022	0.43754

Table 6.11-8 – NCT Array Results with Cellulosic Material

Case ID	Filename	Fissile Mixture Height (cm)	k_{eff}	σ	k_s (k+2σ)
Moderator: Water with 100 g Cellulosic Material					
HC50	NA_K100_H15	15.0	0.78017	0.00044	0.78105
HC51	NA_K100_H20	20.0	0.83462	0.00047	0.83556
HC52	NA_K100_H25	25.0	0.86375	0.00043	0.86461
HC53	NA_K100_H30	30.0	0.87624	0.00045	0.87714
HC54	**NA_K100_H35**	**35.0**	**0.87873**	**0.00041**	**0.87955**
HC55	NA_K100_H40	40.0	0.87524	0.00042	0.87608
HC56	NA_K100_H45	45.0	0.86633	0.00041	0.86715
HC57	NA_K100_H50	50.0	0.85509	0.00038	0.85585
Moderator: Water with 1500 g Cellulosic Material					
HC60	NA_K1500_H40	40.0	0.69615	0.00040	0.69695
HC61	NA_K1500_H45	45.0	0.72143	0.00039	0.72221
HC62	NA_K1500_H50	50.0	0.73626	0.00039	0.73704
HC63	NA_K1500_H55	55.0	0.74237	0.00038	0.74313
HC64	**NA_K1500_H60**	**60.0**	**0.74390**	**0.00037**	**0.74464**
HC65	NA_K1500_H65	65.0	0.74255	0.00037	0.74329
HC66	NA_K1500_H70	70.0	0.73673	0.00037	0.73747
HC67	NA_K1500_H75	75.0	0.72883	0.00034	0.72951
HC68	NA_K1500_H80	80.0	0.72050	0.00033	0.72116
Moderator: Water with 4000 g Cellulosic Material					
HC100	NA_K4000_H85	85.0	0.57976	0.00033	0.58042
HC101	NA_K4000_H90	90.0	0.58604	0.00033	0.58670
HC102	NA_K4000_H95	95.0	0.58907	0.00033	0.58973
HC103	**NA_K4000_H100**	**100.0**	**0.59108**	**0.00031**	**0.59170**
HC104	NA_K4000_H105	105.0	0.58916	0.00031	0.58978
HC105	NA_K4000_H110	110.0	0.58677	0.00031	0.58739
HC106	NA_K4000_H115	115.0	0.58307	0.00032	0.58371

Table 6.11-9 – NCT Array Results with Aluminum

Case ID	Filename	Fissile Mixture Height (cm)	k_{eff}	σ	k_s (k+2σ)
Moderator: Water with 100 g Aluminum					
HC70	NA_A100_H15	15.0	0.80807	0.00047	0.80901
HC71	NA_A100_H20	20.0	0.85445	0.00045	0.85535
HC72	NA_A100_H25	25.0	0.87889	0.00043	0.87975
HC73	NA_A100_H30	30.0	0.88745	0.00043	0.88831
HC74	**NA_A100_H325**	**32.5**	**0.88880**	**0.00043**	**0.88966**
HC75	NA_A100_H35	35.0	0.88808	0.00040	0.88888
HC76	NA_A100_H40	40.0	0.88135	0.00041	0.88217
HC77	NA_A100_H45	45.0	0.87218	0.00038	0.87294
HC78	NA_A100_H50	50.0	0.86069	0.00038	0.86145
Moderator: Water with 1500 g Aluminum					
HC80	NA_A1500_H20	20.0	0.78043	0.00045	0.78133
HC81	NA_A1500_H25	25.0	0.82043	0.00044	0.82131
HC82	NA_A1500_H30	30.0	0.84233	0.00044	0.84321
HC83	NA_A1500_H35	35.0	0.85139	0.00042	0.85223
HC84	**NA_A1500_H40**	**40.0**	**0.85197**	**0.00040**	**0.85277**
HC85	NA_A1500_H45	45.0	0.84700	0.00038	0.84776
HC86	NA_A1500_H50	50.0	0.83791	0.00039	0.83869
HC87	NA_A1500_H55	55.0	0.82724	0.00036	0.82796
HC88	NA_A1500_H60	60.0	0.81461	0.00038	0.81537

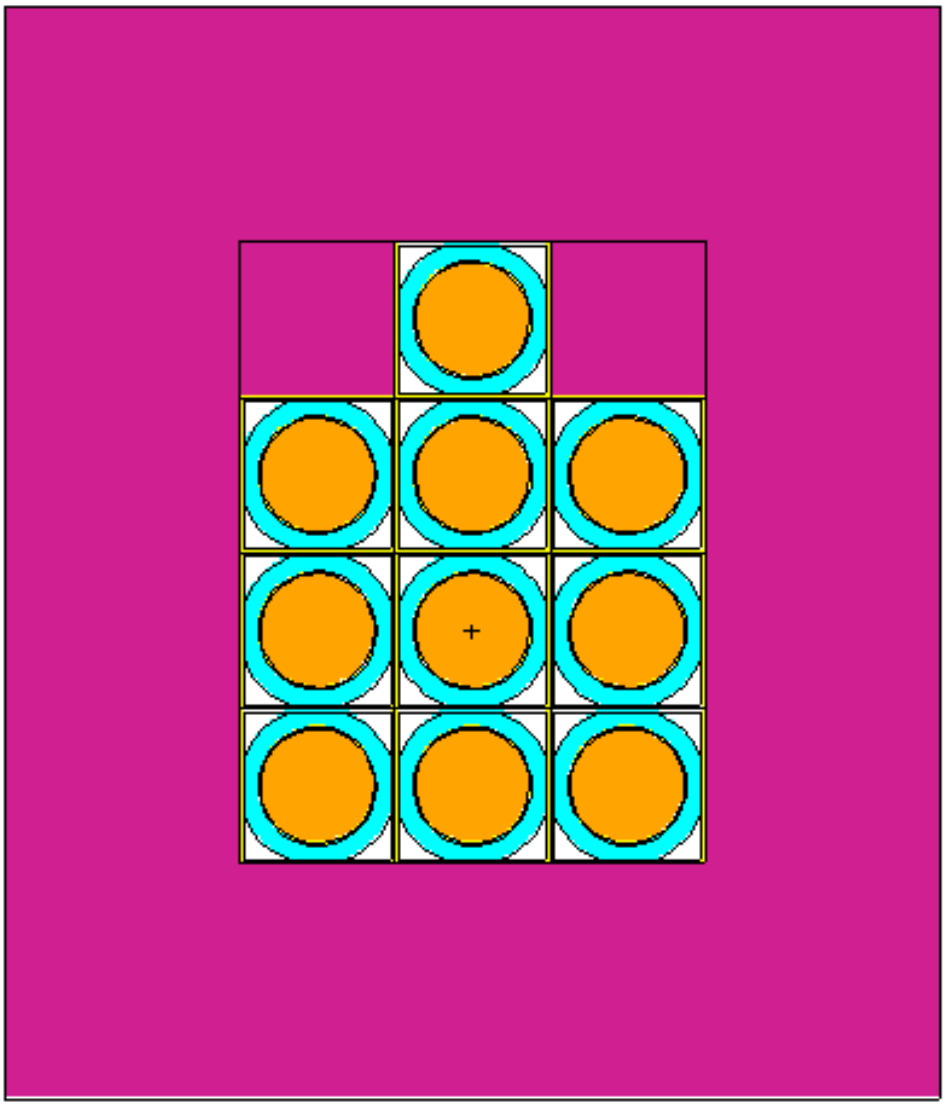

Figure 6.11-4 – NCT Array Geometry

6.11.6 Package Arrays under Hypothetical Accident Conditions

6.11.6.1 HAC Array Configuration

The HAC array model is a 2x2x1 array of the HAC single package model, as shown in Figure 6.11-5. Results are provided in Table 6.11-10. Because it has been demonstrated in the NCT single package, HAC single package, and NCT array cases that adding 100 g of polyethylene to the fissile mixture slightly increases the reactivity, all HAC array cases include 100 g of polyethylene.

In Cases HD1 through HD10, the region between the inner circular tube and outer square tube is filled with full-density water. Therefore, the insulation is replaced with water. The fissile mixture height is varied to find the optimum moderation, and the region above the fissile mixture is filled with full-density water. Of these 10 cases, Case HD4 is the most reactive, with a fissile mixture height of 25.0 cm.

In Cases HD11 through HD15, the most reactive fissile mixture height of 25.0 cm is modeled. The insulation is modeled explicitly, and a range of water densities are modeled between the insulation and outer square tube. These cases are less reactive than Case HD4, indicating that it is conservative to ignore the insulation in the HAC array models.

In Cases HD16 through HD25, Case HD4 is modified for a range of water densities between the inner circular tube and outer square tube. Case HD22 is the most reactive, with k_s = 0.81981 and a water density between tubes of 0.6 g/cm^3. This case is slightly more reactive than Case HD4, for which k_s = 0.81502. However, the reactivity gain by using a reduced water density between the tubes is small.

The most reactive fissile mixture height may change based on the water density between the tubes. For this reason, a limited number of additional cases are run for fissile mixture heights of 22.5 cm, 27.5 cm, and 30.0 cm. In Cases HD26 through HD31, the fissile mixture height is 22.5 cm and the water density is varied between 0.3 and 0.8 g/cm^3. Cases HD32 through HD37 are similar except the fissile mixture height is 27.5 cm, and in Cases HD38 through HD43 the fissile mixture height is 30.0 cm. The most reactive case is Case HD34, which is slightly more reactive than Case HD22.

Therefore, Case HD34 is the most reactive, with k_s = 0.82217. This case has a fissile mixture height of 27.5 cm, the insulation has been replaced with water, and the water density between the inner circular tube and outer square tube is 0.5 g/cm^3. This case is below the USL of 0.9209. Note that the most reactive HAC array case is less reactive than the most reactive NCT array case (Case HC16) because the NCT array uses 10 packages, while the HAC array uses only 4 packages.

6.11.6.2 HAC Array Results

Following are the tabulated results for the HAC array cases. The most reactive configurations are listed in boldface.

Table 6.11-10 – HAC Array Results

Case ID	Filename	Fissile Mixture Height (cm)	Water Density Between Tubes (g/cm^3)	Insulation	k_{eff}	σ	k_s (k+2σ)
HD1	HA_HEUP_H15	15.0	1.0	No	0.77954	0.00115	0.78184
HD2	HA_HEUP_H20	20.0	1.0	No	0.80655	0.00123	0.80901
HD3	HA_HEUP_H225	22.5	1.0	No	0.80899	0.00130	0.81159
HD4	**HA_HEUP_H25**	**25.0**	**1.0**	**No**	**0.81254**	**0.00124**	**0.81502**
HD5	HA_HEUP_H275	27.5	1.0	No	0.81232	0.00124	0.81480
HD6	HA_HEUP_H30	30.0	1.0	No	0.80789	0.00116	0.81021
HD7	HA_HEUP_H325	32.5	1.0	No	0.80247	0.00114	0.80475
HD8	HA_HEUP_H35	35.0	1.0	No	0.79682	0.00119	0.79920
HD9	HA_HEUP_H40	40.0	1.0	No	0.78144	0.00114	0.78372
HD10	HA_HEUP_H45	45.0	1.0	No	0.76909	0.00110	0.77129
HD11	HA_HEUP_H25_IW000	25.0	0	Yes	0.79417	0.00131	0.79679
HD12	HA_HEUP_H25_IW025	25.0	0.25	Yes	0.79759	0.00128	0.80015
HD13	HA_HEUP_H25_IW050	25.0	0.50	Yes	0.80131	0.00121	0.80373
HD14	HA_HEUP_H25_IW075	25.0	0.75	Yes	0.80017	0.00121	0.80259
HD15	HA_HEUP_H25_IW100	25.0	1.0	Yes	0.80331	0.00118	0.80567
HD16	HA_HEUP_H25_W000	25.0	0	No	0.79115	0.00126	0.79367
HD17	HA_HEUP_H25_W010	25.0	0.1	No	0.79794	0.00117	0.80028
HD18	HA_HEUP_H25_W020	25.0	0.2	No	0.80884	0.00133	0.81150
HD19	HA_HEUP_H25_W030	25.0	0.3	No	0.81008	0.00123	0.81254
HD20	HA_HEUP_H25_W040	25.0	0.4	No	0.81535	0.00116	0.81767
HD21	HA_HEUP_H25_W050	25.0	0.5	No	0.81666	0.00129	0.81924
HD22	**HA_HEUP_H25_W060**	**25.0**	**0.6**	**No**	**0.81733**	**0.00124**	**0.81981**
HD23	HA_HEUP_H25_W070	25.0	0.7	No	0.81576	0.00130	0.81836
HD24	HA_HEUP_H25_W080	25.0	0.8	No	0.81435	0.00121	0.81677
HD25	HA_HEUP_H25_W090	25.0	0.9	No	0.81266	0.00130	0.81526
HD26	HA_HEUP_H225_W030	22.5	0.3	No	0.80656	0.00134	0.80924
HD27	HA_HEUP_H225_W040	22.5	0.4	No	0.80968	0.00135	0.81238
HD28	HA_HEUP_H225_W050	22.5	0.5	No	0.81297	0.00126	0.81549
HD29	HA_HEUP_H225_W060	22.5	0.6	No	0.81408	0.00113	0.81634
HD30	HA_HEUP_H225_W070	22.5	0.7	No	0.81343	0.00114	0.81571
HD31	HA_HEUP_H225_W080	22.5	0.8	No	0.81282	0.00123	0.81528
HD32	HA_HEUP_H275_W030	27.5	0.3	No	0.81386	0.00118	0.81622
HD33	HA_HEUP_H275_W040	27.5	0.4	No	0.81679	0.00123	0.81925
HD34	**HA_HEUP_H275_W050**	**27.5**	**0.5**	**No**	**0.81993**	**0.00112**	**0.82217**
HD35	HA_HEUP_H275_W060	27.5	0.6	No	0.81757	0.00123	0.82003
HD36	HA_HEUP_H275_W070	27.5	0.7	No	0.81559	0.00114	0.81787
HD37	HA_HEUP_H275_W080	27.5	0.8	No	0.81315	0.00125	0.81565

(continued)

Table 6.11-10 – HAC Array Results (concluded)

Case ID	Filename	Fissile Mixture Height (cm)	Water Density Between Tubes (g/cm^3)	Insulation	k_{eff}	σ	k_s ($k+2\sigma$)
HD38	HA_HEUP_H30_W030	30.0	0.3	No	0.81016	0.00115	0.81246
HD39	HA_HEUP_H30_W040	30.0	0.4	No	0.81437	0.00121	0.81679
HD40	HA_HEUP_H30_W050	30.0	0.5	No	0.81585	0.00121	0.81827
HD41	HA_HEUP_H30_W060	30.0	0.6	No	0.81631	0.00113	0.81857
HD42	HA_HEUP_H30_W070	30.0	0.7	No	0.81257	0.00108	0.81473
HD43	HA_HEUP_H30_W080	30.0	0.8	No	0.81328	0.00113	0.81554

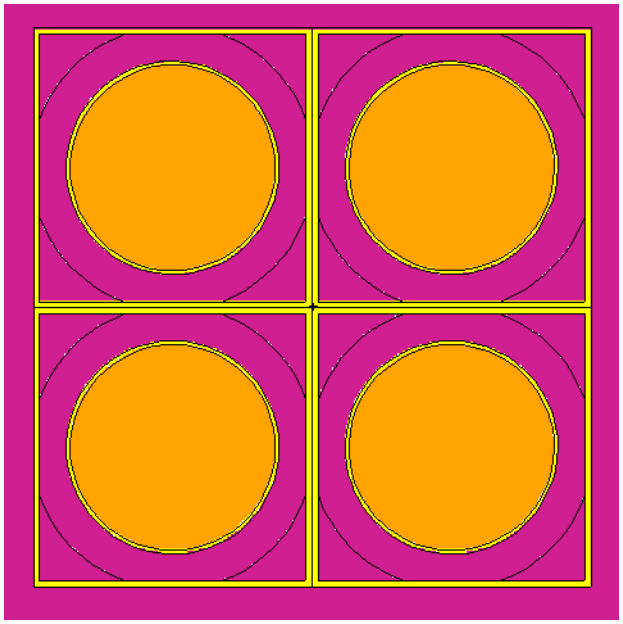

Without insulation

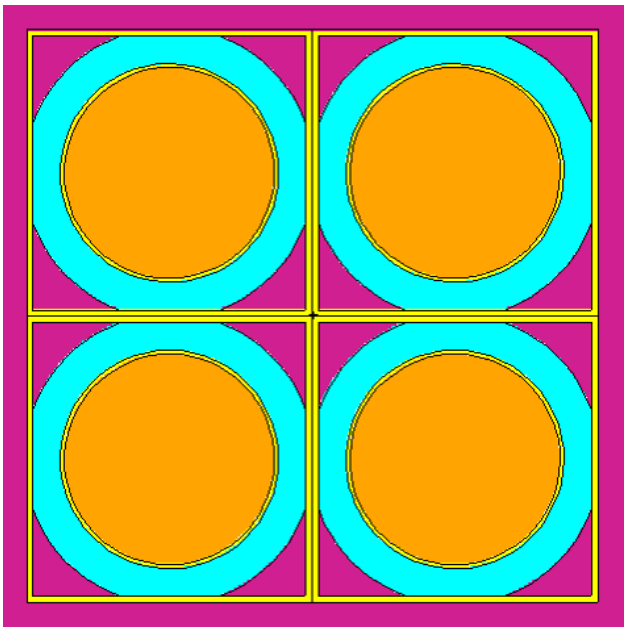

With insulation

Figure 6.11-5 – HAC Array Geometry

6.11.7 Fissile Material Packages for Air Transport

See Section 6.7, which applies to all contents.

6.11.8 Benchmark Evaluations

The Monte Carlo computer program MCNP5 v1.30[12] is utilized for this benchmark analysis. MCNP has been used extensively in criticality evaluations for several decades and is considered a standard in the industry.

The uranium isotopes utilize preliminary ENDF/B-VII cross section data that are considered by Los Alamos National Laboratory to be more accurate than ENDF/B-VI cross sections. ENDF/B-V cross sections are utilized for chromium, nickel, and iron because natural composition ENDF/B-VI cross sections are not available for these elements. The remaining isotopes utilize ENDF/B-VI cross sections. All cross sections utilized are at room temperature. A listing of the cross section libraries used in the ATR FFSC analysis is provided in Table 6.3-4. These cross sections are consistent with the cross sections utilized in the benchmarks.

The ORNL USLSTATS code[13] is used to establish a USL for the analysis. USLSTATS provides a simple means of evaluating and combining the statistical error of the calculation, code biases, and benchmark uncertainties. The USLSTATS calculation uses the combined uncertainties and data to provide a linear trend and an overall uncertainty. Computed multiplication factors, k_{eff}, for the package are deemed to be adequately subcritical if the computed value of k_s is less than or equal to the USL as follows:

$$k_s = k_{eff} + 2\sigma \leq USL$$

The USL includes the combined effects of code bias, uncertainty in the benchmark experiments, uncertainty in the computational evaluation of the benchmark experiments, and an administrative margin. This methodology has accepted precedence in establishing criticality safety limits for transportation packages complying with 10 CFR 71.

6.11.8.1 Applicability of Benchmark Experiments

The critical experiment benchmarks are selected from the *International Handbook of Evaluated Criticality Safety Benchmark Experiments*[14] based upon their similarity to the ATR FFSC and contents. The important selection parameters are high enriched uranium solutions with a thermal spectrum and no strong absorbers such as boron. Ten benchmarks are available that meet this criteria. Because this is a small benchmark set, to supplement these benchmark cases, an additional 45 benchmarks are used for high enriched uranium solutions with boron or cadmium, as well as 42 low enriched (10%) solutions without poisons. The titles for all utilized experiments are listed in Table 6.11-11.

---

[12] MCNP5, "*MCNP – A General Monte Carlo N-Particle Transport Code, Version 5; Volume II: User's Guide*," LA-CP-03-0245, Los Alamos National Laboratory, April, 2003.

[13] USLSTATS, "*USLSTATS: A Utility To Calculate Upper Subcritical Limits For Criticality Safety Applications,"* Version 1.4.2, Oak Ridge National Laboratory, April 23, 2003.

[14] OECD Nuclear Energy Agency, *International Handbook of Evaluated Criticality Safety Benchmark Experiments*, NEA/NSC/DOC(95)03, September, 2006.

6.11.8.2 Bias Determination

The USL is calculated by application of the USLSTATS computer program. USLSTATS receives as input the k_{eff} as calculated by MCNP, the total 1-σ uncertainty (combined benchmark and MCNP uncertainties), and a trending parameter. Two trending parameters have been selected: (1) Energy of the Average neutron Lethargy causing Fission (EALF), and (2) the ratio of the hydrogen to U-235 number density (H/U-235).

The uncertainty value, σ_{total}, assigned to each case is a combination of the benchmark uncertainty for each experiment, σ_{bench}, and the Monte Carlo uncertainty associated with the particular computational evaluation of the case, σ_{MCNP}, or:

$$\sigma_{total} = (\sigma_{bench}^2 + \sigma_{MCNP}^2)^{½}$$

These values are input into the USLSTATS program in addition to the following parameters, which are the values recommended by the USLSTATS user's manual:

- P, proportion of population falling above lower tolerance level = 0.995 (note that this parameter is required input but is not utilized in the calculation of USL Method 1)
- 1-γ, confidence on fit = 0.95
- α, confidence on proportion P = 0.95 (note that this parameter is required input but is not utilized in the calculation of USL Method 1)
- Δk_m, administrative margin used to ensure subcriticality = 0.05.

These data are followed by triplets of trending parameter value, computed k_{eff}, and uncertainty for each case. A confidence band analysis is performed on the data for each trending parameter using USL Method 1. The USL generated for each of the trending parameters utilized is provided in Table 6.11-12. All benchmark data used as input to USLSTATS are reported in Table 6.11-13.

<u>Energy of the Average neutron Lethargy causing Fission (EALF)</u>

The EALF is used as the first trending parameter for the benchmark cases. The EALF comparison provides a means to observe neutron spectral dependencies or trends. USLSTATS is run for all experiments, as well as the subset of experiments that do not contain poisons. The data for the subset of experiments without poisons are plotted in Figure 6.11-6, while the data for all experiments is plotted in Figure 6.11-7. Over the range of applicability, the minimum USL is 0.9344 for the subset of benchmarks that do not contain poisons, and is 0.9309 when all benchmarks are considered. In both cases the USL is trending downward for increasing EALF. Note that for the benchmarks that do not contain poison, the data tests not normal by a small margin (chi = 12.4231, upper bound = 9.49). This behavior is judged to be acceptable, both because the deviation from normal is not large, and the USL generated from this data is bounded by the USL with poison.

EALF for all ATR FFSC small quantity payload cases falls within the range of applicability. The EALF is 4.98E-08 MeV for the most reactive case (Case HC16).

<u>H/U-235 Atom Ratio</u>

The H/U-235 atom ratio is used as the second trending parameter for the benchmark cases. The data for the subset of experiments without poisons are plotted in Figure 6.11-8, while the data for

all experiments is plotted in Figure 6.11-9. Over the range of applicability, the minimum USL is 0.9401 for the subset of benchmarks that do not contain poisons, and is 0.9359 when all benchmarks are considered. The USL is relatively constant over the range of applicability when no poisons are considered, and is trending downward for decreasing H/U-235 when all benchmarks are considered. Note that for the benchmarks that do not contain poison, the data tests not normal by a small margin (chi = 12.4231, upper bound = 9.49). This behavior is judged to be acceptable, both because the deviation from normal is not large, and the USL generated from this data is bounded by the USL with poison.

The H/U-235 atom ratio for all ATR FFSC small quantity payload cases falls within the range of applicability. The H/U-235 atom ratio is 363 for the most reactive case (Case HC16).

Recommended USL

For the H/U-235 trending parameter, the minimum USL is 0.9359, while for the EALF trending parameter, the USL is 0.9309. Therefore, a USL of 0.9309 could be justified. However, a benchmark analysis was also performed for high-enriched plate fuel for the original ATR FFSC criticality analysis (see Section 6.8, *Benchmark Evaluations*). In that section, a USL of 0.9209 is justified. Therefore, a USL of 0.9209 is conservatively selected as the USL for this analysis for consistency.

Table 6.11-11 – Benchmark Experiments Utilized

Series	Title
HEU-SOL-THERM-001	Minimally Reflected Cylinders of Highly Enriched Solutions of Uranyl Nitrate
HEU-SOL-THERM-027	Uranium (89% ^{235}U) Nitrate Solution with Central Boron Carbide or Cadmium Absorber Rod
HEU-SOL-THERM-028	Uranium (89% ^{235}U) Nitrate Solutions with Central Boron Carbide Absorber Rod
HEU-SOL-THERM-029	Uranium (89% ^{235}U) Nitrate Solution with Cluster of Seven Boron Carbide Absorber Rods
HEU-SOL-THERM-030	Uranium (89% ^{235}U) Nitrate Solution with Cluster of Several Boron Carbide Absorber Rods
HEU-SOL-THERM-036	Square-Pitched Lattices of Boron Carbide Absorber Rods In Uranium (89% ^{235}U) Nitrate Solutions
LEU-SOL-THERM-003	Full and Truncated Bare Spheres of 10% Enriched Uranyl Nitrate Water Solutions
LEU-SOL-THERM-004	Stacy: Water-Reflected 10%-Enriched Uranyl Nitrate Solution in a 60-cm-Diameter Cylindrical Tank
LEU-SOL-THERM-007	Stacy: Unreflected 10%-Enriched Uranyl Nitrate Solution in a 60-cm-Diameter Cylindrical Tank
LEU-SOL-THERM-016	Stacy: 28-cm-Thick Slabs of 10%-Enriched Uranyl Nitrate Solutions, Water-Reflected
LEU-SOL-THERM-017	Stacy: 28-cm-Thick Slabs of 10%-Enriched Uranyl Nitrate Solutions, Unreflected
LEU-SOL-THERM-020	Stacy: 80-cm-Diameter Cylindrical Tank of 10%-Enriched Uranyl Nitrate Solutions, Water-Reflected
LEU-SOL-THERM-021	Stacy: 80-cm-Diameter Cylindrical Tank of 10%-Enriched Uranyl Nitrate Solutions, Unreflected

Table 6.11-12 – USL Results

Trending Parameter (X)	Experiment Set	Minimum USL Over Range of Applicability	Range of Applicability
EALF (MeV)	No poison (1-10, 56-97)	0.9344	3.43E-08 ≤ x ≤ 2.95E-07
EALF (MeV)	All	0.9309	3.43E-08 ≤ x ≤ 2.95E-07
H/U-235	No poison (1-10, 56-97)	0.9401	68.2 ≤ x ≤ 1437.5
H/U-235	All	0.9359	68.2 ≤ x ≤ 1437.5

Table 6.11-13 – Benchmark Experiment Data

No	Case	k	σ_{mcnp}	σ_{bench}	σ_{total}	EALF (MeV)	H/U-235
1	HST001_C01	0.99661	0.00100	0.0060	0.0061	8.17E-08	181.8
2	HST001_C02	0.99185	0.00096	0.0072	0.0073	2.76E-07	70.6
3	HST001_C03	0.99921	0.00090	0.0035	0.0036	8.00E-08	185.7
4	HST001_C04	0.99586	0.00094	0.0053	0.0054	2.93E-07	68.2
5	HST001_C05	0.99785	0.00079	0.0049	0.0050	4.28E-08	499.4
6	HST001_C06	1.00159	0.00081	0.0046	0.0047	4.45E-08	458.8
7	HST001_C07	0.99693	0.00092	0.0040	0.0041	7.70E-08	193.3
8	HST001_C08	0.99696	0.00094	0.0038	0.0039	8.18E-08	181.8
9	HST001_C09	0.99087	0.00101	0.0054	0.0055	2.95E-07	68.2
10	HST001_C10	0.99005	0.00086	0.0054	0.0055	4.61E-08	427.4
11	HST027_C01	0.99609	0.00093	0.0046	0.0047	7.42E-08	203.6
12	HST027_C02	0.99522	0.00090	0.0043	0.0044	7.49E-08	203.6
13	HST027_C03	0.99626	0.00089	0.0037	0.0038	7.52E-08	203.6
14	HST027_C04	0.99780	0.00093	0.0037	0.0038	7.53E-08	203.6
15	HST027_C05	0.99563	0.00086	0.0044	0.0045	7.58E-08	203.6
16	HST027_C06	0.99028	0.00095	0.0043	0.0044	7.50E-08	203.6
17	HST027_C07	0.99604	0.00094	0.0038	0.0039	7.50E-08	203.6
18	HST027_C08	0.99772	0.00091	0.0035	0.0036	7.48E-08	203.6
19	HST027_C09	0.99517	0.00090	0.0039	0.0040	7.49E-08	203.6
20	HST028_C01	0.99350	0.00080	0.0023	0.0024	4.72E-08	374.6
21	HST028_C02	0.99332	0.00078	0.0034	0.0035	4.77E-08	374.6
22	HST028_C03	0.99596	0.00080	0.0026	0.0027	4.71E-08	374.6
23	HST028_C04	0.99814	0.00078	0.0028	0.0029	4.76E-08	374.6
24	HST028_C05	0.99070	0.00077	0.0031	0.0032	4.74E-08	374.6
25	HST028_C06	0.99492	0.00080	0.0023	0.0024	4.77E-08	374.6
26	HST028_C07	0.99497	0.00082	0.0038	0.0039	4.77E-08	374.6
27	HST028_C08	0.99433	0.00083	0.0027	0.0028	4.81E-08	374.6
28	HST028_C09	0.99179	0.00088	0.0049	0.0050	1.45E-07	91.5
29	HST028_C10	0.99032	0.00086	0.0053	0.0054	1.46E-07	91.5
30	HST028_C11	0.99179	0.00090	0.0051	0.0052	1.47E-07	91.5
31	HST028_C12	0.99009	0.00083	0.0046	0.0047	1.49E-07	91.5
32	HST028_C13	0.99102	0.00089	0.0058	0.0059	1.49E-07	91.5
33	HST028_C14	0.99180	0.00086	0.0046	0.0047	1.51E-07	91.5
34	HST028_C15	1.00006	0.00092	0.0064	0.0065	1.50E-07	91.5
35	HST028_C16	0.99561	0.00084	0.0052	0.0053	1.52E-07	91.5
36	HST028_C17	0.99144	0.00087	0.0066	0.0067	1.53E-07	91.5
37	HST028_C18	0.99322	0.00085	0.0060	0.0061	1.54E-07	91.5
38	HST029_C01	0.99468	0.00088	0.0066	0.0067	1.58E-07	91.5

(continued)

Table 6.11-13 – Benchmark Experiment Data

No	Case	k	σ_{mcnp}	σ_{bench}	σ_{total}	EALF (MeV)	H/U-235
39	HST029_C02	0.99722	0.00085	0.0058	0.0059	1.58E-07	91.5
40	HST029_C03	0.99112	0.00090	0.0068	0.0069	1.59E-07	91.5
41	HST029_C04	0.99158	0.00087	0.0074	0.0075	1.67E-07	91.5
42	HST029_C05	0.99602	0.00085	0.0067	0.0068	1.69E-07	91.5
43	HST029_C06	0.99484	0.00092	0.0065	0.0066	1.69E-07	91.5
44	HST029_C07	0.99381	0.00089	0.0063	0.0064	1.68E-07	91.5
45	HST030_C01	0.99405	0.00078	0.0039	0.0040	4.78E-08	374.6
46	HST030_C02	0.99786	0.00079	0.0032	0.0033	4.85E-08	374.6
47	HST030_C03	0.99465	0.00075	0.0031	0.0032	4.88E-08	374.6
48	HST030_C04	0.99533	0.00092	0.0064	0.0065	1.58E-07	91.1
49	HST030_C05	0.99334	0.00085	0.0058	0.0059	1.60E-07	91.1
50	HST030_C06	0.99430	0.00084	0.0059	0.0060	1.61E-07	91.1
51	HST030_C07	0.99458	0.00082	0.0064	0.0065	1.65E-07	91.1
52	HST036_C01	0.99355	0.00086	0.0045	0.0046	5.58E-08	302.5
53	HST036_C02	0.99779	0.00084	0.0039	0.0040	5.79E-08	302.5
54	HST036_C03	0.99834	0.00084	0.0044	0.0045	6.05E-08	302.5
55	HST036_C04	0.99971	0.00078	0.0062	0.0062	6.31E-08	302.5
56	LST003_C01	0.99621	0.00040	0.0039	0.0039	4.10E-08	770.3
57	LST003_C02	0.99383	0.00038	0.0042	0.0042	3.91E-08	877.6
58	LST003_C03	0.99926	0.00038	0.0042	0.0042	3.89E-08	897.0
59	LST003_C04	0.99292	0.00036	0.0042	0.0042	3.87E-08	913.2
60	LST003_C05	0.99641	0.00032	0.0048	0.0048	3.59E-08	1173.4
61	LST003_C06	0.99695	0.00030	0.0049	0.0049	3.57E-08	1213.1
62	LST003_C07	0.99535	0.00030	0.0049	0.0049	3.55E-08	1239.8
63	LST003_C08	0.99894	0.00027	0.0052	0.0052	3.45E-08	1411.6
64	LST003_C09	0.99697	0.00025	0.0052	0.0052	3.43E-08	1437.5
65	LST004_C01	1.00136	0.00067	0.0008	0.0010	4.17E-08	719.0
66	LST004_C29	1.00057	0.00065	0.0009	0.0011	4.08E-08	771.3
67	LST004_C33	0.99847	0.00059	0.0009	0.0011	3.96E-08	842.2
68	LST004_C34	1.00148	0.00061	0.0010	0.0012	3.88E-08	895.8
69	LST004_C46	1.00196	0.00052	0.0010	0.0011	3.82E-08	941.7
70	LST004_C51	0.99877	0.00056	0.0011	0.0012	3.78E-08	982.5
71	LST004_C54	1.00160	0.00052	0.0011	0.0012	3.73E-08	1017.5
72	LST007_C01	0.99414	0.00045	0.0009	0.0010	4.25E-08	709.2
73	LST007_C02	0.99734	0.00044	0.0009	0.0010	4.11E-08	770.0
74	LST007_C03	0.99472	0.00041	0.0010	0.0011	3.99E-08	842.2
75	LST007_C04	0.99791	0.00038	0.0011	0.0012	3.91E-08	896.0
76	LST007_C05	0.99628	0.00038	0.0011	0.0012	3.85E-08	942.2
77	LST016_C105	1.00345	0.00047	0.0013	0.0014	5.14E-08	468.7
78	LST016_C113	1.00438	0.00049	0.0013	0.0014	4.89E-08	514.2
79	LST016_C125	1.00368	0.00045	0.0014	0.0015	4.51E-08	608.4
80	LST016_C129	1.00225	0.00041	0.0014	0.0015	4.39E-08	650.2

(continued)

Table 6.11-13 – Benchmark Experiment Data (concluded)

No	Case	k	σ_{mcnp}	σ_{bench}	σ_{total}	EALF (MeV)	H/U-235
81	LST016_C131	1.00227	0.00044	0.0014	0.0015	4.26E-08	699.1
82	LST016_C140	1.00142	0.00041	0.0015	0.0016	4.17E-08	738.9
83	LST016_C196	1.00218	0.00041	0.0015	0.0016	4.11E-08	771.8
84	LST017_C104	1.00273	0.00050	0.0013	0.0014	5.15E-08	468.7
85	LST017_C122	1.00223	0.00049	0.0013	0.0014	4.94E-08	510.8
86	LST017_C123	1.00095	0.00045	0.0014	0.0015	4.52E-08	610.9
87	LST017_C126	1.00158	0.00044	0.0014	0.0015	4.39E-08	650.1
88	LST017_C130	1.00164	0.00046	0.0015	0.0016	4.27E-08	699.2
89	LST017_C147	1.00152	0.00042	0.0015	0.0016	4.20E-08	729.0
90	LST020_C01	0.99867	0.00038	0.0010	0.0011	3.78E-08	971.0
91	LST020_C02	0.99796	0.00034	0.0010	0.0011	3.69E-08	1053.9
92	LST020_C03	0.99807	0.00033	0.0012	0.0012	3.60E-08	1168.0
93	LST020_C04	0.99839	0.00031	0.0012	0.0012	3.54E-08	1239.3
94	LST021_C01	0.99672	0.00038	0.0009	0.0010	3.79E-08	971.0
95	LST021_C02	0.99767	0.00035	0.0010	0.0011	3.71E-08	1052.7
96	LST021_C03	0.99630	0.00034	0.0011	0.0012	3.61E-08	1168.0
97	LST021_C04	0.99786	0.00032	0.0012	0.0012	3.57E-08	1238.9

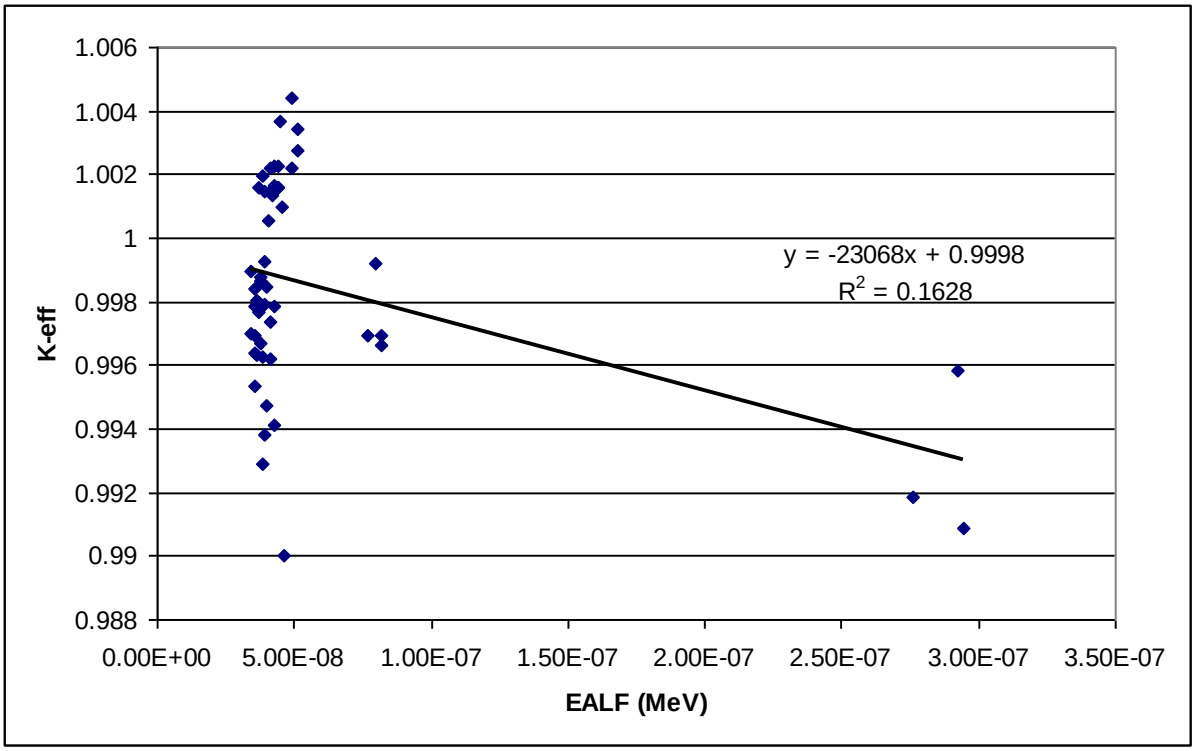

Figure 6.11-6 – Benchmark Data Trend for EALF (no poisons)

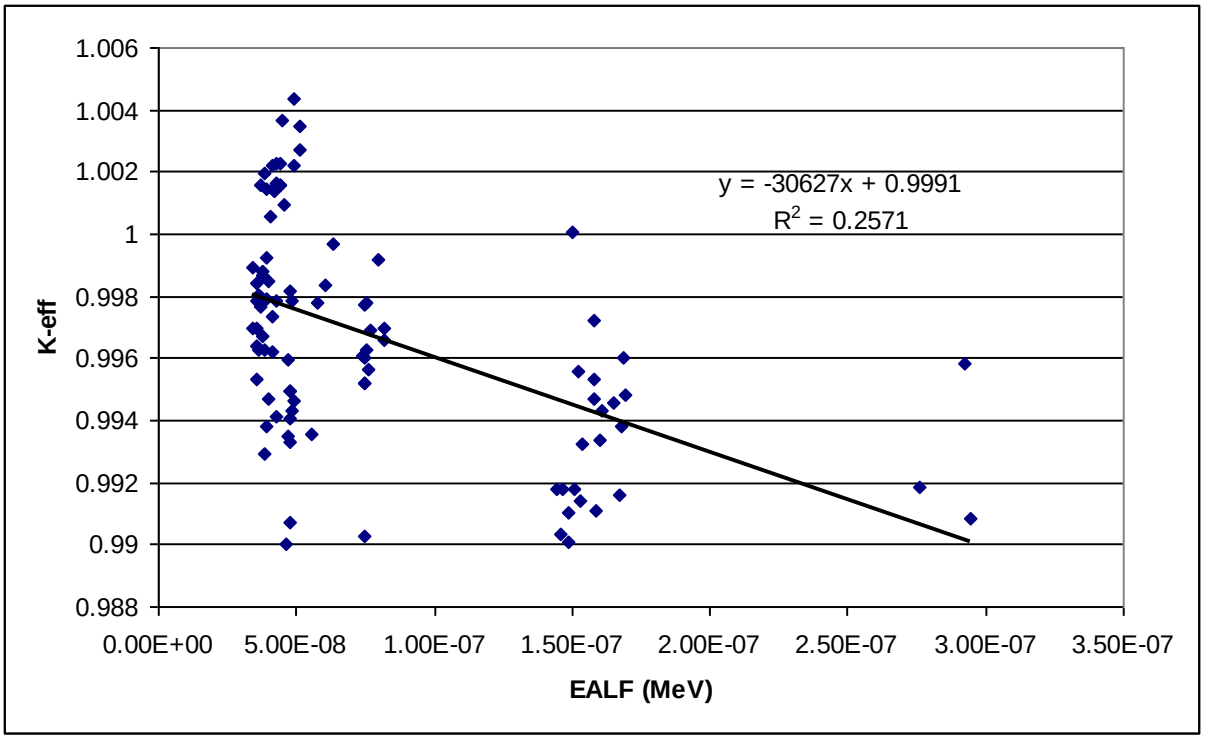

Figure 6.11-7 – Benchmark Data Trend for EALF (all)

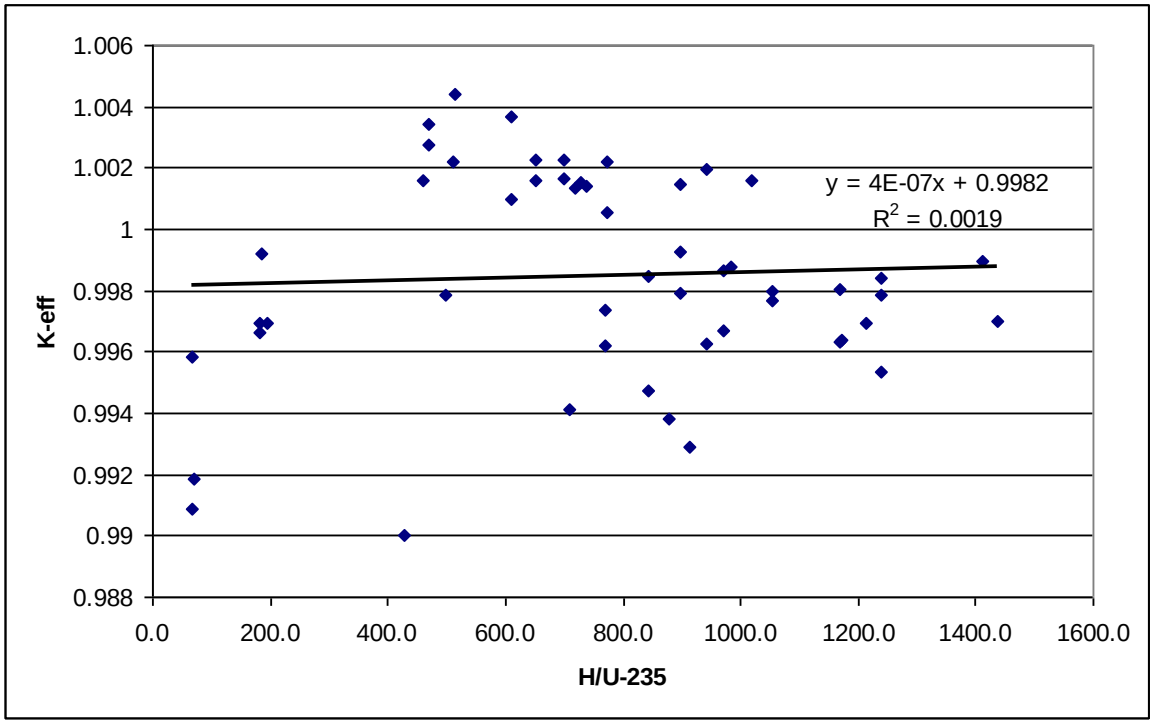

Figure 6.11-8 – Benchmark Data Trend for H/U-235 (no poisons)

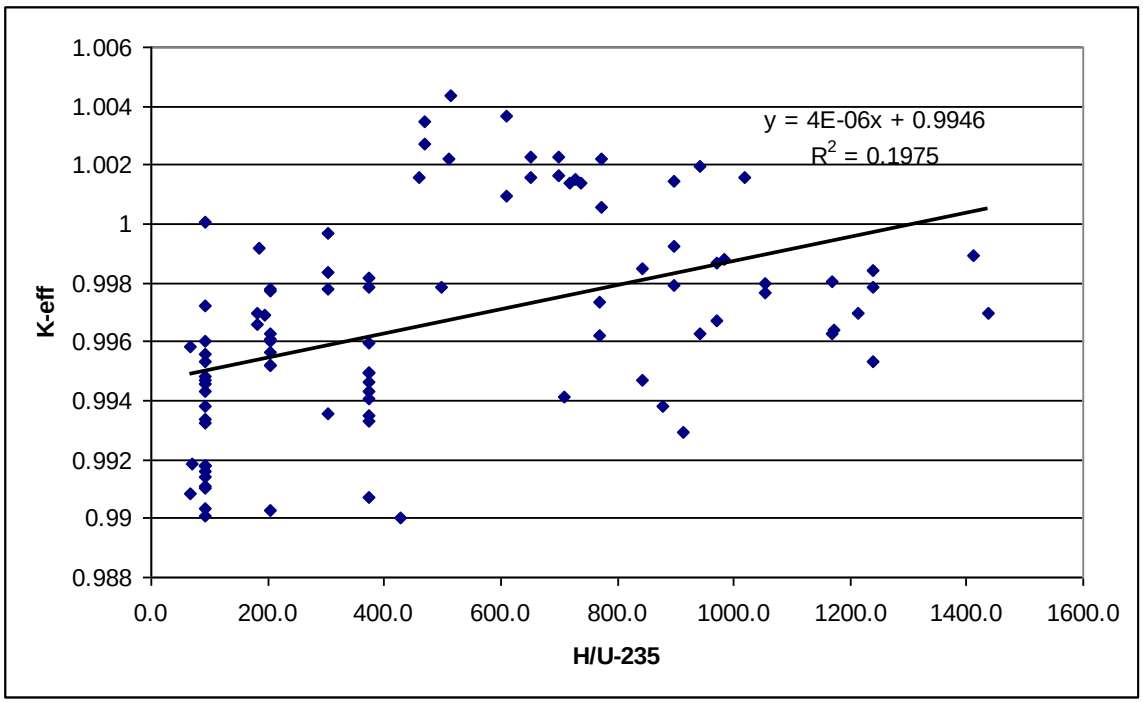

Figure 6.11-9 – Benchmark Data Trend for H/U-235 (all)

6.11.9 Sample Input Files

A sample input file (NA_HEUP_H325) is provided for the most reactive case (Case HC16).

```
ATR Package
999     0      -320:321:-322:323:-324:325                imp:n=0
900     0      310 -311 312 -313 24 -25     fill=3       imp:n=1
901     2 -1.0 (311:-310:313:-312:-24:25) 320 -321 322 -323 324 -325  imp:n=1
c
c       Universe 20: Fuel mixture with pipe
c
200     10 1.0043E-01 -26 -200                 u=20 imp:n=1 $ fuel mix
201     2 -1.0         26 -200                 u=20 imp:n=1 $ water above
fuel
202     4 -7.94     200 -201                   u=20 imp:n=1 $ pipe
203     6 -0.096    201 -203 250 -251 252 -253 u=20 imp:n=1 $ insulation
204     0           203 250 -251 252 -253      u=20 imp:n=1 $ insulation to
tube
205     4 -7.94     -250:251:-252:253          u=20 imp:n=1 $ tube to inf
c
c       Universe 21: Water
c
210     2 -1.0      -204                       u=21 imp:n=1
c
c       Universe 3: Array of Packages
c
300   0    -300 301 -302 303 imp:n=1 u=3 lat=1 fill=-1:1 -1:2 0:0
             20 20 20
             20 20 20
             20 20 20
             21 20 21

24      pz  0             $ bottom of fuel
25      pz  121.92        $ top of cavity (48")
26      pz  32.5          $ top of fuel mix
c
200      cz 7.3838  $ IR pipe
201      cz 7.6581  $ OR pipe
203      cz 10.1981 $ 1" insulation
204      pz 1000    $ dummy
c
250      px  -9.6032 $ square tube
251      px   9.6032
252      py  -9.6032
253      py   9.6032
c
300      px  10.033 $ lattice surfaces/sq. tube
301      px -10.033
302      py  10.033
303      py -10.033
310      px -30.099 $ 3x4 bounds
311      px  30.099
312      py -30.099
313      py  50.165
320      px -60.579 $ outer bounds
321      px  60.579
```

```
322      py -60.579
323      py  80.645
324      pz -30.48
325      pz  152.4

m2      1001.62c  2          $ water
        8016.62c  1
mt2     lwtr.60t
m3      13027.62c 1          $ Al
m4      6000.66c   -0.08     $ SS-304
        14000.60c  -1.0
        15031.66c  -0.045
        24000.50c  -19.0
        25055.62c  -2.0
        26000.55c  -68.375
        28000.50c  -9.5
m5      1001.62c  -0.056920  $ neoprene
        6000.66c  -0.542646
c       17000.66c -0.400434
m6      13027.62c  -26.5     $ insulation material
        14000.60c  -23.4
        8016.62c   -50.2
m10    92234.69c 1.1802E-06 $ HEU fuel H=32.5 M235=400.0 100g Poly
       92235.69c 1.8410E-04
       92236.69c 6.8258E-07
       92238.69c 9.7657E-06
        1001.62c 6.6822E-02
        6000.66c 7.7125E-04
        8016.62c 3.2640E-02
c          Total 1.0043E-01
mt10    lwtr.60t
c
mode   n
kcode  2500 1.0 50 250
sdef    x=d1 y=d2 z=d3
si1     -30 30
sp1     0 1
si2     -30 50
sp2     0 1
si3     0 32.5
sp3     0 1
```

6.12 Appendix D: Criticality Analysis for the U-Mo Demonstration Element

This analysis and any associated results have been removed as the ATR U-Mo demonstration element is no longer a possible payload.

6.13 Appendix E: Criticality Analysis for the Cobra Fuel Element

The ATR FFSC may be utilized to transport a Cobra fuel element. The Cobra fuel element is a plate-type fuel similar to the ATR fuel element analyzed in this chapter, although the fuel geometry is different. The following analyses demonstrate that the ATR FFSC with a Cobra fuel element complies with the requirements of 10 CFR §71.55 and §71.59. Based on a 5x5 array of damaged packages, the Criticality Safety Index (CSI), per 10 CFR §71.59, is 4.0.

The original analysis documented in this appendix is based on a maximum Cobra LEU fuel element U-235 mass of 435.8 g. Some Cobra LEU fuel elements developed after the original analysis will have a maximum U-235 mass of 450 g. This increased U-235 mass is analyzed in Section 6.13.11, *Analysis of Increased U-235 Mass in Cobra LEU Fuel*.

6.13.1 Description of Criticality Design

6.13.1.1 Design Features

No special design features are required to maintain criticality safety. No poisons are utilized in the package. The separation provided by the packaging (outer flat-to-flat dimension of 7.9-in), along with the limit on the number of packages per shipment, is sufficient to maintain criticality safety.

6.13.1.2 Summary Table of Criticality Evaluation

The upper subcritical limit (USL) for ensuring that the ATR FFSC (single package or package array) is acceptably subcritical, as determined in Section 6.13.9, *Benchmark Evaluations*, is:

$$USL = 0.9209$$

The package is considered to be acceptably subcritical if the computed k_{safe} (k_s), which is defined as $k_{effective}$ (k_{eff}) plus twice the statistical uncertainty (σ), is less than or equal to the USL, or:

$$k_s = k_{eff} + 2\sigma \leq USL$$

The USL is determined on the basis of a benchmark analysis and incorporates the combined effects of code computational bias, the uncertainty in the bias based on both benchmark-model and computational uncertainties, and an administrative margin. The results of the benchmark analysis indicate that the USL is adequate to ensure subcriticality of the package.

The packaging design is shown to meet the requirements of 10 CFR 71.55(b)(d)(e). Moderation by water in the most reactive credible extent is utilized in both the normal conditions of transport (NCT) and hypothetical accident conditions of transport (HAC) analyses. In the single package NCT models, full-density water fills the accessible cavity, while in the single package HAC models, full-density water fills all cavities. In all single package and array models, 12-in of water reflection is utilized.

A 9x9x1 array of 81 packages is utilized for the NCT array, while a 5x5x1 array of 25 packages is utilized for the HAC array. In the NCT and HAC array cases, partial moderation is considered to maximize array interaction effects.

The maximum results of the criticality calculations are summarized in Table 6.13-1. The maximum calculated k_s is 0.7643, which occurs for the optimally moderated HAC array case. In

the HAC cases, pitch expansion is postulated as a bounding damaged fuel element condition, and the Cobra fuel handing enclosure is conservatively assumed to fail. The reactivity of the worst case is significantly below the USL of 0.9209.

Table 6.13-1 – Summary of Criticality Evaluation, Cobra Element

Normal Conditions of Transport (NCT)	
Case	k_s
71.55(b)(d): Single Unit Maximum	0.4032
71.55(d), 71.59: 9x9x1 Array Maximum	0.7389
Hypothetical Accident Conditions (HAC)	
Case	k_s
71.55(e): Single Unit Maximum	0.4996
71.55(e), 71.59: 5x5x1 Array Maximum	0.7643
USL = 0.9209	

6.13.1.3 Criticality Safety Index

The criticality safety index is defined in 10 CFR 71.59 as 50/N, where 5N packages are used in the NCT array configuration, and 2N packages are used in the HAC array configuration. A 5x5 array (2N = 25, or N = 12.5) is utilized for the HAC array calculations, while a 9x9 array (5N = 81, or N = 16.2) is utilized for the NCT array calculations. Therefore, the criticality safety index is computed with the smaller value of N, or 50/N = 50/12.5 = 4.0. With a CSI = 4.0, a maximum of 25 packages are allowed per exclusive use shipment, or a maximum of 12 packages per non-exclusive use shipment.

6.13.2 Fissile Material Contents

The fissile material content is either a single high-enriched uranium (HEU) or low-enriched uranium (LEU) Cobra fuel element. The package may transport only a single fuel element per package. The HEU fuel element has a U-235 enrichment < 94% and the fuel meat is uranium metal mixed with aluminum. The LEU fuel element has a U-235 enrichment < 20% and the fuel meat is U_3Si_2 mixed with aluminum. The HEU and LEU Cobra fuel elements are geometrically identical, differing only in the fuel meat composition and enrichment.

A Cobra fuel element consists of six concentric rings of fuel plates. Each ring is comprised of three curved plates and are joined by aluminum spacers, see Figure 6.13-1. The plates fit into slots in the spacers. The fuel plate cladding is aluminum.

The as-modeled isotopic distributions of HEU and LEU fuel are listed in Table 6.13-2. The U-235 enrichment for HEU is set to a bounding value of 94%, and the U-235 enrichment for LEU is set to a bounding value of 20%.

Because the fuel element is comprised of concentric plates, the inner plates are smaller and hence have a lower U-235 loading than the outer plates. The U-235 loading in each plate is provided in Table 6.13-3. Based on the stated tolerances on U-235 per plate and three plates per ring, the total U-235 loading per fuel element is 402.3 ± 10.8 g U-235 for the HEU fuel element and 427.8

± 10.8 g U-235 for the LEU fuel element. In the MCNP models, the U-235 loading per plate is maximized, resulting in a conservative U-235 loading of 402.3 + 10.8 = 413.1 g U-235 for the HEU fuel element and 427.8 + 10.8 = 438.6 g U-235 for the LEU fuel element. The actual U-235 tolerance on the overall fuel element is ± 8.0 g rather than ± 10.8 g. Therefore, the as-modeled U-235 loading per fuel element is conservatively 10.8 – 8.0 = 2.8 g larger than the maximum allowed values.

The fuel element may contain burnable absorbers, such as gadolinium, samarium, or boron. All burnable absorbers are conservatively neglected in this analysis.

Each plate has a nominal fuel meat thickness of 0.063 cm and a nominal cladding thickness of 0.035 cm, or an overall plate thickness of 0.063 + 2*0.035 = 0.133 cm. Tolerances on the cladding and meat thickness are not defined, but the overall tolerance on the plate thickness is 0.005 cm. The active fuel length of each plate ranges from a minimum of 74.95 cm to a maximum of 77.45 cm. The inner radius and maximum fuel meat width for each plate are provided in Table 6.13-4.

To properly match the target U-235 loading in each plate, the density of the fuel meat is explicitly computed for each plate. The first step is to compute the fuel meat volume of each plate, which is the thickness*width*length. An example fuel meat volume calculation is provided in Table 6.13-5 for nominal active fuel length, nominal fuel meat thickness, and maximum width.

For HEU fuel, the density and composition of the fuel meat may be computed for each plate using the following method, which is summarized in Table 6.13-6. The U-235 density (g/cm^3) for each plate is computed based on the U-235 mass and fuel meat volume in each plate. The U-235 density varies slightly between plates to preserve the target U-235 loading. The uranium density (g/cm^3) is computed as the U-235 density/enrichment, where the enrichment is 0.94. The U-238 density (g/cm^3) is then the uranium density minus U-235 density.

The total mixture density includes both uranium and aluminum. It is shown in the original ATR criticality analysis (see Table 6.2-2) that for high-enriched plate-type fuels, the total mixture density is approximately related to the U-235 density as 0.8733*(U-235 density) + 2.5357 g/cm^3. This equation is applied to the average U-235 density in the Cobra fuel element, and then the ratio of the total density to the U-235 density is treated as a constant. Using the data in Table 6.13-6, the U-235 average density is 0.9391 g/cm^3, the corresponding mixture density is 3.3558 g/cm^3, and the ratio of these two values is 3.3558/0.9391 = 3.5734. The total mixture density of each plate is then estimated as 3.5734*(U-235 density), and the aluminum density (g/cm^3) is then the total density minus uranium density.

While the component densities differ for each plate, the weight percent of each component in the fuel mixture is a constant. For the example described above, the composition is summarized in Table 6.13-7.

For LEU fuel, the methodology is similar, although the fuel meat is a mixture of approximately 80 wt.% U_3Si_2 and 20 wt.% aluminum. The computation of the fuel meat density of each plate for a nominal active fuel length, nominal fuel meat thickness, and maximum width is provided in Table 6.13-8. The corresponding fuel meat composition, which is the same for each plate, is provided in Table 6.13-9.

Table 6.13-2 – Modeled Uranium Isotopics

Isotope	HEU (Wt. %)	LEU (Wt. %)
U-235	94.0	20.0
U-238	6.0	80.0

Table 6.13-3 – U-235 Loading

Plate	HEU, U-235 (g)	LEU, U-235 (g)
1 (inner)	11.8 ± 0.5	12.4 ± 0.5
2	16.0 ± 0.5	17.0 ± 0.5
3	20.3 ± 0.6	21.4 ± 0.6
4	24.4 ± 0.6	26.2 ± 0.6
5	28.9 ± 0.7	30.4 ± 0.7
6 (outer)	32.7 ± 0.7	35.2 ± 0.7
Total	134.1 ± 3.6	142.6 ± 3.6
Fuel Element (Total x 3)	402.3 ± 10.8	427.8 ± 10.8

Table 6.13-4 – Plate Dimensions

Plate	Inner Radius (cm)	Max Meat Width (cm)
1 (inner)	1.598	2.800
2	2.030	3.705
3	2.463	4.615
4	2.896	5.525
5	3.328	6.435
6 (outer)	3.761	7.340

Table 6.13-5 – Fuel Meat Volume Example

Plate	Nominal Fuel Meat Thickness (cm)	Nominal Active Length (cm)	Max Fuel Meat Width (cm)	Fuel Meat Volume (cm^3)
1 (inner)	0.063	76.2	2.800	13.442
2	0.063	76.2	3.705	17.786
3	0.063	76.2	4.615	22.155
4	0.063	76.2	5.525	26.523
5	0.063	76.2	6.435	30.892
6 (outer)	0.063	76.2	7.340	35.236

Table 6.13-6 – HEU Fuel Meat Densities Example

	A	B	C = A/B	D	E = C/D	F = E - C	G	H = G - E
Plate	**U-235 (g)**	**Fuel Meat Volume (cm^3)**	**U-235 Density (g/cm^3)**	**Enrich-ment (U-235/U)**	**Uranium Density (g/cm^3)**	**U-238 Density (g/cm^3)**	**Total Density (g/cm^3)**	**Aluminum Density (g/cm^3)**
1 (inner)	12.3	13.442	0.9151	0.94	0.9735	0.0584	3.2699②	2.2964
2	16.5	17.786	0.9277	0.94	0.9869	0.0592	3.3150②	2.3281
3	20.9	22.155	0.9434	0.94	1.0036	0.0602	3.3710②	2.3674
4	25.0	26.523	0.9426	0.94	1.0027	0.0602	3.3681②	2.3654
5	29.6	30.892	0.9582	0.94	1.0193	0.0612	3.4239②	2.4046
6 (outer)	33.4	35.236	0.9479	0.94	1.0084	0.0605	3.3871②	2.3788
Average	-	-	0.9391	-	-	-	3.3558①	-

①Computed based on the average U-235 density as 0.8733*0.9391 + 2.5357 = 3.3558 g/cm^3.
②Computed as G = C*R, where C is the U-235 density and R is the ratio of the total density and the U-235 average density: R = 3.3558/0.9391 = 3.5734.

Table 6.13-7 – HEU Fuel Meat Composition Example

Isotope	**Composition (Wt.%)**
U-235	27.9850
U-238	1.7863
Al	70.2290

Table 6.13-8 – LEU Fuel Meat Densities

	A	B	C = A/B	D	E = C/D	F = E - C	G = E/0.9269①	H = G - E
Plate	**U-235 (g)**	**Meat Volume (cm^3)**	**U-235 Density (g/cm^3)**	**Enrich-ment (U-235/U)**	**Uranium Density (g/cm^3)**	**U-238 Density (g/cm^3)**	**U_3Si_2 Density (g/cm^3)**	**Silicon Density (g/cm^3)**
1 (inner)	12.9	13.442	0.9597	0.2	4.7985	3.8388	5.1769	0.3784
2	17.5	17.786	0.9839	0.2	4.9195	3.9356	5.3075	0.3879
3	22.0	22.155	0.9930	0.2	4.9651	3.9721	5.3566	0.3915
4	26.8	26.523	1.0104	0.2	5.0522	4.0417	5.4505	0.3984
5	31.1	30.892	1.0067	0.2	5.0337	4.0270	5.4306	0.3969
6 (outer)	35.9	35.236	1.0188	0.2	5.0942	4.0753	5.4959	0.4017

	I	J = G/I	K = J - G
Plate	**U_3Si_2 Weight Fraction in Total Density**	**Total Density (g/cm^3)**	**Aluminum Density (g/cm^3)**
1 (inner)	0.8	6.4711	1.2942
2	0.8	6.6343	1.3269
3	0.8	6.6957	1.3391
4	0.8	6.8132	1.3626
5	0.8	6.7883	1.3577
6 (outer)	0.8	6.8698	1.3740

①0.9269 is the weight fraction of uranium in U_3Si_2.

Table 6.13-9 – LEU Fuel Meat Composition

Isotope	Composition (Wt.%)
U-235	14.831
U-238	59.322
Al	20.000
Si	5.8473

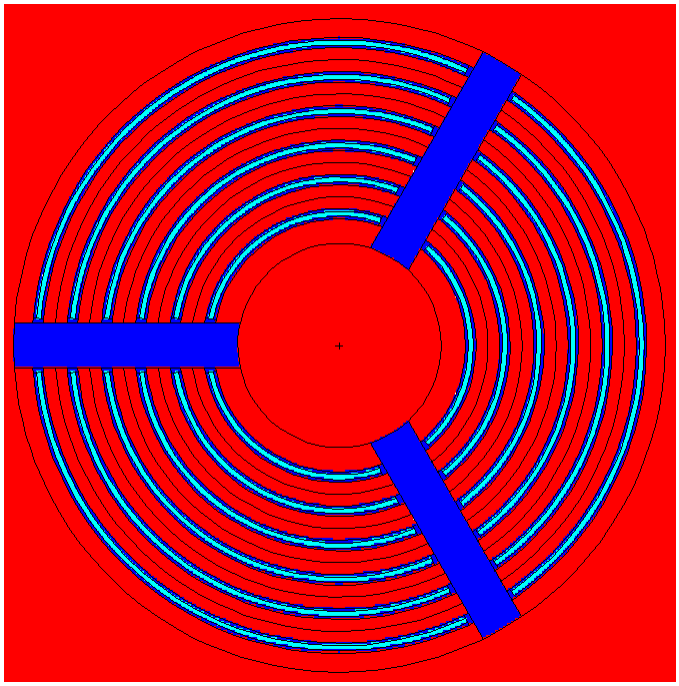

Figure 6.13-1 – Cobra Geometry

6.13.3 General Considerations

6.13.3.1 Model Configuration

The model configuration is relatively simple. Most packaging details are conservatively ignored, particularly at the ends. Because the package is long and narrow, array configurations will stack only in the lateral directions (e.g., 5x5x1). Therefore, the end details, for both the package and the fuel element, are conservatively ignored external to the active fuel region, and these end regions are simply modeled as full-density water. The package length is modeled to match the active length of the fuel element (30 ± 0.5-in), while the actual inner cavity length is 67.88-in as shown on the packaging general arrangement drawing 60501-10. The package is reflected with 12-in of full-density water.

Tolerances on the packaging are selected to result in the most reactive condition, as described in Section 6.3.1, *Model Configuration*. The standard ATR FFSC MCNP models are utilized with no change to the packaging descriptions.

The package consists of two primary structural components, a circular inner tube and a square outer tube. The modeled tube OD is 6.03-in, the modeled wall thickness is 0.108-in, and the modeled tube ID is 5.814-in. The outer tube is modeled with a wall thickness of 0.169-in and outer dimension of 7.9-in.

The fuel element is transported in the Cobra Fuel Handling Enclosure (CFHE). The CFHE supports the fuel element outside the active fuel region and radially centers the fuel element both within the CFHE and within the package cavity. Neoprene pads are attached to the CFHE at the interface between the fuel element and CFHE, although these pads are well outside the active fuel region and are not included in the models. Neoprene also contains chlorine, which acts a neutron poison, and thus it is also conservative to ignore neoprene because it has a negative effect on reactivity. The wall of the CFHE is aluminum with a thickness of 0.19 ± 0.06-in. The nominal inner diameter of the CFHE is 4.1-in. Both maximum and minimum thicknesses for the CFHE are considered in the models.

The dimensions used in the MCNP models as discussed in the preceding paragraphs are summarized in Table 6.13-10.

In the NCT single package models, the CFHE, inner tube, insulation, and outer tube are modeled explicitly, as shown in Figure 6.13-2 and Figure 6.13-3. Although negligible water ingress is expected during NCT, the inner cavity of the package is assumed to be flooded with water because the package lid does not contain a seal. However, the region between the insulation and the outer tube will remain dry because water cannot enter this region.

In the NCT array models, a 9x9x1 array is utilized. The CFHE would survive NCT events with negligible damage and the fuel element remains centered within the CFHE and package cavity. Because the fuel elements may be transported in a thin (< 0.01-in) plastic bag, this plastic bag is assumed to act as a boundary for partial moderation effects. The plastic bag is not modeled explicitly because it is too thin to have an appreciable effect on the reactivity. Therefore, it is postulated that the fuel element channels may fill with full-density water, while the region between the fuel element and CFHE fills with variable density water. Axial movement of the fuel elements is not considered because axial movement would increase the effective active height of the system and reduce the reactivity due to increased neutron leakage.

The HAC single package model is similar to the NCT single package model. Damage in the drop tests was shown to be negligible and concentrated at the ends of the package (see Section 2.12.1, *Certification Tests on CTU-1*). As the ends of the package are not modeled, this end damage does not affect the modeling. The various side drops resulted in only minor localized damage to the outer tube, and no observable bulk deformation of the package. Therefore, the minor damage observed will not impact the reactivity. The insulation is replaced with full-density water, and the region between the insulation and outer tube is also filled with full-density water (see Figure 6.13-4).

During HAC, it is postulated that the CFHE may become damaged. To bound all possible CFHE damage scenarios, HAC models are developed both with and without the CFHE (see Figure 6.13-4). Furthermore, because the ATR FFSC has not been drop tested with a Cobra fuel element, it is postulated that minor damage could occur to the Cobra fuel element. The Cobra fuel element utilizes aluminum cladding plates swaged into spacers, similar in design and construction materials to the ATR fuel element, which showed little damage after drop testing (see Section 2.12.1.5.2, *ATR Fuel Element Inspection*). To conservatively bound the potential fuel damage in the HAC models, the fuel plate pitch is allowed to expand uniformly until constrained by the inner diameter of the package. This pitch expansion increases the moderation and the reactivity. In actuality, such a large uniform expansion of the fuel plate pitch is not credible, and in the worst case scenario would be localized at one end of the fuel element. The modeled damage is intended to bound a fuel element that exhibits minor damage but is otherwise intact.

In the HAC array models, a 5x5x1 array is utilized. As with the HAC single package cases, postulated damage to the CFHE and fuel element are explicitly addressed. Cases are also developed to determine the reactivity effect of allowing variable density water in the region between the inner and outer tubes.

The detailed moderation assumptions for these cases are discussed more fully in Section 6.13.6, *Evaluation of Package Arrays under Normal Conditions of Transport*, and Section 6.13.7, *Package Arrays under Hypothetical Accident Conditions*.

6.13.3.2 Material Properties

The methodologies for computing the fuel meat densities and compositions for HEU and LEU fuel are provided in Section 6.13.2, *Fissile Material Contents*.

The material properties of the packaging materials are provided in Section 6.3.2, *Material Properties*. Pure aluminum with a density of 2.7 g/cm^3 is used for the fuel element cladding and CFHE wall. The inner and outer tubes of the package are constructed from stainless steel 304. Insulation is modeled as Durablanket® S insulation material.

6.13.3.3 Computer Codes and Cross-Section Libraries

MCNP5 v1.30 is used for the criticality analysis. All cross sections utilized are at room temperature (293.6 K). The uranium isotopes utilize preliminary ENDF/B-VII cross section data that are more accurate than ENDF/B-VI cross sections. ENDF/B-V cross sections are utilized for chromium, nickel, and iron because natural composition ENDF/B-VI cross sections are not available for these elements. The remaining isotopes utilize ENDF/B-VI cross sections. Titles of the cross sections utilized in the models have been extracted from the MCNP output or the

user's manual and are provided in Table 6.13-11. The S(α,β) card LWTR.60T is used to simulate hydrogen bound to water.

All cases are run with 5000 neutrons per generation for 850 generations, skipping the first 50. The 1-σ uncertainty is less than 0.001 for all cases.

6.13.3.4 Demonstration of Maximum Reactivity

The U-235 mass is maximized within each fuel plate and exceeds the U-235 fuel element limit allowed by the fuel specification by 2.8 g. It is demonstrated that the HEU fuel element bounds the LEU fuel element, and bounding calculations are performed for the HEU fuel element. The fuel element model is optimized to produce the maximum reactivity by minimizing the active fuel length, cladding thickness, and fuel meat thickness, while maximizing the arc length of the fuel meat, see Section 6.13.4, *Most Reactive Fuel Element Model*. Aluminum spacers that join the fuel plates are conservatively omitted to increase moderation.

The NCT and HAC array cases are significantly more reactive than the corresponding single package cases. Therefore, the following discussion is focused on the array cases.

For NCT, the fuel remains intact and is centered within the CFHE, which is also centered within the package cavity. Water moderation is allowed for all NCT cases because the package lid does not contain a seal, although full moderation under NCT is not credible because the package is dry loaded. A 9x9x1 array of packages is modeled for NCT. Because the fuel elements may be transported in a thin plastic bag, it is assumed the plastic bag may act as a boundary for partial moderation effects. In the NCT array cases, the water density is independently varied within the fuel element, between the fuel element and CFHE, and between the CFHE and the inner diameter of the package. The most reactive condition is with a fully flooded fuel element and CFHE and void between the CFHE and the inner diameter of the package. Case CENA20 is the most reactive NCT array case, with k_s = 0.73887.

For HAC, drop test data on the Cobra fuel element is not available, although the ATR fuel element is a similar plate-fuel design that showed little damage from a 30 foot drop (see Section 2.12.1.5.2, *ATR Fuel Element Inspection*). As a bounding fuel damage scenario, the fuel element plate pitch is allowed to increase under HAC. The CFHE is also assumed to be damaged and is omitted from the models when the fuel element is modeled as damaged. A 5x5x1 array of packages is modeled for HAC. Optimum moderation is achieved with a pitch expansion of 0.5 cm and the fuel element fully moderated. All fuel elements in the array are shifted to the center of the array. Reactivity is increased slightly if 0.8 g/cm^3 water is modeled between the fuel element and the inner diameter of the package. It is also demonstrated that reactivity is maximized if insulation between the inner and outer tube is modeled explicitly. Case CEHA68 is the most reactive HAC array case, with k_s = 0.76431.

Table 6.13-10 – Key Model Dimensions

Parameter	Drawing Dimension (in)	As-Modeled Dimension (in)
ATR FFSC		
Cavity length	67.88	30 ± 0.5
Package Length	73.9	30 ± 0.5
Inner tube outer diameter	6.0	6.03
Inner tube thickness	0.12	0.108
Outer tube flat-to-flat	8.0	7.9
Outer tube thickness	0.188	0.169
Insulation thickness	1.0	1.0
CFHE		
Canister body ID	4.1	4.1
Canister wall thickness	0.19 ± 0.06	0.19 ± 0.06

Table 6.13-11 – Cross Section Libraries Utilized

Isotope/Element	MCNP ID	Cross Section Label
H-1	1001.62c	1-h-1 at 293.6K from endf-vi.8 njoy99.50
C	6000.66c	6-c-0 at 293.6K from endf-vi.6 njoy99.50
O-16	8016.62c	8-o-16 at 293.6K from endf-vi.8 njoy99.50
Al-27	13027.62c	13-al-27 at 293.6K from endf-vi.8 njoy99.50
Si	14000.60c	14-si-nat at 293.6K from endf/b-vi
P-31	15031.66c	15-p-31 at 293.6K from endf-vi.6 njoy99.50
Cr	24000.50c	24-cr-nat at 293.6K from endf/b-v njoy
Mn-55	25055.62c	25-mn-55 at 293.6K from endf/b-vi.8 njoy99.50
Fe	26000.55c	26-fe-nat at 293.6K from endf/b-v njoy
Ni	28000.50c	28-ni-nat at 293.6K from endf/b-v njoy
U-235	92235.69c	92-u-235 at 293.6K from t16 u235la9d njoy99.50
U-238	92238.69c	92-u-238 at 293.6K from t16 u238la8h njoy99.50

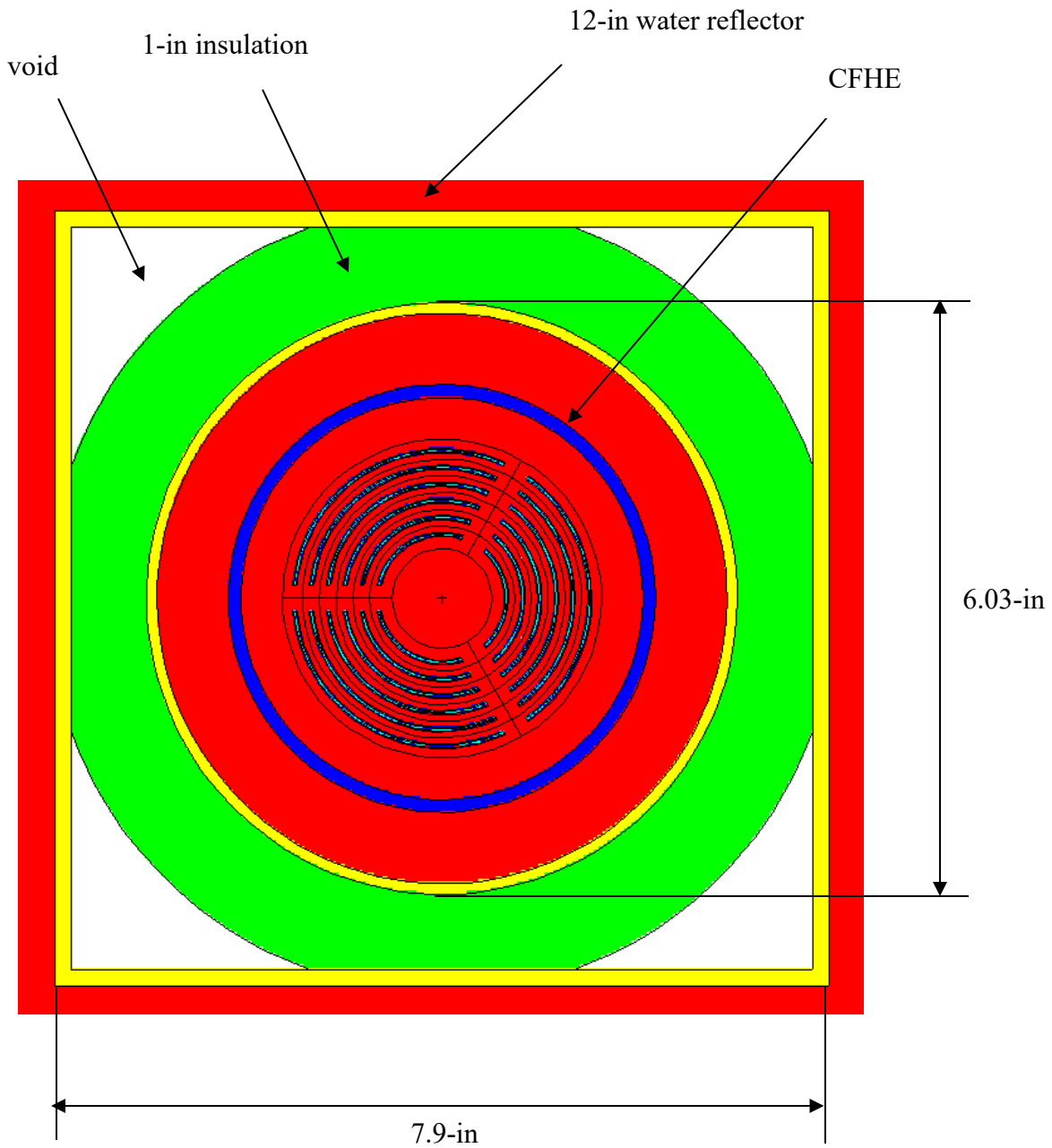

Inner tube thickness = 0.108-in

Outer tube thickness = 0.169-in

Figure 6.13-2 – NCT Single Package Model (planar view)

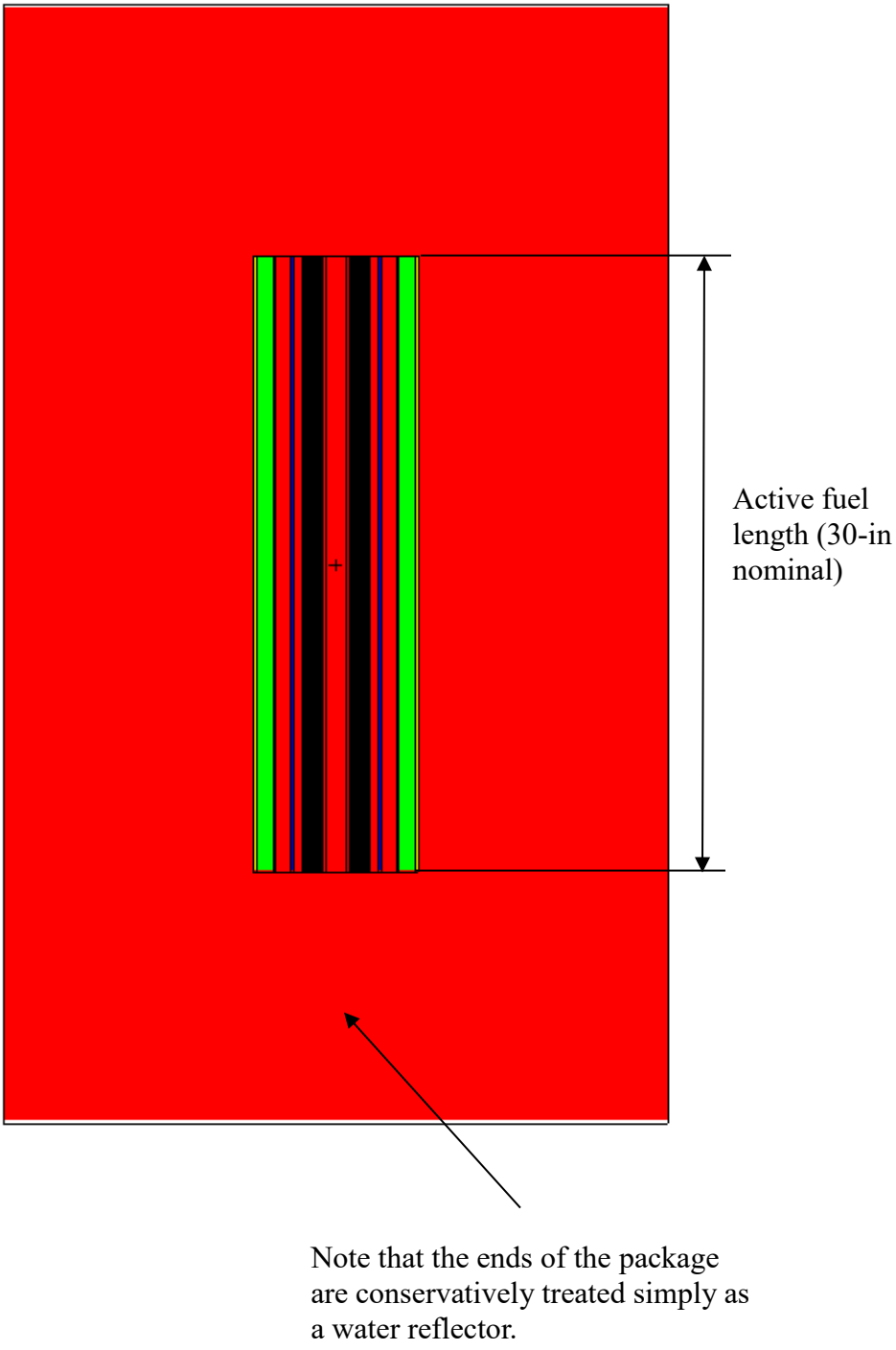

Figure 6.13-3 – NCT Single Package Model (axial view)

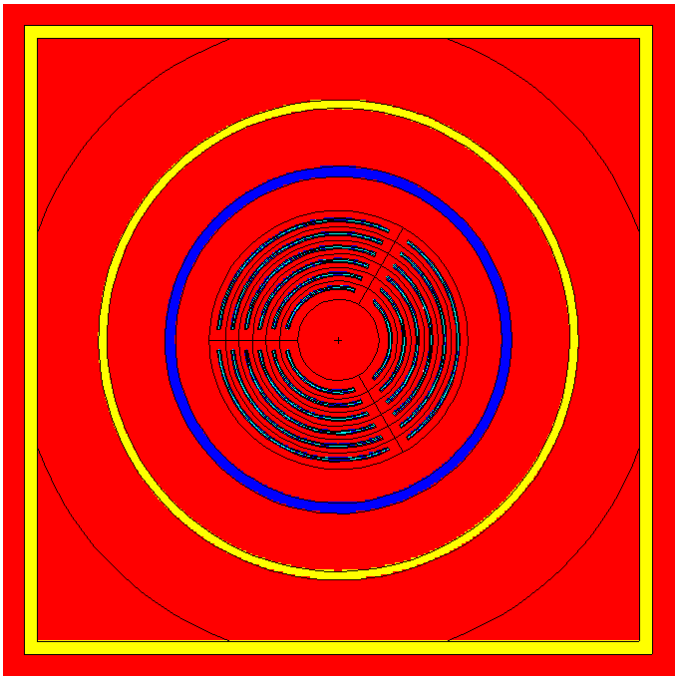

Intact CFHE, Undamaged Fuel

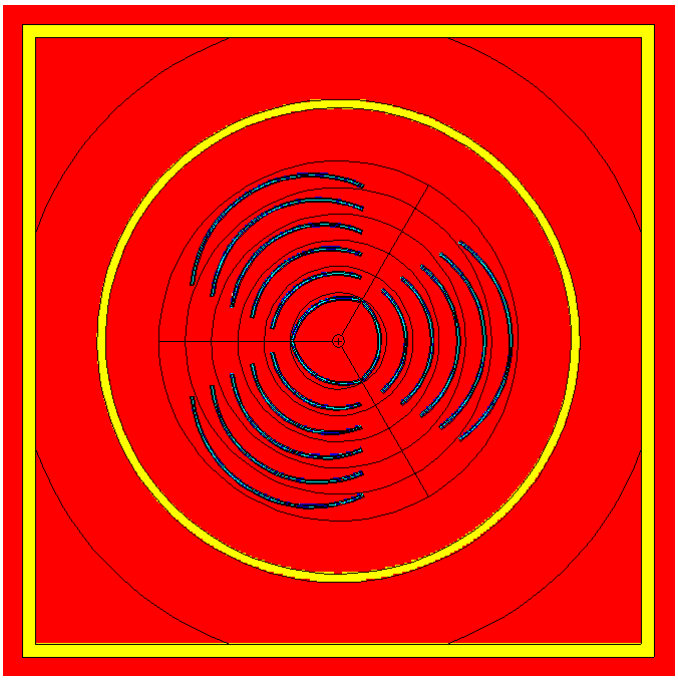

Damaged (absent) CFHE, Damaged Fuel

Figure 6.13-4 – HAC Single Package Model (planar view)

6.13.4 Most Reactive Fuel Element Model

Prior to performing the criticality analysis, a parametric study is performed to determine the most reactive fuel element model. The most reactive fuel element model is then used in subsequent models. Fuel element parameters considered are:

- HEU vs. LEU fuel
- Active fuel length
- Cladding thickness
- Fuel meat thickness
- Fuel meat arc length (or width as a flat plate)
- Presence or absence of aluminum spacers within the fuel

In all cases, the maximum U-235 loading per plate is utilized, including tolerances, as provided in Table 6.13-3. The as-modeled U-235 per plate is summarized in Table 6.13-12. The total U-235 modeled per fuel element conservatively exceeds the maximum allowed by the fuel specification by 2.8 g U-235 for both HEU and LEU fuel.

The cases considered are summarized in Table 6.13-13. Case CEP01 is the base case and features HEU fuel, nominal active fuel length, nominal cladding thickness, nominal fuel meat thickness, maximum arc length, and no aluminum spacers within the fuel. The thickness of the CFHE is modeled at the nominal value of 0.19-in in all models. In Cases CEP02 through CEP10, a single parameter is varied from the base case to determine the effect on the reactivity. Case CEP11 is a combination of the worst-case parameters from Cases CEP01 through CEP10 and is the fuel element model used in subsequent analysis.

The considered variations are:

- HEU fuel vs. LEU fuel is considered.
- Active fuel length
  - Nominal = 76.2 cm
  - Maximum = 77.45 cm
  - Minimum = 74.95 cm
- Cladding thickness
  - Nominal = 0.035 cm
  - Maximum = 0.005 tolerance assumed, 0.035 + 0.005 = 0.04 cm
  - Minimum = 0.005 tolerance assumed, 0.035 – 0.005 = 0.03 cm
- Fuel meat thickness
  - Nominal = 0.063 cm
  - Maximum = 0.005 tolerance assumed, 0.063 + 0.005 = 0.068 cm
  - Minimum = 0.005 tolerance assumed, 0.063 – 0.005 = 0.058 cm
- Fuel meat arc length
  - Maximum = see Table 6.13-14
  - Minimum = -5% tolerance on maximum values assumed, see Table 6.13-14
- Aluminum spacers
  - The base model does not include aluminum spacers so that a water gap exists between the three fuel plates in each ring (see upper half of Figure 6.13-5)
  - A model is developed that includes the aluminum spacers between the three fuel plates in each ring (see lower half of Figure 6.13-5)

The base case (Case CEP01) is developed so that the inner radius of each plate matches the nominal values provided in Table 6.13-15. The centerline radius of each plate is the inner radius + cladding thickness + ½ fuel meat thickness and is also provided in Table 6.13-15. For simplicity, the centerline radius of each plate as defined in Table 6.13-15 is treated as a fixed quantity for all models in the parametric study. Therefore, adjustments to the cladding or fuel meat thicknesses do not affect the centerline radii. To properly preserve the volume of the fuel meat when a flat plate is "bent" into a curved plate, the arc length of the plate is related to the centerline radius based on the geometrical relationship $S = \theta r$, where S is the fuel meat arc length and r is the centerline radius of the fuel meat. This allows computation of θ for each plate, which is used to define the planes that terminate the edge of the plates.

Because the U-235 loading in each plate is fixed at the maximum value, any adjustments to the fuel meat thickness, fuel meat arc length, or active fuel length changes the composition and densities of the fuel meat in the plates. The methodology for computing the fuel meat densities and composition is provided in Section 6.13.2, *Fissile Material Contents*. The composition and densities for each of the cases is summarized in Table 6.13-16 and Table 6.13-17 for HEU and LEU fuel, respectively.

The aluminum spacers between the fuel plates are included in Case CEP09. The spacers are modeled with a thickness of 0.558 cm. For simplicity, the spacers are modeled with an ID and OD to match the overall fuel element boundary, 2.58 cm ID and 8.26 cm OD.

In this parametric study, packages are modeled in a 9x9x1 NCT array to exaggerate the reactivity effect one would observe from a single package. The interior of the package cavity and CFHE are filled with full-density water.

Results are provided in Table 6.13-18. The difference in k_s between the base case and the perturbed case is provided in the far right column. This difference is expressed as Δk_s*10^3. Because the U-235 mass is fixed at the same value for each case, reducing the active fuel length has a small positive effect on reactivity due to decreased neutron leakage (compare Cases CEP03 and CEP01). Reducing the fuel meat arc length (Case CEP04) decreases the reactivity, consistent with the results for ATR fuel (see Section 6.4.1.2.1, *Fuel Element Payload Parametric Evaluation*). Decreasing the cladding thickness (compare Cases CEP05 and CEP01) has a small positive effect on reactivity because the width of the water channel between fuel plates increases, which increases moderation. Likewise, decreasing the fuel meat thickness has a positive effect on reactivity (compare Cases CEP08 and CEP01) because this reduces the overall thickness of the fuel plate, increases the width of the water channel, and increases moderation. Adding the aluminum spacers between the plates (Case CEP09) has a large negative effect on the reactivity due to decreased moderation, and it is conservative to omit the spacers from the model.

The LEU model (Case CEP10) is developed based on Case CEP01 fuel element geometry. The LEU case is less reactive than the base HEU case despite the larger U-235 loading in LEU fuel because LEU fuel has increased parasitic neutron absorption in U-238. Therefore, it is sufficient to perform the Cobra criticality analysis for the HEU fuel element, as it bounds the LEU fuel element.

Considering the results of Cases CEP01 through CEP10, the most reactive fuel element consists of HEU fuel meat, minimum active fuel length, minimum cladding thickness, minimum fuel meat thickness, maximum fuel meat arc length, and no fuel element spacers. Case CEP11 has

these parameters and results in the largest increase in reactivity over the base case, or 7.35 Δk_s*10^3. The geometry and material description of Case CEP11 is used in all subsequent cases.

Table 6.13-12 – U-235 Loading with Maximum Tolerance

Plate	HEU, Max U-235 (g)	LEU, Max U-235 (g)
1 (inner)	12.3	12.9
2	16.5	17.5
3	20.9	22.0
4	25.0	26.8
5	29.6	31.1
6 (outer)	33.4	35.9
Total	137.7	146.2
Fuel Element (Total x 3)	413.1	438.6
Fuel Specification Maximum	410.3	435.8

Table 6.13-13 – Cases for Parameter Study

Case ID	HEU/ LEU	Active length	Cladding Thickness	Fuel Meat Thickness	Fuel Meat Arc Length	Fuel Element Spacers
CEP01	HEU	Nom	Nom	Nom	Max	No
CEP02	HEU	Max	Nom	Nom	Max	No
CEP03	HEU	Min	Nom	Nom	Max	No
CEP04	HEU	Nom	Nom	Nom	Min	No
CEP05	HEU	Nom	Max	Nom	Max	No
CEP06	HEU	Nom	Min	Nom	Max	No
CEP07	HEU	Nom	Nom	Max	Max	No
CEP08	HEU	Nom	Nom	Min	Max	No
CEP09	HEU	Nom	Nom	Nom	Max	Yes
CEP10	LEU	Nom	Nom	Nom	Max	No
Case CEP11 combines the worst-case parameters of the cases above						
CEP11	HEU	Min	Min	Min	Max	No

Note: Changes from base case CEP01 highlighted in yellow.

Table 6.13-14 – Fuel Meat Arc Length

Plate	Maximum (cm)	Minimum (cm)
1 (inner)	2.800	2.660
2	3.705	3.520
3	4.615	4.384
4	5.525	5.249
5	6.435	6.113
6 (outer)	7.340	6.973

Table 6.13-15 – Plate Radii

Plate	Nominal Inner Radius of Plate (cm)	Centerline Radius of Plate (Fixed) (cm)
1 (inner)	1.5980	1.6645
2	2.0300	2.0965
3	2.4630	2.5295
4	2.8960	2.9625
5	3.3280	3.3945
6 (outer)	3.7610	3.8275

Table 6.13-16 – HEU Fuel Meat Densities and Compositions

Case ID →	CEP01 CEP05 CEP06 CEP09	CEP02	CEP03	CEP04	CEP07	CEP08	CEP11
Plate	**Total Fuel Meat Density (g/cm^3)**						
1 (inner)	3.2699	3.2570	3.2832	3.3119	3.2111	3.3388	3.3532
2	3.3150	3.3019	3.3285	3.3576	3.2554	3.3848	3.3995
3	3.3710	3.3577	3.3847	3.4143	3.3104	3.4420	3.4569
4	3.3681	3.3549	3.3819	3.4115	3.3076	3.4391	3.4540
5	3.4239	3.4104	3.4379	3.4680	3.3624	3.4961	3.5112
6 (outer)	3.3871	3.3738	3.4009	3.4307	3.3263	3.4585	3.4735
Isotope	**Fuel Meat Composition (wt. %)**						
U-235	27.9850	27.6420	28.3360	29.0840	26.4020	29.7700	30.1360
U-238	1.7863	1.7644	1.8087	1.8564	1.6852	1.9002	1.9236
Al	70.2290	70.5930	69.8550	69.0600	71.9130	68.3300	67.9410

Table 6.13-17 – LEU Fuel Meat Densities and Composition

Case ID →	CEP10
Plate	**Total Fuel Meat Density (g/cm^3)**
1 (inner)	6.4711
2	6.6343
3	6.6957
4	6.8132
5	6.7883
6 (outer)	6.8698
Isotope	**Fuel Meat Composition (wt. %)**
U-235	14.8310
U-238	59.3220
Al	20.0000
Si	5.8473

Table 6.13-18 – Parametric Study Results

Case ID	Filename	k_{eff}	σ	k_s ($k+2\sigma$)	$\Delta k*10^3$ from Base
CEP01	NA_G1	0.67630	0.00040	0.67710	Base
CEP02	NA_G2	0.67399	0.00038	0.67475	-2.35
CEP03	NA_G3	0.67652	0.00038	0.67728	0.18
CEP04	NA_G4	0.67308	0.00039	0.67386	-3.24
CEP05	NA_G5	0.67187	0.00036	0.67259	-4.51
CEP06	NA_G6	0.67964	0.00038	0.68040	3.30
CEP07	NA_G7	0.67359	0.00038	0.67435	-2.75
CEP08	NA_G8	0.67724	0.00039	0.67802	0.92
CEP09	NA_G1_AL	0.65216	0.00038	0.65292	-24.18
CEP10	NA_G1_LEU	0.66761	0.00039	0.66839	-8.71
CEP11	NA_GMAX	0.68369	0.00038	0.68445	7.35

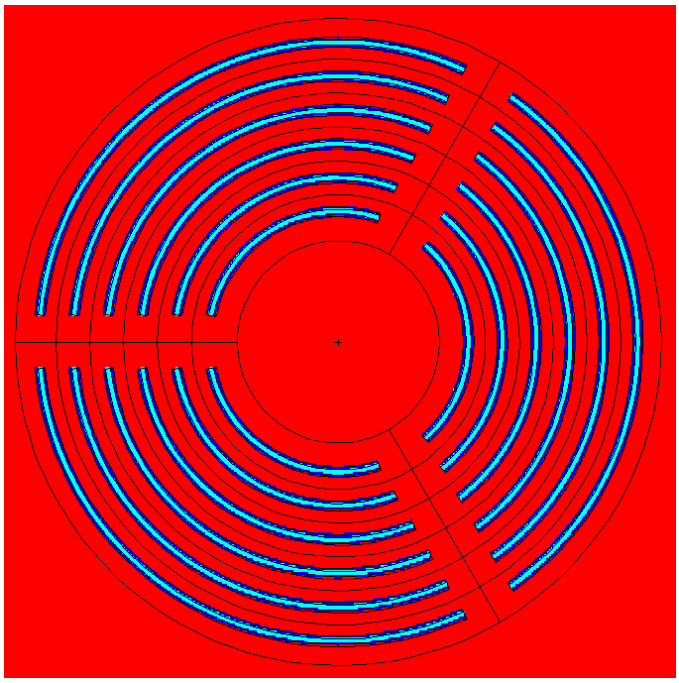

Case CEP1: No aluminum spacers

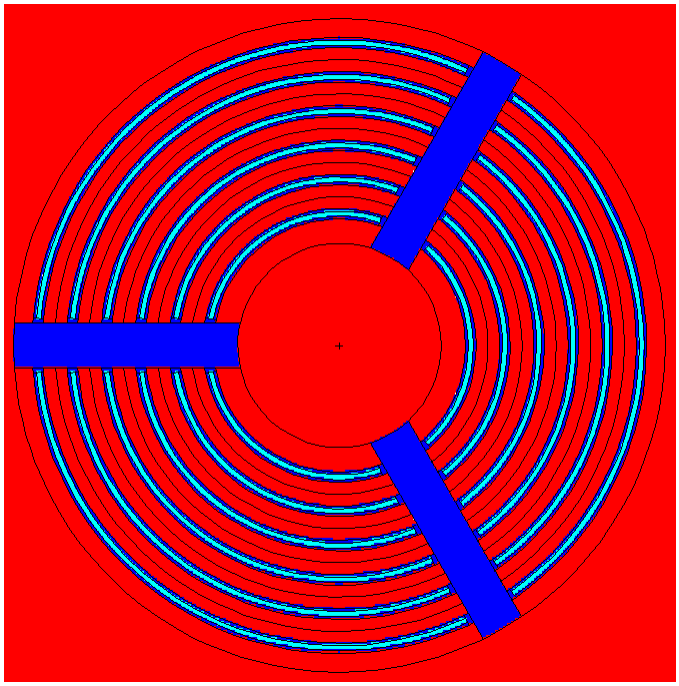

Case CEP9: With aluminum spacers

Figure 6.13-5 – Fuel Element Models

6.13.5 Single Package Evaluation

The most reactive fuel element is determined in Section 6.13.4, *Most Reactive Fuel Element Model* and consists of HEU fuel meat, minimum active fuel length, minimum cladding thickness, minimum fuel meat thickness, maximum fuel meat arc length, and no fuel element spacers. A fuel element with these parameters is used in the following analysis.

6.13.5.1 Single Package Configuration

6.13.5.1.1 NCT Single Package Configuration

The geometry of the NCT single package configuration is discussed in Section 6.13.3.1, *Model Configuration*, and depicted in Figure 6.13-2. A single fuel element is modeled in the center of the CFHE. The package is reflected with 12-in of water.

Results are provided in Table 6.13-19. The first two cases feature a fully flooded package cavity and CFHE. Case CENS1 features a CFHE with maximum thickness (0.25-in), while Case CENS2 features a CFHE with minimum thickness (0.13-in). For a single package, reactivity is maximized for a minimum thickness CFHE because water reflection is enhanced.

In Cases CENS3 through CENS7, the water density within the fuel element is reduced. Full-density water is modeled between the fuel element and CFHE to maximize reflection. Full-density water is also modeled between the CFHE and package inner diameter to maximize reflection. Reactivity decreases as the water density within the fuel element is reduced.

Maximum reactivity is achieved for Case CENS2. This case is fully-flooded with a minimum thickness CFHE. The reactivity of this case is low, with k_s = 0.40321. This case meets the requirements of 71.55(b)(d) and is below the USL of 0.9209.

6.13.5.1.2 HAC Single Package Configuration

The geometry of the HAC single package configuration is discussed in Section 6.13.3.1 and is depicted in Figure 6.13-4. The package is reflected with 12-in of water.

Results for undamaged fuel are provided in Table 6.13-20. Only fully flooded cases are considered because it is demonstrated in the NCT single package cases that reactivity is reduced when the fuel element is moderated with lower density water. In Case CEHS1, the CFHE is modeled at the minimum thickness to maximize water reflection. Reactivity increases compared to the equivalent NCT single package case (Case CENS2) because insulation and void between the inner and outer tubes is replaced with water to increase reflection. In Case CEHS2, the CFHE is omitted from the model entirely to simulate damage to the CFHE. Reactivity increases when the CFHE is omitted from the model due to the increased water reflection.

Results for damaged fuel are provided in Table 6.13-21. The CFHE is conservatively omitted from all damaged fuel models to enhance water reflection and to allow more volume for pitch expansion. In the initial damaged fuel element model (Case CEHS10), the fuel element is compressed by shifting all fuel plates inward by 0.35 cm. In all subsequent damaged fuel element cases, the inner ring of fuel is fixed at the compressed location, while rings 2 through 6 are shifted outward from the base compressed case in 0.1 cm increments. Illustrations of damaged fuel element geometry for several of the damaged fuel cases are provided in Figure 6.13-6.

The reactivity increases with increasing pitch, reaching a maximum k_s = 0.49961 for a pitch expansion of 0.5 cm (Case CEH15). While the pitch expansion has a positive effect on reactivity, the reactivity remains relatively low. This case meets the requirements of 71.55(e) and is below the USL of 0.9209.

6.13.5.2 Single Package Results

Following are the tabulated results for the single package cases. The most reactive configurations are listed in boldface.

Table 6.13-19 – NCT Single Package Results

Case ID	Filename	Water Density within Fuel Element (g/cm^3)	k_{eff}	σ	k_s (k+2σ)
CENS1	NS_W100_MAXFHE	1.0	0.39018	0.00034	0.39086
CENS2	**NS_W100_MINFHE**	**1.0**	**0.40249**	**0.00036**	**0.40321**
CENS3	NS_W050_MINFHE	0.5	0.28811	0.00030	0.28871
CENS4	NS_W060_MINFHE	0.6	0.31051	0.00030	0.31111
CENS5	NS_W070_MINFHE	0.7	0.33316	0.00033	0.33382
CENS6	NS_W080_MINFHE	0.8	0.35609	0.00034	0.35677
CENS7	NS_W090_MINFHE	0.9	0.37976	0.00034	0.38044

Table 6.13-20 – HAC Single Package Results, Undamaged Fuel

Case ID	Filename	k_{eff}	σ	k_s (k+2σ)
CEHS1	HS_FHE	0.43296	0.00034	0.43364
CEHS2	HS_NOFHE	0.44386	0.00036	0.44458

Table 6.13-21 – HAC Single Package Results, Damaged Fuel

Case ID	Filename	Change in Pitch	k_{eff}	σ	k_s (k+2σ)
CEHS10	HS_NOFHE_P0	Base Compressed	0.42535	0.00033	0.42601
CEHS11	HS_NOFHE_P1	0.1 cm from CEHS10	0.45449	0.00035	0.45519
CEHS12	HS_NOFHE_P2	0.2 cm from CEHS10	0.47424	0.00037	0.47498
CEHS13	HS_NOFHE_P3	0.3 cm from CEHS10	0.48837	0.00034	0.48905
CEHS14	HS_NOFHE_P4	0.4 cm from CEHS10	0.49530	0.00036	0.49602
CEHS15	**HS_NOFHE_P5**	**0.5 cm from CEHS10**	**0.49889**	**0.00036**	**0.49961**
CEHS16	HS_NOFHE_P6	0.6 cm from CEHS10	0.49814	0.00033	0.49880
CEHS17	HS_NOFHE_P7	0.7 cm from CEHS10	0.49383	0.00034	0.49451

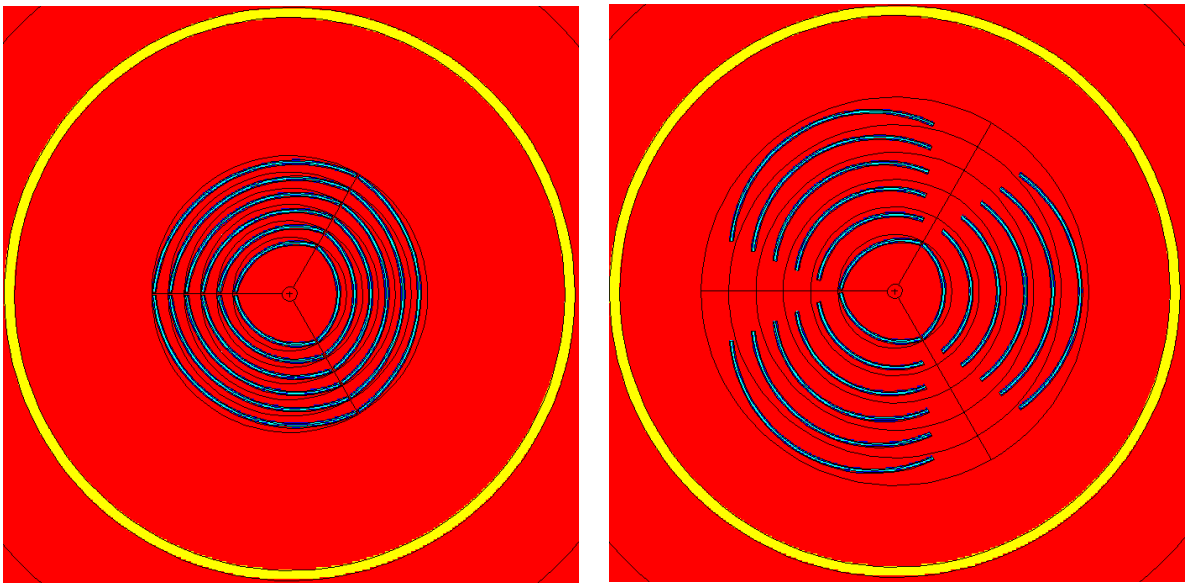

Case CEHS10, base compressed

Case CEHS13, 0.3 cm pitch expansion

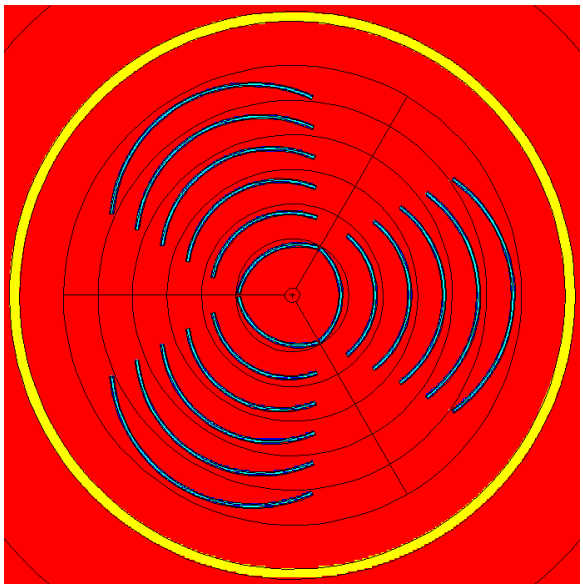

Case CEHS15, 0.5 cm pitch expansion

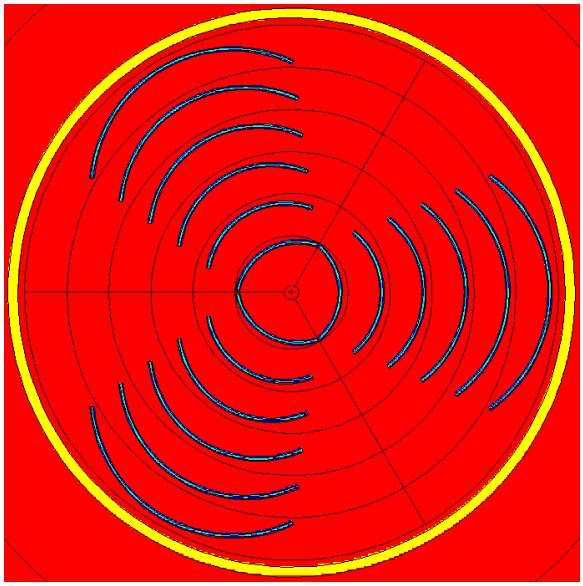

Case CEHS17, 0.7 cm pitch expansion

Figure 6.13-6 – Damaged Fuel Cases

6.13.6 Evaluation of Package Arrays under Normal Conditions of Transport

The most reactive fuel element is determined in Section 6.13.4, *Most Reactive Fuel Element Model* and consists of HEU fuel meat, minimum active fuel length, minimum cladding thickness, minimum fuel meat thickness, maximum fuel meat arc length, and no fuel element spacers. A fuel element with these parameters is used in the following analysis.

6.13.6.1 NCT Array Configuration

The NCT array model is a 9x9x1 lattice for a total of 81 packages, see Figure 6.13-7. Axial stacking configurations would lower the reactivity because the package is long and narrow, and the fuel element active length is significantly shorter than the package length. The geometry of the individual packages is the same as the NCT single package model. The entire array is reflected with 12-in of full-density water.

It is conservatively assumed that water may enter the package cavity. Within the cavity there are three distinct regions that may contain water:

1. Water within the fuel element boundary.
2. Water between the fuel element outer boundary and the inner diameter of the CFHE
3. Water between the CFHE and the inner diameter of the package cavity.

The density of water is independently varied in each of these three regions to determine the most reactive condition.

Results are provided in Table 6.13-22. The parametric study to determine the most reactive fuel element parameters (see Section 6.13.4, *Most Reactive Fuel Element Model*) is based upon a fully flooded NCT array model. The most reactive case from the parameter study, Case CEP11, is used as the base case for the NCT array analysis. Case CEP11 features a CFHE of nominal thickness (0.19-in). Case CENA1 features a CFHE with maximum thickness (0.25-in), while Case CENA2 features a CFHE with minimum thickness (0.13-in). For a package array, reactivity is maximized for a maximum thickness CFHE because aluminum does not appreciably absorb neutrons, and neutron transmission between packages is enhanced for the thicker CFHE. Therefore, all subsequent NCT array cases feature the CFHE modeled at maximum thickness.

In Series 1, the water densities of the three regions are modeled at the same value and varied between 0.5 g/cm^3 and 1.0 g/cm^3. Reactivity is maximized for Case CENA1 (k_s = 0.68564) with full water density in all model regions because maximizing the water density in the fuel element maximizes moderation.

In Series 2, the water density within the fuel element is fixed at 1.0 g/cm^3, while the water density between the fuel element and the CFHE and between the CFHE and package inner diameter is modeled at the same value and varied between 0 g/cm^3 and 1.0 g/cm^3. The maximum reactivity of Series 2 increases compared to Series 1, with a maximum k_s = 0.70962 (Case CENA15). In this case, the water density of the two outer regions is fixed at 0.5 g/cm^3.

In Series 3, the water density within the fuel element and between the fuel element and CFHE is fixed at 1.0 g/cm^3 while the water density between the CFHE and package inner diameter is varied. The maximum reactivity of Series 3 increases compared to Series 2, with a maximum k_s

= 0.73887 (Case CENA20). In this case, void is modeled between the CFHE and package inner diameter.

Because Series 3 indicates maximum reactivity is achieved with void in the outer region, it is possible reactivity could be increased further by reducing the water density between the fuel element and CFHE. Series 4 is essentially the same as Series 3 except the water density between the fuel element and CFHE is fixed at a reduced value of 0.9 g/cm^3. However, the most reactive Series 4 case is less reactive than Series 3, with k_s = 0.73354 (Case CENA30).

The most reactive NCT array case is Case CENA20, with full-density water within the fuel element and CFHE and void between the CFHE and package inner diameter. For this case, k_s = 0.73887, which is below the USL of 0.9209. This case meets the requirements of 71.55(d) and 71.59.

6.13.6.2 NCT Array Results

Following are the tabulated results for the NCT array cases. The most reactive configurations are listed in boldface.

Table 6.13-22 – NCT Array Results

Case ID	Filename	Water Density (g/cm^3)			k_{eff}	σ	k_s (k+2σ)
		Fuel Element	Fuel Element to CFHE	CFHE to Package			
Series 1: Variable water density in all regions							
CEP11	NA_GMAX	1.0	1.0	1.0	0.68369	0.00038	0.68445
CENA1	**NA_W100_FHEMAX**	**1.0**	**1.0**	**1.0**	**0.68486**	**0.00039**	**0.68564**
CENA2	NA_W100_FHEMIN	1.0	1.0	1.0	0.68043	0.00038	0.68119
CENA3	NA_W050	0.5	0.5	0.5	0.58506	0.00037	0.58580
CENA4	NA_W060	0.6	0.6	0.6	0.61932	0.00038	0.62008
CENA5	NA_W070	0.7	0.7	0.7	0.64264	0.00037	0.64338
CENA6	NA_W080	0.8	0.8	0.8	0.66049	0.00039	0.66127
CENA7	NA_W090	0.9	0.9	0.9	0.67470	0.00039	0.67548
Series 2: Full-density water in fuel element, variable water density in remaining regions.							
CENA10	NA_I100_O000	1.0	0	0	0.65080	0.00037	0.65154
CENA11	NA_I100_O010	1.0	0.1	0.1	0.67469	0.00039	0.67547
CENA12	NA_I100_O020	1.0	0.2	0.2	0.69185	0.00039	0.69263
CENA13	NA_I100_O030	1.0	0.3	0.3	0.70272	0.00039	0.70350
CENA14	NA_I100_O040	1.0	0.4	0.4	0.70609	0.00040	0.70689
CENA15	**NA_I100_O050**	**1.0**	**0.5**	**0.5**	**0.70882**	**0.00040**	**0.70962**
CENA16	NA_I100_O060	1.0	0.6	0.6	0.70762	0.00041	0.70844
CENA17	NA_I100_O070	1.0	0.7	0.7	0.70293	0.00038	0.70369
CENA18	NA_I100_O080	1.0	0.8	0.8	0.69780	0.00041	0.69862
CENA19	NA_I100_O090	1.0	0.9	0.9	0.69169	0.00039	0.69247
CENA1	NA_W100_FHEMAX	1.0	1.0	1.0	0.68486	0.00039	0.68564
Series 3: Full-density water in fuel element and CFHE, variable water density CFHE to package ID.							
CENA20	**NA_F100_O000**	**1.0**	**1.0**	**0**	**0.73807**	**0.00040**	**0.73887**
CENA21	NA_F100_O010	1.0	1.0	0.1	0.73353	0.00041	0.73435
CENA22	NA_F100_O020	1.0	1.0	0.2	0.73097	0.00041	0.73179
CENA23	NA_F100_O030	1.0	1.0	0.3	0.72617	0.00039	0.72695
CENA24	NA_F100_O040	1.0	1.0	0.4	0.72085	0.00041	0.72167
CENA25	NA_F100_O050	1.0	1.0	0.5	0.71520	0.00039	0.71598
CENA26	NA_F100_O060	1.0	1.0	0.6	0.70969	0.00040	0.71049
CENA27	NA_F100_O070	1.0	1.0	0.7	0.70467	0.00042	0.70551
CENA28	NA_F100_O080	1.0	1.0	0.8	0.69780	0.00041	0.69862
CENA29	NA_F100_O090	1.0	1.0	0.9	0.69106	0.00038	0.69182
CENA1	NA_W100_FHEMAX	1.0	1.0	1.0	0.68486	0.00039	0.68564

(1/2)

Table 6.13-22 – NCT Array Results (continued)

		Water Density (g/cm^3)					
Case ID	**Filename**	**Fuel Element**	**Fuel Element to CFHE**	**CFHE to Package**	**k_{eff}**	**σ**	**k_s (k+2σ)**
Series 4: Full-density water in fuel element, 0.9 g/cm^3 water in CFHE, variable water density CFHE to package ID.							
CENA30	**NA_F090_O000**	**1.0**	**0.9**	**0**	**0.73274**	**0.00040**	**0.73354**
CENA31	NA_F090_O010	1.0	0.9	0.1	0.73111	0.00042	0.73195
CENA32	NA_F090_O020	1.0	0.9	0.2	0.72801	0.00038	0.72877
CENA33	NA_F090_O030	1.0	0.9	0.3	0.72470	0.00039	0.72548
CENA34	NA_F090_O040	1.0	0.9	0.4	0.71835	0.00039	0.71913
CENA35	NA_F090_O050	1.0	0.9	0.5	0.71497	0.00040	0.71577
CENA36	NA_F090_O060	1.0	0.9	0.6	0.70922	0.00040	0.71002
CENA37	NA_F090_O070	1.0	0.9	0.7	0.70390	0.00040	0.70470
CENA38	NA_F090_O080	1.0	0.9	0.8	0.69831	0.00039	0.69909
CENA19	NA_I100_O090	1.0	0.9	0.9	0.69169	0.00039	0.69247

(2/2)

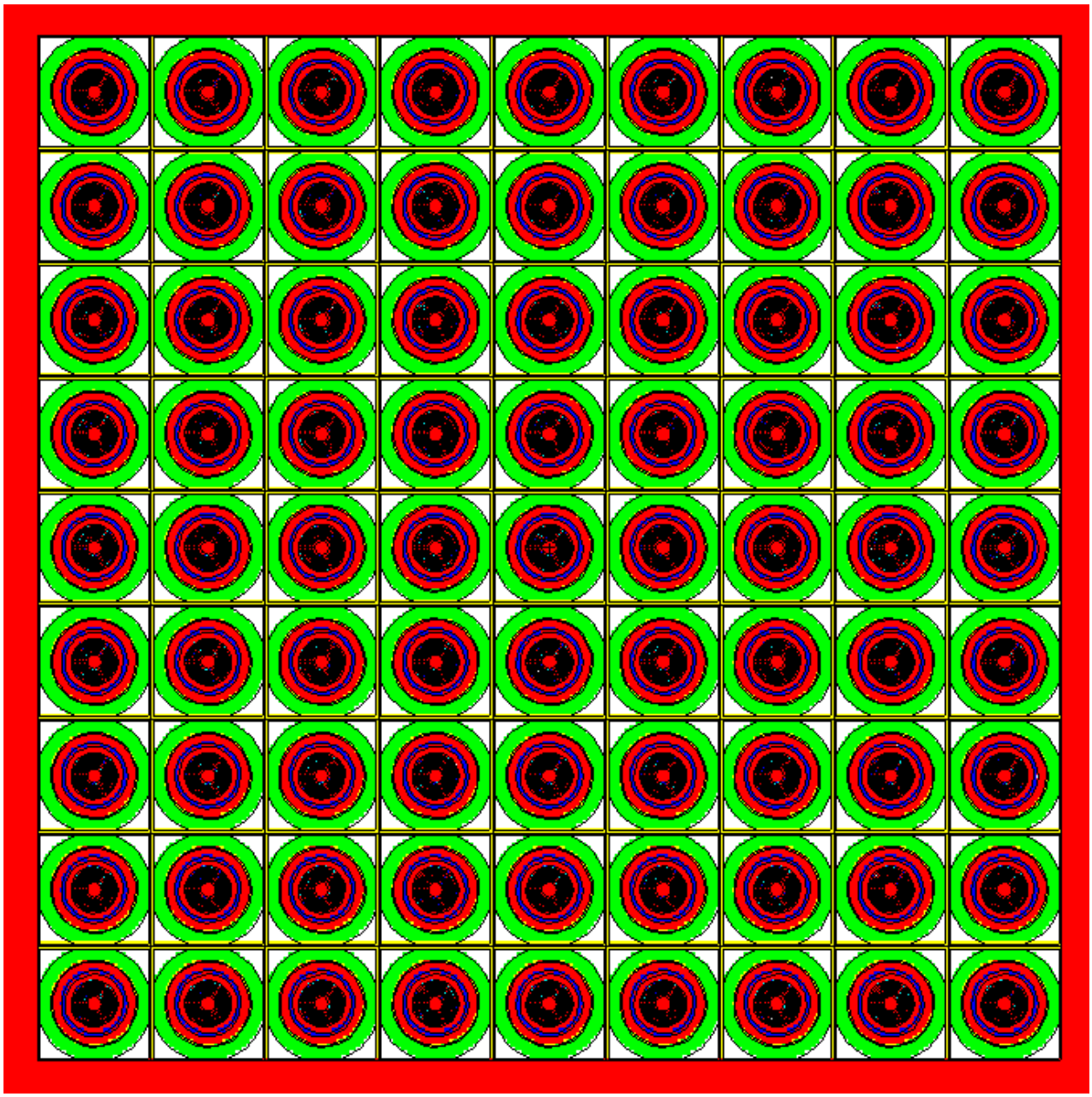

Figure 6.13-7 – NCT Array Geometry

6.13.7 Package Arrays under Hypothetical Accident Conditions

The most reactive fuel element is determined in Section 6.13.4, *Most Reactive Fuel Element Model* and consists of HEU fuel meat, minimum active fuel length, minimum cladding thickness, minimum fuel meat thickness, maximum fuel meat arc length, and no fuel element spacers. A fuel element with these parameters is used in the following analysis.

6.13.7.1 HAC Array Configuration

The HAC array model is a 5x5x1 array of the HAC single package model. Initially it is assumed that the fuel element and CFHE are undamaged in the accident, as shown in Figure 6.13-8.

Results for undamaged fuel and CFHE are provided in Table 6.13-23. If the fuel element and CFHE are undamaged, the configuration is similar to the NCT array but with a smaller array size. Based on the NCT array results, an array configuration with undamaged fuel is most reactive with full-density water within the fuel element and between the fuel element and CFHE and variable density water between the CFHE and package inner diameter. In Series 1, these moderation conditions are considered, and the insulation/void in the outer region is modeled consistent with undamaged geometry. Case CEHA4 is most reactive, with 0.3 g/cm^3 water between the CFHE and package inner diameter and k_s = 0.64964.

For HAC, it is assumed the region between the insulation and the outer boundary of the package may contain variable density water. In Series 2, it is demonstrated that adding water to this region reduces the reactivity because neutron interactions between packages are reduced. In Series 3, it is further assumed that the insulation itself may be replaced with void or variable density water. The system is slightly more reactive when the insulation is present, consistent with the results of the ATR fuel element analysis (see Section 6.6, *Package Arrays under Hypothetical Accident Conditions*).

In the next three series of cases, it is assumed the fuel element and CFHE are damaged. Fuel element damage is modeled as pitch expansion in the same manner as the single package cases, and the CFHE is omitted from the models. Results for the damaged fuel element cases are provided in Table 6.13-24. In Series 4, the pitch is varied from compressed to expanded 0.7 cm relative to the compressed case. The fuel element is centered within the package cavity, as illustrated in Figure 6.13-9, and full-density water is modeled within the fuel element and within the cavity. Case CEHA46 is the most reactive, with k_s = 0.75031 and 0.6 cm pitch expansion.

In Series 5, the fuel elements are shifted to the center of the array, which is a more compact geometry, see Figure 6.13-10. Reactivity increases due to the more compact geometry, with k_s = 0.76369 for Case CEHA55 with 0.5 cm pitch expansion.

In Series 6, the 0.5 cm pitch expansion case from Series 5 is used as the base case and the water between the fuel element and the package inner diameter is varied between 0 and 1.0 g/cm^3. A small increase in reactivity is observed for Case CEHA68, with 0.8 g/cm^3 water in this region and k_s = 0.76431.

Therefore, Case CEHA68 is the most reactive HAC array case with damaged fuel, with k_s = 0.76431, which is below the USL of 0.9209. This case features pitch expansion of 0.5 cm, fully moderated fuel elements, and 0.8 g/cm^3 water between the fuel element and package cavity. This case meets the requirements of 71.55(e) and 71.59.

6.13.7.2 HAC Array Results

Following are the tabulated results for the HAC array cases. The most reactive configurations are listed in boldface.

Table 6.13-23 – HAC Array Results, Undamaged Fuel

Case ID	Filename	Water Density (g/cm^3)			k_{eff}	σ	k_s (k+2σ)
		CFHE to Package	Insulation Region①	Insulation to Package			
Series 1: Water density of 1.0 g/cm^3 within fuel element and between fuel element and CFHE. Variable water density between CFHE and package ID, insulation modeled, void between insulation and package wall.							
CEHA1	HA_FHE_O000	0	Insulation	0	0.64160	0.00039	0.64238
CEHA2	HA_FHE_O010	0.1	Insulation	0	0.64511	0.00040	0.64591
CEHA3	HA_FHE_O020	0.2	Insulation	0	0.64730	0.00039	0.64808
CEHA4	**HA_FHE_O030**	**0.3**	**Insulation**	**0**	**0.64888**	**0.00038**	**0.64964**
CEHA5	HA_FHE_O040	0.4	Insulation	0	0.64870	0.00041	0.64952
CEHA6	HA_FHE_O050	0.5	Insulation	0	0.64778	0.00040	0.64858
CEHA7	HA_FHE_O060	0.6	Insulation	0	0.64649	0.00042	0.64733
CEHA8	HA_FHE_O070	0.7	Insulation	0	0.64407	0.00040	0.64487
CEHA9	HA_FHE_O080	0.8	Insulation	0	0.64226	0.00040	0.64306
CEHA10	HA_FHE_O090	0.9	Insulation	0	0.63958	0.00037	0.64032
CEHA11	HA_FHE_O100	1.0	Insulation	0	0.63536	0.00039	0.63614
Series 2: Water density of 1.0 g/cm^3 within fuel element and between fuel element and CFHE. Water density of 0.3 g/cm^3 between CFHE and package ID, insulation modeled, variable density water between insulation and package wall.							
CEHA4	**HA_FHE_O030**	**0.3**	**Insulation**	**0**	**0.64888**	**0.00038**	**0.64964**
CEHA20	HA_FHE_O030_Z010	0.3	Insulation	0.1	0.64299	0.00040	0.64379
CEHA21	HA_FHE_O030_Z020	0.3	Insulation	0.2	0.63703	0.00038	0.63779
CEHA22	HA_FHE_O030_Z030	0.3	Insulation	0.3	0.62913	0.00039	0.62991
Series 3: Water density of 1.0 g/cm^3 within fuel element and between fuel element and CFHE. Water density of 0.3 g/cm^3 between CFHE and package ID. Variable density water between inner and outer tubes.							
CEHA30	**HA_FHE_O030_ZZ000**	**0.3**	**0**	**0**	**0.64554**	**0.00040**	**0.64634**
CEHA31	HA_FHE_O030_ZZ010	0.3	0.1	0.1	0.62597	0.00039	0.62675
CEHA32	HA_FHE_O030_ZZ020	0.3	0.2	0.2	0.60422	0.00037	0.60496
CEHA33	HA_FHE_O030_ZZ030	0.3	0.3	0.3	0.58257	0.00038	0.58333

①When the insulation is modeled as insulation rather than water or void, "insulation" is denoted.

Table 6.13-24 – HAC Array Results, Damaged Fuel

Case ID	Filename	Change in Pitch	Water Density, Fuel Element to ID (g/cm^3)	k_{eff}	σ	k_s (k+2σ)
Series 4: Damaged fuel with variable pitch, no CFHE, full-density water within cavity, fuel elements centered within package.						
CEHA40	HA_P0	Base Compressed	1.0	0.60171	0.00039	0.60249
CEHA41	HA_P1	0.1 cm from CEHA40	1.0	0.64885	0.00039	0.64963
CEHA42	HA_P2	0.2 cm from CEHA40	1.0	0.68612	0.00040	0.68692
CEHA43	HA_P3	0.3 cm from CEHA40	1.0	0.71493	0.00040	0.71573
CEHA44	HA_P4	0.4 cm from CEHA40	1.0	0.73454	0.00038	0.73530
CEHA45	HA_P5	0.5 cm from CEHA40	1.0	0.74604	0.00038	0.74680
CEHA46	**HA_P6**	**0.6 cm from CEHA40**	**1.0**	**0.74959**	**0.00036**	**0.75031**
CEHA47	HA_P7	0.7 cm from CEHA40	1.0	0.74407	0.00034	0.74475
Series 5: Damaged fuel with variable pitch, no CFHE, full-density water within cavity, fuel elements shifted to center of array.						
CEHA50	HA_CP0	Base Compressed	1.0	0.63734	0.00039	0.63812
CEHA51	HA_CP1	0.1 cm from CEHA40	1.0	0.68523	0.00038	0.68599
CEHA52	HA_CP2	0.2 cm from CEHA40	1.0	0.72004	0.00037	0.72078
CEHA53	HA_CP3	0.3 cm from CEHA40	1.0	0.74422	0.00039	0.74500
CEHA54	HA_CP4	0.4 cm from CEHA40	1.0	0.75836	0.00039	0.75914
CEHA55	**HA_CP5**	**0.5 cm from CEHA40**	**1.0**	**0.76297**	**0.00036**	**0.76369**
CEHA56	HA_CP6	0.6 cm from CEHA40	1.0	0.75998	0.00037	0.76072
CEHA57	HA_CP7	0.7 cm from CEHA40	1.0	0.74748	0.00036	0.74820
Series 5: Damaged fuel with pitch increased 0.5 cm from Case CEHA40, no CFHE, full-density water within fuel element, variable density water between fuel element and ID of package cavity, fuel elements shifted to center of array.						
CEHA60	HA_CP5_O000	0.5 cm from CEHA40	0	0.73839	0.00037	0.73913
CEHA61	HA_CP5_O010	0.5 cm from CEHA40	0.1	0.74329	0.00037	0.74403
CEHA62	HA_CP5_O020	0.5 cm from CEHA40	0.2	0.74833	0.00037	0.74907
CEHA63	HA_CP5_O030	0.5 cm from CEHA40	0.3	0.75285	0.00038	0.75361
CEHA64	HA_CP5_O040	0.5 cm from CEHA40	0.4	0.75600	0.00037	0.75674
CEHA65	HA_CP5_O050	0.5 cm from CEHA40	0.5	0.75924	0.00036	0.75996
CEHA66	HA_CP5_O060	0.5 cm from CEHA40	0.6	0.76080	0.00037	0.76154
CEHA67	HA_CP5_O070	0.5 cm from CEHA40	0.7	0.76314	0.00039	0.76392
CEHA68	**HA_CP5_O080**	**0.5 cm from CEHA40**	**0.8**	**0.76355**	**0.00038**	**0.76431**
CEHA69	HA_CP5_O090	0.5 cm from CEHA40	0.9	0.76312	0.00036	0.76384
CEHA55	HA_CP5	0.5 cm from CEHA40	1.0	0.76297	0.00036	0.76369

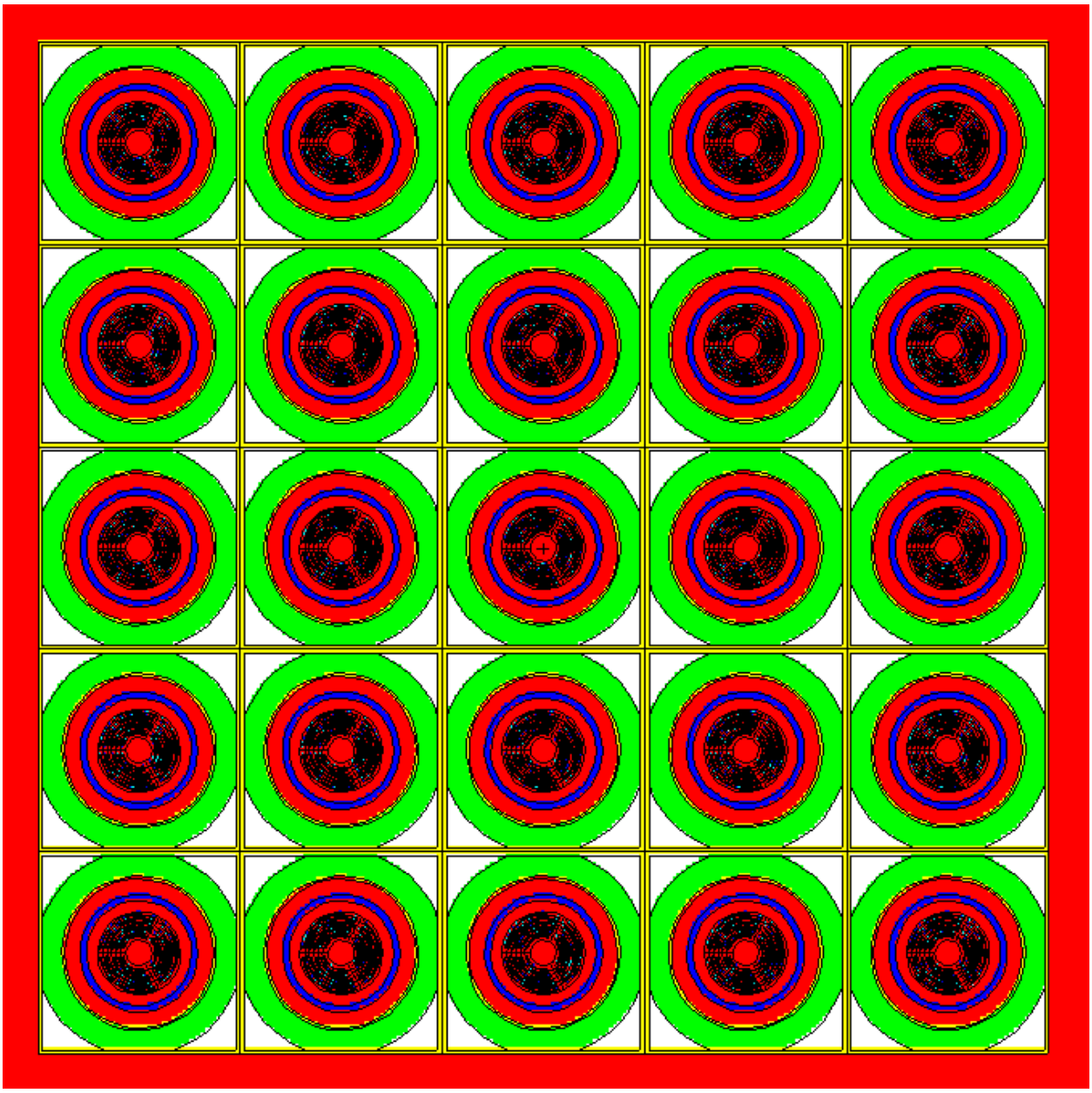

Figure 6.13-8 – HAC Array Geometry, Undamaged Geometry

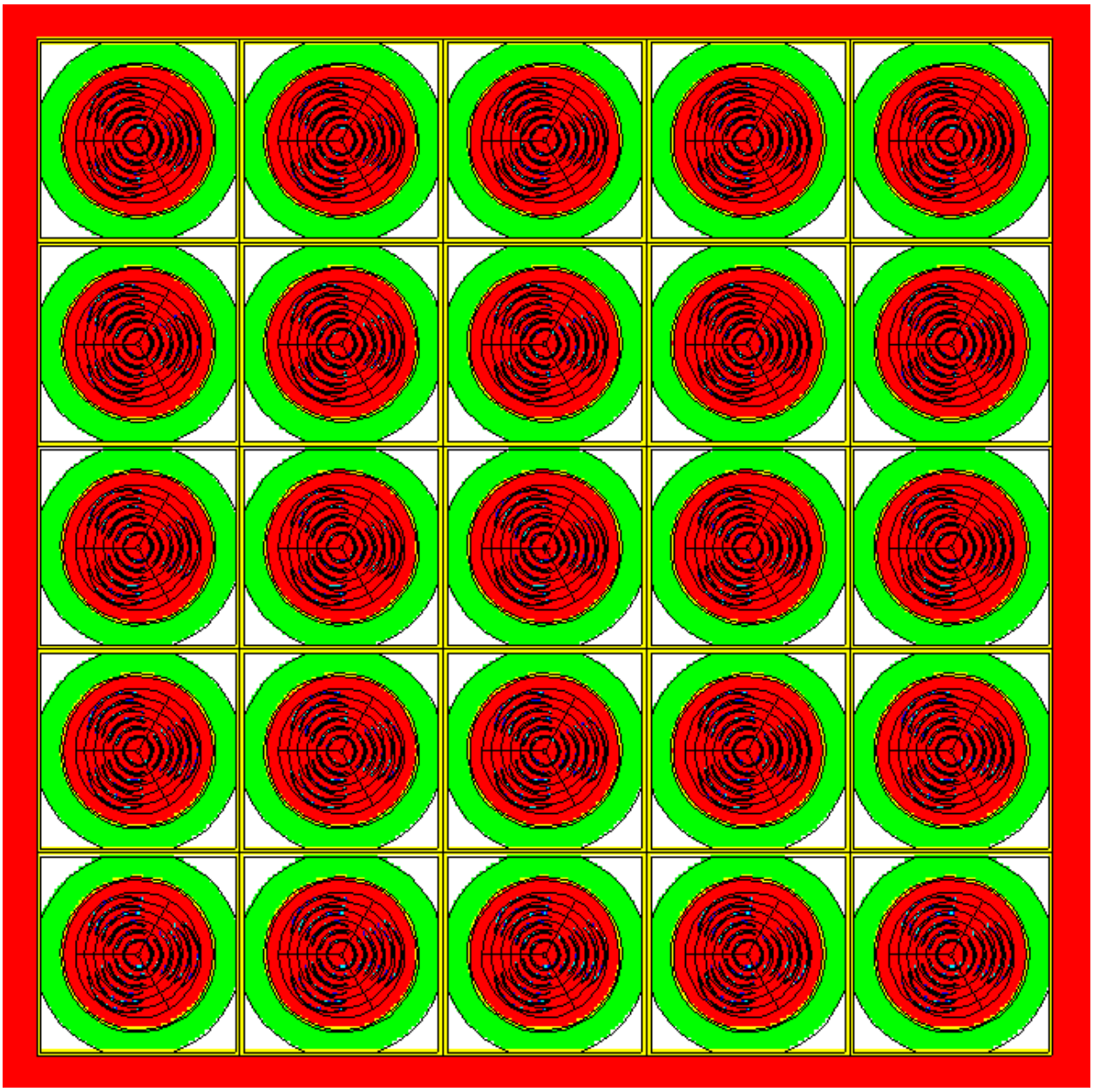

Figure 6.13-9 – HAC Array Geometry, Damaged Geometry, Centered

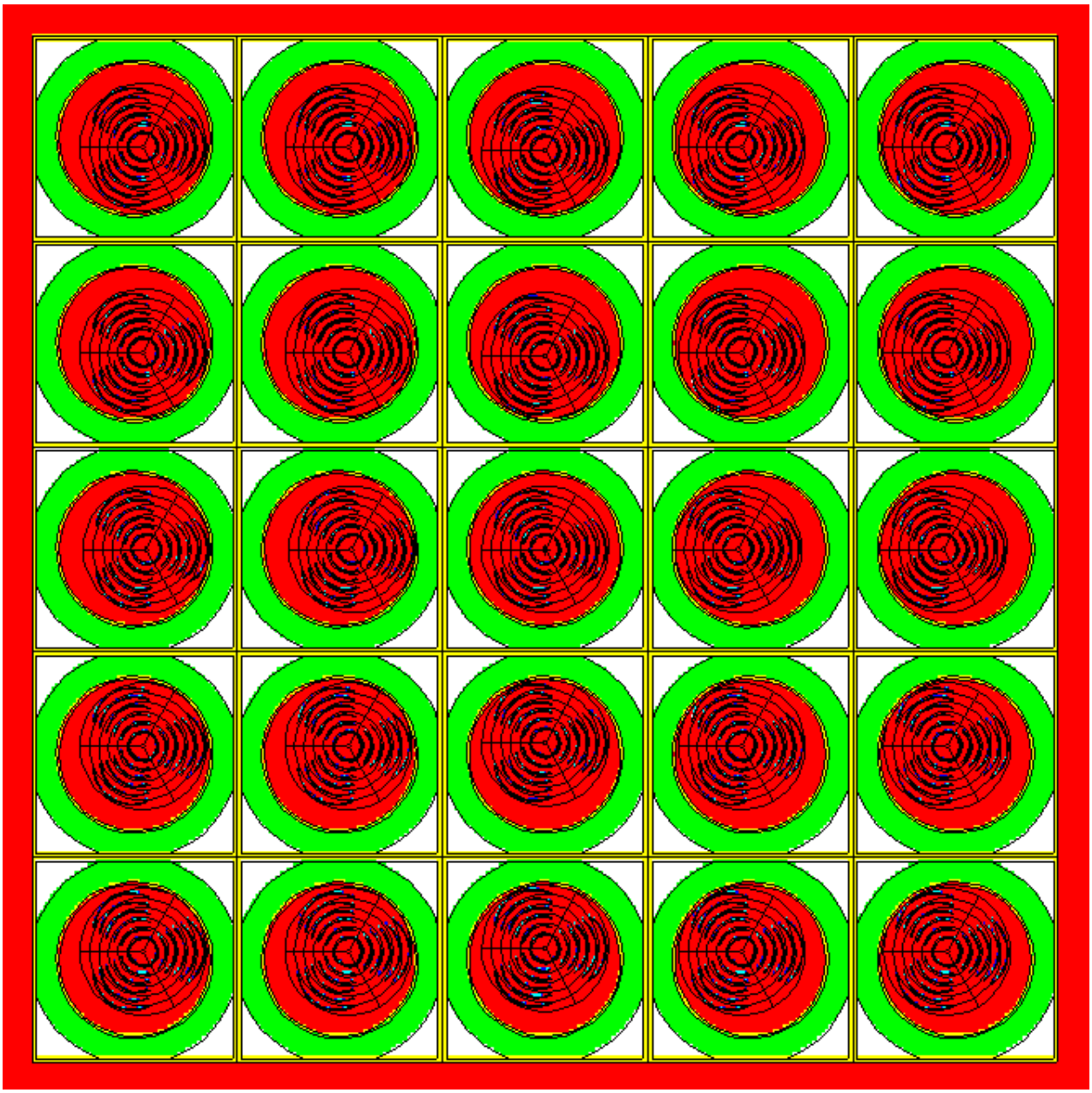

Figure 6.13-10 – HAC Array Geometry, Damaged Geometry, Shifted

6.13.8 Fissile Material Packages for Air Transport

See Section 6.7, which applies to all contents.

6.13.9 Benchmark Evaluations

Cobra fuel is high-enriched plate-type fuel, similar to ATR fuel. Therefore, the benchmarking evaluation performed for ATR fuel documented in Section 6.8, *Benchmark Evaluations*, is applicable to the current analysis, and the USL is 0.9209.

Five parameters were selected for the benchmark evaluation: (1) energy of the average neutron lethargy causing fission (EALF), (2) U-235 number density, (3) channel width, (4) H/U-235 atom ratio, and (5) pitch. The range of applicability of these parameters for the benchmarks utilized is summarized in Table 6.8-2. In the following sections, the range of applicability of the benchmarks is compared with the Cobra criticality analysis.

<u>EALF</u>

The most reactive HAC array case CEHA68 has an EALF = 4.8847×10^{-8} MeV, which is slightly outside the minimum bound of 5.22210×10^{-8} MeV of the benchmark experiments. Because this parameter is only slightly outside the bounds of the benchmark experiments, extrapolation of the USL is acceptable. The USL equation for EALF based on the 17 experiment benchmark set is USL = 0.9171 + (7.9546E+04)*EALF, or USL = 0.9210 for an EALF = 4.8847×10^{-8} MeV. A USL of 0.9210 is larger than the USL of 0.9209 used in the analysis; thus, a USL of 0.9209 is acceptable.

In addition, the small quantity payload criticality analysis utilizes HEU solution benchmarks with a minimum EALF of 3.43×10^{-8} MeV (see Section 6.11.8, *Benchmark Evaluations*), which bounds the EALF of the Cobra analysis. The solution benchmarks resulted in a USL of 0.9309; therefore, adding solution benchmarks to the flat-plate benchmark set would increase the USL. Therefore, it is conservative to apply a USL of 0.9209 for the Cobra criticality analysis, and the EALF parameter is acceptable.

<u>U-235 Number Density</u>

The U-235 number density of the HEU cases is approximately 2.7×10^{-3} atom/b-cm. This is within the range of applicability of $1.849 \times 10^{-3} \leq X \leq 3.926 \times 10^{-3}$ atom/b-cm.

<u>Channel Width, H/U-235 Atom Ratio, and Pitch</u>

The channel width (i.e., water gap between plates), H/U-235 atom ratio, and plate pitch are all related to the system moderation conditions and are somewhat redundant. The EALF parameter is a better metric for determining system moderation than channel width, H/U-235 atom ratio, or plate pitch because it is directly related to the energy range causing fission. Due to the damaged fuel assumption in the analysis and the large channel widths and pitches used in the models, benchmarks with similarly large parameters for a plate fuel element are not available. Because the EALF parameter is shown above to be acceptable for the Cobra fuel analysis, the channel width, H/U-235 atom ratio, and plate pitch parameters are also acceptable.

6.13.10 Sample Input File

A sample input file for the most reactive case (Case CEHA68, HAC array, filename HA_CP5_O080) is included below.

```
ATR
999     0      -320:321:-322:323:-324:325                imp:n=0
900     0      310 -311 312 -313 24 -25     fill=3       imp:n=1
901     2 -1.0 (311:-310:313:-312:-24:25) 320 -321 322 -323 324 -325  imp:n=1
c
c       Universe 1: Fuel Element in FHE
c
101     0      101 -102  110 -111 u=1 fill=20 imp:n=1
102     0      101 -102  111 -112 u=1 fill=21 imp:n=1
103     0      101 -102  112 -113 u=1 fill=22 imp:n=1
104     0      101 -102  113 -114 u=1 fill=23 imp:n=1
105     0      101 -102  114 -115 u=1 fill=24 imp:n=1
106     0      101 -102  115 -116 u=1 fill=25 imp:n=1
c
111     0      -101  100  110 -111 u=1 fill=20(1) imp:n=1
112     0      -101  100  111 -112 u=1 fill=21(1) imp:n=1
113     0      -101  100  112 -113 u=1 fill=22(1) imp:n=1
114     0      -101  100  113 -114 u=1 fill=23(1) imp:n=1
115     0      -101  100  114 -115 u=1 fill=24(1) imp:n=1
116     0      -101  100  115 -116 u=1 fill=25(1) imp:n=1
c
121     0      102 -100  110 -111 u=1 fill=20(2) imp:n=1
122     0      102 -100  111 -112 u=1 fill=21(2) imp:n=1
123     0      102 -100  112 -113 u=1 fill=22(2) imp:n=1
124     0      102 -100  113 -114 u=1 fill=23(2) imp:n=1
125     0      102 -100  114 -115 u=1 fill=24(2) imp:n=1
126     0      102 -100  115 -116 u=1 fill=25(2) imp:n=1
c
130     2 -1.0 -110               u=1            imp:n=1 $ inner water
131     2 -0.8  116               u=1            imp:n=1 $ outer water
c
c       Universe 2: Package, fuel in center
c
201     2 -1.0          -200  fill=1           u=2 imp:n=1
202     4 -7.94     200 -201                   u=2 imp:n=1 $ pipe
203     6 -0.096    201 -203 250 -251 252 -253 u=2 imp:n=1 $ insulation
204     0           203 250 -251 252 -253      u=2 imp:n=1 $ insulation to
tube
205     4 -7.94     -250:251:-252:253          u=2 imp:n=1 $ tube to inf
c
c       Universe 30: Package, fuel shifted left
c
3001    2 -1.0          -200  fill=1(30)       u=30 imp:n=1
3002    4 -7.94     200 -201                   u=30 imp:n=1 $ pipe
3003    6 -0.096    201 -203 250 -251 252 -253 u=30 imp:n=1 $ insulation
3004    0           203 250 -251 252 -253      u=30 imp:n=1 $ insulation to
tube
3005    4 -7.94     -250:251:-252:253          u=30 imp:n=1 $ tube to inf
c
c       Universe 31: Package, fuel shifted right
c
3101    2 -1.0          -200  fill=1(31)       u=31 imp:n=1
```

```
3102    4 -7.94     200 -201                    u=31 imp:n=1 $ pipe
3103    6 -0.096    201 -203 250 -251 252 -253 u=31 imp:n=1 $ insulation
3104    0           203 250 -251 252 -253      u=31 imp:n=1 $ insulation to
tube
3105    4 -7.94     -250:251:-252:253          u=31 imp:n=1 $ tube to inf
c
c       Universe 32: Package, fuel shifted down
c
3201    2 -1.0          -200  fill=1(32)       u=32 imp:n=1
3202    4 -7.94     200 -201                    u=32 imp:n=1 $ pipe
3203    6 -0.096    201 -203 250 -251 252 -253 u=32 imp:n=1 $ insulation
3204    0           203 250 -251 252 -253      u=32 imp:n=1 $ insulation to
tube
3205    4 -7.94     -250:251:-252:253          u=32 imp:n=1 $ tube to inf
c
c       Universe 33: Package, fuel shifted up
c
3301    2 -1.0          -200  fill=1(33)       u=33 imp:n=1
3302    4 -7.94     200 -201                    u=33 imp:n=1 $ pipe
3303    6 -0.096    201 -203 250 -251 252 -253 u=33 imp:n=1 $ insulation
3304    0           203 250 -251 252 -253      u=33 imp:n=1 $ insulation to
tube
3305    4 -7.94     -250:251:-252:253          u=33 imp:n=1 $ tube to inf
c
c       Universe 34: Package, fuel shifted lower left
c
3401    2 -1.0          -200  fill=1(34)       u=34 imp:n=1
3402    4 -7.94     200 -201                    u=34 imp:n=1 $ pipe
3403    6 -0.096    201 -203 250 -251 252 -253 u=34 imp:n=1 $ insulation
3404    0           203 250 -251 252 -253      u=34 imp:n=1 $ insulation to
tube
3405    4 -7.94     -250:251:-252:253          u=34 imp:n=1 $ tube to inf
c
c       Universe 35: Package, fuel shifted lower right
c
3501    2 -1.0          -200  fill=1(35)       u=35 imp:n=1
3502    4 -7.94     200 -201                    u=35 imp:n=1 $ pipe
3503    6 -0.096    201 -203 250 -251 252 -253 u=35 imp:n=1 $ insulation
3504    0           203 250 -251 252 -253      u=35 imp:n=1 $ insulation to
tube
3505    4 -7.94     -250:251:-252:253          u=35 imp:n=1 $ tube to inf
c
c       Universe 36: Package, fuel shifted upper left
c
3601    2 -1.0          -200  fill=1(36)       u=36 imp:n=1
3602    4 -7.94     200 -201                    u=36 imp:n=1 $ pipe
3603    6 -0.096    201 -203 250 -251 252 -253 u=36 imp:n=1 $ insulation
3604    0           203 250 -251 252 -253      u=36 imp:n=1 $ insulation to
tube
3605    4 -7.94     -250:251:-252:253          u=36 imp:n=1 $ tube to inf
c
c       Universe 37: Package, fuel shifted upper right
c
3701    2 -1.0          -200  fill=1(37)       u=37 imp:n=1
3702    4 -7.94     200 -201                    u=37 imp:n=1 $ pipe
3703    6 -0.096    201 -203 250 -251 252 -253 u=37 imp:n=1 $ insulation
```

```
3704    0           203 250 -251 252 -253      u=37 imp:n=1 $ insulation to
tube
3705    4 -7.94     -250:251:-252:253          u=37 imp:n=1 $ tube to inf
c
c       Universe 3: Array of Packages
c
300   0    -300 301 -302 303 imp:n=1 u=3 lat=1 fill=-2:2 -2:2 0:0
            36 36 33 37 37
            36 36 33 37 37
            31 31  2 30 30
            35 35 32 34 34
            35 35 32 34 34
c
c      Universe 10: Wedge 1
c
1000  3  -2.7    1000 -1010 1020 -1030 u=10 imp:n=1
1001  10 -3.3532 1000 -1010 1030 -1040 u=10 imp:n=1
1002  3  -2.7    1000 -1010 1040 -1050 u=10 imp:n=1
1003  2  -1.0   -1000:1010:-1020:1050  u=10 imp:n=1
c
c      Universe 11: Wedge 2
c
1100  3  -2.7    1001 -1011 1021 -1031 u=11 imp:n=1
1101  10 -3.3995 1001 -1011 1031 -1041 u=11 imp:n=1
1102  3  -2.7    1001 -1011 1041 -1051 u=11 imp:n=1
1103  2  -1.0   -1001:1011:-1021:1051  u=11 imp:n=1
c
c      Universe 12: Wedge 3
c
1200  3  -2.7    1002 -1012 1022 -1032 u=12 imp:n=1
1201  10 -3.4569 1002 -1012 1032 -1042 u=12 imp:n=1
1202  3  -2.7    1002 -1012 1042 -1052 u=12 imp:n=1
1203  2  -1.0   -1002:1012:-1022:1052  u=12 imp:n=1
c
c      Universe 13: Wedge 4
c
1300  3  -2.7    1003 -1013 1023 -1033 u=13 imp:n=1
1301  10 -3.4540 1003 -1013 1033 -1043 u=13 imp:n=1
1302  3  -2.7    1003 -1013 1043 -1053 u=13 imp:n=1
1303  2  -1.0   -1003:1013:-1023:1053  u=13 imp:n=1
c
c      Universe 14: Wedge 5
c
1400  3  -2.7    1004 -1014 1024 -1034 u=14 imp:n=1
1401  10 -3.5112 1004 -1014 1034 -1044 u=14 imp:n=1
1402  3  -2.7    1004 -1014 1044 -1054 u=14 imp:n=1
1403  2  -1.0   -1004:1014:-1024:1054  u=14 imp:n=1
c
c      Universe 15: Wedge 6
c
1500  3  -2.7    1005 -1015 1025 -1035 u=15 imp:n=1
1501  10 -3.4735 1005 -1015 1035 -1045 u=15 imp:n=1
1502  3  -2.7    1005 -1015 1045 -1055 u=15 imp:n=1
1503  2  -1.0   -1005:1015:-1025:1055  u=15 imp:n=1
c
c     Universe 20, 21, 22, 23, 24, 25, pitch changes
c
```

```
2000  0         -2000 fill=10(20) u=20 imp:n=1
2001  0         -2000 fill=11(21) u=21 imp:n=1
2002  0         -2000 fill=12(22) u=22 imp:n=1
2003  0         -2000 fill=13(23) u=23 imp:n=1
2004  0         -2000 fill=14(24) u=24 imp:n=1
2005  0         -2000 fill=15(25) u=25 imp:n=1

24      pz -37.475                  $ bottom of fuel
25      pz  37.475                  $ top of fuel
c
100     py 0
101     p  1.7321 -1 0 0
102     p -1.7321 -1 0 0
110  cz  0.2     $inner bound
111  cz  1.5305  $mid-
112  cz  2.463  $mid-
113  cz  3.396  $mid-
114  cz  4.3285  $mid-
115  cz  5.261  $mid-
116  cz  6.2  $outer bound-
120  cz  5.207   $FHE inner
121  cz  5.6896  $FHE outer
c
200      cz 7.3838 $ IR pipe
201      cz 7.6581 $ OR pipe
203      cz 10.1981 $ 1" insulation
204      pz 1000    $ dummy
c
250      px  -9.6032 $ square tube
251      px   9.6032
252      py  -9.6032
253      py   9.6032
c
300      px  10.033 $ lattice surfaces/sq. tube
301      px -10.033
302      py  10.033
303      py -10.033
310      px -50.164 $ 5x5 bounds
311      px  50.164
312      py -50.164
313      py  50.164
320      px -80.644 $ outer bounds
321      px  80.644
322      py -80.644
323      py  80.644
324      pz -67.955
325      pz  67.955
c
1000  p  1.1181  -1  0  0  $upper
1001  p  1.2186  -1  0  0  $upper
1002  p  1.2923  -1  0  0  $upper
1003  p  1.3479  -1  0  0  $upper
1004  p  1.3921  -1  0  0  $upper
1005  p  1.4249  -1  0  0  $upper
1010  p  -1.1181  -1  0  0  $lower
1011  p  -1.2186  -1  0  0  $lower
1012  p  -1.2923  -1  0  0  $lower
```

```
1013  p  -1.3479  -1  0  0  $lower
1014  p  -1.3921  -1  0  0  $lower
1015  p  -1.4249  -1  0  0  $lower
1020  cz  1.6055  $ r1
1021  cz  2.0375  $ r1
1022  cz  2.4705  $ r1
1023  cz  2.9035  $ r1
1024  cz  3.3355  $ r1
1025  cz  3.7685  $ r1
1030  cz  1.6355  $r2
1031  cz  2.0675  $r2
1032  cz  2.5005  $r2
1033  cz  2.9335  $r2
1034  cz  3.3655  $r2
1035  cz  3.7985  $r2
1040  cz  1.6935  $r3
1041  cz  2.1255  $r3
1042  cz  2.5585  $r3
1043  cz  2.9915  $r3
1044  cz  3.4235  $r3
1045  cz  3.8565  $r3
1050  cz  1.7235  $r4
1051  cz  2.1555  $r4
1052  cz  2.5885  $r4
1053  cz  3.0215  $r4
1054  cz  3.4535  $r4
1055  cz  3.8865  $r4
c
2000  so 10000

m2      1001.62c  2          $ water
        8016.62c  1
mt2     lwtr.60t
m3      13027.62c 1          $ Al
m4      6000.66c   -0.08     $ SS-304
        14000.60c  -1.0
        15031.66c  -0.045
        24000.50c  -19.0
        25055.62c  -2.0
        26000.55c  -68.375
        28000.50c  -9.5
m6      13027.62c  -26.5     $ insulation material
        14000.60c  -23.4
        8016.62c   -50.2
m10     92235.69c  -3.0136E-01  $meat
        92238.69c  -1.9236E-02
        13027.62c  -6.7941E-01
c
*tr1    0 0 0 120 30 90 150 120 90 $ 120 deg CCW
*tr2    0 0 0 120 150 90 30 120 90 $ 120 deg CW
*tr20  -0.35  0  0
*tr21  0.15  0  0
*tr22  0.65  0  0
*tr23  1.15  0  0
*tr24  1.65  0  0
*tr25  2.15  0  0
tr30  -1.1828  0  0  $ shift left
```

```
tr31  1.1828  0  0  $ shift right
tr32  0  -1.1828  0  $ shift down
tr33  0  1.1828  0  $ shift up
tr34  -0.8364  -0.8364  0  $ fuel shifted lower left
tr35  0.8364  -0.8364  0  $ fuel shifted lower right
tr36  0.8364  0.8364  0  $ fuel shifted upper left
tr37  -0.8364  0.8364  0  $ fuel shifted upper right
c
mode   n
kcode  5000 1.0 50 850
sdef    x=d1 y=d2 z=d3
si1     -50 50
sp1     0 1
si2     -50 50
sp2     0 1
si3     -40 40
sp3     0 1
```

6.13.11 Analysis of Increased U-235 Mass in Cobra LEU Fuel

The original analysis of the Cobra LEU fuel is based on a maximum U-235 mass of 435.8 g. Some Cobra LEU fuel elements developed after the original analysis will have a maximum U-235 mass of 450 g. This analysis reconfirms the conclusion that Cobra HEU fuel is more reactive than Cobra LEU fuel and thus shows that the original analysis remains of conservative evaluation following the increase in LEU U-235 mass.

References for this analysis are documented in Section 6.13.11.5, *References*.

6.13.11.1 Methodology

The reactivity of the Cobra fuel when transported in the ATR FFSC is evaluated using MCNP. The comparison of reactivity between HEU and LEU fuel originally performed in Section 6.13.4, *Most Reactive Fuel Element Model*, is repeated with an increased U-235 mass in the LEU fuel element of 450 g. The original cases are designated CEP01 and CEP10. U-235 mass in the LEU fuel element is increased by adjusting fuel meat densities. New densities are calculated consistent with the original methodology. No other changes are made except for modernization of material definitions.

6.13.11.2 Updated Fuel Meat Densities

LEU fuel meat densities are original calculated in Table 6.13-8. The LEU fuel meat densities are plate-specific and are derived from the plate fuel meat volumes and U-235 masses. New fuel meat densities are calculated by scaling the original fuel meat densities by a common factor such that the relative distribution of U-235 between plates in unchanged and the new fuel element total U-235 mass is 450 g.

Calculation of new LEU fuel meat densities is shown in Table 6.13-25. The calculation shown is for one sector of fuel plates, with a fuel Cobra fuel element consisting of three identical sectors (18 fuel plates). The original modeling of Cobra LEU fuel used 438.6 g of U-235 per element rather than the maximum allowable quantity of 435.8 g. The following ratios are utilized consistent with the original calculation:

- The LEU fuel uranium enrichment is 20 wt.% U-235.
- The LEU fuel meat consists of uranium silicide (U_3Si_2) mixed with aluminum. The uranium silicide is 92.69 wt.% uranium.
- The mass ratio of uranium silicide to aluminum is 4-to-1.

Table 6.13-25 – Updated Cobra LEU Fuel Meat Densities

Plate #	New U-235 Mass (g)	Fuel Meat Volume (cm^3)	Uranium Mass (g)	U_3Si_2 Mass (g)	Fuel Meat Mass (g)	Fuel Meat Density (g/cm^3)
1	13.2	13.442	66.18	71.40	89.24	6.6392
2	18.0	17.786	89.77	96.85	121.07	6.8069
3	22.6	22.155	112.86	121.76	152.20	6.8698
4	27.5	26.523	137.48	148.33	185.41	6.9904
5	31.9	30.892	159.54	172.12	215.15	6.9647
6	36.8	35.236	184.17	198.69	248.36	7.0485

6.13.11.3 Material Definition Modernization

All criticality modeling is performed using MCNP6.2 [1]. Default .80c and .90c (H-1 only) continuous energy neutron cross-sections are utilized, which are based on ENDF/B-VII.1 and processed at 293.6 K. Thermal neutron scattering data, based on ENDF/B-VII.0 and processed at 293.6 K, is applied to fuel plate aluminum (al27.22t, Al-27 in metal), package stainless steel (fe56.22t, Fe-56 in metal), and water (lwtr.20t, hydrogen in light water).

In accordance with guidance in [1], material compositions originally used in analysis of Cobra fuel are converted to isotopic compositions using the "mattool" utility [2] included with MCNP6.2. An exception is made for materials with carbon, where elemental carbon is utilized as this cross-section is actively updated rather than carbon isotopes. For materials with oxygen, the O-18 mass is proportionally redistributed into the O-16 and O-17 masses since O-18 cross-sections are not available. Cross-sections available for use in MCNP6.2 are discussed in [3].

The material compositions for the Cobra HEU fuel meat, Cobra LEU fuel meat, stainless steel, water, and Durablanket S are shown in Table 6.13-26, Table 6.13-27, Table 6.13-28, Table 6.13-29, and Table 6.13-30 respectively. Aluminum is modeled as solely Al-27.

Table 6.13-26 – Cobra HEU Fuel Meat Composition

Isotope	ZAID	Weight Fraction
U-235	92235	2.798492E-01
U-238	92238	1.786295E-02
Al-27	13027	7.022879E-01

Table 6.13-27 – Cobra LEU Fuel Meat Composition

Isotope	ZAID	Weight Fraction
U-235	92235	1.483096E-01
U-238	92238	5.932182E-01
Al-27	13027	1.999994E-01
Si-28	14028	5.371693E-02
Si-29	14029	2.826359E-03
Si-30	14030	1.929536E-03

Table 6.13-28 – Stainless Steel Composition

Isotope	ZAID	Weight Fraction
C	6000	8.000000E-04
Si-28	14028	9.186649E-03
Si-29	14029	4.833629E-04
Si-30	14030	3.299884E-04
P-31	15031	4.500000E-04
Cr-50	24050	7.930004E-03
Cr-52	24052	1.590288E-01
Cr-53	24053	1.837982E-02
Cr-54	24054	4.661392E-03
Mn-55	25055	2.000000E-02
Fe-54	26054	3.860150E-02
Fe-56	26056	6.283767E-01
Fe-57	26057	1.477152E-02
Fe-58	26058	2.000272E-03
Ni-58	28058	6.383782E-02
Ni-60	28060	2.543716E-02
Ni-61	28061	1.124191E-03
Ni-62	28062	3.643081E-03
Ni-64	28064	9.577429E-04

Table 6.13-29 – Water Composition

Isotope	ZAID	Weight Fraction
H-1	1001	1.118727E-01
H-2	1002	2.571391E-05
O-16	8016	8.877422E-01
O-17	8017	3.593948E-04

Table 6.13-30 – Durablanket S Composition

Isotope	ZAID	Weight Fraction
O-16	8016	5.012956E-01
O-17	8017	2.029452E-04
Al-27	13027	2.647353E-01
Si-28	14028	2.147528E-01
Si-29	14029	1.129939E-02
Si-30	14030	7.714015E-03

6.13.11.4 Results and Conclusions

Calculated effective multiplication factors, k_{eff}, along with associated standard deviations, σ, for the Cobra HEU and LEU payloads are shown in Table 6.13-31. As was done originally, the comparison is performed using a 9 × 9 × 1 array of packages under normal conditions of transport (NCT). The Cobra fuel handling enclosure and ATR FFSC fuel cavity are filled with full-density water.

Both models are run using 600 generations, with the first 100 generations skipped for calculation of k_{eff} and 100,000 neutrons per generation. These runs parameters are sufficient to ensure proper convergence behavior for k_{eff} and Shannon entropy. Furthermore, the run parameters ensure a high degree of confidence in the final results as k_{eff} values do not overlap at the 99% confidence level.

The results reconfirm the following statement in Section 6.13.4, *Most Reactive Fuel Element Model*:

> *"The LEU case is less reactive than the base HEU case despite the larger U-235 loading in LEU fuel because LEU fuel has increased parasitic neutron absorption in U-238. Therefore, it is sufficient to perform the Cobra criticality analysis for the HEU fuel element, as it bounds the LEU fuel element."*

No additional analysis is necessary as the original analysis remains conservative following the increase in Cobra LEU U-235 mass.

Table 6.13-31 – Updated Cobra Fuel Enrichment Comparison

Fuel Enrichment	k_{eff}	σ	99% Confidence Interval
HEU	0.67829	0.00011	[0.67800, 0.67859]
LEU	0.67472	0.00011	[0.67443, 0.67502]

6.13.11.5 References

1. C. J. Werner et al., *MCNP® User's Manual: Code Version 6.2*, LA-UR-17-29981, Revision 0, Los Alamos National Laboratory, Los Alamos NM, October 27th 2017 (Available for Radiation Safety Information Computational Center as CCC-850)
2. C. J. Solomon, *The Intrinsic Source Constructor Package: Installation and Use*, LA-UR-17-22234, Los Alamos National Laboratory – XCP-3, Los Alamos NM, March 30th 2017
3. J. L. Conlin, *Listing of Available ACE Data Tables*, LA-UR-17-20709, Los Alamos National Laboratory – Nuclear Data Team (XCP-5), Los Alamos NM, October 12th 2017

6.14 Appendix F: Criticality Analysis for ATR, MURR, MIT, and NBSR LEU Fuel Elements and/or DDEs

The ATR FFSC may be utilized to transport LEU versions of the ATR, MURR, and MIT fuel elements analyzed previously in this chapter. These fuel elements are plate-type fuels with similar geometry and layout to the previously-discussed HEU versions. The ATR FFSC may also be utilized to transport LEU DDEs for the MURR and MIT. DDEs have minor dimensional variations from standard fuel elements to support design verification and testing but are otherwise very similar to the LEU fuel elements.

Additionally, the ATR FFSC may be utilized to transport the LEU DDE for the NBSR. Similar to the other LEU payloads, this DDE is a plate-type fuel.

Due to significant similarities in materials, construction, and criticality behavior, the aforementioned LEU fuel elements and DDEs are jointly analyzed within this section. The following analyses demonstrate that the ATR FFSC when transporting ATR, MURR, MIT, and NBSR LEU fuel elements and/or DDEs complies with the requirements of 10 CFR 71.55 and 71.59. The Criticality Safety Index (CSI), per 10 CFR 71.59, is 4.0 for the ATR, MURR, MIT, and NBSR LEU fuel elements and/or DDEs.

6.14.1 Description of Criticality Design

6.14.1.1 Design Features

No special design features are required to maintain criticality safety. No poisons are utilized in the package. The separation provided by the packaging (outer flat-to-flat dimension of 7.9-in), along with the limit on the number of packages per shipment, is sufficient to maintain criticality safety.

6.14.1.2 Summary Table of Criticality Evaluation

The USL for ATR, MURR, MIT, and NBSR LEU fuel elements and/or DDEs is calculated on a case-by-case basis in Section 6.14.6, *Benchmark Evaluations*. The package is considered to be acceptably subcritical if the computed k_{safe} (k_s), which is defined as $k_{effective}$ (k_{eff}) plus twice the statistical uncertainty (σ), is less than or equal to the USL, or:

$$k_s = k_{eff} + 2\sigma \leq USL$$

The USL is determined on the basis of a benchmark analysis and incorporates the combined effects of code computational bias, the uncertainty in the bias based on both benchmark-model and computational uncertainties, and an administrative margin. The results of the benchmark analysis indicate that the USL is adequate to ensure subcriticality of the package.

The packaging design is shown to meet the requirements of 10 CFR 71.55(b)(d)(e) [8] (Note: references for this section are found in Section 6.14.7, *References*). Moderation by water in the most reactive credible extent is utilized in both the normal conditions of transport (NCT) and hypothetical accident conditions (HAC) analyses. In the single package NCT models, full-density water fills the accessible cavity, while in the single package HAC models, full-density water fills all cavities. In all single package and array models, 12-in of water reflection is utilized. In the NCT and HAC array cases, partial moderation is considered to maximize array interaction effects.

The maximum results of the criticality calculations are summarized in Table 6.14-1.

Table 6.14-1 – Summary of Criticality Evaluation (LEU Fuel Elements and DDEs)

	ATR LEU	MURR LEU	MIT LEU	NBSR LEU
Normal Conditions of Transport (NCT)				
Case	k_s	k_s	k_s	k_s
Single Unit Maximum	0.42385	0.5063	0.42693	0.39137
Array Maximum	0.79375 (8×8)	0.86146 (8×8)	0.68613 (9×9)	0.65257 (9×9)
Hypothetical Accident Conditions (HAC)				
Case	k_s	k_s	k_s	k_s
Single Unit Maximum	0.45393	0.58572	0.52045	0.50968
Array Maximum	0.72607 (5×5)	0.86625 (5×5)	0.72735 (5×5)	0.74897 (5×5)
Upper Subcritical Limit (USL)				
	0.91942	0.92071	0.92288	0.92348
Air Transport Analysis				
	k_s = 0.71171		USL = 0.90868	

6.14.1.3 Criticality Safety Index

The CSI, as defined in 10 CFR 71.59, is calculated as follows:

$$CSI = \frac{50}{N_{min}} \quad N_{NCT} = \frac{\#\ NCT\ Array\ Packages}{5} \quad N_{HAC} = \frac{\#\ HAC\ Array\ Packages}{2}$$

For the ATR, MURR, MIT, and NBSR LEU fuel elements and/or DDEs, the NCT and HAC arrays have ≥ 64 and 25 packages respectively, resulting in N values of ≥ 12.8 and 12.5. The CSI, calculated using N_{HAC}, is 4. A maximum of 12 packages (nonexclusive use) or 25 packages (exclusive use) are allowed per shipment.

6.14.2 Fissile Material Contents

All of the LEU fuel elements and DDEs consist of multiple fuel plates slotted into opposing side plates, with the opposing side plates restricting the movement of the fuel plates relative to each other. Each fuel plate consists of aluminum cladding surrounding a centrally-located fuel foil or 'meat'. The fuel meat and cladding are separated by 0.001-inch thick layers of zirconium (all dimensions nominal unless otherwise stated).

All fuel meat is U-10Mo. The molybdenum content is 10 ± 1 wt.%, with impurities limited to 1,200 ppm. The remaining alloy content is uranium, with a U-235 enrichment of 19.75 ± 0.20 wt.%. The uranium isotopic composition is shown in Table 6.14-2. The fuel meat density and dimensions are different for each fuel type.

Table 6.14-2 – LEU U-10Mo Uranium Composition

Isotope	Units	Limit
U-232	µg/gU	≤ 0.002
U-234	wt.% U	≤ 0.260%
U-235	wt.% U	19.75 ± 0.20%
U-236	µg/gU	≤ 4600
U-238	*Remaining mass*	

6.14.2.1 ATR LEU Fuel Element

The ATR LEU fuel element assembly consists of 19 curved fuel plates. Each ATR LEU fuel plate contains a 0.008-inch to 0.016-inch thick fuel meat. The total thickness of each plate is 0.050 inches to 0.100 inches. Fuel plate widths (by arc length) vary significantly and are between 2 inches and 4 inches, with cladding side widths between 0.160 inches to 0.190 inches. Fuel plate #1 is the smallest plate by midplane radius, with the size progressively increasing until the final and largest plate, fuel plate #19. The fuel meat height is 48 inches, while the fuel plate height is 49.5 inches. The channel thickness between fuel plates is 0.078 inches.

The nominal fuel meat volume and U-235 mass for each fuel plate is shown in Table 6.14-3. The total U-235 loading of an ATR LEU fuel element is 1,648 g ± 2%, with a nominal U-10Mo alloy density of 16.5 g/cm^3. The modeled U-235 loading is 1,699.2 g as shown in Table 6.14-9. The bounding value for transport is 1,681 g as shown in Table 1.1-1.

6.14.2.2 MURR LEU Fuel Element and DDE

The MURR LEU fuel element assembly consists of 23 curved fuel plates. Each fuel plate contains a 0.009-inch to 0.020-inch thick fuel meat. The total thickness of each plate is 0.044 inches to 0.049 inches, with cladding thicknesses between 0.0110 inches and 0.0165 inches. Fuel plate widths (by arc length) vary significantly and are between 1.9 inches and 4.4 inches. Fuel plate #1 is the smallest plate by midplane radius, with the size progressively increasing until the final and largest plate, fuel plate #23. The fuel meat height is 24 inches, while the fuel plate

height is 25.5 inches. The channel thickness between fuel plates is 0.092 inches to 0.093 inches. The MURR DDE will use the same fuel plates as the MURR LEU fuel element.

The U-235 mass loadings for each fuel plate are shown in Table 6.14-4. The total U-235 loading of a MURR LEU fuel element is 1,507 g ± 15.1 g, with a nominal U-10Mo alloy density of 17.0 g/cm^3. The tolerance on total U-235 mass is less than the sum of the individual plate tolerances. The modeled U-235 loading is 1,664.7 g as shown in Table 6.14-11. The bounding value for transport is 1,660 g as shown in Table 1.1-1.

6.14.2.3 MIT LEU Fuel Element and DDE

The MIT LEU fuel element assembly consists of 19 offset flat plates, forming a rhombus-shaped assembly. Each fuel plate contains a 0.013-inch to 0.025-inch thick fuel meat. The total thickness of each plate is 0.049 inches, with cladding thicknesses between 0.011 inches and 0.017 inches. There are three types of fuel plates: Type T (2 outermost plates in assembly), Type F (13 innermost plates), and Type Y (remaining 4 plates). The fuel meat height is 22.375 inches, while the fuel plate height is 23.00 inches. The channel thickness between fuel plates is at most 0.082 inches, with the fuel assembly average channel thickness not to exceed 0.079 inches. The MIT DDE will use the same fuel plates as the MIT LEU fuel element.

The U-235 mass loadings for each fuel plate are shown in Table 6.14-5. The total U-235 loading of a MIT LEU fuel element is 968 g ± 9.7 g, with a nominal U-10Mo alloy density of 17.0 g/cm^3. The tolerance on total U-235 mass is less than the sum of the individual plate tolerances. The modeled U-235 loading is 1,092.45 g as shown in Table 6.14-13. The bounding value for transport is 1,070 g as shown in Table 1.1-1.

6.14.2.4 NBSR DDE

The NBSR LEU DDE consists of 34 curved fuel plates. The fuel plates are axially stacked within the assembly, with a 2-inch gap separating two sets of 17 plates. Each fuel plate contains a 0.0085-inch thick fuel meat. The total thickness of each plate is 0.050 inches. The fuel meat height is up to 11.635 inches, while the fuel plate height is 13.000 inches. The fuel plate is manufactured flat, with a width of 2.79 inches, before being rolled to a curvature radius of 5.500 inches. The channel thickness between fuel plates is 0.116 inches.

The U-235 fuel loading of a single fuel plate is 11.27 g ± 0.24 g, resulting in a total U-235 loading of 383.18 g ± 8.16 g for a single NBSR DDE. The nominal density of the U-10Mo alloy density is 17.2 g/cm^3. The modeled U-235 loading is 481 g. The bounding value for transport is 460 g as shown in Table 1.1-1.

Table 6.14-3 – ATR LEU Fuel Meat Nominal Parameters

Plate #	Fuel Meat Volume (cm^3)	U-235 Mass (g)
1	11.15	33.5
2	19.26	57.9
3	20.29	60.9
4	26.24	78.8
5	27.50	82.6
6	28.77	86.4
7	30.03	90.2
8	31.30	94.0
9	32.56	97.8
10	33.83	101.6

Plate #	Fuel Meat Volume (cm^3)	U-235 Mass (g)
11	35.09	105.4
12	36.36	109.2
13	37.62	113.0
14	38.89	116.8
15	40.15	120.6
16	33.65	101.1
17	21.34	64.1
18	21.98	66.0
19	22.73	68.3
Total	*548.74*	*1648.1*

Table 6.14-4 – MURR LEU U-235 Mass by Fuel Plate

Plate #	U-235 Mass (g)	Tolerance (g)
1	18.09	2.01
2	25.66	2.14
3	36.26	2.27
4	47.89	2.39
5	50.45	2.52
6	52.99	2.65
7	55.53	2.78
8	58.07	2.90
9	60.61	3.03
10	63.16	3.16
11	65.70	3.28
12	68.24	3.41

Plate #	U-235 Mass (g)	Tolerance (g)
13	70.78	3.54
14	73.32	3.67
15	75.86	3.79
16	78.41	3.92
17	80.95	4.05
18	83.49	4.17
19	86.03	4.30
20	88.59	4.43
21	91.15	4.56
22	93.71	4.69
23	81.87	4.82
Total	*1507*	*15.1*

Table 6.14-5 – MIT LEU U-235 Mass by Fuel Plate

Plate #	Plate Type	U-235 Mass (g)	Tolerance (g)
1	T	30.02	1.05
2	Y	39.26	1.37
3	Y	39.26	1.37
4	F	57.74	2.02
5	F	57.74	2.02
6	F	57.74	2.02
7	F	57.74	2.02
8	F	57.74	2.02
9	F	57.74	2.02
10	F	57.74	2.02
11	F	57.74	2.02
12	F	57.74	2.02
13	F	57.74	2.02
14	F	57.74	2.02
15	F	57.74	2.02
16	F	57.74	2.02
17	Y	39.26	1.37
18	Y	39.26	1.37
19	T	30.02	1.05
Total		*968*	*9.7*

6.14.3 General Considerations

6.14.3.1 Model Configuration

All relevant design features of the LEU fuel elements, DDEs, and ATR FFSC are modeled in MCNP. Since the package is long and narrow, array configurations are stacked only in the lateral directions. All models are surrounded by 12 inches of water reflection.

Fuel element and DDE modeling is limited to the fuel plates. Non-fuel components such as end boxes and side plates are conservatively not modeled and instead replaced by variable-density moderator. For NCT, the side plates are assumed to maintain the fuel plates in a fixed spacing. This fixed spacing assumption is also applied for the ATR LEU fuel element under HAC. For all other fuel elements and DDEs under HAC, it is assumed that the side plates could fail and thus the fuel plates can freely separate. No damage to the fuel plates themselves is modeled. The zirconium interlayers within each fuel plate are not modeled and are instead included as part of the aluminum cladding. Fuel modeling is axially limited to the region encompassing the respective fuel meat. For conservatism, the fuel plates are modeled using worst-case tolerances.

Due to the simplifications used in modeling, separate models are not necessary to evaluate fuel elements and DDEs of the same type.

Due to its moderating qualities, neoprene material which may be present in FHEs is accounted for. Neoprene is modeled without chlorine and assumed to possibly become homogenized with water inside the ATR FFSC cavity. Neoprene is only credited when its presence is concluded to increase reactivity.

NCT and HAC single package models are shown in Figure 6.14-1 through Figure 6.14-4. The figures show the fuel meat (green, may not be visible due to size), fuel cladding (pink), flooded water (blue), insulation (yellow), and steel (brown). Empty space is modeled as void (white). The outline of the MURR LEU FHE and MIT FHE inner cavities, with NCT dimensions as-built and HAC dimensions following damage, can be seen on the respective figures. On all figures, the fuel bag region can be seen to encompass the channels between fuel plates.

6.14.3.1.1 ATR FFSC

The ATR FFSC is modeled consistent with the other criticality analyses in this chapter. The ATR FFSC model consists of the inner tube, insulation, and the outer shell. Material volumes are conservatively minimized to minimize parasitic absorption.

The inner tube is 6.0-inch outer diameter, 0.120-inch thick ASTM A269 tubing. Tolerances for ASTM A269 tubing of that diameter are ± 0.030 inches for outer diameter and ± 10% for wall thickness [1]. Thus, the inner tube is modeled with a 6.03-inch outer diameter (maximizing cavity volume and minimizing insulation) and 0.108-inch wall thickness. Similarly, the outer shell is 8.0-inch outer side length, 0.188-inch thick ASTM A554 tubing. Tolerances for ASTM A554 tubing of that size are ± 0.060 inches for side length and ± 10% for wall thickness [2]. Using a bounding tolerance of 0.1 inches for side length, the outer shell is modeled with a 7.9-inch outer side length and 0.169-inch wall thickness. Insulation is modeled as 1-inch thick, starting at the inner tube outer diameter and truncated as necessary to fit within the square outer shell. During HAC, the insulation may be lost and thus is not credited. No other changes are made to the ATR FFSC model during HAC as damage is limited to the not-modeled package ends.

The fuel plates are assumed to be transported in a bag, for which the moderator density can vary independently from the rest of the ATR FFSC inner tube. The bag region is defined to be between the fuel plates and limited by the fuel plate widths. Up to 200 grams of polyethylene may be shipped in the cavity and assumed to possibly become homogenized with water inside the ATR FFSC cavity (either within or outside the bag region). Polyethylene is only credited when its presence is concluded to increase reactivity.

ATR FFSC model dimensions are summarized in Table 6.14-6.

6.14.3.1.2 ATR LEU Fuel Element

Fuel meat volume is maximized by modeling the maximum allowable fuel meat arc length and height, while fuel plate volume (i.e. fuel meat plus cladding) is minimized by modeling the minimum fuel plate thickness. All other dimensions do not have explicitly specified tolerances and thus are modeled as nominal.

Plate-specific modeled dimensions are shown in Table 6.14-8. The modeled fuel meat height is 48.25 inches. The modeled NCT channel thicknesses either meet or exceed the nominal channel thicknesses. The modeled meat volume and U-235 mass for each fuel plate is shown in Table 6.14-9. The individual fuel meat U-235 masses are at least 2.3% greater than nominal masses, with the total U-235 mass 3.1% greater than nominal. This exceeds the ± 2% tolerance on U-235 mass specified in Section 6.14.2.1. The modeled U-235 mass also exceeds the authorized maximum of 1,681 g (see Table 1.1-1).

The ATR FHE is not modeled, but neoprene rub strips are accounted for based on the ATR FHE design. The total volume of the neoprene rub strips is 62.65 in^3.

6.14.3.1.3 MURR LEU Fuel Element and DDE

Fuel meat mass is increased beyond specified tolerances by first increasing the fuel meat density to a maximum possible density of 17.2 g/cm^3 and then increasing the fuel meat thickness an additional 0.003 inches. This is done to bound possible adjustments to the fuel design. Fuel plate volume (i.e. fuel meat plus cladding) is minimized by modeling the minimum fuel plate thickness. All other dimensions do not have explicitly specified tolerances and thus are modeled as nominal.

Plate-specific modeled dimensions are shown in Table 6.14-10. The modeled fuel meat height is 24.2 inches. The modeled NCT channel thicknesses exceed nominal channel thicknesses. The modeled fuel meat U-235 mass for each fuel plate is shown in Table 6.14-11. The individual fuel meat U-235 masses are at least 5.0% greater than the respective nominal plus tolerance masses, with the total U-235 mass 9.4% greater than the total nominal plus tolerance mass. The modeled U-235 mass also exceeds the authorized maximum of 1,660 g (see Table 1.1-1).

Credit is taken for the MURR LEU FHE in restricting the movement of the fuel plates, but the aluminum material of the FHE is not modeled. Fuel plate movement is limited to within the confines of the FHE during both NCT and HAC. HAC damage to the FHE is modeled per Figure 2.12.3-4. The total volume of the FHE neoprene rub strips is 22.41 in^3.

6.14.3.1.4 MIT LEU Fuel Element and DDE

Fuel meat mass is increased beyond specified tolerances by first increasing the fuel meat density to a maximum possible density of 17.2 g/cm^3 and then increasing the fuel meat thickness an additional 0.001 inches. This is done to bound possible adjustments to the fuel design. Fuel meat volume is maximized by modeling maximum fuel meat width and height. Fuel plate volume (i.e. fuel meat plus cladding) is minimized by modeling the minimum fuel plate thickness and width. Fuel plate thickness is reduced an additional 0.002 inches so that all channel thicknesses meet or exceed the maximum allowable average.

Plate-specific modeled dimensions are shown in Table 6.14-12. The modeled fuel meat height is 22.390 inches. The modeled NCT channel thicknesses exceed the nominal channel thicknesses. The modeled fuel meat U-235 mass for each fuel plate is shown in Table 6.14-13. The individual fuel meat U-235 masses are at least 8.5% greater than the respective nominal plus tolerance masses, with the total U-235 mass 11.7% greater than the total nominal plus tolerance mass. The modeled U-235 mass also exceeds the authorized maximum of 1,070 g (see Table 1.1-1).

Credit is taken for the MIT FHE in restricting the movement of the fuel plates, but the aluminum material of the FHE is not modeled. Fuel plate movement is limited to within the confines of the FHE during both NCT and HAC. HAC damage to the FHE is modeled per Figure 2.12.3-3. The total volume of the FHE neoprene rub strips is 20.74 in^3.

6.14.3.1.5 NBSR DDE

Fuel meat mass is increased beyond the specified tolerances by increasing the fuel meat thickness an additional 0.001 inches. This is done to bound possible adjustments to the fuel design. Fuel meat volume is maximized by modeling maximum fuel meat width and height. Fuel plate volume (i.e. fuel meat plus cladding) is minimized by modeling the minimum thickness and height.

Plate-specific modeled dimensions are shown in Table 6.14-7. The modeled U-235 mass is 14.16 g per fuel plate, resulting in 481 g U-235 per DDE. The total U-235 mass is 23% greater than the total nominal plus tolerance mass. The modeled U-235 mass also exceeds the authorized maximum of 460 g (see Table 1.1-1).

Table 6.14-6 – Key ATR FFSC Model Dimensions

Item	Nominal (in)	Modeled (in)
Inner round tube outer diameter	6.0	6.03
Inner round tube wall thickness	0.120	0.108
Insulation thickness	1.0	1.0
Outer square tube outer side length	8.0	7.9
Outer square tube wall thickness	0.188	0.169

Table 6.14-7 – Key NBSR LEU Model Dimensions

Item	Nominal (in)	Modeled (in)
Fuel Meat Thickness	0.0085	0.0095
Fuel Meat Flat-to-Flat Width	2.5030 (prior to rolling)	2.5030
Fuel Meat Height	11.625	11.635
Fuel Plate Thickness	0.050	0.048
Fuel Plate Flat-to-Flat Width	2.7930 (prior to rolling)	2.7930
Fuel Plate Height	13.000	12.010
Plate Curvature Radius	5.500	5.500
Channel Thickness	0.116	0.123

Table 6.14-8 – Key ATR LEU Model Dimensions

Plate #	Fuel Meat Thickness (in)	Fuel Plate Thickness (in)	Fuel Meat Arc (deg)	Fuel Plate Arc (deg)	NCT Channel Thickness (in)
1	0.008	0.079	34.7	40.0	-
2	0.013	0.049	35.2	39.1	0.080
3	0.013	0.049	35.5	39.3	0.079
4	0.016	0.049	35.9	39.5	0.078
5	0.016	0.049	36.2	39.8	0.079
6	0.016	0.049	36.5	39.9	0.079
7	0.016	0.049	36.8	40.1	0.079
8	0.016	0.049	37.1	40.3	0.079
9	0.016	0.049	37.3	40.4	0.079
10	0.016	0.049	37.5	40.5	0.079
11	0.016	0.049	37.8	40.7	0.079
12	0.016	0.049	38.0	40.8	0.079
13	0.016	0.049	38.2	40.9	0.079
14	0.016	0.049	38.4	41.0	0.078
15	0.016	0.049	38.5	41.1	0.079
16	0.013	0.049	38.7	41.2	0.079
17	0.008	0.049	38.9	41.3	0.079
18	0.008	0.049	39.0	41.4	0.079
19	0.008	0.099	39.2	42.2	0.078

Table 6.14-9 – ATR LEU Fuel Meat Model Parameters

Plate #	Fuel Meat Volume (cm^3)	U-235 Mass (g)
1	11.68	35.0
2	20.15	60.3
3	21.17	63.4
4	27.33	81.9
5	28.60	85.7
6	29.87	89.5
7	31.15	93.3
8	32.41	97.1
9	33.69	100.9
10	34.95	104.7

Plate #	Fuel Meat Volume (cm^3)	U-235 Mass (g)
11	36.22	108.5
12	37.50	112.3
13	38.77	116.1
14	40.04	119.9
15	41.30	123.7
16	34.60	103.6
17	21.92	65.7
18	22.56	67.6
19	23.32	69.8
Total	*567.24*	*1699.2*

Table 6.14-10 – Key MURR LEU Model Dimensions

Plate #	Fuel Meat Thickness (in)	Fuel Plate Thickness (in)	Fuel Meat Arc (deg)	Fuel Plate Arc (deg)	NCT Channel Thickness (in)
1	0.010	0.042	34.9	40.8	-
2	0.013	0.042	35.3	41.0	0.095
3	0.017	0.042	35.8	41.2	0.095
4	0.021	0.042	36.2	41.4	0.095
5	0.021	0.042	36.5	41.5	0.095
6	0.021	0.042	36.9	41.7	0.094
7	0.021	0.042	37.2	41.8	0.094
8	0.021	0.042	37.4	41.9	0.094
9	0.021	0.042	37.7	42.0	0.094
10	0.021	0.042	38.0	42.1	0.094
11	0.021	0.042	38.2	42.2	0.094
12	0.021	0.042	38.4	42.3	0.094
13	0.021	0.042	38.6	42.4	0.094
14	0.021	0.042	38.8	42.5	0.094
15	0.021	0.042	39.0	42.5	0.094
16	0.021	0.042	39.2	42.6	0.094
17	0.021	0.042	39.3	42.7	0.094
18	0.021	0.042	39.5	42.7	0.094
19	0.021	0.042	39.6	42.8	0.094
20	0.021	0.042	39.7	42.8	0.095
21	0.021	0.042	39.9	42.9	0.095
22	0.021	0.042	40.0	42.9	0.095
23	0.018	0.047	40.1	43.0	0.095

Table 6.14-11 – MURR LEU Fuel Meat Model Parameters

Plate #	U-235 Mass (g)	Mass Above Max Allowable (g)	Plate #	U-235 Mass (g)	Mass Above Max Allowable (g)
1	21.31	1.21	13	78.00	3.68
2	29.33	1.53	14	80.81	3.82
3	40.53	2.00	15	83.62	3.97
4	52.77	2.49	16	86.42	4.09
5	55.60	2.63	17	89.23	4.23
6	58.41	2.77	18	92.01	4.35
7	61.22	2.91	19	94.82	4.49
8	64.00	3.03	20	97.65	4.63
9	66.80	3.16	21	100.46	4.75
10	69.61	3.29	22	103.29	4.89
11	72.42	3.44	23	91.14	4.45
12	75.22	3.57	*Total*	*1664.67*	*142.57*

Table 6.14-12 – Key MIT LEU Model Dimensions

Plate #	Fuel Meat Thickness (in)	Fuel Meat Width (in)	Fuel Plate Thickness (in)	Fuel Plate Width (in)	NCT Channel Thickness (in)
1	0.014	2.177	0.044	2.521	-
2	0.018	2.177	0.044	2.521	0.080
3	0.018	2.177	0.044	2.521	0.079
4	0.026	2.177	0.044	2.521	0.080
5	0.026	2.177	0.044	2.521	0.080
6	0.026	2.177	0.044	2.521	0.079
7	0.026	2.177	0.044	2.521	0.080
8	0.026	2.177	0.044	2.521	0.079
9	0.026	2.177	0.044	2.521	0.080
10	0.026	2.177	0.044	2.521	0.080
11	0.026	2.177	0.044	2.521	0.079
12	0.026	2.177	0.044	2.521	0.080
13	0.026	2.177	0.044	2.521	0.079
14	0.026	2.177	0.044	2.521	0.080
15	0.026	2.177	0.044	2.521	0.080
16	0.026	2.177	0.044	2.521	0.079
17	0.018	2.177	0.044	2.521	0.080
18	0.018	2.177	0.044	2.521	0.079
19	0.014	2.177	0.044	2.521	0.080

Table 6.14-13 – MIT LEU Fuel Meat Model Parameters

Plate #	U-235 Mass (g)	Mass Above Max Allowable (g)
1	34.92	3.85
2	44.90	4.27
3	44.90	4.27
4	64.85	5.09
5	64.85	5.09
6	64.85	5.09
7	64.85	5.09
8	64.85	5.09
9	64.85	5.09
10	64.85	5.09

Plate #	U-235 Mass (g)	Mass Above Max Allowable (g)
11	64.85	5.09
12	64.85	5.09
13	64.85	5.09
14	64.85	5.09
15	64.85	5.09
16	64.85	5.09
17	44.90	4.27
18	44.90	4.27
19	34.92	3.85
Total	*1092.45*	*115.75*

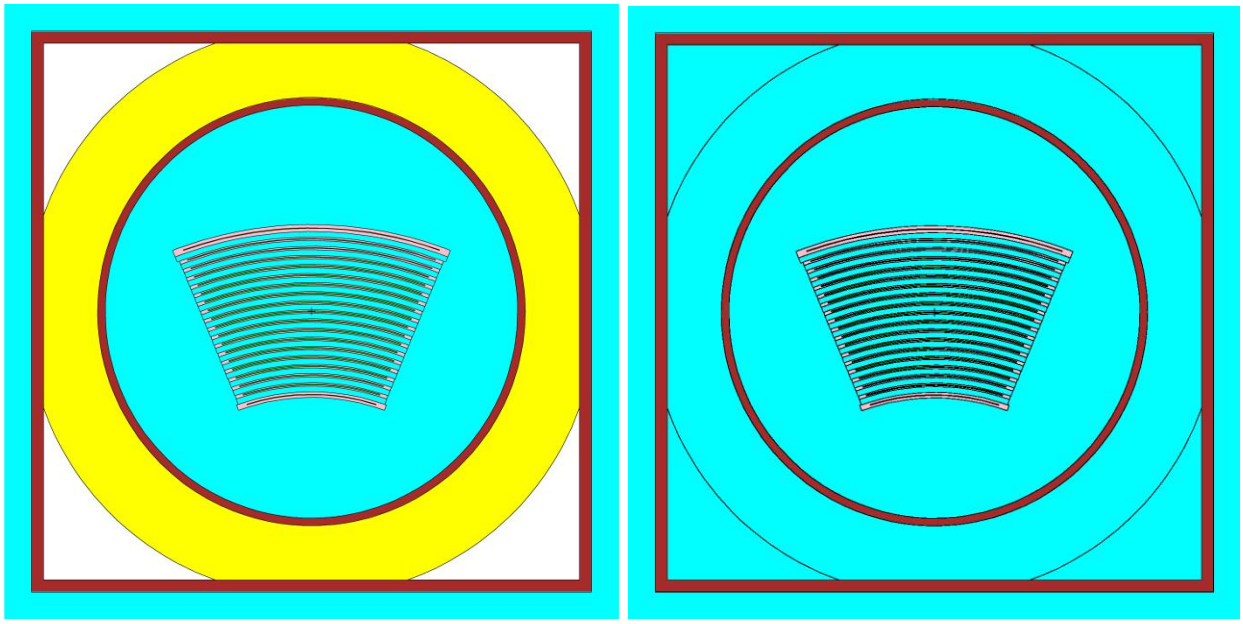

Figure 6.14-1 – ATR LEU Single Package, NCT and HAC

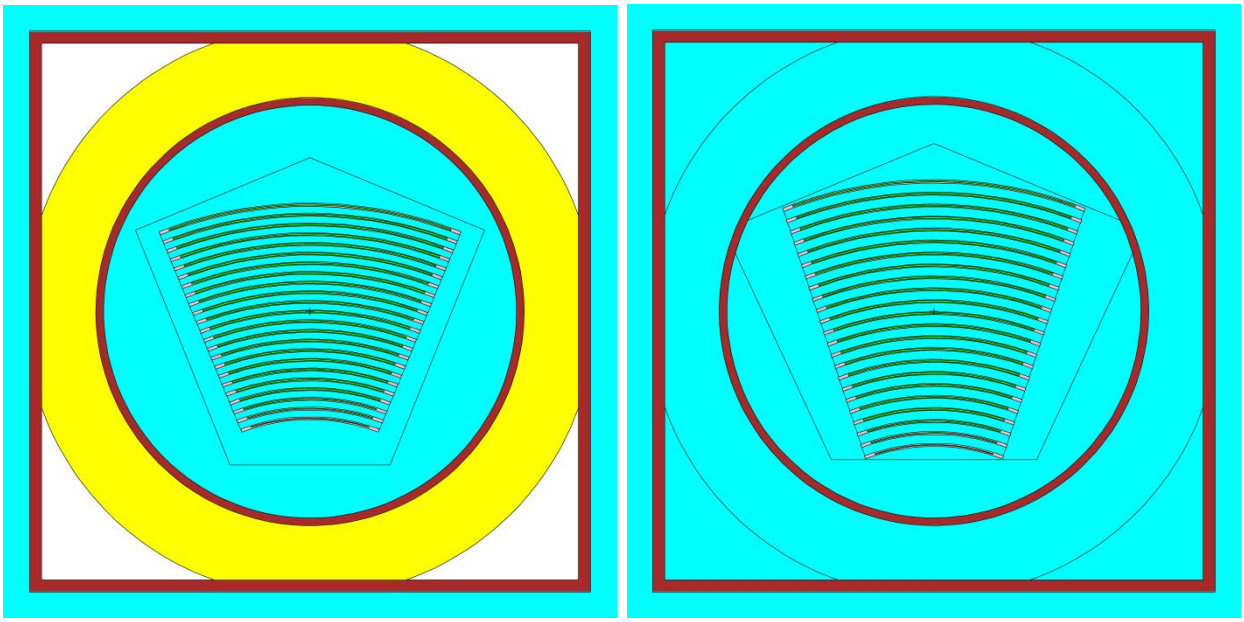

Figure 6.14-2 – MURR LEU Single Package, NCT and HAC

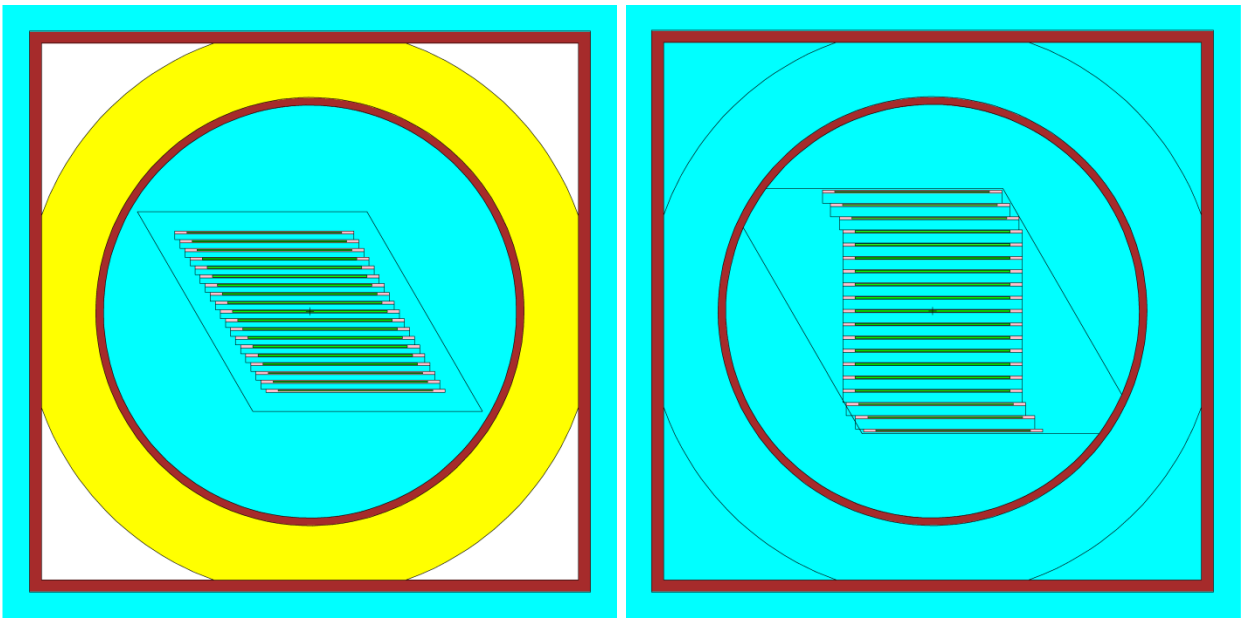

Figure 6.14-3 – MIT LEU Single Package, NCT and HAC

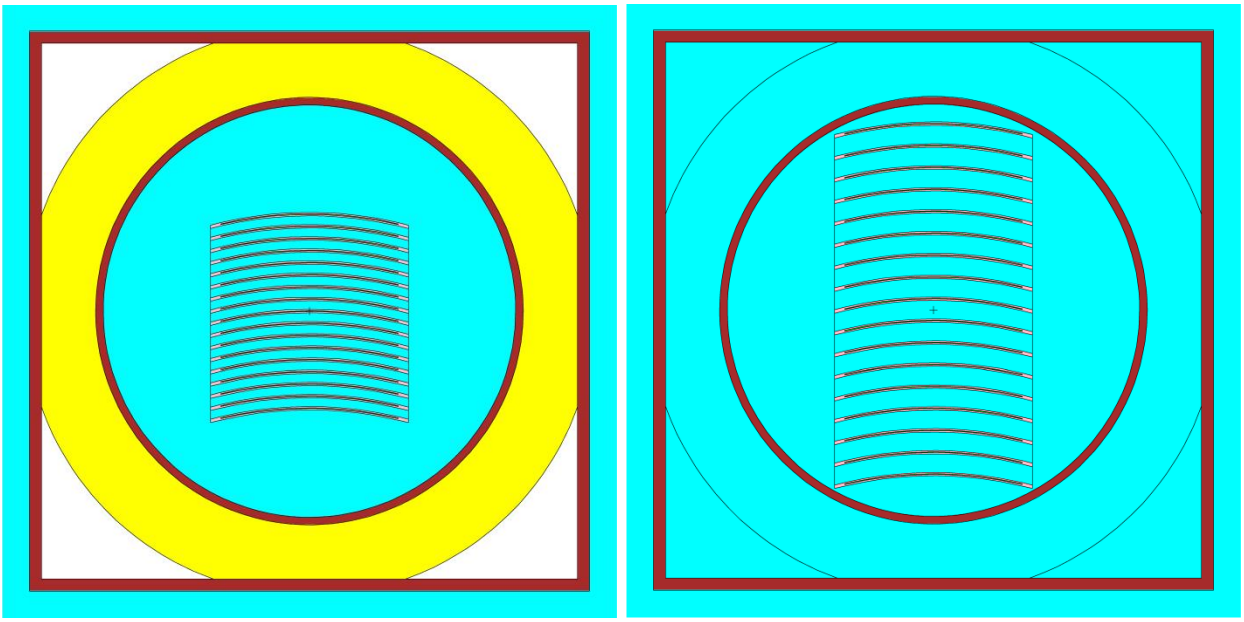

Figure 6.14-4 – NBSR LEU Single Package, NCT and HAC

6.14.3.2 Material Properties

In accordance with MCNP developer guidance, elemental compositions are converted to isotopic compositions using the "mattool" utility [3] included with MCNP6.2. An exception is made for materials with carbon, where elemental carbon is utilized as this cross-section is actively updated rather than carbon isotopes. For materials with oxygen, O-18 mass is redistributed into O-16 and O-17 masses since O-18 cross-sections are not available. Cross-sections available for use in MCNP6.2 are discussed in [4].

The fuel meat is constructed of U-10Mo fuel. The fuel is modeled such that uranium content is maximized (9% Mo, 91% wt.% U) and the enrichment is also maximized (19.95 wt.% U-235). All other uranium isotopes are modeled at their respective limits with the remaining mass filled by U-238. The U-10Mo composition is shown in Table 6.14-14. The fuel meat density is 16.5 g/cm^3 for the ATR LEU and 17.2 g/cm^3 for all other fuel types. Fuel density is increased beyond nominal values, up to a manufacturing maximum of 17.2 g/cm^3, to ensure fuel masses exceed respective tolerances and bound possible adjustments to fuel designs.

The fuel plate cladding is aluminum alloy 6061-O. The ATR FFSC structural tubing is type 304 stainless steel. The compositions for these materials are obtained from [5] and shown in Table 6.14-17 and Table 6.14-19 respectively.

Consistent with other analyses in this chapter, Durablanket S insulation is modeled as equal parts Al_2O_3 and SiO_2 by weight. The density is 6 pounds per cubic foot (0.096 g/cm^3). The Durablanket S composition is shown in Table 6.14-15.

Compositions for neoprene, polyethylene, and water are obtained from [5]. Water may be modeled as pure or homogenized with neoprene and/or polyethylene. Neoprene is conservatively modeled without chlorine, which is a neutron absorber. Neoprene density is adjusted to reflect the loss of chlorine. Materials are homogenized by (1) calculating the mass and volume of each sub-material, (2) calculating the isotopic masses for each sub-material using weight fractions and sub-material mass, and (3) summing isotopic masses into a homogenized material definition. The homogenized material density is calculated using the total mass and volume. The compositions for neoprene, polyethylene, and water are shown in Table 6.14-18, Table 6.14-20, and Table 6.14-16 respectively. For cases in which the homogenized material density is adjusted, the input water density is adjusted while the neoprene and/or polyethylene densities remain constant.

The composition of wood, for use in the air transport analysis, is taken from [5] and shown in Table 6.14-21. This material is discussed in Section 6.14.5.

Table 6.14-14 – U-10Mo Composition

Reference			*Modeled*	
Element	**ZAID**	**Wt. Fraction**	**ZAID**	**Wt. Fraction**
Mo	42000	9.00000E-02	42092	1.273450E-02
			42094	8.131011E-03
			42095	1.415610E-02
			42096	1.500685E-02
			42097	8.690852E-03
			42098	2.221755E-02
			42100	9.063129E-03
U-232	92232	1.82000E-09	92232	1.820000E-09
U-234	92234	2.36600E-03	92234	2.366000E-03
U-235	92235	1.81545E-01	92235	1.815450E-01
U-236	92236	4.18600E-03	92236	4.186000E-03
U-238	92238	7.21903E-01	92238	7.219030E-01

Table 6.14-15 – Durablanket S Composition (Density = 0.096 g/cm^3)

Reference			*Modeled*	
Element	**ZAID**	**Wt. Fraction**	**ZAID**	**Wt. Fraction**
O	8000	50.2	8016	5.012956E-01
			8017	2.029452E-04
Al	13000	26.5	13027	2.647353E-01
Si	14000	23.4	14028	2.147528E-01
			14029	1.129939E-02
			14030	7.714015E-03

Table 6.14-16 – Water Composition (Density = 1.0 g/cm^3)

Reference			*Modeled*	
Element	**ZAID**	**Wt. Fraction**	**ZAID**	**Wt. Fraction**
H	1000	0.111894	1001	1.118683E-01
			1002	2.571290E-05
O	8000	0.888106	8016	8.877466E-01
			8017	3.593967E-04

Table 6.14-17 – Aluminum Alloy 6061-O Composition (Density = 2.7 g/cm^3)

Reference			*Modeled*	
Element	**ZAID**	**Wt. Fraction**	**ZAID**	**Wt. Fraction**
Mg	12000	0.010000	12024	7.794921E-03
			12025	1.028000E-03
			12026	1.176980E-03
Al	13000	0.972000	13027	9.719903E-01
Si	14000	0.006000	14028	5.511934E-03
			14029	2.900148E-04
			14030	1.979911E-04
Ti	22000	0.000880	22046	6.969614E-05
			22047	6.421984E-05
			22048	6.498300E-04
			22049	4.868279E-05
			22050	4.756247E-05
Cr	24000	0.001950	24050	8.138607E-05
			24052	1.632121E-03
			24053	1.886331E-04
			24054	4.784012E-05
Mn	25000	0.000880	25055	8.799912E-04
Fe	26000	0.004090	26054	2.309010E-04
			26056	3.758735E-03
			26057	8.835819E-05
			26058	1.196495E-05
Cu	29000	0.002750	29063	1.883159E-03
			29065	8.668135E-04
Zn	30000	0.001460	30064	6.887649E-04
			30066	4.116611E-04
			30067	6.127886E-05
			30068	2.884319E-04
			30070	9.848649E-06

Table 6.14-18 – Neoprene Composition
(No Chlorine, Density = 0.737 g/cm^3)

Reference			*Modeled*	
Element	**ZAID**	**Wt. Fraction**	**ZAID**	**Wt. Fraction**
H	1000	0.056920	1001	9.491352E-02
			1002	2.181585E-05
C	6000	0.542646	6000	9.050647E-01

Table 6.14-19 – Type 304 Stainless Steel Composition (Density = 8.00 g/cm^3)

Reference			*Modeled*	
Element	**ZAID**	**Wt. Fraction**	**ZAID**	**Wt. Fraction**
C	6000	0.000400	6000	3.999960E-04
Si	14000	0.005000	14028	4.593278E-03
			14029	2.416790E-04
			14030	1.649926E-04
P	15000	0.000230	15031	2.299977E-04
S	16000	0.000150	16032	1.420716E-04
			16033	1.156799E-06
			16034	6.753296E-06
			16036	1.682534E-08
Cr	24000	0.190000	24050	7.929925E-03
			24052	1.590272E-01
			24053	1.837963E-02
			24054	4.661345E-03
Mn	25000	0.010000	25055	9.999900E-03
Fe	26000	0.701730	26054	3.961618E-02
			26056	6.448942E-01
			26057	1.515980E-02
			26058	2.052851E-03
Ni	28000	0.092500	28058	6.215726E-02
			28060	2.476752E-02
			28061	1.094596E-03
			28062	3.547175E-03
			28064	9.325298E-04

Table 6.14-20 – Polyethylene Composition (Density = 0.930 g/cm^3)

Reference			*Modeled*	
Element	**ZAID**	**Wt. Fraction**	**ZAID**	**Wt. Fraction**
H	1000	0.143716	1001	1.436830E-01
			1002	3.302550E-05
C	6000	0.856284	6000	8.562840E-01

Table 6.14-21 – Wood Composition (Density = 0.64 g/cm^3)

Reference			***Modeled***	
Element	**ZAID**	**Wt. Fraction**	**ZAID**	**Wt. Fraction**
H	1000	0.059642	1001	5.962835E-02
			1002	1.370556E-05
C	6000	0.497018	6000	4.970185E-01
N	7000	0.00497	7014	4.950631E-03
			7015	1.937388E-05
O	8000	0.427435	8016	4.272625E-01
			8017	1.729736E-04
Mg	12000	0.001988	12024	1.549647E-03
			12025	2.043686E-04
			12026	2.339861E-04
S	16000	0.00497	16032	4.707357E-03
			16033	3.832904E-05
			16034	2.237617E-04
			16036	5.574856E-07
K	19000	0.001988	19039	1.847591E-03
			19040	2.377463E-07
			19041	1.401736E-04
Ca	20000	0.001988	20040	1.921638E-03
			20042	1.346592E-05
			20043	2.876710E-06
			20044	4.548182E-05
			20046	9.117818E-08
			20048	4.447989E-06

6.14.3.3 Computer Codes and Cross-Section Libraries

All criticality modeling is performed using MCNP6.2 [6]. Default .80c and .90c (H-1 only) continuous energy neutron cross-sections are utilized, which are based on ENDF/B-VII.1 and processed at 293.6 K. Thermal neutron *S(α, β)* scattering data, based on ENDF/B-VII.0 and processed at 293.6 K, is applied to aluminum cladding (al27.22t, aluminum-27 metal), stainless steel (fe56.22t, iron-56 metal), and all pure or homogenized water (lwtr.20t, hydrogen in light water). All cases are run using 250 generations, with the first 50 generations skipped for calculation of k_{eff} and 10,000 neutrons per generation. These run parameters are sufficient to ensure proper convergence behavior for k_{eff} and Shannon entropy.

Calculation of USL is performed based on select cases using Whisper-1.1 [7] with Whisper default options. Cases are re-run in MCNP6.2 to calculate sensitivity coefficients using 600 generations, with the first 100 generations skipped and 10,000 neutrons per generation. The cases are analyzed in Whisper using 988 benchmarks (113 outliers identified by the developers are excluded from full set of 1,101 benchmarks).

6.14.3.4 Demonstration of Maximum Reactivity

The U-235 mass is maximized within each fuel plate by maximizing fuel meat volume, uranium content, and enrichment without any offsetting reductions in fuel density or composition. Fuel plate cladding is minimized and structural components such as the fuel plate side plates, fuel plate end boxes, and FHE are not modeled except for moderating materials such as FHE neoprene. Volumes otherwise filled by these components can be filled by variable-density moderator or movement of the fuel plates. Moderating materials are allowed to become perfectly homogenized with water to maximize their effect.

No modeling of the ends of the ATR FFSC is performed. Modeling is axially limited to the maximum length of the fuel meat, reducing the amount of neutron absorbing materials. Axial water reflection begins at the ends of the fuel meat, maximizing the reflection of neutrons back into fuel.

For NCT, the fuel plates remain in a fixed spacing but may move freely as a group within the package cavity to maximize reactivity. For array cases, all fuel plates are shifted towards the center of the array. Water moderation is allowed within the package cavity because the package lid does not contain a seal. Since fuel elements may be transported in a thin bag, the level of moderation is allowed to vary independently between the fuel plates and outside the fuel plates but within the package cavity. Bag moderation is adjusted to have ideal moderation between fuel plates, while inner tube moderation is adjusted to either maximize reflection (single package) or balance leakage and moderation between packages (array cases). Moderating materials may become homogenized with water in either region (or not, if materials decrease reactivity).

For HAC, the side plates of the fuel elements are assumed to fail and the fuel plates are allowed to move independent of each other (except for ATR LEU fuel elements, which maintain a fixed spacing). Fuel plate spacing is adjusted to maximize reactivity. For array cases, all fuel plates are reoriented towards the center of the array. Water moderation is allowed within the package cavity or within the outer shell as damage may allow water into any region of the package. The insulation in the outer shell may be lost and thus is replaced by variable-density moderator. The bag holding the fuel plates is assumed to remain intact for altered fuel plate spacing. The level of moderation is allowed to vary independently between the fuel plates, outside the fuel plates but within the inner tube, and outside the inner tube but within the package outer shell. Similar to NCT, bag moderation is adjusted to have ideal moderation between fuel plates, while inner tube and outer shell moderation is adjusted to either maximize reflection (single package) or balance leakage and moderation between packages (array cases). Moderating materials may become homogenized with water in the two regions within the package cavity.

Maximum reactivity for the air transport analysis is discussed in Section 6.14.5.

6.14.4 Package Criticality Calculations

The package is considered to be acceptably subcritical if the computed k_{safe}, which is defined as $k_{effective}$ (k_{eff}) plus two standard deviations (σ), is less than or equal to the USL for all cases.

$$k_{safe} = k_{eff} + 2\sigma \leq USL$$

Results are reported using k_{safe}. The standard deviation for all cases is less than or equal to 0.00070. The maximum k_{safe} for each series of cases is listed in boldface.

6.14.4.1 NCT Single Package Evaluation

6.14.4.1.1 Configuration

The NCT single package baseline configuration is the fuel plates centered in the cavity with full density pure water in both the fuel plate bag and inner tube. This configuration maximizes moderation between the fuel plates and reflection outside of the fuel plates. In the first series of cases, the water density inside the fuel plate bag and inside the inner tube are both lowered to confirm that maximum moderation and reflection are most conservative. In the second series of cases, the two regions of water are homogenized with neoprene and/or polyethylene (as applicable) to determine the most reactive locations for those materials.

6.14.4.1.2 Results

NCT single package results are shown in Table 6.14-22 through Table 6.14-25. It can be seen that the fuel plates are under-moderated, and thus a decrease in fuel plate bag water density decreases k_{safe}. Similarly, a decrease in inner tube water density results in a decrease in reflection and therefore k_{safe}. With respect to neoprene and polyethylene, it is seen that the addition of polyethylene to either region increases k_{safe} while the addition of neoprene to either region decreases k_{safe}. The most reactive configuration is maximum density water in all regions and polyethylene in the fuel plate bag.

Table 6.14-22 – ATR LEU NCT Single Package Results

Bag Water Density (g/cm^3)	Inner Tube Water Density (g/cm^3)	Neoprene Location	Polyethylene Location	k_{safe}
Series 1: Water Density Adjustment				
1	**1**	**-**	**-**	**0.42115**
0.9	1	-	-	0.40399
0.8	1	-	-	0.38707
1	0.9	-	-	0.40323
1	0.8	-	-	0.38190
Series 2: Homogenized Material Location				
1	1	Bag	-	0.40284
1	**1**	**-**	**Bag**	**0.42385**
1	1	Bag	Bag	0.40510
1	1	Inner Tube	-	0.41764
1	1	-	Inner Tube	0.42207
1	1	Inner Tube	Inner Tube	0.41820

Table 6.14-23 – MURR LEU NCT Single Package Results

Bag Water Density (g/cm^3)	Inner Tube Water Density (g/cm^3)	Neoprene Location	Polyethylene Location	k_{safe}
Series 1: Water Density Adjustment				
1	**1**	**-**	**-**	**0.50062**
0.9	1	-	-	0.47599
0.8	1	-	-	0.45182
1	0.9	-	-	0.48408
1	0.8	-	-	0.46458
Series 2: Homogenized Material Location				
1	1	Bag	-	0.48870
1	**1**	**-**	**Bag**	**0.50630**
1	1	Bag	Bag	0.49337
1	1	Inner Tube	-	0.49801
1	1	-	Inner Tube	0.50184
1	1	Inner Tube	Inner Tube	0.49978

Table 6.14-24 – MIT LEU NCT Single Package Results

Bag Water Density (g/cm^3)	Inner Tube Water Density (g/cm^3)	Neoprene Location	Polyethylene Location	k_{safe}
Series 1: Water Density Adjustment				
1	**1**	**-**	**-**	**0.42227**
0.9	1	-	-	0.40764
0.8	1	-	-	0.39258
1	0.9	-	-	0.40197
1	0.8	-	-	0.38075
Series 2: Homogenized Material Location				
1	1	Bag	-	0.40892
1	**1**	**-**	**Bag**	**0.42693**
1	1	Bag	Bag	0.41531
1	1	Inner Tube	-	0.42058
1	1	-	Inner Tube	0.42349
1	1	Inner Tube	Inner Tube	0.42153

Table 6.14-25 – NBSR LEU NCT Single Package Results

Bag Water Density (g/cm^3)	Inner Tube Water Density (g/cm^3)	Polyethylene Location	k_{safe}
Series 1: Water Density Adjustment			
1	**1**	**-**	**0.38796**
0.9	1	-	0.36870
0.8	1	-	0.34843
1	0.9	-	0.37027
1	0.8	-	0.35170
Series 2: Homogenized Material Location			
1	**1**	**Bag**	**0.39137**
1	1	Inner Tube	0.38896

6.14.4.2 NCT Package Array Evaluation

6.14.4.2.1 Configuration

The NCT package array baseline configuration is an array of packages, with fuel plates in each package shifted towards the center of the array. Full density pure water is in both the fuel plate bag and inner tube. In the first series of cases, the water density in the inner tube is first lowered to find the optimal level of moderation between packages. Then, the water density in the fuel plate bag is lowered to confirm that the individual fuel elements are under-moderated and thus maximum density moderator between the fuel plates is most reactive. In the second series of cases, the two regions of water are homogenized with neoprene and/or polyethylene (as applicable) to determine the most reactive locations for those materials. Inner tube water density is adjusted after homogenization to verify the optimal density is being used.

The package array configurations are shown in Figure 6.14-5 through Figure 6.14-8. The size of the NCT array is 8×8×1 for ATR LEU and MURR LEU and 9×9×1 for MIT LEU and NBSR LEU.

6.14.4.2.2 Results

NCT package array results are shown in Table 6.14-26 through Table 6.14-29. It can be seen that a significantly reduced inner tube water density, optimizing moderation and leakage between packages, results in the highest k_{safe}. Like the NCT single package configuration, a reduction in fuel plate bag water density decreases k_{safe} since the individual fuel elements are under-moderated. With respect to neoprene and polyethylene, k_{safe} is maximized when these materials are homogenized with water within the package (though the effect is relatively small).